Copy - Kathy Hedi

NHMFL

NATIONAL HIGH MAGNETIC FIELD LABORATORY

Operated by:
Florida State University
University of Florida
Los Alamos National Laboratory

Supported by:
National Science Foundation
State of Florida

1995 ANNUAL REPORT

NHMFL

National High Magnetic Field Laboratory

1995 Annual Report

Operated by:

Florida State University
University of Florida
Los Alamos National Laboratory

Supported by:

National Science Foundation
State of Florida

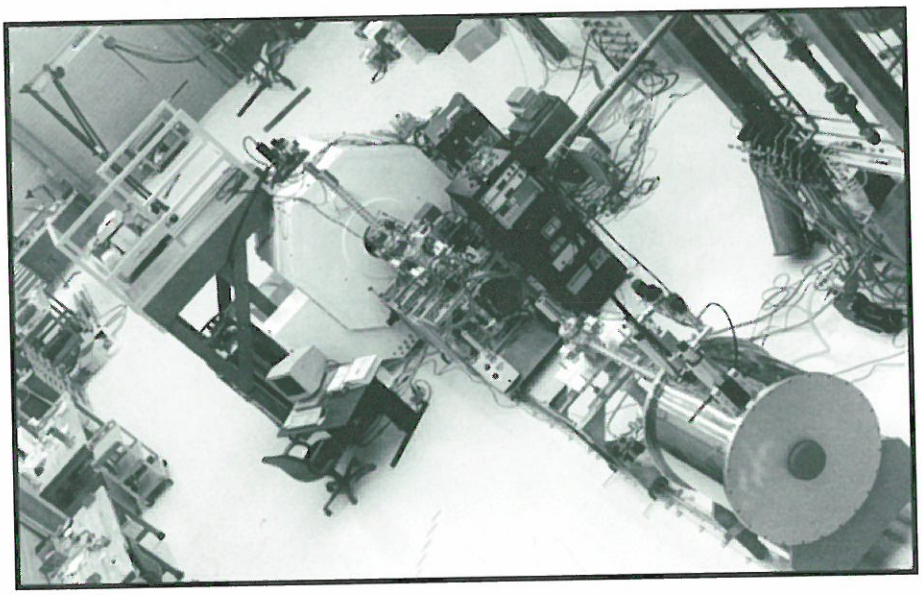

ON THE COVER: The 9.4 T FT-ICR mass spectrometer at the NHMFL. The large white object just left of center is the shielded 9.4 T magnet. The darker objects in the center are the electrospray ion source and system controls. A 6 T, 150 mm bore magnet is shown lower right.

This document is available upon request in alternate formats for individuals with print-related disabilities.

Contact: **National High Magnetic Field Laboratory**
1800 East Paul Dirac Drive
Tallahassee, Florida 32310

Phone: (904) 644-0311
Fax: (904) 644-9462
e-mail: patten@magnet.fsu.edu
World Wide Web: *http://www.magnet.fsu.edu/*

TABLE OF CONTENTS

INTRODUCTION

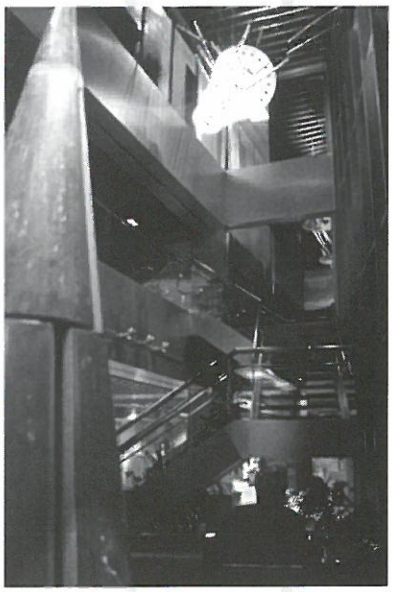

Year five for the National High Magnetic Field Laboratory (NHMFL)—1995—was an exciting year of transition, as the laboratory moved aggressively from building and developing the world-class infrastructure to supporting vigorous user and science programs. This year also completes the first funding cycle, and a thoughtful renewal proposal describing our vision for the next five years was submitted to the NSF and will be considered by the National Science Board in early 1996. The next phase of the NHMFL will build upon the synergy of three principal missions: (1) activities in *support of the users' needs* in broad areas of science and technology, (2) activities in *close partnership with the private sector* that advance magnet technology and magnet materials engineering, and (3) the development of an *in-house science program* that uses the existing facilities for excellent research and enhances those facilities on behalf of all users. The laboratory's outreach efforts in education, international cooperation, and partnerships with industry span all three areas and have been vigorously pursued during this year.

The laboratory marked its move from the construction phase to a science-driven phase with numerous conferences and workshops. Most notable was the *International Conference on Physical Phenomena at High Magnetic Fields-II* held in Tallahassee on May 6-9. This conference was the second in a series of conferences focusing on science areas where high magnetic fields play an important role. The conference brought together approximately 300 experts to assess the current status of such research and to identify

- ***Support of users' needs***
- ***Close partnership with the private sector***
- ***In-house science program***

November SESAPS meeting

promising new directions for science and applications. The conference proceedings will be published by World Scientific. Two workshops were held in conjunction with this conference: one focused on research opportunities at and beyond 1000 tesla (T) and the other was the first workshop on European-United States cooperation on magnet and magnet materials technology for non-destructive 100 T capability. Later in the year the NHMFL hosted five other major meetings including the *Advanced Materials for Pulsed Magnets—Cooperation with Industry Workshop* held on October 12-13, at Los Alamos; the annual meeting of the *Southeastern Section of the American Physical Society*, November 9-11, Tallahassee; the *Southeastern Magnetic Resonance Conference*, November 30-December 2, Tallahassee; a meeting of the *Hypersonic Magnet Levitation Group*, December 12, Tallahassee; and the *Third International Symposium on Magnetic Suspension Technology*, December 13-15, Tallahassee. The Southeastern Magnetic Resonance Conference was developed initially around a regional focus but has grown into an important international meeting: over 200 participants from around the world came to Tallahassee for the conference.

Not only are leading scientists, researchers, and engineers coming to the NHMFL for conferences and meetings, they are coming—more importantly—to use the facilities. In 1995, user groups doubled over the previous year and fifty percent of

Users' research activity has increased significantly at the DC Field Facilities in Tallahassee and the Pulsed Field Facilities in Los Alamos.

Los Alamos Facility

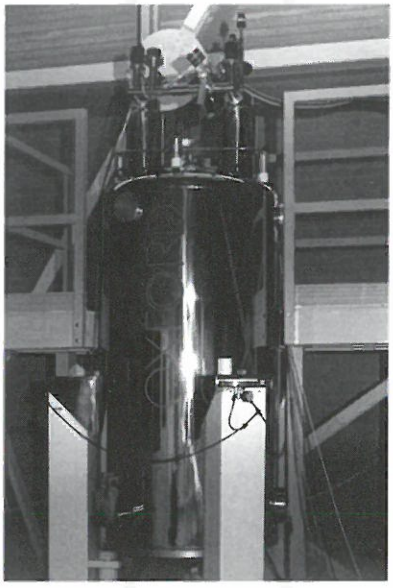

720 MHz NMR Magnet

the users were from the external community. The NHMFL's in-house, interdisciplinary research groups, which bring together theory and experimental efforts, have developed into an invaluable resource for users of the facility. The laboratory sponsored numerous seminars during the year, and presenters included both users and guests of the laboratory. Partial support for external users is provided by the NHMFL Visitors Program funded by the state of Florida. Within the NHMFL, the multi-institutional program called the Center for Interdisciplinary Magnetic Resonance (CIMAR) started users' programs that are supported by in-house scientists.

One of the great strengths of the NHMFL is the full integration of laboratory programs across the three sites of the NHMFL at Gainesville, Los Alamos, and Tallahassee. This inter-institutional cooperation has proven to be extremely successful and has exceeded all expectations. During 1995, two new and unique facilities were initiated that will expand future research opportunities significantly. In Gainesville, construction was started on a new system capable of generating temperatures as low as 500 microkelvin in a field of 20 T. This new user facility will be completed early in 1996 and will provide the highest B/T ratio in the world.

The second initiative is the start of a design program that will lead to the construction of a non-destructive pulsed magnet system capable of reaching 100 T with a pulse length of at

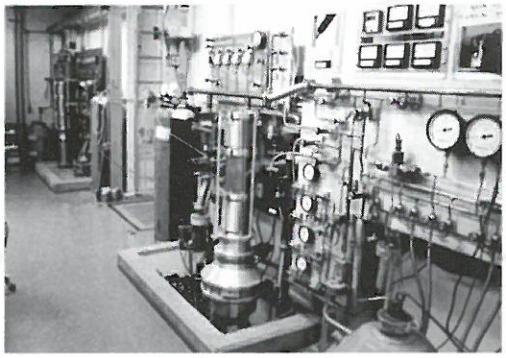

One of the great strengths of the NHMFL is the full intergration of laboratory programs across the three sites of the NHMFL at Gainesville, Los Alamos, and Tallahassee.

Ultra-High B/T Facility at University of Florida

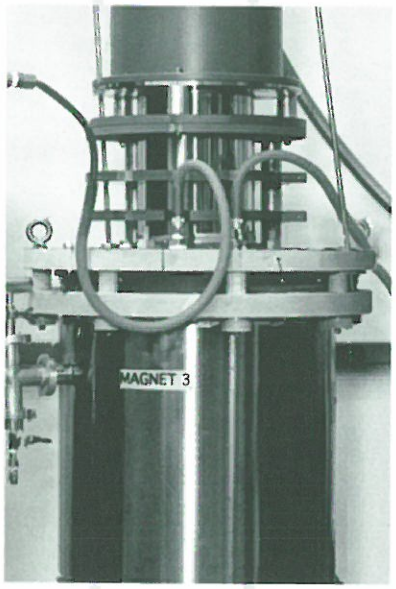

Dilution Refrigerator Mounted on the 50 T Pulsed Magnet

least 20 ms above 50 T, i.e., more than 1,000 times longer than existing, destructive facilities. This impressive and challenging project is jointly funded by the U.S. Department of Energy and National Science Foundation, and is an outstanding example of the NHMFL's quest to provide facilities in response to user needs. This effort, when combined with a currently available dilution refrigerator and pressure cell capabilities at Los Alamos, will provide unique science opportunities covering the extremes in parameter space (100 T, 20 mK, 25 GPa), and is planned to be available for the user community by 1998. Other significant additions to the NHMFL user facilities include:

- The new 9.4 T Ion Cyclotron Resonance (ICR) Mass Spectrometer significantly enhances the mass resolution and trapping time over that which is available with the roughly dozen 7 T ICR mass spectrometer systems located around the world. Prior to the installation and commissioning of the 9.4 T system at the NHMFL, the highest field available for mass spectroscopy was 7 T.

- The Pulsed Field Facilities at Los Alamos acquired a dilution refrigerator for use in pulsed magnets. This added capability extends the range of temperatures available to users down to 25 mK.

- Several new nuclear magnetic resonance (NMR) systems were installed during 1995. These included the 720

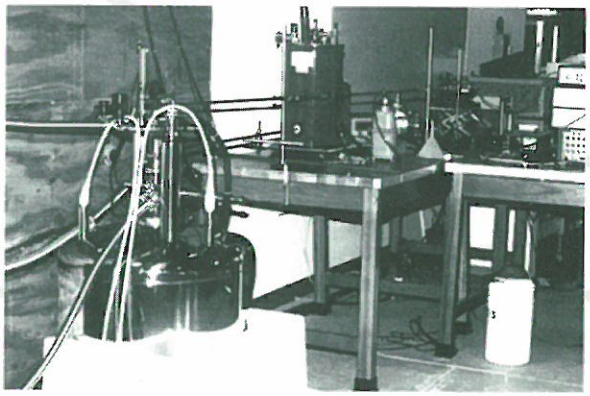

15/17 T EMR Magnet

600 MHz Wide Bore NMR Magnet

MHz high resolution NMR spectrometer given to the laboratory by Oxford Instruments and Varian, and the 600 MHz wide bore, high resolution NMR spectrometer that was procured from Bruker. The 600 MHz wide bore is the first of its type in the world. At the end of 1995, Magnex delivered and installed the 20 T (i.e., 850 MHz for proton NMR) solid state NMR magnet that reached 19.4 T in preliminary tests. After a minor reconfiguration, it is expected to achieve its design field of 20 T. These new instruments significantly enhance our capacity to respond to the challenges and opportunities for high field NMR. In addition to the superconducting NMR magnets, a new magnet was developed by the NHMFL's Magnet Science and Technology Group—a 24.5 T high homogeneity resistive magnet. The magnet has less than 20 ppm variation over 15 mm along the magnet axis and temporal stability of 10 ppm. Efforts to further stabilize the magnet and to improve its homogeneity are underway. Since its installation in July 1995, this magnet has been used extensively for NMR studies of high T_c superconductors and quantum wells.

- The 15-17 T high resolution Electron Magnetic Resonance (EMR) spectrometer, which is the highest field, high resolution EMR system in the world, was installed during the fall of 1995. Within a few days of installation, this new spectrometer was used by several external research groups. This instrument and

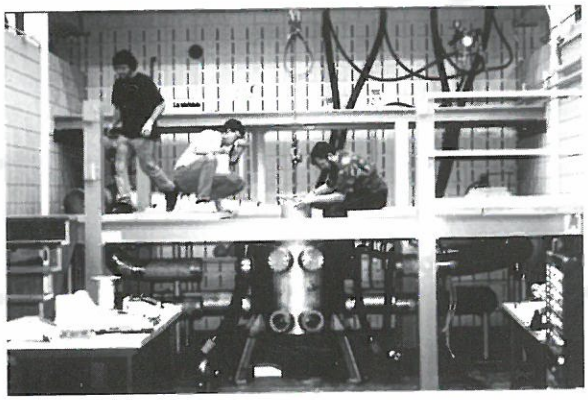

New instruments significantly enhance our capacity to respond to the challenges and opportunities for high field NMR.

30 T Powered Magnet

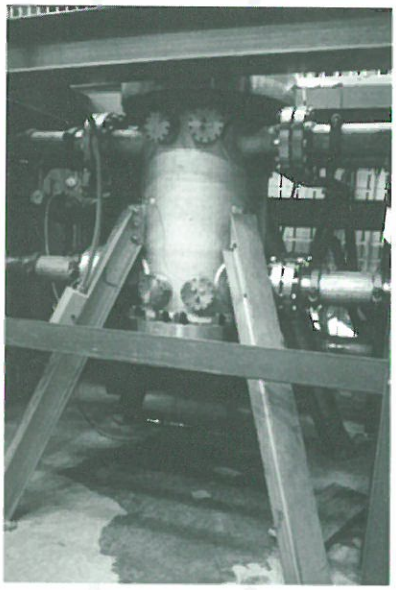

24.5 T High Resolution Resistive Magnet

the resistive magnets, including the 24 T with 20 ppm homogeneity powered magnet, provide new research opportunities in EMR not available anywhere else in the world.

This year, the Magnet Science and Technology Group added to the successes of previous years. The world record 27 T powered magnet that was commissioned in June of 1994 logged more than 1,100 operating hours before being retired to build the 24.5 higher homogeneity magnet. This extraordinary number of operating hours is more than double the typical operation time for such magnet systems. The success of the 27 T magnets was eclipsed in March 1995 by the commissioning of a 30 T magnet, which set a new world record for powered magnets. The NHMFL is hopeful that the 30 T magnet will be superseded by an even more impressive accomplishment of the 34 T powered magnet that is nearing completion and should be operating in early 1996.

The NHMFL is adding significantly to the high resolution research capabilities of the laboratory. The 1.1 GHz (25 T) high resolution NMR magnet program got a boost from the establishment of a partnership between the NHMFL and Intermagnetics General Corporation (IGC) on the fabrication of the 900 MHz (21.1 T) very wide bore, high resolution NMR magnet. The contract signed between the NHMFL and IGC

The commissioning of a 30 T magnet set a new world record for powered magnets.

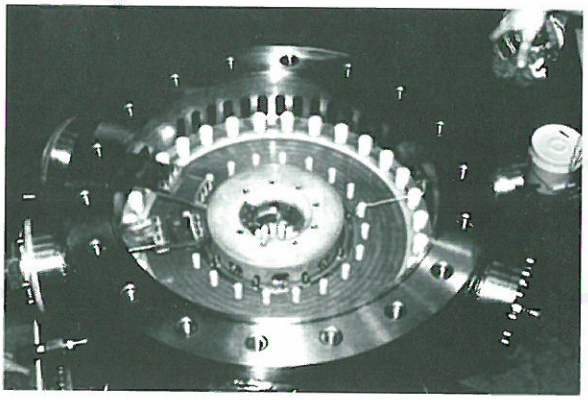

View of the Top of the Three Concentric Magnet Stacks

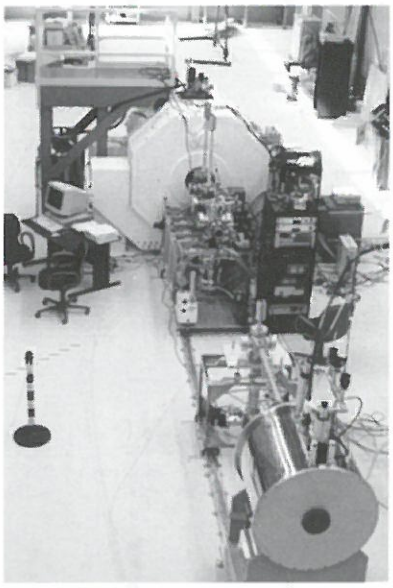

9.4 T FT-ICR Mass Spectrometer

on January 11, 1996, includes a collaboration on the engineering design and fabrication of this unique magnet system and an IGC commitment of $1,000,000 to the project. IGC has played another critical role in the laboratory's program to build a 1.1 GHz NMR magnet by partnering with the NHMFL on an NIH-funded Phase II SBIR program to build a 2.5 T, high transition temperature, superconducting coil as a prototype for the 5 T insert; this will be coupled with the wide bore 900 MHz (21.1 T) outer magnet to reach the "Holy Grail" of the NMR community: 1 GHz high resolution NMR. The partnership with IGC is only an example of the NHMFL's outreach to the private sector. These cooperative alliances utilize the laboratory's unique facilities and resources to advance magnet and magnet materials technology and at the same time provide a return on the private sector investment in the form of new technological capacity and improved market position.

In addition to the advances made in the facilities area, we have had numerous scientific successes in the first year of full operation of both the continuous and pulsed field facilities. The following is a glimpse of the breadth of users' research over the past year.

- A user group headed by Roy Weinstein, University of Houston, attained a world record field for trapped field magnets—

Cooperative alliances with industry utilize the laboratory's unique facilities and resources.

Magnet Cell with Resistive Magnet

10.1 tesla at a temperature of about 42 kelvin. This benchmark was achieved in a 2 cm diameter by 3.2 cm long, high temperature superconductor, containing four quasi-crystals, produced at the University of Houston. Ten tesla had been the group's goal for several years. The group's achievement was acknowledged with *The Workshops Materials/Device Performance Award* at the 1995 International Workshop on Superconductivity, jointly sponsored by the International Superconductivity Technology Center and the Materials Research Society.

- An international team from the University of Nijmegen, the Electrotechnical Laboratory in Tsukuba, Japan, and the NHMFL led by NHMFL scientist James Brooks, used a specialized pressure device to apply uniaxial stress to induce and enhance superconductivity in low-dimensional molecular conductors. Very high magnetic fields (near 30 T) allowed a magnetic "x-ray" to monitor the changes in structure and electron behavior that produced the higher superconducting transition temperature. Such analysis is not possible by any other method. Further theoretical work is underway to determine what parameters may lead to higher transition temperatures in molecular conductors. These organic-based materials provide an alternative path to the quest for superconductivity at higher, economically viable temperatures.

- R.G. Mani, K. von Klitzing, and K. Ploog from the Max-Planck-Institut für

500 MHz NMR Magnet

Festkorperforschung in Stuttgart, Germany, conducted measurements on "multiply connected" quantum Hall systems in which it is possible to realize two quantum Hall effects in a single sample. These studies have addressed fundamental questions related to the nature of edge currents in the Hall effect as well as practical questions related to the breakdown of the quantum Hall effect at high voltages with important implications for metrology.

18/20 T NMR Magnet

- Russell Bowers of the University of Florida used a 20 T, 50 mm bore magnet and laser system to dynamically polarize the nuclei at high magnetic fields, thereby permitting the NMR observation of spins within several semiconducting systems. The combination of high field and rapid ramp rate of resistive magnets allowed these unique studies of optical pumping efficiency as a function of magnetic field strength.

- William Halperin of Northwestern University used the 24.5 T high homogeneity magnet for NMR study of the flux lattice/ flux melting /flux glass phase diagram to fields much higher than the previous 9 T measurements.

- Stan Tozer and Scott Hannahs of the NHMFL have extended the frontier for optical and electrical transport studies at high pressures and high magnetic fields simultaneously using diamond-anvil cells in DC and pulsed fields and to temperatures of 20 mK. These studies of reduced dimensional

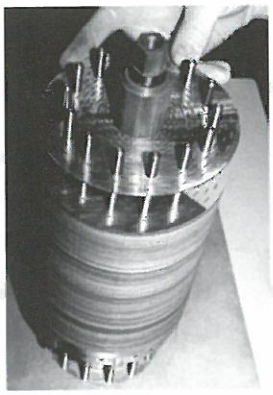

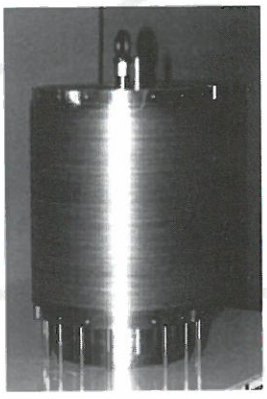

Innermost Coil of the 30 T Resistive Magnet

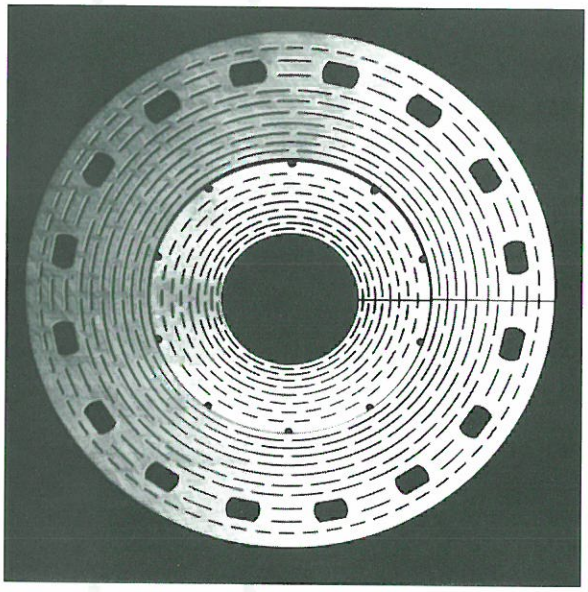

Plates of the 34 T Resistive Magnet

systems are being carried out with the hope of observing a reentrant behavior predicted to occur at fields in excess of 75 T. To obtain this magnitude of field, advanced materials being studied at NHMFL and a pulse magnet optimization code developed at NHMFL will be brought together to achieve what will be a world record field for this type of magnet. Extensively nonmetallic diamond or sapphire-anvil cells also are required to minimize eddy current heating during the pulse. These new developments will feed directly into the 100 T, magnetization, and NMR high pressure programs planned for the future.

National laboratories have unique resources of scientists, engineers, and facilities that can be used in innovative ways to strengthen learning experiences in science. The NHMFL shared its resources with over 150 undergraduate and graduate students who worked on research or affiliated programs at the laboratory during 1995. The NHMFL also continued to provide challenging educational and research opportunities for minority and women scholars, as well as young students. This year the laboratory expanded its educational outreach programs, particularly those for the grades K-12, and since the NHMFL open officially in 1994, several thousand K-12 students have toured and listened to lectures at the Tallahassee facility. On September 30, 1995, the anniversary of the dedication of

The NHMFL shared its resources with over 150 undergraduate and graduate students.

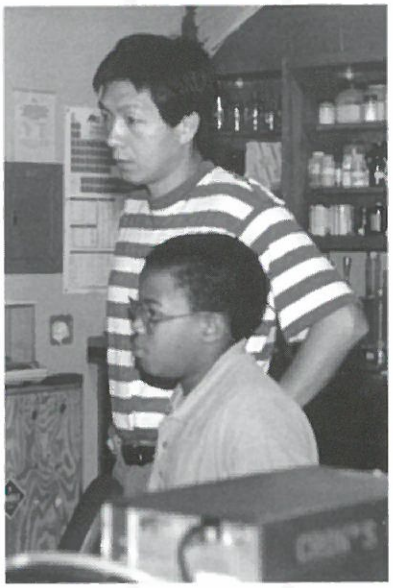

the laboratory, the NHMFL held its second annual open house. The open house attracted over 800 visitors, and the majority were young people who enjoyed the numerous hands-on exhibits displayed throughout the laboratory.

Thanks to a collaboration with nearby Tallahassee Community College, which assigned an educator to the NHMFL, we are exploring new cooperative programs among the universities, community colleges, and regional school systems that will build on the state-federal partnership and the investments made in the NHMFL. The Florida Department of Education has provided the NHMFL with a $75,000 grant to begin a summer mentorship program at the NHMFL for Florida science teachers. One of the objectives of this grant is to provide a number of science teachers selected from throughout the state with an opportunity and the tools to develop new educational units by utilizing the laboratory's facilities and interacting with the NHMFL's faculty. These units will be made available to other teachers in Florida (and eventually elsewhere) via the Internet and other modes of electronic communications. During the fall semester, twenty-three local gifted middle school students participated in a scientist-mentorship program at the NHMFL. Each week, these students participated in hands-on research projects under the direction of their mentors and made oral presentations of their research results at a mini-workshop held at the NHMFL on January 9, 1996. This program proved to be so successful that it will be repeated in the fall of 1996.

We are exploring new cooperative programs among the universities, community colleges, and regional school systems.

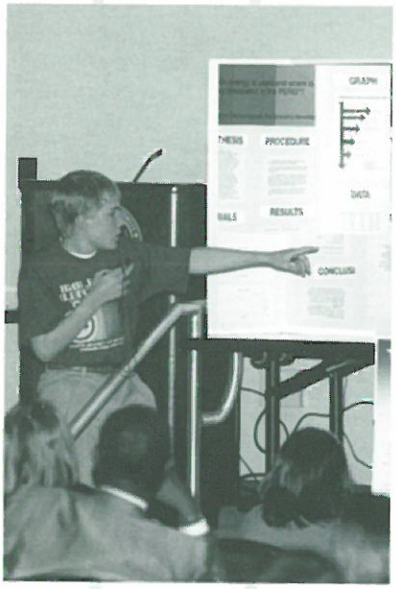

For the third consecutive year, the laboratory provided research opportunities for scholars from groups underrepresented in the fields of science and engineering. For the first time this year, the NHMFL expanded its minority and women summer research program to include all three sites, i.e., Tallahassee, Gainesville, and Los Alamos. Ten students participated. A 1995 participant, Larry Sears, commented, "...the entire experience was just what my education needed. Books and classrooms are fine but application of all those theories is so much more beneficial." This program received considerable assistance from the Florida-Georgia Alliance for Minority Participation (AMP) and other AMP directors around the country. The laboratory will continue to expand this program and will work with AMPs to develop and introduce new programs that offer exciting research participation opportunities for undergraduates from underrepresented groups.

This annual report provides the reader with an overview of the research, collaborative, and educational activities accomplished by the NHMFL during 1995. The laboratory has established itself as a world leader in magnet-related research and development, and the future looks extremely bright.

- ***Support of users' needs***
- ***Close partnership with the private sector***
- ***In-house science program***

RESEARCH REPORTS 1

An Overview of the NHMFL's 1995 Research Reports

The year 1995 marked the last year of the National High Magnetic Field Laboratory's (NHMFL) initial five-year funding period and during this period, a majority of the efforts of the labaoratory were devoted to the construction and establishment of the facilities. This last year, however, has witnessed impressive progress including science and user activity, as is indicated by the large number of research reports following this introduction, and the achievements in facility development, as reflected by new research capacity. With the transition from construction to science and engineering as the drivers of the future, the laboratory has emerged with a clear vision and commitment to the expectations and optimism for magnet-related research and technology as envisioned in the Seitz-Richardson report and the specific goals of the U.S. National Science Foundation (NSF).

The significant increase in the number of research reports (from 125 last year to over 180 this year) reflects the growing use of the NHMFL facilities, the increased scientific activities over a broad range of areas, and the progress in magnet science and technology. These unique facilities offer unprecedented research opportunities and others are planned for the coming years. The NHMFL has achieved a high degree of success in a wide range of activities, covering all aspects of scientific research in high magnetic fields as well as magnet science for the generation of these fields.

Within five short years, the NHMFL has become the world's major facility devoted to the promotion of science and technology with magnetic fields. In pursuing the challenges and new opportunities, the NHMFL joins the other magnet laboratories in the world to promote scientific and technological excellence. The NHMFL is unique, however, in that its mission is to respond to the needs of *all* areas of magnet-related science and technology including physics, chemistry, biology, materials, engineering, medical science, and earth sciences.

The core of the in-house science program is an outstanding collection of international interdisciplinary scientists. Building on this unique personnel infrastructure, the in-house science activities utilize the facilities to carry out high quality research at the forefront of science and advance the facilities and its scientific capabilities. The Science Program Committee, with representation from all participating institutions, oversees these mandates by promoting and monitoring in-house research and encouraging collaborations with external users. The science program is directed by rotating internal scientists, who also serve as the chair of the Science Program Committee. This new structure has increased unity and coherence in the science program with excellent cooperation in all respects.

New horizons in science are underpinned by the numerous successes of the Magnet Science and Technology Group (MST) and the integration of all NHMFL activities, i.e., extraordinary teams will use the best magnets in the world to produce new results at exceptional levels. The MST generated two world records for resistive magnets—27 T and 30 T—and put into service several other unique high field magnet systems. In field strengths, they are comparable to the highest fields available at other laboratories in the form of hybrid magnets, while in user quality, i.e., accessibility, extremely low vibration level and reliability, they are unparalleled. Together with the unique features of the 40 MW power supply (1 ppm rms ripple), a high field user facility has been established that allows measurements of extreme sensitivity. As a result, the new generation of resistive magnets at the NHMFL has a field quality similar to superconducting magnets, however, without their inherent disadvantages such as slow ramp rates and limited maximum field. Nearing completion is the 60 T quasi-continuous magnet at the pulsed field facilities at Los Alamos, which will provide users with new opportunities to explore innovative science at field strengths not available with continuous fields.

Interactions among science and user groups and MST have progressed well and have resulted in proposals for new magnet systems, such as high field, high gradient magnets; magnets with field modulation; resistive magnets with high homogeneity; and pulsed magnets with new enhancements for users, for example, the 100 T non-destructive pulsed magnet. A good example of the synergy available and exploited at the NHMFL is the research activity on superconductivity that ranges from theory, basic science, and development of new high temperature superconductors, to the production and characterization of short samples, to the manufacture of longer lengths of wires, and finally to the application and technology development of windings, insulation systems, and joints. Another example of such synergy is the very interesting link between materials science and magnetic fields. Magnets require new materials with high strength and other advanced characteristics and stronger insulation systems. Such new materials and insulation systems are being developed at the NHMFL. Conversely, new materials can be developed through the use of magnetic fields. For example, crystal growth in magnetic fields is a relatively new technology. The NHMFL is exploring this technology by building a magnet for NASA that will allow for the possibility of growing crystals in magnetic fields on a spaceship. Other examples of materials development through the use of magnetic fields include the polymerization of long molecule chains in strong magnetic fields. Research reports on these subjects illustrate the synergism among the science and user groups and MST.

The research reports in this chapter reflect the activities of the laboratory in 1995. These reports are organized according to the following categories: Biology (page 3), Chemistry (page 9), Superconductivity–Basic (page 18), Superconductivity–Applied (page 29), Kondo/Heavy Fermion Systems (page 34), Molecular Conductors (page 44), Semiconductors (page 54), Magnetism and Magnetic Materials (page 68), Other Condensed Matter (page 87), Magnetic Resonance Techniques (page 91), and Magnet Science and Technology (page 97). The Magnet Science and Technology section has been sub-divided by program. Each sub-section, for example, Large Superconducting Magnet Systems, High Field Magnetic Resonance Systems, Pulse Magnets, etc., begins with a program overview of the ongoing major activities within the area, followed by the associated research reports.

BIOLOGY

Characterization of "Catalytic" Solvent Molecules in Polypeptide Structural Interconversions by Solution NMR Spectroscopy

Cross, T.A., NHMFL/FSU-Chemistry and Institute of Molecular Biophysics
Xu, F., NHMFL/FSU-Chemistry and Institute of Molecular Biophysics
Wang, A., NHMFL/FSU-Chemistry
Vaughn, J., NHMFL/FSU-Chemistry and Institute of Molecular Biophysics

Very little is known about the interactions of proteins with solvent in hydrophobic environments, such as the interstices of a lipid bilayer. Almost all protein structures determined to date have been water soluble proteins. The aqueous environment destabilizes electrostatic interactions within the protein. For instance, hydrogen bonds on the protein's surface are considerably weakened by the presence of water. The absence of a protic solvent can be expected to stabilize electrostatic interactions. Consequently, we would expect membrane bound proteins to have a very stable structure.

To investigate the influence of solvent on protein structure we have prepared samples of the polypeptide, gramicidin A, in organic solvents. In relatively high dielectric solvents such as ethanol, gramicidin forms a variety of structures that are intertwined helices. These helices can be parallel or antiparallel, left-handed or right-handed. In alcohols a complicated mixture of these conformations is present and they interconvert slowly on the ms timescale so that sharp resonances are obtained for each conformer in the NMR spectra, but this exchange rate is rapid on the hr timescale required for chromatographic separation. In low dielectric solvents the exchange rate becomes slow on the timescale of a week. Both chromatographic separation and NMR spectral analysis can be performed on isolated conformers in dioxane. The addition of ethanol to dioxane (1:99; v/v) results in rapid interconversion of the conformers. The protic solvent appears to act as a catalyst for structural interconversion.

Using recently developed techniques in solution NMR to characterize bound solvent molecules on a protein's surface, we have identified polypeptide binding sites for 12 ethanol molecules on gramicidin in a benzene/ethanol mixed solvent (95:5; v/v). Four of these sites appear to involve hydrogen bonding of the ethanol to amide backbone sites participating in hydrogen bonds between the polypeptide monomers. Such interactions will destabilize the dimer and the ethanol will be in position to stabilize a structural intermediate in the conformer interconversion pathway. Such catalytic activity by protic solvents is an extension of our current chemical knowledge of acid/base catalysis. Catalysis by acids and bases involves monopole-dipole interactions; here we have demonstrated catalysis with dipole-dipole interactions.

Furthermore, we have shown that specific non-minimum energy conformers of gramicidin can be kinetically trapped in the lipid bilayer in a metastable state. This is exactly analogous to the metastable states we have seen for gramicidin in dioxane. We speculate that another regulatory mechanism for membrane protein function may exist—that proteins may be inserted into membranes in inactive conformations and later activated when the protein's biological function is required.

High Resolution Protein Structure and Biological Implications from Solid State NMR Spectroscopy

Cross, T.A., NHMFL/FSU-Chemistry and Institute of Molecular Biophysics
Tian, F., NHMFL/FSU-Chemistry and Institute of Molecular Biophysics
Ketchem, R.R., NHMFL/FSU Institute of Molecular Biophysics

High resolution membrane bound polypeptide and protein structures have been exceptionally hard to achieve. These systems are difficult to crystallize and high resolution NMR spectroscopy methods are not readily applicable. Solid state NMR of hydrated lipid bilayer membranes that have been aligned between glass plates can be used to generate structural constraints for molecules in these model membranes. Here we have incorporated into the aligned bilayers the 15 amino acid polypeptide, gramicidin A, that forms a monovalent cation selective channel across such membranes. From specific isotopically labeled samples, numerous orientation dependent nuclear spin interactions have been observed. Each such observation constrains the molecular structure with respect to the magnetic field direction and the channel axis that are arranged parallel to each other. These constraints have been shown to have a high degree of accuracy and have been demonstrated to yield a high resolution three dimensional structure from a hydrated lipid bilayer environment.

During this past year extensive studies have been performed at the NHMFL on samples containing Na^+. While the channel structure shows a 0.4 nm diameter pore, it is not certain how the carbonyl groups that line this pore solvate the cations. How many carbonyls solvate the cation at one time? What is the orientation of the carbonyls with respect to the cation? Our previous work has described the details of the channel structure in the absence of cations. Models based on computational methods have indicated that four carbonyls solvate the cation and that considerable structural deformation occurs upon cation binding. It has been shown here that there is essentially no structural change upon cation binding. Only one site shows a change in carbonyl orientation greater than 2° and that is as a change of just 4° for the Leu-10 carbonyl bond. This means that a maximum of two carbonyls are involved in solvating the Na^+ at any one time anywhere within the channel. It also means that the Na^+ ion passes through the channel on a helical path following the carbonyl oxygens. It is known that there is not a very large potential energy barrier for cations to enter the channel, i.e. for four of six waters in the primary hydration sphere to be stripped off and replaced with the polypeptide solvation environment. Consequently, these carbonyls are very effective for solvating Na^+ in the channel. More importantly, it suggests that when cations bind there is not a deep potential energy well formed, which would make it hard for the cation to continue on its transit across the membrane. This is contrary to the general understanding of ion channels, which assumes that cations are bound by the channel with a nearly ideal binding geometry requiring considerable structural rearrangements. The effort here suggests that cations are marginally solvated by the protein so that the potential energy barriers are minimized for cation movement through the channel.

Multi-Nuclear NMR Studies of Single Muscle Cells and Muscle Cell Bundles

Ellington, W.R., NHMFL/FSU, Biology Dept.
Combs, C.A., NHMFL/FSU, Biology Dept.
Kinsey, S.T., NHMFL/FSU, Biology Dept.

Our research efforts have focused on high field NMR studies of energetics, membrane transport, and acid-base balance in isolated muscle cells (fibers) and cell bundles. The major constraint in doing studies such as these is the maintenance of cells in good physiological condition. To this end, NMR spectra were acquired using a dual-tuned (^1H,^{31}P) micro-solenoid probe (coil internal diameter [ID] = 2.2 mm). Cells were mounted in a

1.9 ID glass tube that was inserted into a superfusion assembly machined from nylon. Physiological saline solution, brought to the desired temperature by a heat-exchanger mounted at the base of the probe, was circulated through the muscle chamber by peristaltic pumps. Large lobster abdominal muscle cells (10 mm x 125 micrometers) were utilized in most studies. NMR studies were conducted using a Bruker DMX 600 WB spectrometer fitted with XYZ gradients (maximum gradient strength = 100 G/cm). ^{1}H-NMR spectra and ^{31}P-NMR spectra were acquired at 600 MHz and 242 MHz, respectively.

We have used the above system to investigate the mechanism of membrane permeation of lactic acid, the major end product of energy metabolism when cells lack oxygen. Lactate influx and efflux rates were measured by monitoring changes in intracellular lactate levels while the muscles were superfused with, and subsequently cleared of, extracellular lactate. Under our experimental conditions, three lactate-containing compartments exist: intracellular, extracellular, and interstitial. To eliminate the latter two compartments (and observe only intracellular lactate), we employed a diffusion-weighted, stimulated-echo sequence (a non-localized DRYSTEAM experiment). Since lactate in the extracellular and interstitial compartments has a high molecular mobility (especially under our flow conditions), the signal from these compartments is rapidly attenuated with increasing diffusion weighting, leaving only the intracellular signal. We have found that this methodology can be used with preparations of a single cell or a few cells (where no interstitial compartment exists), as well as with multiple cell bundles. Using this technique, we were able to measure initial velocities of lactate transport using ^{1}H-NMR while interleaved ^{31}P-spectra allowed us to monitor intracellular pH and energetic stability of the preparation with excellent time resolution. ^{1}H- and ^{31}P-spectra could each be accumulated in as little as 15 seconds. Our results (supported by NSF grant IBN-9104548) indicate that a stereospecific L-lactate:H^{+} carrier protein is not involved in lactate transport in this muscle.

EPR of Muscle Contraction

Fajer, P., FSU, Biology Dept./NHMFL
Fajer, E.A., FSU, Biology Dept.
Adhikari, B., FSU, Inst. Molec. Biophysics
Raucher, D., FSU, Inst. Molec. Biophysics
Li, H., FSU, Biology Dept.
Griffin, P., FSU, Biology Dept.
Somerset, J., FSU, Inst. Molec. Biophysics
Madden, S., NHMFL

Since moving the laboratory in June 1995 from the main FSU campus to the NHMFL, we have concentrated our efforts on investigating the myosin essential light chain (ELC) involvement in the regulation of muscle contraction. By measuring the protein dynamics of catalytic domain and of the regulatory domain we have proven existence of a hinge within the myosin head. A hinge between the two domains was postulated but never observed by Rayment et al. (1993). This particular project is now being written up by Adhikari. (In the summer, Adhikari also wrote a paper on the dynamics of myosin heads when perturbed by osmotic compression; it has been accepted in the Biophysical Journal. Most of the experimental work was accomplished before our move to NHMFL.)

Adhikari and Somerset have begun a project on the effects of ionic strength, divalent metal ions, and phosphorylation on the dynamics of the ELC. Their work was presented at SEMRC and at the Biophysical Society Meeting in Baltimore (February 1996). The biological significance of this project is in the correlation of protein dynamics with regulation of muscle function. It seems that the agents that promote association of myosin to actin filaments also promote large scale rotations of myosin heads. We stipulate that the activation process might simply be due to increased Brownian motion that allows docking of the two-protein complex.

Li has extended her studies of troponin C orientation (Li and Fajer, Biochemistry 1994) to TnC dynamics. It seems that the disordering observed during Ca activation of muscle is static i.e. there is only a small change of protein mobility.

This project was also presented at SEMRC and Biophysical Society meeting, and Li is in the final stages of writing the manuscript. We have also accomplished specific labeling of other regulatory proteins (troponin I, tropomosin) and reconstituted them successfully in the muscle fibers. This will allow us to follow path of Ca binding signal from TnC all the way to actin.

Very High Frequency EPR of Metalloproteins

Gaffney, B.J., John Hopkins Univ., Chemistry Dept.
Maguire, B.C., John Hopkins Univ., Chemistry Dept.
Doctor, K.S., John Hopkins Univ., Chemistry Dept.
Tevelrakh, E., John Hopkins Univ., Chemistry Dept.
Hassan, A., NHMFL
Krzystek, J., NHMFL
Pardi, L., NHMFL
Brunel, L.C., NHMFL

Electron paramagnetic resonance (EPR) spectroscopy of paramagnetic metal centers in biological molecules affords an intimate view of structure and bonding in such localized regions as enzyme active sites and locations of specialized structure. The most abundant metal in biomolecules is iron, which can be found in paramagnetic spin states from S=1/2 to S=5/2. The precision with which the geometry of iron centers can be determined, through measurement of zero field splittings, and with which structural details of metal ligands can be obtained, through nuclear interactions with the paramagnets, is predicted to increase dramatically as the frequency of the measurement is increased. New steps to realize this potential have been taken in recent experiments using a newly constructed EPR spectrometer designed by Louis-Claude Brunel and coworkers at the National High Magnetic Field Laboratory in Tallahassee. In collaboration with Betty J. Gaffney of Johns Hopkins University, three proteins containing high-spin, ferric iron have been examined at 5 K and at frequencies to 330 GHz. Samples chosen for study contained high-spin, ferric sites representative of heme, and of non-heme, iron proteins. At 330 GHz, the effective perpendicular g-value of polycrystalline methemoglobin (from horse) was approximately 5.5, providing a direct measure of the zero field splitting (~9 cm-1). Crystals of methemoglobin gave lower effective g-values when exposed to a 4 T field before they were frozen, demonstrating that they were oriented by the magnetic field. Other samples examined contained non-heme iron sites: in the iron transfer protein, transferrin, and in the enzyme, lipoxygenase. Transferrin gave a signal at 12.2 T, consistent with the very small zero field splitting in this metalloprotein. Multiple signals were observed from lipoxygenase in multifrequency experiments with the spectrometer operating from 44 to 330 GHz.

Future applications of very high frequency EPR of biomolecules are expected to include studies of single crystals of the dimensions used for x-ray analysis and ENDOR studies leading to details of metal-ligand geometry and of enzyme-substrate complexes.

Analysis of Electrophoretic Transport of Macromolecules Using Pulsed Field Gradient NMR

Moerland, T., FSU, Biology Dept./NHMFL
Locke, B.R., FAMU-FSU Dept. Chemical Engineering

The objective of this project is to apply pulsed field gradient NMR (PFG-NMR) to the analysis of electrophoretic and diffusive transport of biological molecules in solutions of polymers, in gels, and in gel-like media. These measurements will provide fundamental transport properties that are necessary for the design and operation of separation and purification processes for these macromolecules. Particular applications are to NASA's microgravity research, however the work is also relevant to ground based separation methods. This project is funded by NASA (UGS95-0041) and began September 1995.

Preliminary experiments for this project have been directed toward obtaining 1H-PFG-NMR measurements of the apparent diffusion coefficient for water (D) in polyacrylamide and agarose gels of varying percent composition. Preliminary data obtained at a diffusion time of 30 ms suggest a linear relationship between the water self diffusion coefficient and the percent composition (%T) of polyacrylamide gels. This result is in contrast with expectations stemming from an Ogston type model (Ogston, 1958),[1] which predicts an exponential relationship between D and acrylamide composition. The Ogston model was formulated for spherical particles in a random, uniform suspension of fibers, and thus there may be deviations from this relationship for the diffusion of water in a gel matrix.

Data reported in our study considered variation of the percent of the monomer acrylamide with a fixed concentration of crosslinking agents. Work reported in the literature by Pavesi and Rigamonti (1995)[2] gave a power law dependence for water self diffusion as a function of crosslinker density for fixed total acrylamide concentration. No theoretical justification was given for this functional relationship for the effect of crosslinking density; however, studies from gel swelling data (Richards and Temple, 1971)[3] also suggest an exponential relationship between mobility and concentration of crosslinking agent. Thus, both our data and that of Pavesi and Rigamonti (both obtained using PFGNMR) suggest deviations from Ogston behavior for water self diffusion. It is worth noting that data obtained by Gibbs and Johnson (1991)[4] found the diffusion coefficients of a range of small probes followed an empirically modified form of the Ogston model whereby the diffusion coefficient was proportional to the exponential of the acrylamide concentration raised to an empirical power law coefficient. Therefore, further experimental and theoretical studies are needed to fully understand transport in these gel media.

References:

1 Ogston, A.G., Transactions of Faraday Society, 54:1754-1757 (1958).

2 Pavesi, L., et al., Phys. Rev. E, 51(4), 3318 (1995).

3 Richards, R., et al., Nature Physical Science, 230, 92 (1971).

4 Gibbs, S.G., et al., Macromolecules, 24, 6100 (1991).

Effects of Temperature on Diffusive Mobility of Phosphorous Metabolites in Skeletal Muscle

Moerland, T., FSU, Biology Dept./NHMFL
Locke, B.R., FAMU-FSU Dept. Chemical Engineering
Hubley, M., FSU, Biology Dept./NHMFL/UF Center for Structural Biology

This project utilizes pulsed-field gradient NMR (PFG-NMR) to investigate the effects of temperature on diffusion and mobility of the phosphorous metabolites phosphocreatine (PCr) and ATP in skeletal muscle. Such changes in temperature are relevant clinically, in the context of accidental and surgical hypothermia, and to poikilothermic animals.

Diffusion coefficients of ATP and PCr were determined using the pulsed gradient spin echo method, with homonuclear decoupling of the B-ATP resonance during spin evolution (Hubley et al., 1995).[1] Muscle preparations consisted of isolated bundles of goldfish skeletal muscle, which is composed of a uniform population of white (fast, glycolytic) muscle fiber types. Intracellular diffusion coefficients were measured with a short diffusion time (9 ms) to minimize the effects of boundaries on measurements of intracellular diffusion coefficients. Diffusion coefficients of ATP and PCr also were measured in aqueous solutions with an ionic composition similar to that of the intracellular environment.

Intracellular diffusion of PCr and ATP was significantly influenced by temperature in a manner that is consistent with the Stokes-Einstein relationship (Figure 1). A mathematical reaction-diffusion model to analyze the distribution of phosphorous metabolites during muscular contraction was developed. This model incorporates NMR-measured diffusion coefficients, enzyme rate constants, and NMR-derived metabolite concentrations. Concentrations of ATP and PCr were calculated as functions of time and position from the primary cellular sites of synthesis, mitochondria. This model indicates that there is little change in the intracellular concentration profile of ATP from that in resting (unstimulated) cells under any condition examined (Figure 2). However, muscular contraction may result in significant decreases in PCr with time and distance from mitochondria (Figure 2).

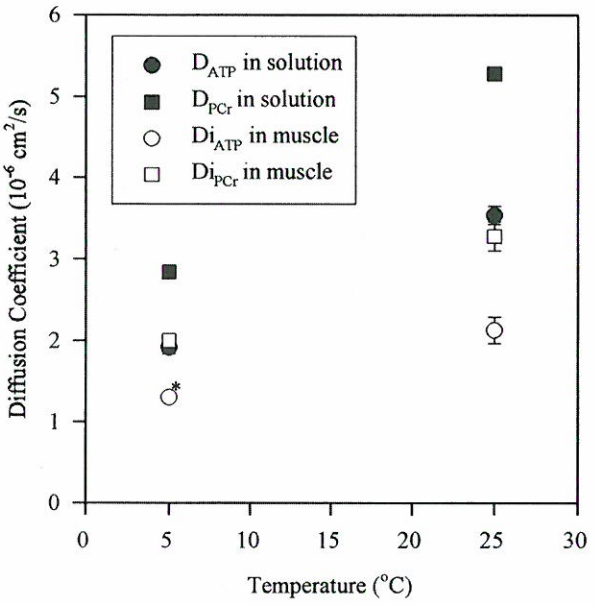

Figure 1. Diffusion coefficients of ATP and PCr in goldfish skeletal muscle and in solution.

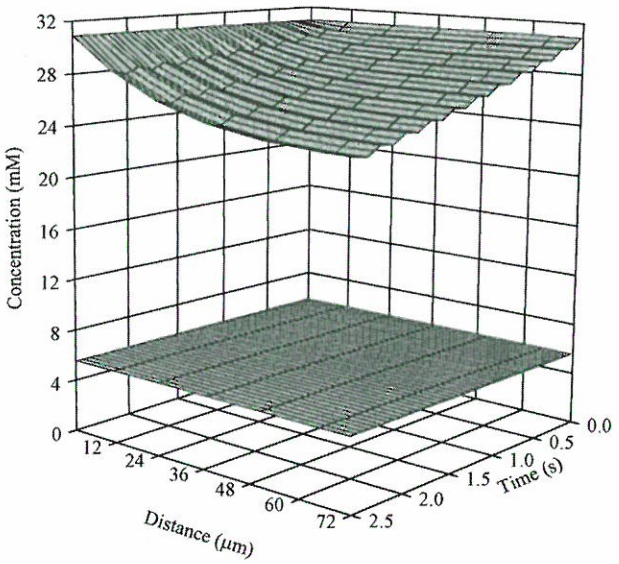

Figure 2. Concentration profiles for ATP and PCr in goldfish skeletal muscle. [PCr] is the upper curve and [ATP] is the lower curve.

Reference:

1 Hubley, et al., NMR in Biomedicine, 8:113-117.

Solution Structure of a Lewis^X Analogue Taking into Account Its Internal Dynamics

Berthault, P., CEA CE/Saclay
Birlirakis, N., CEA CE/Saclay
Rubinstenn, G., Ecole Normale Supérieure
Sinaÿ, P., Ecole Normale Supérieure
Desvaux, H., NHMFL

We have investigated the structural and dynamic properties of a synthetic C/O-trisaccharide analogue of sialyl Lewis^X using off-resonance ROESY. The measurements have been done at various mixing times, at various angles between the static and the effective field in the rotating frame and using selective excitation techniques. Thus the longitudinal and transverse cross-relaxation rates between 30 pairs of protons have been determined with a very high accuracy (224 cross-relaxation rates measured). These parameters have been transformed into a geometrical parameter (an internuclear distance) and a dynamic parameter (a correlation time per proton pair), assuming that the correlation function of each considered proton pair can be described by a different exponential function. A simulated annealing procedure using these distance restraints resulted in low energy structures without covalent nor nOe violations.

The comparison of the back-calculated distances with the NMR distances has shown a very good agreement for all considered protons (pyranosid as well as methyl protons) showing that this method can take into account possible variations of internal dynamics along the molecule. Complete cross-validation has been used to check the quality of the NMR set of distances derived by this method in comparison with the results obtained assuming a global isotropic Brownian motion and considering a given proton pair as internal distance reference. Whatever the reference pair, the results are always worse in this latter model, proving that the solution structure obtained by assuming different correlation functions for each proton pair is both more accurate and more precise. Finally, the quality of the NMR results enabled us to give a definite answer to the question of the number of structural families for this molecule.

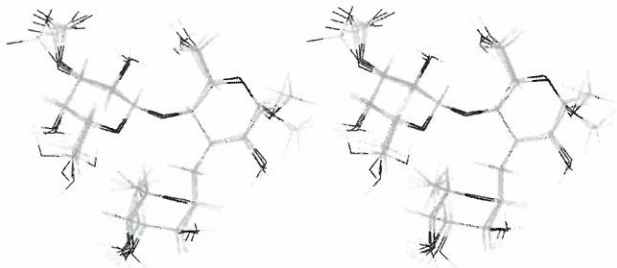

Figure 1. Solution structure of the trisaccharide taking into account its internal dynamics.

High Frequency EPR of NO Biradicals

Brunel, L.C., NHMFL
Chachati, C., C. E. N. Saclay, France
Fabre, C., Ecole Normale Superieure Paris, France
Gambarelli, S., Ecole Normale Superieure Paris, France
Jaouen, D., Ecole Normale Superieure Paris, France
Rassat, A., Ecole Normale Superieure Paris, France

To check the accuracy of the structural information obtained from high-field EPR, the studies of biradicals for which full structural information is available have been performed.[1,2] In the fast exchange approximation the spin Hamiltonian writes:

$$H = \beta \mathbf{B.g.S} + \mathbf{I.A.S} + \mathbf{SJS} + \mathbf{SDS}$$

where all the symbols have their usual meaning and **S** is the total spin.

In Figure 1 are the experimental spectra and the theoretical fit for a biradical of approximate D2h symmetry.[1]

The combination of 9 GHz and high frequency EPR gave an accurate determination of the magnetic **g**, **A** and **D** tensors of the biradical, in particular the high field spectra appeared to be very sensitive to the principal values of the **g** tensor. Structural information about biradicals may not be that important, but the methodology developed in References 1 and 2 will be of tremendous significance when applied to biological systems.

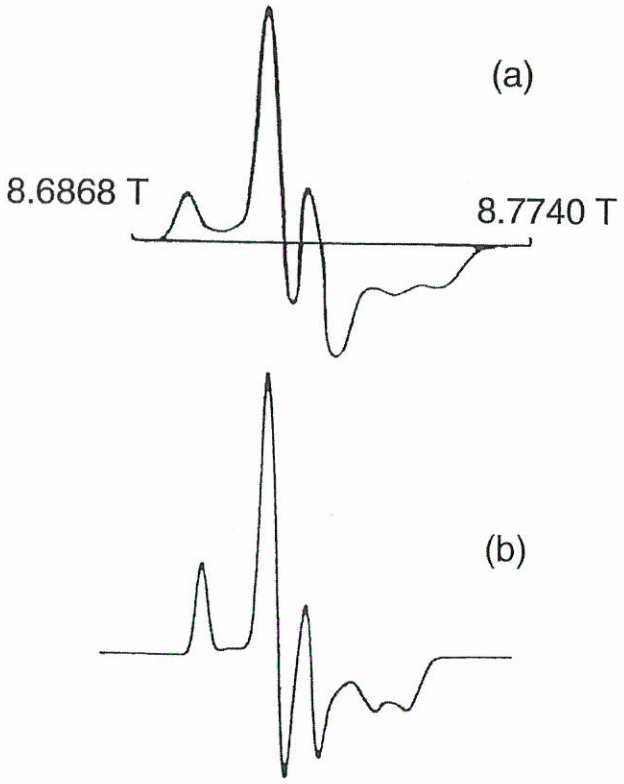

Figure 1. 245 GHz EPR spectrum of a nitroxyl biradical. (a) Recorded at 25 K. (b) Theoretical fit.

References:

1 Fabre, C., et al., Mag. Res. in Chemistry, in print, (1996).

2 Gambarelli, S., et al., to be published.

Determination of Scalar Coupling Constants by Pattern Recognition in Band-Selective NMR Correlation Spectroscopy

Jeannerat, D., NHMFL

Bodenhausen, G., NHMFL/FSU, Chemistry Dept.

In a band-selective high-resolution NMR experiment, the first hard pulse of the sequence for *d*ouble-*q*uantum *f*iltered *co*rrelation *s*pectroscop*y* (DQF-COSY) is replaced by a selective pulse thus allowing one to "zoom" onto a strip of a correlation spectrum. The resulting improvement in the digital resolution in the ω_1 dimension allows one to access the fine structure of cross-peak multiplets.

First, we compare two complementary band-selective experiments: a conventional reference spectrum and a modified spectrum with a selective inversion pulse applied in the middle of t_1 to refocus some couplings. The multiplet structures are similar except that the displacement due to the coupling between the selectively excited spin and the inverted spin collapses. The determination of the coupling constant is possible using convolution with a doublet of delta functions for different trial coupling constants.

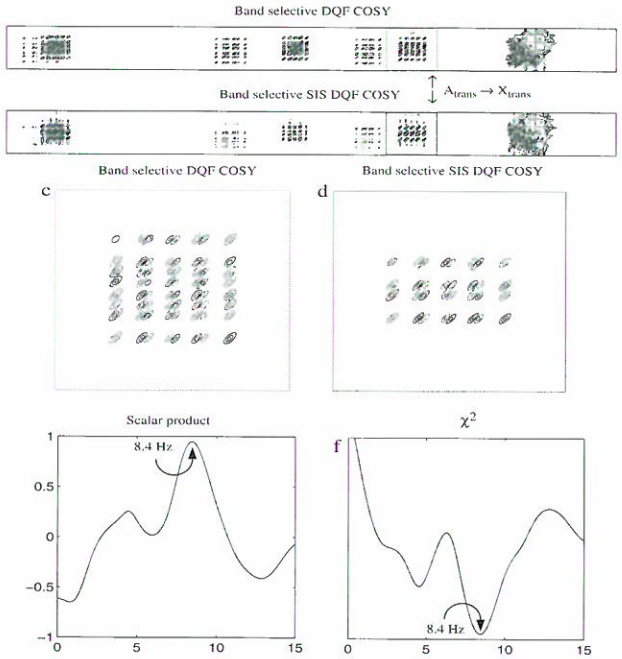

Figure 1. (a) Band selective DQF-COSY centered on the spin A_{trans} of trans-phenylcyclopropane-

carboxylic acid in the ω_1 dimension acquired on a 300 MHz Bruker DMX spectrometer at 303 K. (b) SIS version of (a) where the spin K_{trans} has been inverted. (c,d) Zoom of (a,b). Similarity functions using the χ^2 method (e) and the scalar product (f) giving the same value for the coupling constant J_{AK}.

The second application is a band-selective DQF-COSY where the flip angles of both hard mixing pulses are 75°. The resulting cross-peak multiplets show structures with dominant peaks corresponding to the pattern of E-COSY spectra and recessive peaks which are also observed in 90° DQF-COSY. Two-dimensional *deconvolution* allows one to decompose the structure of such multiplets and to determine the coupling constants, not only between the active spins, but also between the active and passive spins. A graphical representation of the couplings that contribute to the structure of a multiplet facilitates the assembly of a "chromatic graph" of the coupling network.

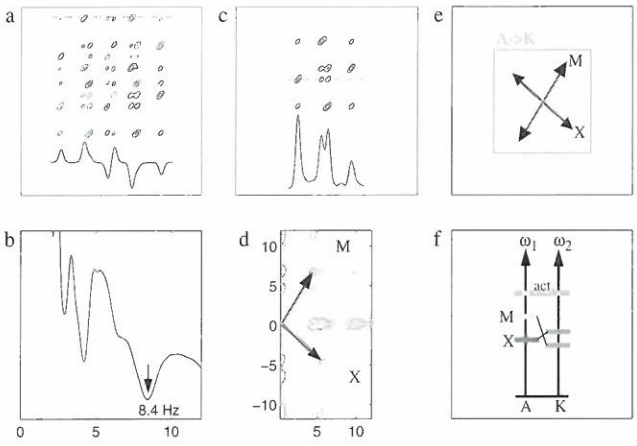

Figure 2. (a) Multiplet correlating spins A_{trans} and K_{trans} in trans-phenylcyclopropanecarboxylic acid. (b) Determination of the active coupling constant $J(A_{trans}, K_{trans})$. (c) Spectrum after deconvolution of the active coupling constant. (d) Contour plot of the function giving the passive coupling constants. (e) Two-dimensional (f) "One-dimensional" representations of the coupling constants.

FT-ICR Mass Spectral Analysis of Complex Mixtures

Marshall, A.G., NHMFL/FSU, Chemistry Dept.
Guan, S., NHMFL/FSU, Chemistry Dept.
Scheppele, S.E., Univ. Illinois Chicago, Chemistry Dept.
Marto, J.A., NHMFL/Ohio State Univ., Chemistry Dept.
White, F.M., NHMFL/FSU, Chemistry Dept.
Seldomridge, S., FSU, Chemistry Dept.
Pasa-Tolic, L., NHMFL
Huang, Y., NHMFL
Kim, H.S., NHMFL/Ohio State Univ., Chemistry Dept.

In 1995, we showed that FT-ICR mass spectrometry at 3 tesla could identify more than a thousand chemically distinct compounds of molecular weight 100-600 u, without prior chromatographic separation, in a complex mixture of aromatics in a crude oil distillate.[1] Even better results should be possible at higher magnetic field.

We also showed that "tandem" mass spectrometry (or "MS/MS") makes it possible to analyze mixtures of phospholipids (the constituents of biological cell membranes), to identify their distinguishing features: polar head group (e.g., choline, serine, inositol) from positive-ion mass spectra, and fatty acid side chains (and which is which) from negative-ion mass spectra.[2]

Unlike all other mass analyzers, in which detection is inherently destructive, FT-ICR allows for repeated remeasurement of the same ions for increased signal-to-noise ratio, much like signal-averaging in FT-NMR spectroscopy. We have been able to reduce FT-ICR detection limit to 8 *attomoles* of a peptide (see Figure 1) and 40 *attomoles* of a phospholipid.[3] Those levels represent the total amount of sample introduced into the instrument, and approach the amounts of such compounds found in a single living cell.

Detailed analysis of complex mixtures requires high resolution as well as high sensitivity. Figure 2 shows the highest mass resolution yet reported for a peptide.[4] Such high resolving power is made

possible by our ability to detect a time-domain signal persisting for more than a minute (Figure 2, top).

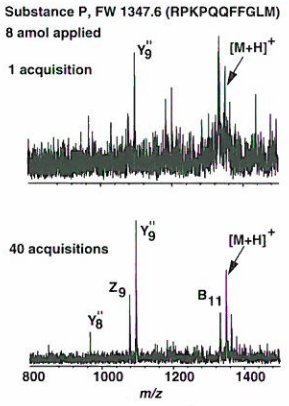

Figure 1. Reduction in FT-ICR detection limit to attomole level, by remeasurement of quasimolecular ions from a small peptide.

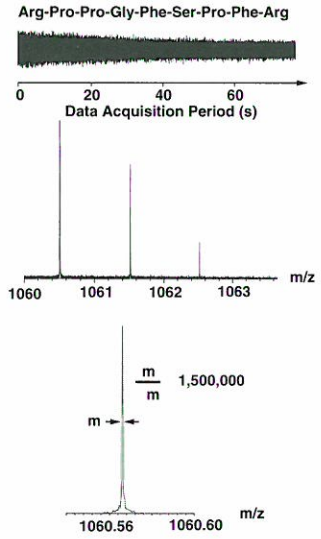

Figure 2. Ultrahigh-resolution FT-ICR mass spectrum of bradykinin quasi-molecular ions, $(M+H)^+$, produced by matrix-assisted laser desorption/ ionization.

References:

1 Guan, S., et al., Anal. Chem. 67, 0000-0000 (1995).

2 Marto, J.A., et al., Anal. Chem. 67, 3979-3984 (1995).

3 Solouki, T., et al., Anal. Chem. 67, 4139-4144 (1995).

4 Pasa-Tolic, L., et al., J. Mass Spectrom. 30, 825-833 (1995).

Separate Measurement of In-Phase and Antiphase Contributions to Transverse Relaxation in NMR

Meersmann, T., NHMFL

Bodenhausen, G., NHMFL/FSU, Chemistry Dept.

Although transverse relaxation under conditions of free precession or in the presence of a spin-locking radio-frequency field plays an essential factor in many modern NMR methods involving coherence transfer, empirical knowledge of relaxation rates is very scarce. This work focused on the interplay of J-couplings and transverse relaxation in proton spin systems. Similar effects are to be expected in ^{31}P NMR, ^{19}F NMR and ^{13}C NMR of enriched samples. We have taken the first experimental ^{1}H NMR measurements that allow one to compare the T_2 rates with the decay rates $T_{1\rho}$ of anti- and in-phase coherences.

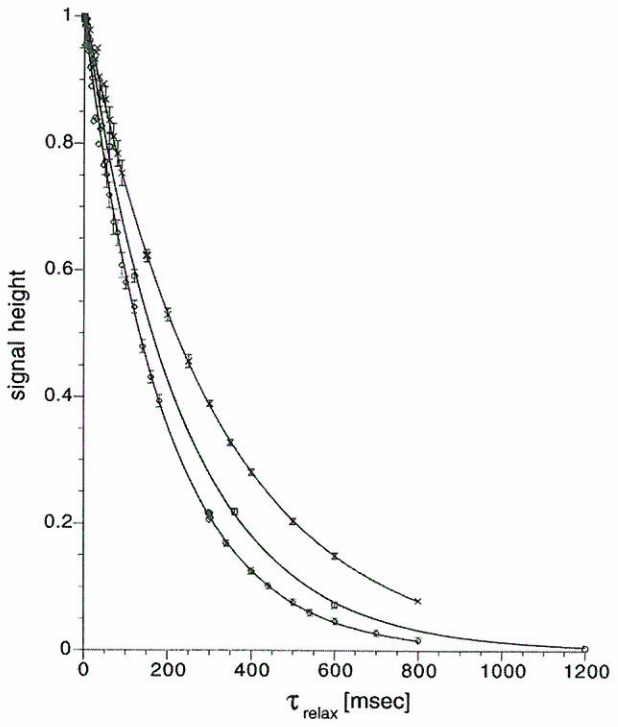

Figure 1. Decay of the different components of proton transverse magnetization in cyclosporin A. In-phase coherence shows the slowest decay rate (upper curve) and antiphase coherence (lower curve) the fastest. Under free precession the magnetization relaxes at an average rate (middle curve).

The rates that have been measured for protons of the cyclic undecapeptide Cyclosporin A or of a self-complementary duplex B-DNA dodecamer are consistent with the predicted behavior, and show that

$$\frac{1}{T_2} = \frac{1}{2}\left\{\frac{1}{T_{1\rho}^{in-phase}} + \frac{1}{T_{1\rho}^{antiphase}}\right\}.$$

Relaxation measurements on some protons in Taxol, however, demonstrate a dramatic deviation from this equation while measurements on other protons of the same molecule are in agreement. The unexpected deviations from the predicted rates are (at least in part) due to effects originating from long-range scalar couplings. These "remote" couplings are not visible in the spectrum since the natural linewidth exceeds the corresponding coupling constants.

Determination of Scalar Coupling Constants in Taxol Using Selective Two-Dimensional NMR Spectroscopy in Combination with Convolution Algorithms

Peng, C., NHMFL
Jeannerat, D., NHMFL
Bodenhausen, G., NHMFL/FSU, Chemistry Dept.

Proton-proton scalar coupling constants give important information on the connectivity and the conformation of organic molecules. The determination of coupling constants is the subject of numerous methods, none of which appear to be universally applicable. We have developed a method for the accurate determination of proton-proton scalar coupling constants using a pair of selective two-dimensional experiments containing complementary information. The two spectra are convoluted with suitable arrays of delta functions. A measure of similarity between the two convoluted spectra is then obtained to extract the coupling information.

Calculation of Molecular Properties in High Magnetic Fields

Runge, K., UF, Physics Dept.
Sabin, J.R., UF, Physics Dept.

During the past year, we have initiated development of a program for the calculation of electronic and geometric properties of molecules in high (>100 tesla (T)) magnetic fields.

Preliminary consideration and computation indicate that molecules in high magnetic fields (ca. 100 T) experience changes in their electronic structure with concomitant changes in their geometries. In most of the few cases studied, molecular bond lengths decrease and electronic binding energies increase.[1] Similarly, minima in molecular potential surfaces deepen, and in fact, new vibrational degrees of freedom may appear. These changes are expected to lead to chemical effects such as field dependent reaction rates, catalysis, production and stability of new molecules, improved reaction branching ratios, and modified nonlinear optical properties. Many of these effects are amenable to experimental verification with minimal difficulty.

Since, however, high magnetic fields, either continuous or pulsed, have not been routinely available up to this time, little has been done in this field to date. Although there has been some work in Europe, primarily by the group headed by Professor Cederbaum at Heidelberg, little has been done in this country. This program is being designed to explore the possibilities.

Presently, the design and coding of a molecular properties program is underway. This program includes the external field as a parameter, and the program is designed to work in the low field region—that is, for field strengths up to those where the magnetic and coulomb binding energies are of equal magnitude (ca. 100 kT). Even at these field strengths, consideration must be given to basis set choice, gauge problems, the Born-Oppenheimer separation, and many other of the commonly used quantum chemical concepts.

We anticipate the availability of semi-continuous magnetic fields of the order of 100 tesla, which we expect to be available at the NHMFL in the near future, will be sufficient to produce the effects mentioned above. This work, which we believe is the first work on the effects of high fields on chemical structure and reactivity, will serve to stimulate cooperative experimental efforts at the NHMFL. Discussions with experimentalists indicate that many of the planned investigations are amenable to experimental exploration. In particular, questions of molecular electron density changes brought about by large fields will be reflected in the molecular electronic excitation spectra that can be probed optically. Discussions with Dr. Neil Sullivan (UF) indicate that he would be interested in designing optical experiments to be carried out at NHMFL in order to confirm theoretical prediction of effects of magnitude large enough to be scientifically (or technologically) interesting.

Reference:

1 Schmelcher, P., et al., in Conceptual Trends in Quantum Chemistry, Vol. 2, Kluwer, 1994.

Invoking Polymer Order: High Magnetic Field Orientation of Liquid Crystalline Thermosets

Smith, M.E., LANL
Armijo, E.V., LANL
Benicewicz, B.C., LANL
Douglas, E.P., LANL
Lacerda, A., NHMFL/LANL–FSU
Earls, J.D., Dow Chemical
Priester, R.D., Jr., Dow Chemical

Liquid crystalline thermosets (LCT's) provide a unique opportunity to produce anisotropic solids of varying degree. Our laboratory has been involved in the synthesis and characterization of LCT's and their specific properties. Once ordered into the liquid crystalline phase, the crosslinking reaction rate for these monomers is enhanced as compared to the isotropic state.[1] The cured samples possess a glass transition temperature significantly higher than the reaction temperature as a result of the liquid crystalline network structure.[2] The ability to align these systems molecularly using magnetic fields has been demonstrated on small scale samples.[3,4] The principle material used in our experiments is the diglycidyl ether of dihydroxy-α-methylstilbene (DGE-DHAMS) cured with sulfanilamide (SAA). This isotropic monomer mixture forms a smectic phase as the molecules build into rod-like structures during the curing reaction.

Feasibility experiments were conducted on the 20 T superconducting magnet at NHMFL–LANL. Several difficulties were overcome by the judicious design of an instrument probe and sample mold system. The probe was designed with the following characteristics: sample chamber (~22mm diameter) to accommodate central support rod, wiring, and sample mold; a surrounding vacuum chamber; a surrounding liquid nitrogen chamber; and finally an outer vacuum chamber. During operation, a temperature gradient of 315°/cm with an internal thermal mass of 34g exists. Bar shaped samples of ~3.5g were produced at field strengths up to 18 T and magnetic field exposure times as long as 9 hours. The second phase of this experimental work was the production of larger samples for mechanical

testing and analysis. By using a 20 T, room temperature bore magnet at NHMFL–FSU, samples of sizes 10 to 30g were obtained under various field strengths. This larger sample size enabled more stringent characterization of the orientation effects.

Results of mechanical, thermal, and morphological analyses are presented for samples cured under field for 1 hour, standard deviations are shown in parentheses:

	0 T Field	**18 T Field**
Tensile Modulus [ksi]	443 (54)	1174 (166)
Transverse Modulus [ksi]	454	475
Strain @ Break [%]	8.9 (0.42)	1.0 (0.03)
Stress @ Break [psi]	13,010 (1001)	9985 (500)
Coefficient of Thermal Expansion parallel to field [μm/m/°C]	54	4.3
Coefficient of Thermal Expansion perpendicular to field [μm/m/°C]	55	111
Order Parameter (x-ray diffraction)	0	0.90

For the first time, magnetic field oriented polymers of sufficient size to undergo tensile testing have been produced and analyzed. There is a near three-fold increase in tensile modulus without sacrifice of the transverse value.

References:

1 Douglas, E.P., et al., Chem. Mat., 6, 1925 (1994).

2 Langlois, D.A., et al., Polym. Mater. Sci. Eng., 74 (1996).

3 Barclay, G.G., et al., J. Polym. Sci., Part A, 30, 1845 (1992).

4 Barclay, G.G., et al., Macromol., 25, 2947 (1992).

Alignment of Xanthan Liquid Crystals in Magnetic Fields and Relaxation at Zero Field

Van Winkle, D.H., FSU, Physics Dept. and Martech

Szabo, T., FSU, Physics Dept. and Martech

Rill, R.L., FSU Chemistry Dept. and Martech

Liu, Y.-J., FSU Chemistry Dept. and Martech

Dharia, J., FSU Chemistry Dept. and Martech

Locke, B.R., FAMU–FSU CoE, Chemical Engr. and Martech

The research project focused on determining whether xanthan fragments in aqueous solution exhibit a significant diamagnetic anisotropy. Xanthan is a hydrophillic polymer often used as a thickening agent in foods. We reduced the average molecular weight by sonication and formed liquid crystal phases of the aqueous solution by increasing the polymer concentration. Liquid crystalline materials that exhibit a diamagnetic anisotropy will reorient in sufficiently high magnetic fields. It was not known whether Xanthan has a diamagnetic anisotropy, and if so what critical magnetic field is required to reorient the liquid crystal.

A preliminary experiment was performed during 1994, which involved hanging a meter stick holding a microscope slide with liquid crystalline Xanthan in the field, removing the sample from the field and investigating it by optical microscopy to determine whether any persistent reorientation occurred. There was no evidence of a reorientation.

A probe was designed and built to hold a room temperature Xanthan liquid crystalline sample between two polarizers in the magnetic field. This probe was used and a run at the NHMFL was performed on 1/19/95. The results were inconclusive and it was determined that modifications of the probe design were needed in order to make quantitative measurements of the birefringence change as a function of field. This means that a Cotton-Mouton experimental setup needs to be designed and built in order to continue the magnetic aspects of our research.

The research was supported by Martech and NSF #BCS-9311901.

Measurement of Cross-Relaxation between Amide Protons in ^{15}N-Enriched Proteins with Suppression of Spin Diffusion

Vincent, S.J.F., NHMFL
Zwahlen, C., NHMFL
Bolton, P.H., Wesleyan Univ., Chemistry Dept.
Logan, T.M., FSU, Structural Biology Dept.
Bodenhausen, G., NHMFL/FSU, Chemistry Dept.

This variant of two-dimensional nuclear Overhauser effect spectroscopy (NOESY) allows one to observe cross-relaxation pathways between protons that have heteronuclear scalar couplings to nitrogen-15 or carbon-13 nuclei. In ^{15}N-enriched proteins, it is possible to focus attention on Overhauser effects between amide protons that are due to a direct one-step transfer of longitudinal magnetization, while eliminating two-step spin-diffusion pathways. This can be achieved by inverting the longitudinal magnetization of all amide protons that are scalar-coupled to ^{15}N in the middle of the relaxation time τ_m. Such an inversion can obtained by inserting a "*bi*linear *r*otation *d*ecoupling" (BIRD) pulse sandwich in τ_m (Figure 1).

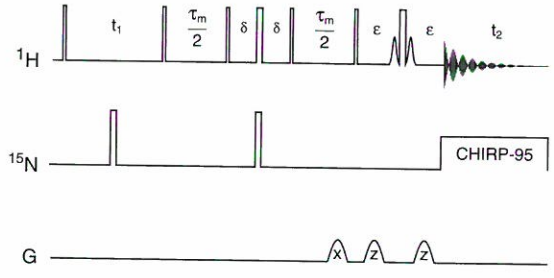

Figure 1. Pulse sequence for QUIET-BIRD-NOESY.

Application to ^{15}N-labeled FKBP (Figure 2) shows a dramatic effect of this procedure on the number and intensities NOESY peaks.

Four peaks are emphasized for the sake of illustration (Figure 2): (1) H^N(R13) ~~~> H^N(T14) is due to a one-step Overhauser effect between two amide protons located 0.206 nm apart; (2) H^N(F36) ~~~>H^δ(F36) is eliminated in the QUIET-BIRD-NOESY spectrum although their distance is 0.177 nm; (3) H^δ(Y82) ~~~> H^ε(Y82) nOe survives unperturbed (the distance is of 0.244 nm); and (4) H^N(K73) ~~~> H^N(L74) is strongly attenuated in QUIET-BIRD-NOESY (the direct effect survives but is rather small, since the internuclear distance is 0.394 nm).

If one records build-up curves due to one-step processes between amide protons of consecutive amino acids in a protein, this would allow accurate estimates of the structurally important distances between amide protons to be obtained.

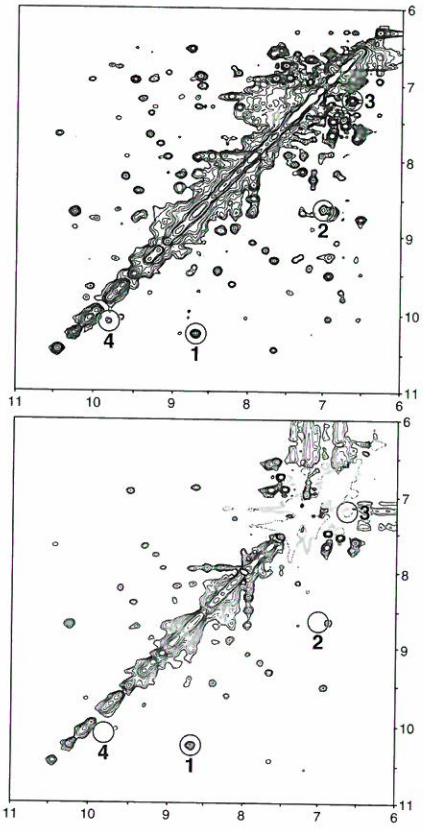

Figure 2. (Bottom) Quiet window (amide region) enlarged from the QUIET-BIRD-NOESY spectrum. Both spectra show four numbered circles highlighting chosen cross-peaks. (Top) Enlarged plot of the corresponding window extracted from a conventional NOESY spectrum recorded under identical conditions.

Structural Information Obtained by Quenching of Spin Diffusion in Nuclear Overhauser Spectroscopy

Zwahlen, C., NHMFL
Vincent, S.J.F., NHMFL
Bodenhausen, G., NHMFL/FSU, Chemistry Dept.

The primary source of structural information in biomolecules in solution is the nuclear Overhauser effect. For isolated two-spin systems, cross-peak intensities in two-dimensional *n*uclear *O*verhauser *e*ffect *s*pectroscop*y* (NOESY) can be directly related to proton-proton distances. However, NOESY spectra can be misleading if spin-diffusion effects are not properly taken into account. Spin diffusion can often be recognized by recording cross-peak amplitudes as a function of the mixing time τ_m. However, the accuracy of the determination of internuclear distances can be greatly improved if spin diffusion is suppressed, since in this case cross-peak intensities reflect a single internuclear distance. This can be achieved by using a method dubbed QUIET-BAND-NOESY.

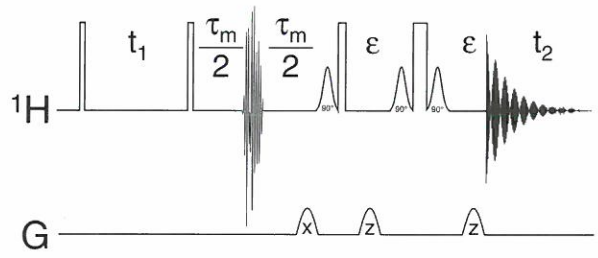

Figure 1. Pulse sequence for two-dimensional QUIET-BAND-NOESY with the water-flip-back implementation of WATERGATE.

In QUIET-BAND-NOESY, selected regions are transformed into direct nuclear Overhauser effects that can be easily analyzed as the cross-peaks reflect real two-spin systems.

Two-dimensional QUIET-BAND-NOESY experiments are straightforward to implement and their analysis does not require any novel tools.

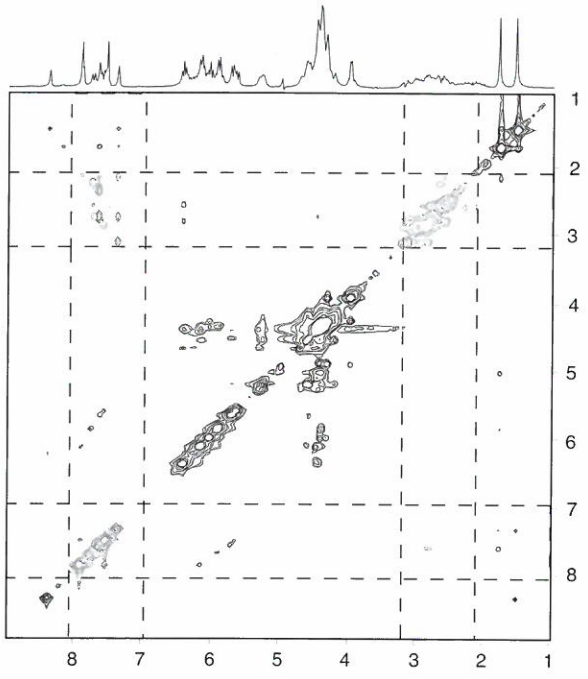

Figure 2. QUIET-BAND-NOESY of Dickerson's dodecamer B-DNA d(CGCGAATTCGCG)$_2$ with a mixing time τ_m = 200 ms, doubly-selective Q^3 of 12 ms duration applied at $\tau_m/2$ to invert two frequency bands, each of 1 ppm width, centered at 7.50 ppm and 2.70 ppm respectively.

Effects of Pr, Tb and Zn Doping in $YBa_2Cu_3O_7$ on Magneto-Resistivity and Magnetic Phase Boundaries

Crow, J.E., NHMFL
Cao, G., NHMFL
Freibert, F., FSU, Physics Dept.
McCall, S., FSU, Physics Dept.
Shepard, M., FSU, Physics Dept.

Transverse AB-plane magneto-resistivity ρ_{AB} (C-axis||H) of $(Y_{1-X}Pr_X)Ba_2Cu_3O_{7-\delta}$ and $YBa_2(Cu_{1-X}Zn_X)_3O_{7-\delta}$ thin films and $(Y_{1-X}Tb_X)Ba_2Cu_3O_{7-\delta}$ thin films and single crystals has been measured as a function of $0.0 \leq X < X_c$, $2K < T < 300K$ and $0T \leq H < 20T$. Mean-field upper critical field H_{C2} and vortex-glass transition field H_G phase boundaries have been determined and are discussed in terms of proposed theories. Tb doping of $YBa_2Cu_3O_7$ reflects an enhanced pinning or "stiffening" of the vortex system without apparent alteration to T_c or the slope of the mean-field normal phase-mixed phase boundary line, $dH_{C2}/dT|_{T=Tc}$. However, Pr and Zn doping of $YBa_2Cu_3O_7$ tends to depress both T_c and $dH_{C2}/dT|_{T=Tc}$ and shows a "softening" of the vortex system. This behavior may be understood in terms of the magnitude of the superconducting pair coherence length, which is controlled by doping, and the divergence of the vortex-glass correlation length as it relates to flux line coupling of vortices in the CuO_2 planes. These systems are compared with other high T_c superconducting systems that possess similar phase boundary properties.

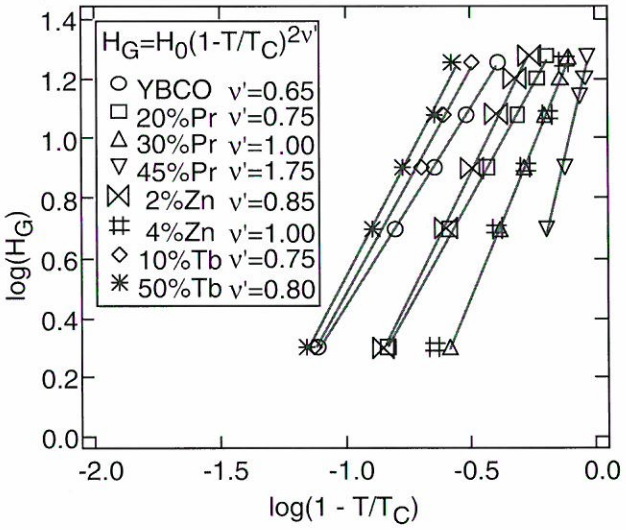

Figure 1. Log-log plot of vortex glass phase boundary H_G (symbols) vs. reduced temperature (1- T/T_c) exhibiting fits to power-law behavior (lines).

Thermal Conductivity in Magnetic Fields of Doped High Temperature Superconductors

Crow, J.E., NHMFL
Cao, G., NHMFL
Henning, P., FSU, Physics Dept.
Hirschfeld, P., UF, Physics Dept.
Putikka, W., NHMFL

The thermal conductivity of high temperatures is an ideal probe of the scattering mechanisms of the charge carriers and the phonons because it remains a non-zero probe into the superconducting state. In these materials, the thermal conductivity has unusual behavior: a sharp upturn at T_c and a peak near $T_c/2$. This peak has been attributed to both the phonons and the charge carriers. The phonon scenario uses the fact that as the carriers condense and thus no longer scatter phonons, the phonon mean free path and thus thermal conductivity should rise at T_c and peak when the declining phonon population overtakes the longer

mean free path. The carrier scenario is based on measurements of the normal fluid conductivity via microwaves in YBCO. The observation is that the carriers' scattering rate is reduced immediately at T_c presumably from their very condensation and causes a peak in the normal fluid conductivity at the same position that the peak in thermal conductivity is seen. Further, extending the Wiedmann-Franz law into the superconducting state and the substitution of the measured normal fluid conductivity shows close agreement with the measured thermal conductivity data on YBCO. Our measurements of the thermal conductivity focus on the selective doping of YBCO single crystals. The doping serves to change T_c in a controlled way. Comparisons of these measurements with the phonon theory of thermal conductivity in superconductors allow us to separate out the phonon and carrier contributions. Magnetic field measurements of the thermal conductivity further serve to separate the behavior of the phonons and the behavior of the charge carriers, as both have radically different responses to the application of magnetic field. Figure 1 shows the behavior in magnetic field of one such compound, a $Y_{0.85}Pr_{0.15}Ba_2Cu_3O_{7-\delta}$ single crystal with heat flow along the a-b plane. T_c = 78 K in this compound. In contrast to YBCO, there is no sharp break at T_c, although a peak in the value below T_c remains. Additional measurements of both the doping and field dependence of K(T) will be pursued.

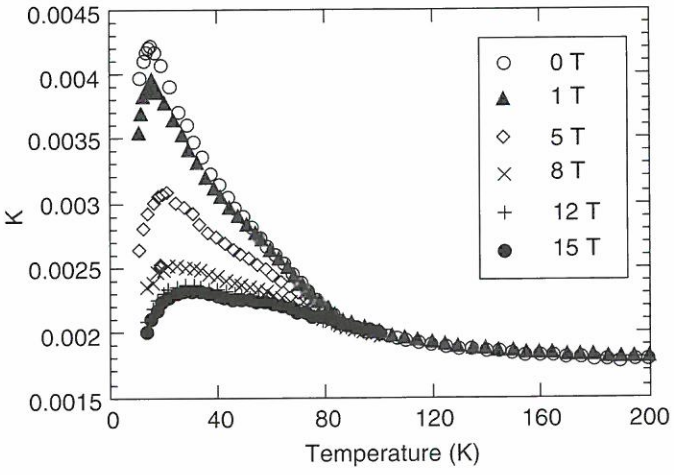

Figure 1. Thermal conductivity vs. temperature and magnetic field for $Y_{1-x}Pr_xBa_2Cu_3O_{7-\delta}$ with x = 0.15 (T_c = 78 K).

Effect of Li-Doping in La_2Cu0_4

Fisk, Z., NHMFL/FSU, Physics Dept.
Sarrao, J., NHMFL
Cassady, L.S., NHMFL/FSU, Physics Dept.
Hammel, P.C., LANL
Yoshinari, Y., LANL
Thompson, J.D., LANL

La_2CuO_4, the prototypic single layer cuprate, can be hole-doped in two ways chemically: out-of-plane Sr-doping and in-plane Li-doping. In both cases, one hole is added to the CuO_2-planes per dopant atom. In the Li case, the doped material never becomes metallic or superconducting. It is therefore remarkable that the Li-doping in other respects is identical to Sr-doping. Namely, in-plane lattice parameter versus x is identical, the orthorhombic-tetragonal transition temperature as a function of x is identical, and the magnetic phase diagram as a function of x is the same. There is also the observation that in both cases the initial doping leads to substantial reduction in the room temperature resistivity. The surprise in all this is that the lack of metallic behavior and eventually superconductivity in the Li-doped materials suggests that the holes added are bound.

In addition to the experiments demonstrating the points above, we have worked on $La_2Cu_{0.5}Li_{0.5}O_4$, which is atomically ordered: each Cu connects in-plane through an O to a Li, and vice versa. This compound, with formally d^8 Cu is a diamagnetic insulator. Cu NMR experiments by Hammel find a remarkable result: $1/T_1$ is activated with characteristic temperature 1800 K. Moreover, the decay mechanism is magnetic, as shown by the ratio of the T_1's for the Cu 63 and 65 nuclei.

There appears to be a magnetic singlet here, with characteristic energy 1800 K, involving the Cu spins and the one hole per Cu that is presumably in the O-ligands. This appears to be a new and unexpected result in the physics of the doped CuO_2-planes.

Spectrum of Lightly Doped Cuprates

Gor'kov, L.P., NHMFL
Kumar, P., UF, Physics Dept.

We have considered in some more details the three-band model for the electronic spectrum of CuO_2-planes in cuprates to account for the electron-hole asymmetry of the doping process. The basic ingredient of this model is the charge-transfer (CT) gap seen optically in the insulating state of all cuprates. Here are listed several our results.

Virtual transitions of electrons between oxygen and copper sites results in additional destruction of the antiferromagnetic long range order-the mechanism alternative to the thermal and quantum fluctuations in the Heisenberg model.

An effective Hamiltonian can be derived for the hole bands. However, there is the Kondo-like term in the Hamiltonian leading to the strong interactions of holes with local (copper) spins. The interaction would always result in formation of spin clusters of atomic size dressing up an added hole. (Antiferromagnetic order plays a secondary role in this phenomenon). The difference with the so-called "Zhang-Rice singlet" is that the spin cluster has an internal structure and possesses excited levels.

A new optical process of the second order in the perturbation theory may, therefore, become possible: its matrix element can be constructed from the electric dipole matrix element for virtual transition of an electron between oxygen and copper sites, and the hybridizing matrix element that annihilates, after that, the electron-hole pair. Therefore, the coupling of carriers to local spins could result in a transition where the initial and final spin configurations differ. To consider these ideas, as a possible explanation for the weak absorption structure in the 0.2 - 0.6 eV range (Falk et al.), extended numerical calculations are necessary. That has not been done yet.

The manuscript of the paper, describing the qualitative part of these results, is in preparation.

Liaison Between Superconductivity and Phase Separation

Haas, S., FSU Physics Dept./NHMFL/SCRI
Nazarenko, A., FSU Physics Dept./NHMFL
Dagotto, E., FSU Physics Dept./NHMFL
Riera, J., Univ. of Rosario, Physics Dept., Argentina

Models of strongly correlated electrons that tend to phase separate are studied including a long-range 1/r repulsive interaction. It is observed that charge-density-wave states become stable as the strength of the 1/r term, V_{coul}, is increased. Due to this effect, the domain of stability of the superconducting phases that appear near phase separation at $V_{coul} = 0$ is not enlarged by a 1/r interaction as naively expected. Nevertheless, superconductivity exists in a finite region of parameter space, even if phase separation is suppressed. Our results have implications for some theories of the cuprates.

Evidence for an Unusual Electron Transmission Rate from the Measurement of the Intrinsic Josephson Coupling Energy between Cu-O Bilayers in a High-T_c Superconductor at High Magnetic Fields

Hettinger, J.D.*, MSD/ANL
Gray, K.E., MSD/ANL
Washburn, B.W., MSD/ANL
Veal, B.W., MSD/ANL
Paulikas, A.P., MSD/ANL
Kostic, P., MSD/ANL

Previous work[1] suggested that the Josephson coupling between adjacent layers in oxygen deficient $YBa_2Cu_3O_{7-\delta}$ was larger than predicted by conventional models based on the normal state c-axis resistivity (ρ_c), implying an unusual electron transmission along the c-axis Josephson junctions (JJ). The ρ_c is found to be qualitatively similar to conventional tunnel junctions where reducing temperature (T) from room-T causes the junction resistivity to increase due to a reduction of thermal activation over the tunnel barrier.

Based on conventional ideas about tunnel junctions and JJ, two predictions of physical properties at high magnetic fields can be investigated. As thermal activation of charge carriers over the tunnel barrier decreases in a tunnel junction, the resistivity increases. Eventually a constant resistivity should be realized which is related to the temperature independent tunneling probability. Due to the presence of the superconductivity, this tunneling conductivity is "shorted-out" by the Josephson supercurrent and never measured. By applying a large field the superconductivity may be destroyed making possible a measure of ρ_c to low-T where the tunneling conductivity can be observed. Also, by extracted Josephson coupling energies, a parameter corresponding to the resistivity for pair transmission (ρ_c^*) may be determined. The ρ_c^* has been shown to decrease at T below T_c in contrast to conventional JJ and has no apparent relation to ρ_c. However, it is not expected that this T-dependent ρ_c^* can continue to low T. High fields allow a probe of the magnetoresistance and ρ_c^* to low-T.

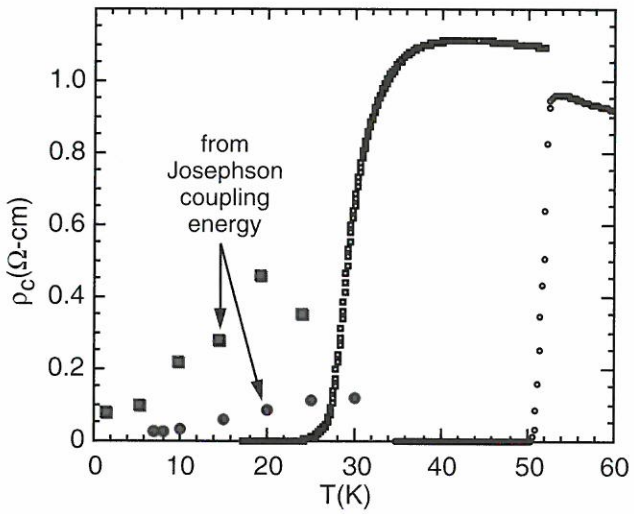

Figure 1. Evidence for an unusual electron transmission rate from the measurement of the intrinsic Josephson coupling energy between Cu-O Bilayers in a high-T_c superconductor at high-magnetic fields.

We have measured ρ_c of oxygen deficient $YBa_2Cu_3O_{7-\delta}$ in magnetic fields up to 27 T and from T_c down to 4 K. Three samples with T_c ranging from 70 K to 20 K which have different anisotropies were measured. The ρ_c for each sample is similar and can be qualitatively understood as a conventional superconducting tunnel junction. We did not observe the anticipated crossover to a constant resistivity which is characteristic of conventional tunnel junctions. As the magnetic field was increased so that measurements could be made to much lower T, a constant ρ_c was not observed. Instead the ρ_c continued to increase implying that tunneling through the barrier is small.

When we extracted the Josephson coupling energy and then recast that coupling energy into an equivalent ρ_c^*, we found that as T-decreased, ρ_c^* continued to decrease suggesting that conduction along the c-axis became more coherent as T was reduced. While this was expected to occur to some T from extrapolation of the low-field results, we observed the T dependence to the lowest temperatures measured (demonstrated in the figure).

Reference:

1 Hettinger, J.D., et al., Phys. Rev. Lett., 74, 4726 (1995).

* Present address: Rowan College of NJ, Dept. of Chemistry and Physics.

Gd^{3+} EPR Determination of the Local Spin Susceptibility in Gd: YBCO

Janossy, A., Univ. of Budapest, Physics Dept.
Brunel, L.C., NHMFL
Cooper, J.R., Univ. of Cambridge, Physics Dept.

We have shown that Gd^{3+} EPR at high fields in Gd doped high T_c superconductors is a precise probe of the conduction electron static spin susceptibility χ. The Gd^{3+} EPR Knight shift at 245 GHz and the spin relaxation broadening at 245 GHz (8.75 tesla) and 9.2 GHz in $Gd_{0.01}\ Y_{0.99}\ Ba_2Cu_3\ O_y$ (with various value of y between 6.05 and 7.0) are in agreement with published ^{89}Y NMR data above 70 K taken at the same magnetic field. These EPR data are the first measurements at the rare earth site at low temperatures. In the superconducting compounds $\chi(T)$ differs strongly from the Yoshida function and at low temperature it follows a T or T^2 dependence. An anomalous EPR lineshape is

observed at low T in the superconducting state; we tentatively attribute this to a small (10^{-2} - 10^{-3} μ_B) static magnetic moment on planar Cu sites.

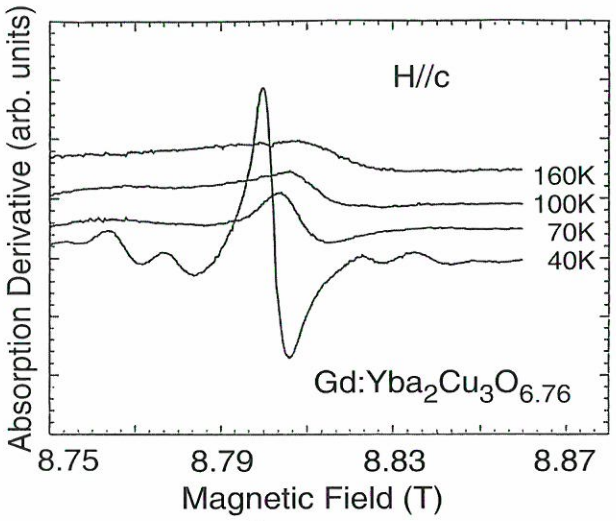

Figure 1. Typical Gd^{3+} EPR spectra at 245 GHz for y= 6.76. Note the shift and broadening with T. At 40 K the "wiggles" apart the central transition are -3/2 —> - 1/2 and 1/2 —> 3/2 transitions.

High Field IV Measurements on Bulk YBCO Samples

Joshi, R.J., Univ. of Mass., Physics Dept.
Hallock, R.B., Univ. of Mass., Physics Dept.

We study the magnetic field and morphology dependent characteristics of the superconducting transition in polycrystalline YBCO. An experimental analysis of the I-V characteristics in the vicinity of the transition into the vortex glass phase can be used to extract the scaling exponents n and z. Our I-V measurements are done at small current densities 10^{-3} < I < 10 A/cm^2 with an electric field sensitivity of 2 nV/cm and a maximum of six decades in voltage. Previous studies on sintered YBCO involved either high or low magnetic fields with differences in the dynamic exponent z extracted from each regime.[1-3] We have recently performed extensive sets of I-V runs on selected samples of YBCO in magnetic fields accessible to us in our laboratory where 0.05 mT < H < 500 mT. Our low to intermediate field I-V measurements are consistent with predictions of I-V scaling with n ~ 1.1-1.5 and z showing some morphology and field dependence. For the small grain size samples z ~ 3.5 - 4.5, which is somewhat consistent with earlier high field data (where z > 4) and consistent with the predictions of the glassy models. For an intermediate grain size sample z shows some evolution from 3 to 4 in the intermediate field range, 0.1 T < H < 0.5 T. For the small grain size samples, z ~ 3 consistent with the data of Tiernan and Hallock[1] but lower than the values predicted by the glassy models, where z > 4. The work at the NHMFL involved I-V measurements at much higher fields on the same samples in order to explore the role of the higher magnetic fields on the exponents. Taken together the high and low field data should provide us with a comprehensive picture of the superconducting transition in granular YBCO over its entire range of experimental accessibility.

At the NHMFL, I-V and resistivity data were taken on four YBCO samples in selected high magnetic fields, 1 T < H < 14 T. Judging from their resistive transitions, two samples had large grains, one sample had intermediate size grains and one sample had small grains (subject to confirmation from a grain size analysis). For each of the samples we performed extensive sets of I-V isotherm measurements in two selected high magnetic fields. All our data showed qualitative features predicted by the Fisher, Fisher and Huse scaling hypothesis.[4] Moreover, the static exponents extracted from the data were consistent with predictions of the glassy models. However the values for the dynamic exponent, z ~ 3 are lower than what is predicted by the glassy models. Moreover for the small and intermediate grain size samples the high field z ~ 3 is lower than the value measured in intermediate fields where z ~ 4.

References:

1 Tiernan, W.M., et al., Phys. Rev. B, 48, 3423 (1993).

2 Worthington, T.K., et al., Phys. Rev. B, 43, 10538 (1993).

3 Koch, R.H., et al., Phys. Rev. Lett., 63, 1511 (1989).

4 Fisher, D.S., et al., Phys. Rev. B, 43, 130 (1991).

^{7}Li NMR in the NHMFL Resistive Magnets and ^{139}La NQR in $La_2Cu_{1-x}Li_xO_4$

Kleinhammes, A., NHMFL
Kuhns, P.L., NHMFL
Moulton, W.G., NHMFL/FSU Physics Dept.
Sarrao, J., NHMFL
Fisk, Z., NHMFL
Sullivan, N.S., NHMFL/UF Physics Dept.

The underlying physics of highly correlated electron systems is still not well understood after two decades of experimental and theoretical effort. Microscopic probes, such as NMR, that can probe the correlations and their symmetries through site specific measurement of the relaxation times, Knight shifts, quadrupole coupling, and static internal fields in the ordered state are needed to distinguish between theoretical models and make further progress. In Li doped La_2CuO_4 the Li substitutes in the Cu site and introduces holes, which unlike the Sr doping, are localized. The effect of Li doping on the AF transition, however, is much like that of Sr in that the transition is rapidly depressed at low doping concentrations and disappears at 3-4% Li. The spin-lattice relaxation times of the ^{7}Li NMR and ^{139}La NQR have been measured in $La_2Cu_{1-x}Li_xO_{4+\delta}$ for x=0, 0.01, and 0.10. Measurements have been made in both oxygen rich, as-grown, crystals and deoxygenated crystals. The measurements have been made at fields of 16 T and 26 T, and between room temperature and 77 K.

Even though the data are far from complete, several unusual and interesting features stand out. The ^{7}Li T_1 data for x=0.10 show two relaxation times, indicating the presence of Li sites with different local fields and/or fluctuation spectra. The x=0.01 relaxation data show only a single exponential, indicating a single site. The T_1's for all data increase more rapidly with decreasing temperature than any Korringa–like mechanism would predict. The relaxation times all increase with increasing field. The NMR T_2 and T_1 also have been measured in an x=0.015 doped powder sample from 4.2 to 300 K at 16 T. The spectrum shows only a small increase in T_2 below the transition over that 300 K, considerably less than the nearest neighbor dipole contribution. T_2^* and T_2 as a function of temperature are shown in the figure. The values of T_1 also show no dramatic difference above and below the transition; however, the ^{139}La NQR data show the expected splitting due to an internal field below the ordering temperature. This is consistent with the possibility that the exchange of the nearest neighbor Cu spins is modified to the extent that they do not participate in the AF order. In addition to this work, Kuhns, Kleinhammes, and Moulton have collaborated with a number of users on NMR at high fields in the resistive magnets. These include A.P. Reyes and Bill Halperin, Northwestern University, ^{17}O NMR in superconducting cuprates, James Brooks, NHMFL, ^{77}Se NMR in 1D conducting organics, and C. R. Bowers, UF, on optical pumped NMR in GaAs and InP. This work is described in detail elsewhere in the report.

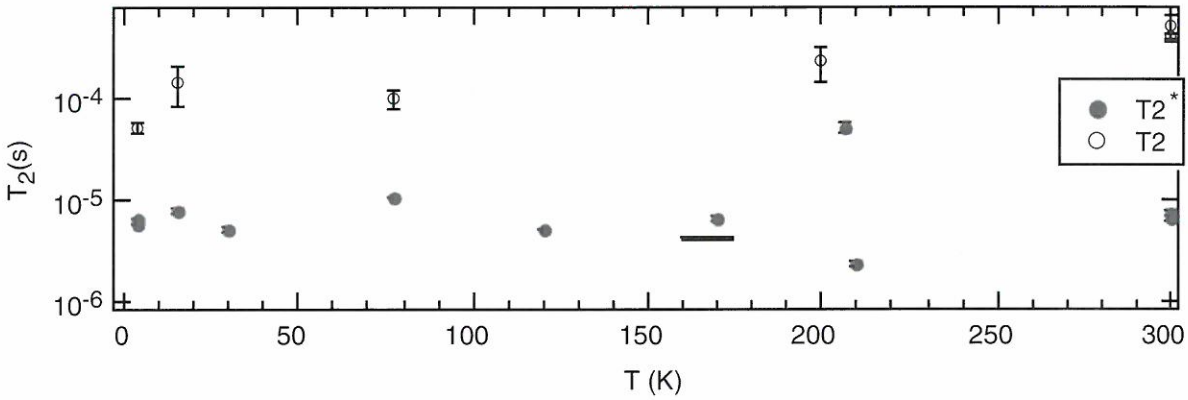

Figure 1. ^{7}Li NMR in the NHMFL resistive magnets and ^{139}La NQR in $La_2Cu_{1-x}Li_xO_4$.

A Model of Correlated Fermions with $d_{x^2-y^2}$ Superconductivity

Nazarenko, A., NHMFL
Moreo, A., FSU Physics Dept./NHMFL/ MARTECH
Riera, J., Inst. de Fisica de Rosario, Argentina
Dagotto, E., FSU Physics Dept./NHMFL/ MARTECH

Motivated by the phenomenology of the high-T_c cuprates, a two dimensional fermionic model with attractive interactions is here discussed. The exact solution to the two particle problem leads to a bound state in the $d_{x^2-y^2}$ subspace. Numerical techniques suggest that the model has $d_{x^2-y^2}$ superconductivity (SC) in the ground state at low fermionic density. Within a self-consistent RPA diagrammatic study, the density dependence of the critical temperature is calculated. We argue that in the context of d-wave SC this model fulfills the role that the attractive on-site Hubbard model has played for s-wave SC. We also show that another candidate, the attractive "t-U-V" model, which has d-wave SC at the mean-field level is actually not useful as a realization of this family of condensates for a variety of reasons.

Photoemission Spectra of $Sr_2CuO_2Cl_2$: A Theoretical Analysis

Nazarenko, A., FSU Physics Dept./NHMFL
Vos, K.J.E., Queen's University, Physics Dept. Kingston, Ontario, Canada
Haas, S., FSU Physics Dept./NHMFL/SCRI
Dagotto, E., FSU Physics Dept./NHMFL
Gooding, R.J., Queen's University, Physics Dept., Kingston, Ontario, Canada.

Recent angle resolved photoemission (ARPES) results for the insulating cuprate $Sr_2CuO_2Cl_2$ have provided the first experimental data that can be directly compared to the (theoretically) well-studied problem of a single hole propagating in an antiferromagnet. The ARPES results reported a small bandwidth, providing evidence for the existence of strong correlations in the cuprates. However, in the same experiment some discrepancies with the familiar 2D $t-J$ model were also observed. Here we discuss a comparison between the ARPES results and the quasiparticle dispersion of both (i) the $t-t'-J$ Hamiltonian and (ii) the three-band Hubbard model in the strong—coupling limit. Both model Hamiltonians show that the experimentally observed one-hole band structure can be approximately reproduced using reasonable values for t', or the direct oxygen hopping amplitude t_{pp}.

Magnetic Raman Scattering in Two-Dimensional Spin-1/2 Heisenberg Antiferromagnets: Spectral Shape Anomaly and Magnetostrictive Effects

Nori, F., Univ. of Michigan, Physics Dept.
Merlin, R., Univ. of Michigan, Physics Dept.
Haas, S., FSU Physics Dept./NHMFL/SCRI
Sandvik, A., NHMFL
Dagotto, E., FSU Physics Dept./NHMFL

We calculate the Raman spectrum of the two-dimensional (2D) spin-1/2 Heisenberg antiferromagnet by exact diagonalization and quantum Monte Carlo techniques on clusters of up to 144 sites. On a 16-site cluster, we consider the phonon-magnon interaction that leads to random fluctuations of the exchange integral. Results are in good agreement with Raman scattering experiments on various high-T_c precursors, such as La_2CuO_4 and $YBa_2Cu_3O_{6.2}$. In particular, our calculations reproduce the broad lineshape of the two-magnon peak, the asymmetry about its maximum, the existence of spectral weight at high energies, and the observation of nominally forbidden A_{1g} scattering.

ESR and Magnetic Susceptibility Studies in Eu_2CuO_4

Rettori, C., San Diego State Univ., Physics Dept.
Oseroff, S., San Diego State Univ., Physics Dept.
Rao, D., Universidade Estadual de Campinas, Physics Dept.
Valdivia, J.A., Universidade Estadual de Campinas, Physics Dept.
Barberis, G.E., Universidade Estadual de Campinas, Physics Dept.
Martins, G., NHMFL
Sarrao, J., NHMFL
Fisk, Z., NHMFL
Brunel, L.C., NHMFL
Tovar, M., Centro Atomico Bariloche

Being in the frontier between superconductivity (SC) and weak ferromagnetism (WF) in the rare-earth (RE) cuprates series (RE_2CuO_4, RE = Pr, Nd, Sm, Eu, Gd) makes Eu_2CuO_4 a quite interesting material. When grown in alumina crucibles and CuO flux (Al_2O/CuO) it can be made superconducting (by Ce or Th doping) and shows no WF.[1] On the other hand, Eu_2CuO_4 grown in Pt crucibles and PbO (Pt/PbO) flux shows WF when field cooled, and does not become superconducting.[2] The presence of WF is usually associated with canting of the copper moments in the ab-plane away from perfect AF alignment. In the T' structure WF order is forbidden, and lattice distortions in the CuO_2 planes need to be invoked to account for it. Thus, it is well established that for RE = Eu there is a subtle instability of the T'-type structure.

Previous ESR experiments on Gd^{3+} in Eu_2CuO_4 single crystals grown in Pt/PbO showed an internal magnetic field and crystal field distortions at the Gd^{3+} site[3], for $T< T_N$. However, the poor resolution of the ESR spectra led to an ambiguous assignment of the direction of the magnetic field at the RE site caused by the AF ordering of the Cu moments. So this prompted us to perform and analyze ESR of Gd^{3+} and Magnetic Susceptibility experiments in Eu_2CuO_4 single crystals grown in Al_2O/CuO, which is basically 'free' of local distortions and so of WF.

The ESR experiment reveals for $T<T_N$ the presence of an internal magnetic field of $H_i = \pm$ 310 Oe along [100] and [010] directions at the RE sites. We should emphasize that, within the sensitivity of our magnetization measurements, this internal field is observed in the absence of WF, and it has a similar value to that found in Eu_2CuO_4 grown in Pt/PbO that has a large WF component. We showed that the strength and directions of H_i can be calculated from a non-collinear AF array of Cu moments with 0.30(4) μ_B / Cu ion. This result is in good agreement with recent results obtained in magnetic-field-dependent neutron-diffraction experiments. It is important to mention, however, that while neutron-diffraction experiments show that the AF order in Pr_2CuO_4 is the same as that of Eu_2CuO_4 (non-collinear), *paradoxically* ESR experiments[4] did not find any evidence for the existence of an internal field in Pr_2CuO_4. Finally, we want to strongly emphasize that our ESR data[4] on Gd^{3+} in Pr_2CuO_4 are incompatible with both the collinear and non-collinear AF ordering.

References:

1 Alvarenga, A.D., et al., accepted in Phys. Rev. B.

2 Markert, J.T., et al., Physica C, 158, 178 (1989).

3 Rao, D., Phys. Rev. B, 38, 8920 (1988).

4 Martins, G.B., Phys. Rev. B, 51, 11909 (1995).

High Field ^{17}O NMR Studies in $YBa_2Cu_3O_7$

Reyes, A.P., Northwestern Univ., Physics Dept.
Halperin, W.P., Northwestern Univ., Physics Dept.
Moulton, W.G., NHMFL
Kuhns, P.L., NHMFL
Kleinhammes, A., NHMFL
Hammel, P.C., LANL
Martindale, J.A., LANL

Central to the current models extending BCS theory is the possibility of unconventional pairing mechanisms for superconductivity. Although

several experimental results favor symmetries whose electronic excitations exhibit d-wave pairing, other results such as NMR Knight shift do not preclude s-wave states. The Knight shift probes the carrier spin susceptibility whose temperature dependence depends on the symmetry of the energy gap function. Previous NMR results on Cu and O Knight shifts do not have enough accuracy to display the leading order temperature dependence, at low temperatures, which depends on the symmetry of the order parameter. The experimental difficulty has been in the determination of the local magnetic field in the sample which, due to effects of superconductivity remains largely unknown. At high magnetic fields these corrections are relatively small (~1/H), allowing more precise determination of the shift. Our preliminary results at fields at 24 T (Figure 1) indicate that the normal state spin shift (0.02%) is about an order of magnitude smaller than previously measured (0.16%, H<9 T) for the planar O(2,3) oxygen for field parallel to the *c*-axis. Measurement of the temperature dependence of the Knight shift at high fields should provide an important insight to the understanding of high T_c superconductivity.

First order phase transition of the Abrikosov vortex lattice to a vortex flux liquid has been observed below the superconducting transition in several transport experiments up to 9 T. The local nature of the NMR method is utilized to probe the field distribution in the vortex state. Above the melting transition but below T_c, rapid fluctuations of the vortex liquid average local field inhomogeneities producing a motionally narrowed NMR line. When the vortices freeze into an Abrikosov lattice, it produces a characteristic field distribution that is broadened. Our preliminary results on aligned powder samples indicate that apart from the solid and liquid phase, there is a coexistence regime exhibited by a double peak structure in the ^{17}O NMR lineshape. At 24 T the onset of this regime T_m is quite steep (Figure 2) and not understood in terms of known theoretical models. Below the lower transition T_g, the double peak structure collapses and the system becomes homogeneous. This phase is consistent with a vortex glass (solid) phase as was observed in films and twinned single crystals. A complete mapping of the melting phase diagram is necessary to understand this technologically relevant phenomenon and provide important constraints on current theories.

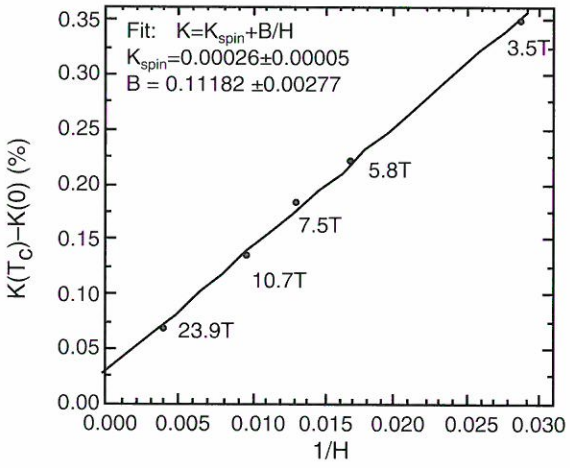

Figure 1. Field dependence of total Knight shift.

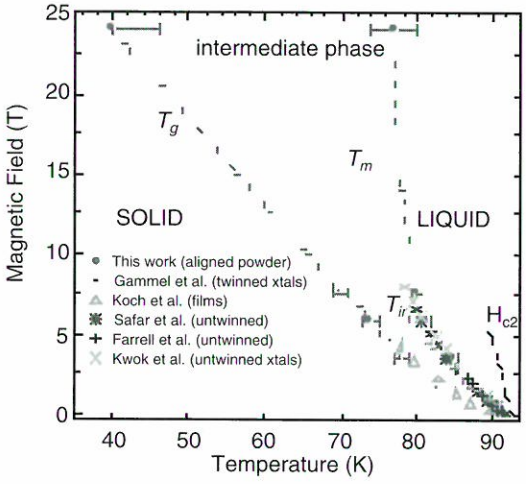

Figure 2. YBCO Hllc melting transition.

Composite Particle Interaction for Odd Gap Superconductors

Schrieffer, J.R., FSU Physics Dept./NHMFL
Balatsky, A.V., LANL

We have derived the effective composite particle interaction V_c for odd gap superconductors from a spin fermion or periodic Kondo model. The interaction leads to a BCS-Gor'kov-Eliashberg type gap equation with the fermion pair propagator replaced by a propagators for two fermions and a

boson or a spin fluctuation, coupled to total momentum and frequency zero and spin one for s- or d-wave type pairing and spin zero for p-wave pairing. This potential includes retardation and damping effects, as in the strong coupling theory of superconductivity, both of which are important since the onset of odd gap behavior only occurs for coupling constant greater than a critical value of order unity. This work provides the basis for the composite order parameter description of such systems.

Furthermore, in the case of an odd gap, we prove that three particle composite condensation implies the existence of an odd frequency pairing condensation and visa versa. Hence the composite particle condensation is a convenience and not a necessity in describing odd gap superconductors.[1]

Reference:

1 Abrahams, E., et al., Phys. Rev. B, 53, 1271 (1995).

Odd Gap Superconductors

Schrieffer, J.R., FSU Physics Dept./NHMFL
Abrahams, E., Rutgers Univ., Physics Dept.
Balatsky, A.V., LANL
Scalapino, D.J., Univ. California, Santa Barbara, Physics Dept.

We have shown that the order parameter Λ of odd frequency gap superconductors corresponds to a three particle composite condensate, involving two fermions and a boson (or spin fluctuation).[1] This result follows from the fact that the equal time Gor'kov F function vanishes by symmetry so that the conventional order parameter is zero. A convenient choice for Λ is dF/dt at t=0, which from the Heisenberg equations of motion leads to the conversion of an s-wave triplet pair to a singlet pair coupled to a spin one excitation, e.g., a spin fluctuation. By introducing a composite particle model interaction analogous to the BCS Hamiltonian for fermion pairs, we have shown that superconductivity onsets above a critical coupling constant of order unity.

Using this model we have worked out many physical properties of odd gap superconductors, including the superfluid density which we find to be positive, in contrast to previous authors who have obtained unphysical negative values for this quantity. In addition, we have derived expressions for the NMR relaxation rate, the heat capacity and transport rates, as well as showing that Josephson tunneling does not occur between even and odd frequency superconductors.

Reference:

1 Abrahams, E., et al., Phys. Rev. B, 53, 1271 (1995).

Strongly Correlated Electrons: Spin Fluctuations and Superconductivity

Schrieffer, J.R., NHMFL/FSU, Physics Dept.

Using the coherent spin path integral formulation of the periodic Kondo problem, we have constructed the action functional that determines the coupling between a dressed fermion quasi particle and a spin fluctuation mode.[1] In the case of antiferromagnetic spin fluctuations we have proved that in contrast to the coupling of bare fermions to spin modes, the dressed coupling obeys a spin deformation potential theorem, which suppresses the spin fluctuation coupling invoked by the nearly antiferromagnetic fermi liquid (NAFL) approach[2] to explain the origin of high temperature superconductivity. In essence, the vertex function $\Gamma_{k,q}$ renormalizing the coupling J_q is proportional to $v_k \cdot (q-Q)/J_q$ where Q is the SDW wave vector and k and q are the quasi particle and spin fluctuation momenta respectively. Since the pairing interaction is given by $V_{kq} = \Gamma_{kq}^2 J_q^2 G_q$ it follows that the large peak of χ_q.

$$\chi_q = \chi_o Q^2 / \{(q-Q)^2 + \xi^{-2}\}$$

for q=Q is canceled by the two factors of Γ. Therefore, we are presently constructing a new approach to high temperature superconductivity based on a real space formulation that fully includes

retardation and nonlinear effects, i.e. multi spin fluctuation effects, such as are present in the spin bag approach.[3,4]

References:

1 Schrieffer, J.R., J. Low Temp. Phys., 99, 397 (1995).

2 Pines, D., J. Phys. Chem. Solids, 54, 1447 (1993).

3 Schrieffer, J.R., et al., Phys. Rev. Lett., 60, 944 (1988).

4 Bishop, A.R., et al., Phys. Rev. Lett., 61, 2709 (1988).

High Field Magnetoresistance in $La_{1.85}Sr_{0.15}CuO_4$

Torikachvili, M.S., San Diego State Univ., Physics Dept.
Rodriguez, J.P., Cal. State Univ., Los Angeles, Physics Dept.
Lacerda, A., NHMFL/Los Alamos
Sarrao, J., NHMFL/FSU
Fisk, Z., NHMFL/FSU

The high temperature superconductor $La_{1.85}Sr_{0.15}CuO_4$ has a superconducting transition temperature $T_c \approx 38$ K. The electrical resistivity of the normal phase is linear with temperature from just above T_c to past room temperature. We performed an investigation on polycrystalline $La_{1.85}Sr_{0.15}CuO_4$ that consisted of the measurement of magnetoresistance in the normal phase in fields to 18 T. We found that the isothermal magnetoresistance $\delta\rho/\rho$ was nearly quadratic with fields in the temperature range from 100 K to 300 K. The isofield magnetoresistance in fields in the 10 to 18 T range is positive, it can be very large near 100 K, then it drops displaying a minimum in the 150 to 200 K temperature range, and it raises again forming a plateau above 250 K. This behavior is not expected from Koehler's rule. We are using these data to test current models in high-T_c materials.

Infrared Measurements in High Magnetic Fields

Zibold, A., UF, Physics Dept.
Liu, H.L., UF, Physics Dept.
Tanner, D.B., UF, Physics Dept.
Wang, Y.J., NHMFL
Grüninger, M., Univ. of Karlsruhe, Germany
Geserich, H.P., Univ. of Karlsruhe, Germany
Li, M.Y., National Tsing Hua Univ., Taiwan
Wu, M.K., National Tsing Hua Univ., Taiwan

Midgap infrared absorption in the insulating phases of the cuprate superconductors. We measured the magnetotransmittance on (001) surfaces of semiconducting cuprates in magnetic field up to 30 tesla. To study CuO in- and out-of-plane effects, the magnetic field was applied either normal to the CuO-planes or at an angle of 30 degrees from the normal. The frequency range was between 800 and 5000 cm^{-1}; the temperature was changed between 5 and 110 ~ K. The spectra show a variety of weak electronic absorption features, some of which seem to be generally intrinsic in the semiconducting limit of the cuprates. In $Y_{1-x}Pr_xBa_2Cu_3O_6$ for different x (x=0,0.4,1) three features occur, two possibly due to magnon excitations and the third to the 4f shell configuration in the Pr ion. In addition, we have studied the 123-bilayer material and the single-layer compound $Sr_2CuO_2Cl_2$. The main effect is a very small shift of the two magnon-peak in the single-layer compound to higher frequencies with increasing field.

Far-infrared studies of high-T_c films in high magnetic fields. We have performed both transmittance and reflectance for highly *ab*-plane oriented $YBa_2Cu_3O_{7-\delta}$ thin films (thickness ~ 40 nm; MgO substrates) over the frequency range from 35 to 360 cm^{-1} at temperatures between 10 K and 300 K and in magnetic field up to 30 T. The zero-field transmittance is consistent with a two component dielectric function consisting of Drude (free-carrier) and midinfrared (bound-carrier) absorption. There is no evidence in our spectra for a superconducting gap in the 50-300 cm^{-1} range.

The magneto-transmittance measurements with H perpendicular to the *ab*-plane and with unpolarized light did not show any discernible field dependence at low temperatures, in contradiction to several previous reports. At temperatures where the DC resistance was not zero-on account of flux motion-there is a corresponding change in infrared transmittance. The interpretation is that the infrared absorption is related to the vortex motion in this temperature/field regime.

SUPERCONDUCTIVITY - APPLIED

Self Field Measurements and Current Distribution Calculations in Superconductors

Gielisse, P.J., NHMFL/FAMU-FSU CoE, Mech. Eng.
Niculescu, H., FAMU-FSU CoE, Mech. Eng.
Khankhasayev, M., FAMU-FSU CoE, Mech. Eng.

Self field measurements and calculation procedures have yielded a methodology for the determination of critical current density distributions in superconductors. Axial components of the self field, generated by polycrystalline superconductors of different geometries and composition, have been measured at grid points in planes above the sample. The measurements were made with a precision custom designed and computer controlled x-y scanning assembly at liquid nitrogen temperature, using a Hall probe or a superconducting magnetic field sensor developed in our laboratory.

A method for calculating current distributions, based on inverse matrix and iteration procedures, has been developed for flat samples of arbitrary shape.

The method makes possible the evaluation of persistent current patterns in thin superconducting samples, using experimental field data and "inverted" matrix equations relating currents and fields. Analytical and numerical calculations of fields and currents were performed and convergence and uniqueness of the iterative solutions of the method were tested.

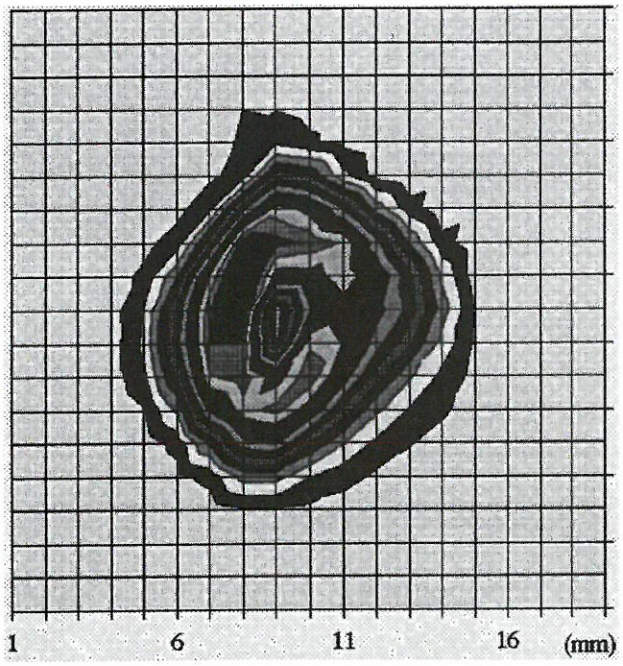

Figure 1. Critical current density distribution calculated by I M Method from experimental field map.

Thermal Expansion of Superconducting Composites by Digital Micro-Image Processing

Gielisse, P.J., NHMFL/FAMU-FSU CoE, Mech. Eng.
Tu, M., FAMU-FSU CoE, Mech. Eng.
Xu, Y., FAMU-FSU CoE, Mech. Eng.
Kulisic, I., FAMU-FSU CoE, Mech. Eng.

Thermal expansion measurements of Nb_3Sn and NbTi superconducting composites have been carried out by a digital micro-image processing

technique. The schematic of the system for thermal expansion measurement at low temperatures is shown in Figure 1. In this method, the deformation of the sample is simultaneously recorded with two CCD cameras equipped with long distance micro objective lenses. The system consists of a cryogenic chamber, a set of temperature sensors, a receiver assembly and a computer image processing system. The specimen is located inside the cryogenic vacuum chamber, which is covered with a transparent and optically flat window. Heat can only be removed from the sample by conduction to the two refrigeration stations, the upper and lower flanges.

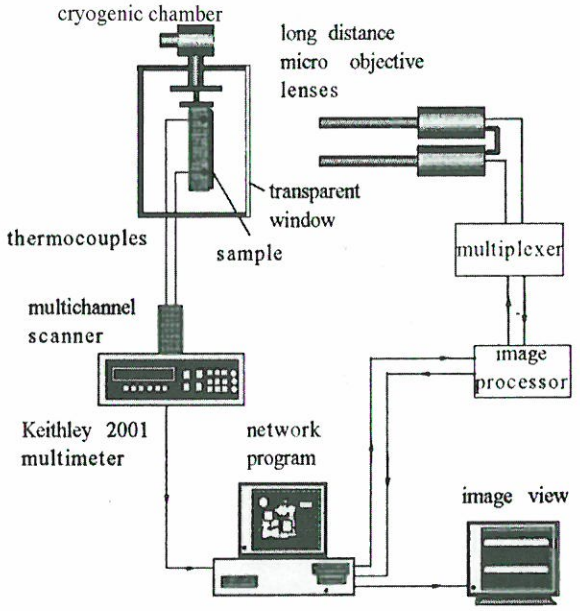

Figure 1. Thermal expansion measurements at low temperatures.

A network program controls all instruments and acts as a command post. With temperature increasing, the two CCD cameras take pictures of the grating patterns, which are then digitized and installed in a PC memory. This procedure repeats itself every ten degrees until room temperature is reached. The images and the positions of the grating patterns can then be analyzed by means of a program written in C language.

The experimental data resulting from the measurement of the linear thermal expansion of samples Nb_3Sn #1, #2, and #3 from 73 K to 293 K are plotted in Figure 2, using a 3rd-order polynomial equation for curve fitting.

For comparison purposes, data from the open literature (G. K. White, R. Driver, and R. B. Roberts, *Int'l. J. of Thermophysics*, 12(4), 1991) for pure Cu and Nb_3Sn have also been plotted. The thermal expansion coefficient of pure copper is higher than that of Nb_3Sn. The thermal expansion values of the composites lies between that of Cu and Nb_3Sn as end members.

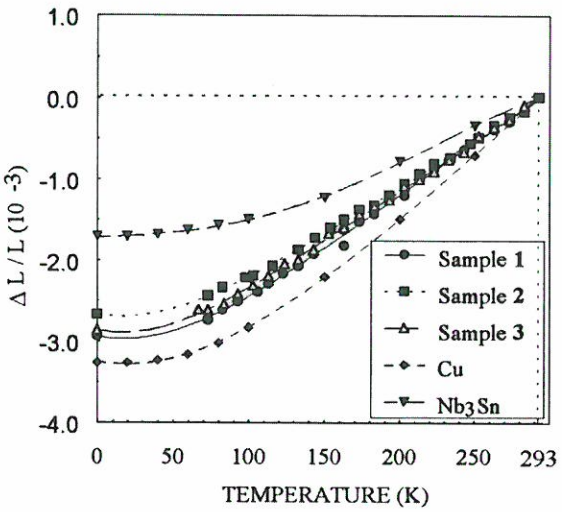

Figure 2. Linear thermal expansion measurements.

Critical Current Measurements in Bismuth-Cuprate Superconducting Tapes

Gubser, D.U., Naval Research Laboratory, Washington DC
Soulen, Jr., R.J., Naval Research Laboratory, Washington DC
Fuller-Mora, W.W., Naval Research Laboratory, Washington DC

We have measured the critical current density, $J_c(H,T)$, of a number of commercially manufactured bismuth-cuprate superconducting tapes. Magnetic fields up to 20 T were applied to samples immersed in liquid cryogens; helium (T = 4.2 K), neon (T = 27.3 K), and nitrogen (T = 77 K and 65 K). These measurements are part of a continuing collaboration among universities (University of Wisconsin, Florida State University, and State University of New York), industry (American Superconductor Corporation, Intermagnetics General Corporation, and Trans-Science Corporation) and government laboratories (Naval Research Laboratory, Naval Surface

Weapons Center, and Concurrent Technologies Incorporated). This collaboration, supported by funding from the Advanced Research Project Agency, ARPA, and the Navy, is focused on improving high temperature superconducting wires and tapes for magnet applications. Of immediate Navy interest are magnets for ship propulsion and mine sweeping.

This past year, the cryostat for measuring critical currents was modified to increase the current capacity to 200 amperes. Also, the liquid neon facility at the NHMFL was used for measurements at 27 K. These modifications permitted a more complete mapping of the H,T space over the region of interest.

Results of our measurements at liquid neon temperatures are shown in Figure 1 where we plot the measured critical currents, in a direction parallel to the face of the tape but perpendicular to current flow, as a function of magnetic field, H. It should be noted that current densities approaching 10^5 amp/cm^2 are achieved at zero magnetic field and at 27 K temperature. The zero field value is depressed from the 4.2 K value by only about 20 percent; however, the value falls by an additional 50 percent at a field of 5 tesla.

For viable Naval applications we believe it will be necessary to raise the critical current density of the superconductor by at least a factor of three at 5 tesla, up to a value over 10^5 amp/cm^2. Continuing research and development on superconducting oxide wires will be necessary to achieve this goal.

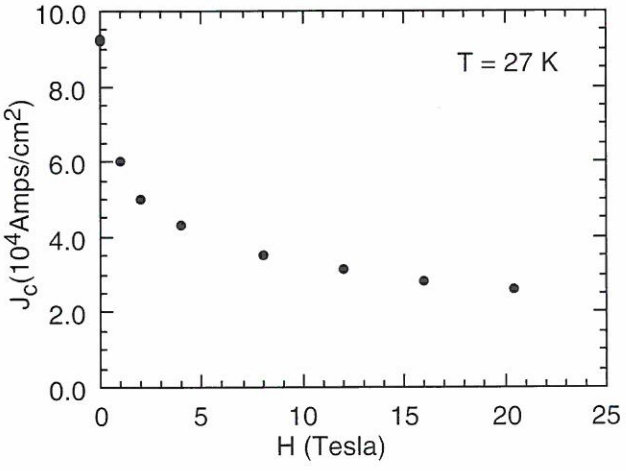

Figure 1. Critical current measurements in bismuth-cuprate superconducting tapes.

Investigation of Transport Properties at High Magnetic Fields in Highly Anisotropic Layered High-T_c Superconductors

Maley, M.P., LANL
Coulter, J.Y., LANL
Safar, H.F., LANL
Cho, J.H., LANL
Bulaevskii, L.N., LANL

The layered crystal structure of the cuprate high temperature superconductors, HTS, is well known to lead to highly anisotropic transport properties. The Bi-based compounds, Bi-2212 and Bi-2223 represent an extreme limit in which two-dimensional superconducting layers are weakly coupled by Josephson tunneling currents and where semiconducting behavior (resistance rising with decreasing temperature) is observed for current flow normal to the layers (along the c axis) prior to the onset of superconductivity. The purpose of this investigation was to study the effects of high magnetic fields on the c-axis resistivity, ρ_c, of single crystals of Bi-2212 in order to observe the underlying transport mechanism when superconductivity is suppressed. We measured ρ_c of single crystals of Bi-2212 in DC fields up to 26 T applied both parallel and perpendicular to the c-axis over the temperature range 4-150 K.

With the magnetic field aligned along the c-axis we observe an extension of the semiconducting behavior to below 50 K with an exponential dependence on 1/T. At fixed temperatures above the peak, we observe a negative magnetoresistance that is well described by a fluctuation model based on the BCS theory for Josephson coupled layered superconductors. In this model the effect of superconducting fluctuations in the normal state is to decrease the density of states (DOS) for quasi-particle tunneling along the c-axis, thus increasing the resistivity. Large magnetic fields suppress fluctuations leading to an enhancement of DOS and thus a negative magnetoresistance. The suppression of superconductivity at 26 T also allows observation of the normal state c-axis transport in the absence of superconducting fluctuations over an extended temperature range. The strongly diverging nature of this normal-state resistivity cannot be accounted

for by superconducting fluctuations and suggests an underlying thermally assisted c-axis transport that, as yet, is unexplained. This result contradicts previous work that attributes the semiconducting behavior to the effects of superconducting fluctuations.

With the magnetic field aligned nearly parallel to the CuO_2 layers, we measured ρ_c as a function of angle θ with respect to the layer plane in fields up to 20 T. We observed a sharp peak in $\rho_c(\theta)$ near parallel alignment that had been previously observed at lower fields. It is interesting that a field of 20 T is insufficient to destroy the Josephson coupling between layers at 30 K. The peak in the dissipation is caused by the interaction between the c-axis transport current and the Josephson vortices, which causes phase-slip to occur between planes along the planar direction. With small misalignments, the c-axis component of the field causes 2D "pancake" vortices to form in the plane that are strongly pinned, anchoring the vortex system and resulting in a steep drop in resistivity. We also observed a shoulder in the $\rho_c(\theta)$ peak that we believe indicates a commensurate structure in the Josephson-pancake vortex system. A model has been developed that describes the essential features of the data.

Critical Current Testing Nb_3Sn Wire

McKinnell, J.C., Teledyne Wah Chang
Jablonski, P.D., Teledyne Wah Chang
Siddall, M.B., Teledyne Wah Chang
Dilley, F.H., Teledyne Wah Chang

Large diameter Nb_3Sn wires manufactured by the Modified Jelly Roll Process (0.5 mm to 1.2 mm) were tested for critical current properties from 12 T to 20 T. The data obtained added to the high field data obtained in 1994 on small wire diameters. In addition to the testing on TWC's standard wire designs, testing was also performed on a wire design with enhanced J_o and reduced copper fraction. This wire showed a 40% increase in critical current at 20 T relative to the standard wire design. The data obtained in these tests is directly applicable to high field magnet design.

Magnetic Field Dependence of the Critical Currents of YBaCuO Thick Films Deposited on Flexible Metallic Substrates

Safar, H.F., STC-LANL
Coulter, J.Y., STC-LANL
Maley, M.P., STC-LANL
Wu, X.D., STC-LANL
Foltyn, S., STC-LANL
Arendt, P., STC-LANL
Willis, J.O., STC-LANL

The recent demonstration that flexible $YBa_2Cu_3O_{7-d}$ (YBCO) thick films with high critical currents can be produced has stirred considerable interest, because it brings the possibility of large-scale conductors with excellent physical properties. An outstanding question is which is the most important source of flux pinning in these materials. This is of great importance, since the relative effectiveness of different pinning mechanisms can make substantial differences in the current-carrying capabilities of these conductors, particularly at high fields and temperatures. We have performed detailed studies of the anisotropy and magnetic field dependence of the critical currents of these materials. Overall, we find that the critical current shows a clear Lorentz force dependence and two distinctive peaks, one for fields parallel to the ab plane due to bulk intrinsic pinning by the layered structure of the superconductor, and

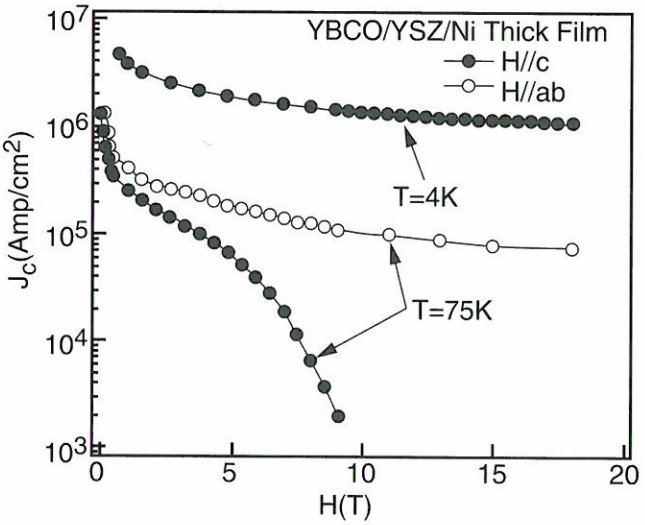

Figure 1. Field dependence of the critical current density for selected orientations.

the other for fields parallel to the c-axis, which we attribute to twin boundary c-axis correlated pinning, as suggested by its Lorentz force dependence. The field dependence of the critical current density for selected orientations is shown in Figure 1. In addition to these measurements, we are working in the study of the vortex-solid-to-liquid transition in these samples. Preliminary measurements performed at NHMFL-Los Alamos suggest that it is a "Bose-Glass" transition, induced by the naturally occurring c-axis correlated disorder (i.e. grain boundaries, twin boundaries).

Quasi Permanent Magnets Made of High T_c Superconductor

Weinstein, R., Univ. of Houston, Physics Dept.
Ren, Y., Univ. of Houston, Physics Dept.
Liu, J., Texas Southern Univ., Math Dept.
Sawh, R., Univ. of Houston, Physics Dept.
Obot, V., Texas Southern Univ., Math Dept.
Foster, C., Indiana Univ. Cyclotron Facility

We have continued the study of superconducting Trapped Field Magnets (TFMs) based on $YBa_2Cu_3O_7$ (Y123).

Post Activation Cooling: The TFMs are activated by cooling in an applied field, B_A. B_A is then turned off (this is the usual Field Cooled method, FC). Creep rates in the temperature range 60-77 K are generally 5% - 8% per decade of time. However, if the TFM is cooled an additional ΔT, *after* activation, the creep is greatly diminished. The current, J, in the TFM is fixed during FC. If the FC is done at T_1, the critical current $J_c(T_1)$ results. At ΔT lower, the TFM is *capable* of a critical current $J_c(T_2)$, but still carries a current of $J_c(T_1)$. The creep behaves as though a time τ has elapsed, where τ is the time period in which $J_c(T_2)$ would be reduced by creep to $J_c(T_1)$. In a TFM activated by FC at 65 K, post activation cooling (PAC) reduces creep by a factor of 6.25 for $\Delta T = 2K$, 197 for $\Delta T = 4K$, and ≥ 1000 for $\Delta T = 6K$.[1] The PAC phenomenon makes it possible to reduce creep, practically, to zero.

Cracking: An activated TFM has a gradient in vortex currents that is equivalent to a circulating current. This circulating current interacts with the field it creates to produce an outward pressure. We studied the cracking of TFMs under this pressure. Previous literature considered cracking after activation. We observed that cracking occurs not after activation, when only trapped field and persistent current are present, but rather during activation, when applied field is also present. We extended the theory of cracking to include the more general conditions during activation.[2] Theory and experiment[2] are now in excellent agreement relative to: (a) the shape of the cracks (radial), (b) their origin (near the center), and (c) the cracking strength. The latter was measured to be within 5% of the value measured for Y123 by mechanical engineering methods.

Record Trapped Fields: During this period we also established a new record for magnetic field trapped in an ingot of any material at any temperature. 10.1 tesla was trapped at 42 K.[3] In order to achieve this, field cracking was avoided by using B_A as low as possible consistent with the trapped field aimed at. We also used the PAC method to diminish creep. We used it, however *during* the FC activation, i.e., we used intra-activation cooling (IAC) to reduce creep during activation.

Based on a series of high trapped fields an award for Materials/Device Development was presented to this group by the MRS/ISTEC Program Committee of the International Workshop on Superconductivity at Hawaii, in June 1995.

Also in this period, a processing method was developed to produce short homogeneous isotropic columnar pinning centers. Processing in this way, Y123 trapped 3.1 tesla at 77, a record field at 77 K.

References:

1 Liu, J., et al., Proc. 1995 Internat. Workshop on Supercon., Maui, June 1995.

2 Ren, Y., et al., Physica C, 251, 15 (1995).

3 Weinstein, R., et al., submitted to Eighth Internat. Workshop on Critical Currents in Supercon., Kitakyushu, Japan, May 1996.

KONDO/HEAVY FERMION SYSTEMS

Low-Temperature Magnetoresistance Study of UNiAl and UNiGe

Bruck, E., Van der Waals-Zeeman Institute, Univ. of Amsterdam
Havela, L., Charles University, The Czech Republic, Dept. of Metal Physics
Sechovsky, V., Charles University, The Czech Republic, Dept. of Metal Physics
Nakotte, H., LANSCE-LANL
Lacerda, A., NHMFL/Los Alamos

The aim of this study is to observe effects connected with metamagnetic transitions in the context of giant magnetoresistance (GMR) phenomena, and to investigate the field development of excitations at very low temperatures. Due to the failure of the dilution refrigerator we were able to complete the program for UNiGe only, whereas for the heavy-fermion antiferromagnet UNiAl an additional experiment in the millikelvin range is necessary. For this compound, we observed how the anomaly in $\rho(T)$ connected with the antiferromagnetic transition is gradually shifted toward lower temperatures with increasing field. Above B = 10 T, it changes into the first-order transition and disappears completely near B = 11.5 T. The low-temperature ρ-value is reduced by more than 50 percent comparing to the zero-field value. The type of the low-temperature behavior, however, could not be deduced from experiments performed only down to T = 2.5 K. The results are summarized in the Figure 1. For UNiGe we were particularly interested in the development of resistivity parameters over three different magnetic phases with the coupling: 1.+ - + -, 2.+ + - + + -, 3. + + +. For the current along the a-axis, the residual resistivity ρ_0 systematically decreases in the sequence 1-2-3 (see Figure 2). All these $\rho(T)$ data can be fitted to the formula: $\rho = \rho_0+aT^2+bT(1+2T/\Delta)\exp(-\Delta/T)$, the last term of which accounts for the electron magnon scattering. The width of the gap in the magnon spectrum Δ is comparable with the strength of the in-plane magnetic anisotropy and increases significantly with axial symmetry imposed by external field. For i//c the resistivity in the intermediate phase is enhanced with respect to the ground state one. This proves that the resistivity in AF state does not scale with the concentration of + - boundaries (lower in the phase 2 comparing to 1).

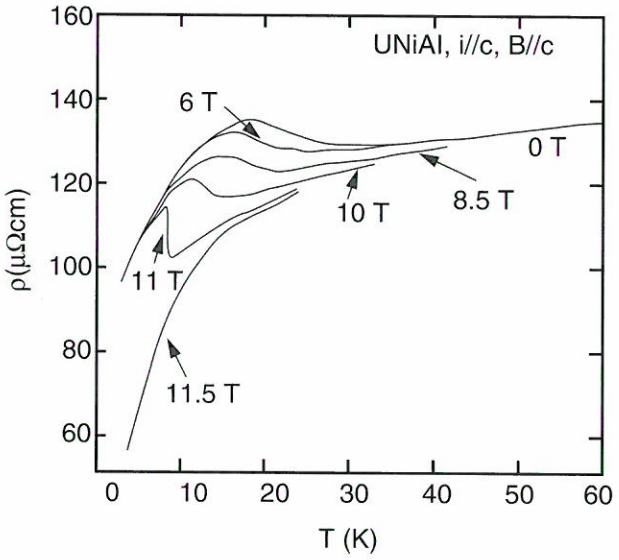

Figure 1: Resistivity versus temperature of UNiAl, with illc, Bllc.

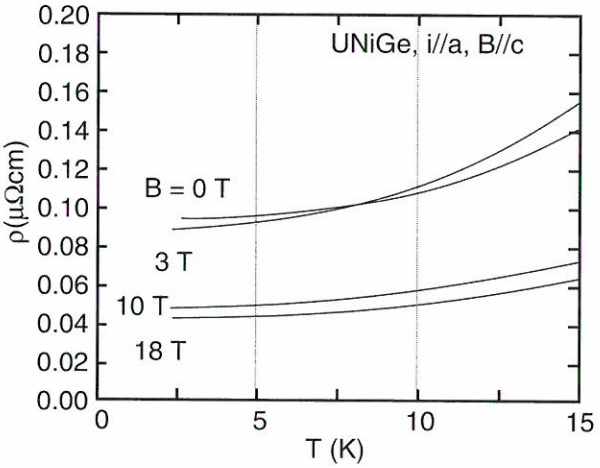

Figure 2: Resistivity versus temperature of UNiGe with illa, Bllc.

Kondo Insulators

Fisk, Z., NHMFL/FSU, Physics Dept.
Sarrao, J., NHMFL
Young, D., NHMFL/FSU, Physics Dept.
Torelli, M.T., NHMFL/FSU, Physics Dept.
Boebinger, G.S., AT&T Bell Labs
Ott, H.R., ETH, Zurich
Sharifi, F., NHMFL/UF, Physics Dept.
Aeppli, G., AT&T Bell Labs

The Kondo insulators are a class of small gap semiconducting rare earth compounds, with gap typically 10-100 K.[1] The unusual aspect of these materials is that thermal excitations across the gap carry magnetic moment corresponding to the Hund's Rule ground state of the +3 rare earth ion; the gap closes at characteristic temperature $3.5\ k_B T^* \approx \Delta$, the gap temperature, as is seen in optical conductivity experiments, with spectral weight redistribution over an energy scale an order of magnitude larger than the gap; and the magnetic moments when thermally present are non-interacting. The goal of this program has been to understand where these materials fit into the general picture of highly correlated metals and the general competition between magnetic ground state and moment compensated ground state. Our tools have been the materials variables of chemical substitution, both isoelectronic and not, and external variables of magnetic field, pressure and temperature.

In collaboration with Boebinger, we have studied the magnetoresistance and Hall effect in $Ce_3Bi_4Pt_3$ and SmB_6. The gap scale is a factor of 3 smaller in the first material, and pulsed fields of 60 T lead at low temperatures to a state with conduction electron concentration of approximately 0.03 e/formula unit. The idea here is that the 60 T field partially collapses the gap, in a continuous fashion.

We also are investigating, in collaboration with Ott, the development of the Kondo insulating state from the insulating side. Namely, we start with an insulator and dope with a material which at x=1 doping produces a Kondo insulator. For this, we are doping Sm into SrB_6. To date the experiments have determined, at the SrB_6 end, that the Sr material is in fact a semi-metal, not a semiconductor. This does not seriously alter the experiment. However, detailed single crystal refinement on the SrB_6 single crystals, combined with band structure calculations from the Lausanne group have discovered that SrB_6 possesses electronic characteristics similar to grey tin, where there is a Fermi point. In this case, there is finite direct band overlap in a small region of k-space. This is an unusual situation and the SrB_6 shows puzzling transport properties below 1 K, which we are now exploring.

Finally, we are conducting a number of studies on FeSi. These include doping experiments, which produce magnetically ordered phases, plus some paramagnetic metallic phases. Tunneling experiments are in progress in collaboration with Sharifi. These indicate that the gap that opens does not show a region with no density of states, rather a region with very low density of states. The important question with FeSi is whether the same phenomena are shown as in the rare earth materials, and the extent to which band structure can account for the experiments.

Reference:

[1] Fisk, Z., et al., to appear in Physica B (1995).

The Physics of $YbInCu_4$

Fisk, Z., NHMFL/FSU, Physics Dept.
Sarrao, J., NHMFL
Lawrence, J.M., Univ. of CA, Irvine, Physics Dept.
Thompson, J.D., LANL

$YbInCu_4$ is a cubic intermetallic compound that has a first order volume collapse to a non-magnetic ground state at T = 45 K. We have been studying this α-Ce type structural change using single crystals that show particularly clean properties. This type of first order structural change bears a number of similarities to a gas-liquid phase transition, and part of our motivation for studying this system is to determine the extent to which we can regard the development of the so-called "coherent" ground

state in heavy Fermion materials as a gas-liquid phase transition, but generally one beyond the critical point. In this particular system, we have alloyed the system into the region beyond the first order range. The full range of compounds $YbIn_{1-x}Ag_xCu_4$ ($0 \leq x \leq 1$) have been synthesized as single crystals, and we observe a smooth evolution of physical properties from $YbInCu_4$ to $YbAgCu_4$, a "normal" heavy Fermion.[1] We also are performing high pressure experiments on the materials: pressure suppresses the transition temperature. What we have not been able to determine yet is whether the structural phase transition can be pushed to T = 0 K, or whether it becomes continuous at high enough pressure. The initial indications are that this second possibility is what happens. The high temperature state carries the full Yb (J = 7/2) magnetic moment, so there is in addition strong field dependence in the phase diagram. We have prepared an extensive set of single crystals to investigate these questions. The goal is first the full determination of the phase diagram in composition, pressure, magnetic field, and temperature space. We want to use this to refine the minimal description of the underlying physics. The ultimate objective is to apply such a minimal description to all concentrated "Kondo-type" systems.

Reference:

1 Sarrao, J.L., et al., to appear in Physica B (1995).

Interplay Between the Kondo Effect and RKKY Interactions

Gor'kov, L.P., NHMFL
Kim, J.H., NHMFL

Physics of the single impurity Kondo model is often used as a basis for interpreting the properties of a dense (impurity) lattice system. To examine whether the Kondo physics is applicable for describing the dense systems, we start from the dilute limit and study the effect of finite impurity concentration x with the increase in x. For the effect of finite x, it is natural to start with a problem dealing only two impurity spins in the sea of conduction electrons.

We have studied the two-impurity Kondo problem by using a perturbation analysis in three dimensions[1] and by applying the Bethe ansatz approach[2] in one dimension. There are two important energy scales in this problem: one is the Kondo temperature, Tk, and the other is the RKKY interaction energy between two impurity spins, I. The RKKY interaction for T << Tk and for T > Tk may differ because the impurity spins tend to be screened at low temperatures due to the Kondo effect. The perturbation analysis indicates that the zero temperature magnetic susceptibility for two impurity spins differs significantly from the independent impurities due to the RKKY interactions when Tk ~ I. By applying the Bethe ansatz approach, we show that the exact solution to the two-impurity Kondo problem can be constructed in one dimension. We diagonalize the model for the impurity singlet and triplet state, separately. For Tk >> I, we find that the impurity spins are quenched independently, as expected. However, for Tk << I, the impurity contribution to thermodynamic quantities from the triplet state differs from the singlet state. For the triplet case, the solution indicates that the interaction contribution is negligible compared to the Kondo effect at low temperatures (i.e., T << Tk). This suggests that the ground state is of a Fermi liquid type with quenched impurity spins. For the singlet state, on the other hand, the impurity spins behave as an effective spin zero scatterer. This is consistent with the results of perturbative scaling analysis[3] and recent numerical renormalization group study.[4]

These results indicate that Kondo Hamiltonian may not be an appropriate model even for magnetic alloys such as $Ce_x\ La_{1-x}\ Cu_6$ and $Ce_x\ La_{1-x}\ Pb_3$. The specific heat C and the magnetic susceptibility χ increase linearly in x as La ions are substituted by Ce ions for a wide range of x. The data on C and χ in these alloys suggest that the contributions from the RKKY interaction is either absent or much smaller than the Kondo effect. However, this linear dependence on x is different from an expectation

that the RKKY contribution appears in the finite x regime as suggested by the two-impurity Kondo model. Therefore, we conclude that the Kondo physics may not be applicable in describing the dense systems.

References:

1 Gor'kov, L.P., et al., Interplay Between the Kondo Effect and the RKKY Interaction in the Two-Impurity Model, 1995 (To appear in the Philosophical Magazine).

2 Gor'kov, L.P., et al., Exact Solution to the Two-Impurity Kondo Problem in One-Dimension, (unpublished).

3 Jayaprakash, C., et al., Phys. Rev. Lett. 47, 737 (1981).

4 Silva, J. B. et al., (unpublished).

Polaronic Effects in Mixed Valence Problem

Gor'kov, L.P., NHMFL

It is emphasized that the usual description of the mixed valence phenomenon in terms of the atomic f- or d- orbitals has, strictly speaking, no justified meaning. Electronic "configurations," however, can be formed on a timescale of a characteristic phonon's frequency provided non-linear electron-lattice interactions are taken into account. Such an involvement of slow lattice degrees of freedom may naturally introduce a small parameter for low energy scales characteristic for the physical phenomena in heavy fermions or the mixed valence compounds. A simple quasiclassical model is formulated to illustrate the idea. So far, the idea has been applied to the properties of an local magnetic center imbedded into the conduction sea of other electrons. A more elaborated treatment is now in progress.

Reference:

1 Gor'kov, L.P., "Phase Transitions in Mixed Valence Systems," 1995, to be published in Physica B.

Symmetry of Low Temperature Phase Below Magnetic Transitions in Mixed Valence Materials

Gor'kov, L.P., NHMFL
Barzykin, V., Univ. of British Columbia

Initially the idea of these studies[1] was to make use of basic symmetry arguments for classification of possible magnetic phases where the corresponding order parameter differs from the familiar staggered Néel magnetization of sublattices. A number of materials show such a behavior experimentally. The emphasis has been to account for effects of strong anisotropy in these materials.[2] The symmetry considerations, in particular, would allow one to make predictions regarding the influence of an external magnetic field on the phase transition.

Among numerous problems related to the aforementioned topics, the most intricate phenomenon is the existence of the so-called "tiny" moments (~0.04 μ_B) phase, which e.g. sets on in URu_2Si_2 at 17.5 K. The recent experiments have shown, first, that even at low magnetic fields the variation of the transition temperature seriously disagrees with predictions of the phenomenological analysis implying the need of a microscopic approach. Secondly, the neutron experiments have also revealed importance of the mixed valence features in the compound. We generalized our analyses by introducing the concept of a coherent wave function for the f-electrons which is a combination of the two components corresponding to different occupations for the 5f-shells.[3]

References:

1 Gor'kov, L.P., NHMFL, Annual Report 1994, p. 41.

2 Gor'kov, L.P., et al., "Non-Néel Ordering in Presence of Strong Anisotropy," Physica B, 206 & 207, 116 (1995).

3 Gor'kov, L.P., et al, "Singlet Magnetism in Heavy Fermions," Phys. Rev. Lett., 74, 4301 (1995).

Correlated Electron Theory

Ingersent, K., NHMFL/UF Physics Dept.
Schiller, A., NHMFL/UF Physics Dept.

Theoretical Treatment of Correlated Lattice Electrons. This work aims to achieve an understanding of the properties of correlated electron systems through theoretical calculations for lattice (e.g., Hubbard-like) models in large but finite spatial dimensionalities, d. In the limit $d = \infty$, correlated lattice electron models can be treated exactly within a dynamical mean-field theory for a single lattice site embedded in an effective medium which represents the remainder of the lattice. This approach has successfully recovered much of the physics of correlated Fermion systems. However, it ignores the effects of spatial fluctuations, which are believed to play an important role, for instance, in the competition between magnetic ordering and the Kondo effect within heavy-fermion systems.

In order to address this deficiency, we have developed[1] a systematic expansion in powers of $1/d$ about the limit $d = \infty$. At first order in $1/d$, the method entails a self-consistent mapping of the lattice onto coupled one- and two-site problems. To date, we have applied a simplified version of our scheme to the Falicov-Kimball model, finding only small deviations from $d = \infty$ results even for two dimensions. The next stage of our work will require large-scale numerical implementation of our scheme for fully interacting models such as the Hubbard and periodic Anderson Hamiltonians, for which the existence of small many-body energy scales makes marked deviations from $d = \infty$ behavior highly probable.

Magnetic Impurities in Unconventional Fermi Systems. The experimental study of quantum wires and quantum Hall systems has led to great theoretical activity in the area of one-dimensional Fermi systems. Such systems must be treated within the Luttinger-liquid picture, rather than the more familiar Fermi-liquid theory that applies in two and three dimensions. The response of Luttinger liquids to local probes is of particular interest at present. We are studying the behavior of magnetic impurities within Luttinger liquids using a variety of theoretical approaches.[2] We have been able to explain and predict several differences between the behavior of local moments in Fermi and Luttinger liquids. Our ultimate goal is to utilize these differences to gain a deeper understanding of the host electron gas.

Another type of unconventional Fermi behavior can arise even in two or three dimensions. Certain anisotropic superconductors and semiconductors have a quasiparticle density of states which vanishes in a power-law fashion at the Fermi energy. The heavy-fermion superconductors are strong candidates for this class of materials. Our studies[3] indicate that the conventional Kondo effect is, for practical purposes, completely suppressed in such systems. Nonetheless, doping with magnetic impurities may lead to a clear signature of the pseudogap in thermodynamic and transport properties. Further work is under way to obtain improved predictions of these properties.

References:

1 Schiller, A., et al., Phys. Rev. Lett. 76, 113 (1995).

2 Schiller, A., et al., Phys. Rev. B 51, 4676 (1995); unpublished.

3 Ingersent, K., to appear in Physical Phenomena at High Magnetic Fields II, eds. L. P. Gor'kov et al. (World Scientific, Singapore); submitted to Phys. Rev. Lett.

Magnetic Field Dependence of the Energy Gap of SmB_6

Lacerda, A., NHMFL/Los Alamos
Goettee, J.D., NHMFL/Los Alamos
Smith, J.L., STC–LANL
Kebede, A., North Carolina State Univ., Physics Dept.

Recently, materials having a small semiconductor-like gap, such as $Ce_3Bi_4Pt_3$ and SmB_6, and FeSi have gained interest due to the unusual nature of the energy gap formation. Each of these three materials forms in a cubic crystal structure, which appears favorable to the

appearance of a gap in the electronic spectrum. To probe the magnetic field effect on the energy gap, we have measured the transverse magnetoresistance in magnetic fields to 50 T and temperature between 4 K to 40 mK of the SmB_6 (gap of the order of 40 K) compound. At 4 K a very large negative and quadratic-in-field magnetoresistance was found. At 4 K and 50 T the magnetoresistance approaches -45%.[1] A striking point of our results is that even with the high magnetic field applied (comparable to the energy gap), the magnetoresistance is quadratic in the entire field range investigated. Recently, making use of an all-plastic dilution refrigerator for the pulse magnets, we have measured the transverse magnetoresistance of SmB_6 from 1 K down to 40 mK. In Figure 1, we show the transverse magnetoresistance at 40 mK to 50 T. An inflection point is clearly seen near 35 T, which may indicate the closing of the energy gap and the onset of closed orbits in the SmB_6 compound.

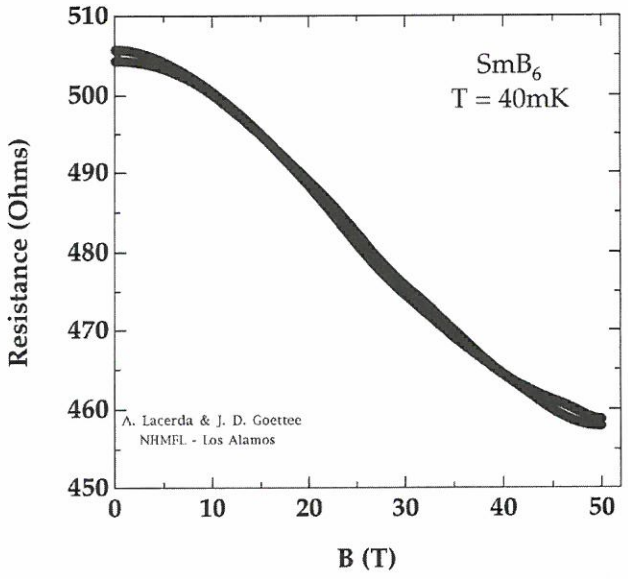

Figure 1. Resistance versus applied magnetic field to 50 T at 40 mK of SmB_6.

Reference:

1 Lacerda, A., et al., Physica B, 199&200, (1994) 469.

Magnetic Phase Transitions in CeB_6

Lacerda, A., NHMFL/Los Alamos
Torikachvili, M.S., San Diego State Univ., Physics Dept.
Sarrao, J.L., NHMFL
Fisk, Z., NHMFL/FSU, Physics Dept.

CeB_6 is a heavy fermion dense Kondo system that displays two magnetic phase transitions at low temperatures, at 2.4 K and 3.3 K respectively. Neutron scattering and magnetization data by Effantin et al.[1] suggest that the transition at 3.3 K is the onset of a quadrupolar antiferromagnetic (QA) phase, while that transition at 2.4 K is due to the onset of antiferromagnetism. We performed measurements of magnetoresistance and magnetization in CeB_6 above 2 K in magnetic fields to 18 T in order to elucidate the transition from paramagnetism to the QA phase. We found that the features in the electrical resistivity and magnetization (Figure 1) as a function of magnetic field coincide in temperature, and that the transition temperature from paramagnetism to the QA phase increases nearly quadratically with magnetic field.

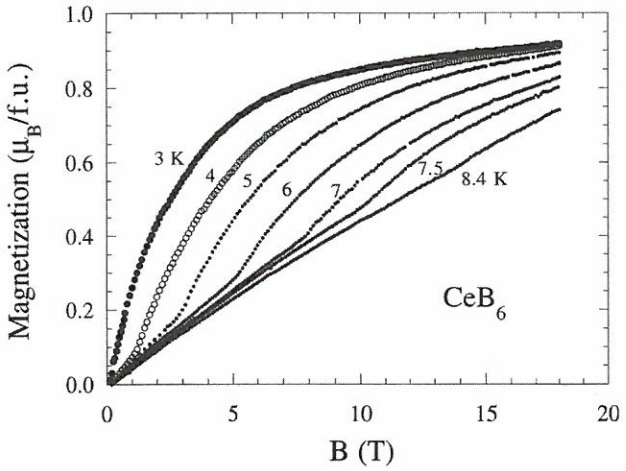

Figure 1. Magnetic phase transitions in CeB_6

Reference:

1 Effantin, J. M., et al., J. Magn. Mat., 47&48, 145 (1985).

Magnetization of CePtPb

Lawrence, J.M., UC Irvine, Physics Dept.
Lacerda, A., NHMFL/Los Alamos

CePtPb is a new hexagonal compound that orders antiferromagnetically at $T_N = 0.9$ K and for which the susceptibility is highly anisotropic, with the ratio χ_{ab}/χ_c extrapolating to the value 65 at T_N. In order to better understand this anisotropy, we measured the magnetization for fields in the range 0 to 18 T, for two orientations of the crystal with respect to the field, and for 2.4, 4, 20 and 100 K (Figure 1). The solid line in Figure 1a fits the data at 2.4 K to a mean field Brillouin form, where the saturation magnetization $M_{s,ab} = 0.92\mu_B$ and Weiss temperature $\theta = 1.3$ K compare reasonably well to the values $1.17\mu_B$ and 0.8 K (Figure 1b, dashed line); these values do not agree so well with the values $0.42\mu_B$ and 0 K obtained from the low temperature susceptibility cc. Addition (Figure 1b, solid line) of a linear term $\chi_{0,c}B$, where $\chi_{0,c}$ is the measured c-axis van Vleck susceptibility, makes clear that the overall fits require an additional susceptibility that is nonlinear in B.

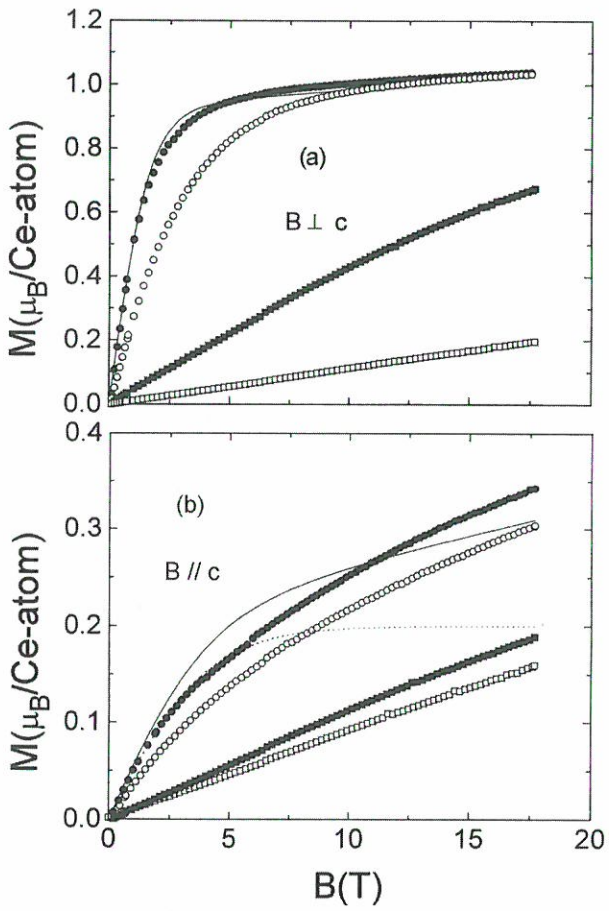

Figure 1. Magnetization as a function of field of CePtPb.

Better agreement between the fits to the magnetization and susceptibility require a full crystal field calculation, nonlinear in field. For the case of CePtPb where the point symmetry (mm) is very low, this would be difficult. Nevertheless, this work makes clear that magnetization data obtained in the high fields accessible at the NHMFL are very sensitive to crystal field effects, and given a calculation appropriate to the given point symmetry, such magnetization data could in principle be used to determine accurately the crystal field parameters. Indeed, such studies would be superior to specific heat studies in that the effective temperatures (50 T ~ 50 K) are larger than for the typical specific heat measurements (20 K) and that the magnetization is sensitive to orientation.

High Field Magnetoresistance of URu_2Si_2

Mentink, S.A.M., Univ. of Toronto
Mason, T.E., Univ. of Toronto
Mydosh, J.A., Leiden Univ.
Goettee, J.D., NHMFL

The nature of the antiferromagnetic transition at T_N=17.5K in the heavy fermion superconductor URu_2Si_2 is still unclear. Despite a very small ($0.04\mu_B$/U-atom) ordered magnetic moment, the accompanying anomalies in specific heat and thermal expansion are very large. High field experiments are particularly useful towards understanding these discrepancies. Resistivity experiments in constant fields up to 25 T performed in Toronto and Nijmegen show that the anomaly at T_N, which indicates the formation of an energy gap, slowly shifts towards lower T, with a critical field of 40 T. Neutron diffraction, however, shows that the ordered magnetic moment decreases strongly with field, with an estimated critical field of 14.5 T. The existence of these two energy scales suggests that the principal order parameter in URu_2Si_2 is not the antiferromagnetic ordering of small U-moments, but possibly an ordering of quadrupoles.[1] We have attempted to extend these data by

magnetoresistance in pulsed field up to 50 T to better define the critical field. A new resistance probe for use at variable temperatures was constructed, but up to now we have not been able to obtain reliable data on these low-resistance (1mΩ) crystals. Further experiments are needed to complete the phase diagram of URu_2Si_2.

Reference:

1 Mentink, et al., submitted to Phys. Rev. B., Rapid Commun.

Disorder Driven Non-Fermi Liquid Behavior in Kondo Alloys

Miranda, E., NHMFL
Dobrosavljevic, V., NHMFL
Kotliar, G., Rutgers Univ., Physics Dept.

Several non-magnetic Kondo alloys (e.g., $UCu_{5-x}Pd_x$, $U_{1-x}Th_xPd_2Al_3$, $U_{0.2}Y_{0.8}Pd_3$, $La_{0.9}Ce_{0.1}Cu_2Si_2$) show an anomalous low temperature behavior in thermodynamic and transport properties which cannot be described by Landau's Fermi liquid theory. As a rule, the specific heat at low temperatures behaves as $C_v/T \sim -A\ln(T/T_0)$ and the resistivity is linear $\rho \sim \rho_0(1-T/T_0)$, where T_0 can be negative or positive. The spin susceptibility shows either a logarithmic behavior or a weak power law. Attempts to explain this phenomenon have focused on the proximity to a magnetic transition or have invoked some exotic single-impurity mechanism.[1] One of the main difficulties for these theories, however, has been the leading linear temperature dependence of the resistivity.

We have proposed that the linear in T resistivity can be explained by a simple model of disorder. Experimental support for this idea has come from NMR measurements on $UCu_{5-x}Pd_x$, [2], which have provided compelling evidence that disorder plays a central role in the low temperature behavior of these systems. Due to the exponential nature of the Kondo temperature, even relatively weak disorder leads to an extremely broad distribution of Kondo temperatures.[3] Spins belonging to regions with very small Kondo temperatures are unquenched and their combined incoherent scattering leads, in general, to a linear resistivity. Our results suggest that the linear resistivity is a very robust feature with respect to changes in the form of disorder. Further investigation will focus on whether the same model can explain existing data on the dynamical spin response and the behavior under applied magnetic field. Besides, it needs to be established whether disorder can explain the non-Fermi liquid behavior of all the studied Kondo alloys.

References:

1 Andraka, B., et al., Phys. Rev. Lett., 67, 2886, (1991); Cox, D.L., Phys. Rev. Lett. 59, 1240, (1987).

2 Bernal, O.O., et al., Phys. Rev. Lett., 75, 2023, (1995).

3 Dobrosavljevic, V., et al., Phys. Rev. Lett., 69, 1113 (1992).

Superconductivity at a Magnetic Critical Point

Miranda, E., NHMFL
Bonesteel, N.E., NHMFL

Until recently, $CeCu_2Si_2$ was the only known Ce-based heavy fermion superconductor. The discovery of pressure-induced superconductivity in three other Ce-based heavy fermion compounds $CeCu_2Ge_2$, $CePd_2Si_2$ and $CeRh_2Si_2$[1] has revealed a trend unprecedented in the field of heavy fermion superconductivity. The three compounds share the same lattice structure as $CeCu_2Si_2$ and differ only in the conduction electron count. These studies have shown that external pressure can suppress the Néel temperature T_N to zero. At this pressure-induced critical point all three compounds have been found to exhibit a small superconducting phase. The role of the external pressure seems to be to bring their unit cell volume to the value of $CeCu_2Si_2$ at ambient pressure. The latter compound, on the other hand, has been shown to be extremely sensitive to internal strains, being at the threshold of the magnetic and superconducting phases. Though several experimental facts still need to be settled it is tempting to assume that these compounds share a common pairing mechanism.

The proximity to a magnetic critical point suggests that the overdamped gapless magnetic fluctuations might be responsible for pairing. The effect of scattering off gapless bosons on the normal state electronic spectrum has been the subject of many recent studies.[2] We have focused, instead, on the possibility that these processes might lead to a superconducting instability.[3] The localized nature of the magnetic response in *k*-space leads to the formation of "hot lines" on the 3D Fermi surface,[4] where the scattering amplitude is greatest. We have started the study of the competition between the pair-breaking and pair-forming effect of such scattering within an Eliashberg formalism. The rather universal form of the magnetic response near a metallic quantum critical point makes these systems an ideal testing ground of theories of spin fluctuation mediated superconductivity and can shed new quantitative light on this scenario.

References:

1 Jaccard, D., et al., Phys. Lett. A, 163, 475 (1992); Grosche, F.M., et al. (preprint); Movshovich, R., et al. (preprint).

2 See, e.g., Halperin, B.I., et al., Phys. Rev. B, 47, 7312 (1993).

3 Bonesteel, N.E., Phys. Rev. B, 48, 11484 (1993).

4 Hlubina, R., et al., Phys. Rev. B, 51, 9253 (1995).

Non-Fermi-Liquid Behavior in $UCu_{3.5}Al_{1.5}$ Tested by Magnetization Experiments

Nakotte, H., LANSCE – LANL
Lacerda, A., NHMFL/Los Alamos
Torikachvili, M.S., San Diego State Univ., Physics Dept.
Bruck, E., Univ. of Amsterdam, Van der Waals–Zeeman Laboratory, The Netherlands
Prokes, K., Univ. of Amsterdam, Van der Waals–Zeeman Laboratory, The Netherlands
de Boer, F.R., Univ. of Amsterdam, Van der Waals–Zeeman Laboratory, The Netherlands

The existence of a single energy scale, the Fermi liquid temperature (T_{EF}), is a central premise in the Fermi-liquid theory. While such a single energy scale was proposed for many "pure" heavy-fermion compounds, strong deviations from the Fermi-liquid behavior were observed experimentally in a number of dilute systems.[1,2] Non-Fermi-liquid behavior is reflected by certain divergences in the specific heat and the magnetic susceptibility. Recently, we found that $UCu_{3.5}Al_{1.5}$ exhibits a scaling behavior very similar to that of $UCu_{3.5}Pd_{1.5}$ [2], which is one of the most popular non-Fermi-liquid materials. Various scenarios (ranging from single-ion two-channel Kondo mechanism to collective effects) have been proposed for the occurrence of non-Fermi-liquid behavior,[1] but a detailed understanding was not achieved yet. In the case of $UCu_{3.5}Pd_{1.5}$, the magnetization was, however, predicted to scale with $H/T^{2/3}$ (above 10 T and 10 K) if the single impurity picture holds.[2] Similar temperature behavior is expected for the $UCu_{3.5}Al_{1.5}$ compound. For the latter we have tested this prediction by measuring the magnetic response of $UCu_{3.5}Al_{1.5}$ at various temperatures between 2.5 and 300 K. For this purpose, we used the vibrating sample magnetometer in the 20 T superconducting magnet at the NHMFL Pulsed Field Facility at Los Alamos National Laboratory. For $UCu_{3.5}Al_{1.5}$, we do not find any evidence for a $H/T^{2/3}$ scaling of the magnetization in any temperature range, which may indicate collective effects to be responsible for non-Fermi-liquid behavior in this compound. In order to gain additional insight in the non-Fermi-liquid behavior of this compound, we plan to perform magnetoresistance studies down to mK temperatures.

References:

1 Lohneysen, H.v., Physica B, 206&207, (1995) 101.

2 Aronson, M.C., et al., Physica B (in press).

High Field Studies of $YbInCu_4$

Thompson, J.D., LANL
Lacerda, A., NHMFL/Los Alamos
Sarrao, J.L., NHMFL
Fisk, Z., NHMFL/FSU, Physics Dept.

$YbInCu_4$ is a correlated electron compound that exhibits a weakly first-order isostructural volume collapse and associated valence change at $T_V = 40$ K that apparently is similar to the γ-α transition in elemental Ce. Substitution of Ag for In increases T_V, whereas replacing Yb with Y decreases T_V. From magnetization measurements to 18 T, we have found that a magnetic field applied to $Yb_{.875}Y_{.125}InCu_4$ at $T << T_V(0) = 14.7$ K induces a first-order transition at a field $H^*(T)$ from a reduced moment-to-nearly trivalent moment state. H^* and T_V are related simply by $((H^*(T)/H^*(0))^2 + ((T(H)/T_V(0))^2 = 1$. Further, $H^*(0)$ and $T_V(0)$ follow the same linear relationship found earlier[1] for $YbIn_{1-x}Ag_xCu_4$, indicating that T_V and H^* track each other irrespective of how the valence-transition temperature is tuned by substitutions.

We also have measured the transverse magnetoresistance of an $YbInCu_4$ crystal at 50 mK and magnetic field to 20 T. Oscillations, reproduced on field increasing and decreasing, are superimposed on a very large positive magnetoresistance. See Figure 1. The possibility that these are quantum oscillations needs to be confirmed by further experiments but are highly suggestive.

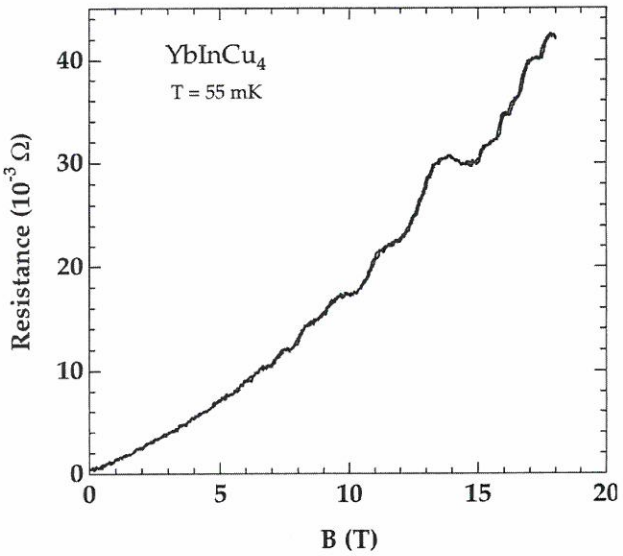

Figure 1. Resistance versus applied magnetic fields to 18 T at 55 mK of $YbInCu_4$.

Reference:

1 Katori, H.A., et al., Physica B 201, 159, (1994).

Magnetic Breakdown in a Molecular Conductor

Agosta, C.C., Clark Univ., Physics Dept.
Mielke, C.H., Clark Univ., Physics Dept.
Ivanov, S.A., Clark Univ., Physics Dept.
Howe, D.A., Clark Univ., Physics Dept.
Goettee, J.D., NHMFL–Los Alamos
Lacerda, A., NHMFL–Los Alamos
Tokumoto, M., ETL, Japan
Tanaka, Y., ETL, Japan
Kinoshita, N., ETL, Japan

We saw clear Shubnikov de Haas oscillations at 40 mK and up to 50 T due to the breakdown between an open and closed Fermi surface in the organic conductor k-$(BEDT\text{-}TTF)_2Cu(NCS)_2$ by using a dilution refrigerator in a pulsed magnetic field. These were the first measurements performed in the dilution refrigerator that was installed in the 50 T pulsed magnetic field apparatus at Los Alamos.

The transport measurements were made using AC detection at a frequency of ~900 kHz on small platelet shaped samples. The rise time of the pulsed magnet was approximately 6.5 ms and caused no appreciable sample heating on the time scale of the experiment, based on the identical data collected from both the up sweep and down sweep of the magnet pulse. However, the entire mixing chamber rose to approximately 100 mK after the pulse.

Figure 1 shows the magnetoresistance of $(ET)_2Cu(NCS)_2$ at 40 mK up to 50 T. The superconducting transition is seen at ~3 T, and large oscillations corresponding to the closed or α orbit indicate a frequency of 596 T. In the high field region the high frequency oscillations corresponding to the breakdown or β orbit can be easily seen. We used digital filtering to isolate the breakdown oscillations, shown in the inset, and found beats that match the phase and frequency of the α oscillations.

Our direct observation is that the amplitude of the β orbit is modulated and has nodes when the α oscillation is at a maxima or a minima. A straightforward cause of the β amplitude modulation would be a variation of the probability of tunneling across the band gap commensurate with the α oscillation. Thus we suggest that the tunneling probabilities across the Fermi surface gap are modulated by the Landau level filling on the 2D Fermi surface. More details of this experiment can be found in our paper.[1]

We would like to acknowledge National High Magnetic Field Laboratory at Los Alamos and D. Rickel in particular for his support. This work at Clark University is supported by the Air Force URI program grant #F49620-92-J-0525.

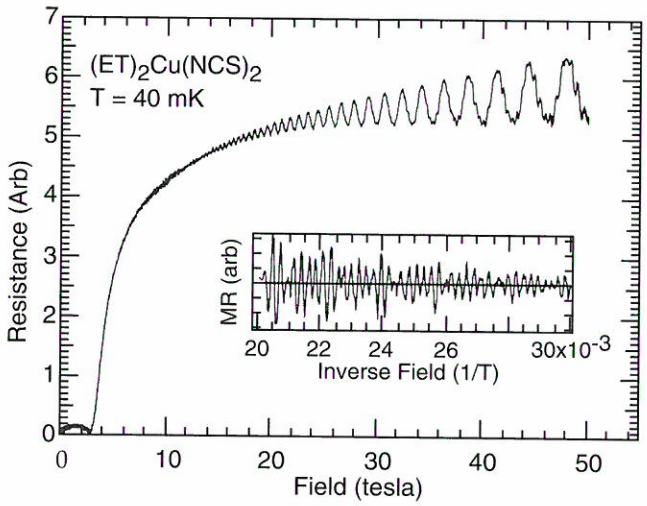

Figure 1. Magnetoresistance of a molecular superconductor. The inset shows only the resistance high frequency oscillations of the breakdown orbit.

Reference:

1 Agosta, C.C., et al., to be published in the proceedings of the Physical Phenomena in High Magnetic Field Conference by World Scientific (1995).

Superconductivity and Correlated Electron Properties of Molecular Conductors

Agosta, C.C., Clark Univ., Physics Dept.
Mielke, C.H., Clark Univ., Physics Dept.
Ivanov, S.A., Clark Univ., Physics Dept.
Howe, D.A., Clark University, Physics Dept.
Montgomery, L.K., Indiana Univ., Chemistry Dept.

We have done a number of experiments on new and old molecular conductors probing the superconducting properties and measuring the Fermi surfaces through quantum oscillations. As one example we measured the RF penetration in the superconductor λ-$(BETS)_2GaCl_4$ as a function of magnetic field at temperatures down to 0.25 mK. These measurements were done with the applied DC field parallel to the conducting planes. Combining these results with previous measurements we had made with the field perpendicular to the conducting planes we found the anisotropy of the critical magnetic field $H_{c\parallel}/H_{c\perp}$ to be 3.3. We also measured the penetration depth and transport properties of the related compound κ-$(BETS)_2GaCl_4$. We observed no superconductivity or quantum oscillation down to 25 mK in this material.

In another experiment a sample of $(TMTSF)_2ClO_4$ was placed in the dilution refrigerator in an attempt to measure the FISDW cascade. In contrast to previous experiments on $(TMTSF)_2ClO_4$ we placed the sample in the small coil of a self resonant circuit powered by a tunnel diode to measure susceptibility. The sample was cooled at a rate of about 25 mK/min. Because the FISDW phase transitions are thermodynamic in nature, we expected the oscillator to show a large frequency shift as the field swept through the different phases. Interestingly, only about half of the expected FISDW phases appeared on the signal. This was true at all the temperatures we tried, between 1500 and 40 mK. More work is needed to determine why only certain FISDW phases were seen.

In other newer compounds we failed to see superconductivity or a clear Fermi surface. This

work at Clark University is supported by the Air Force URI program grant #F49620-92-J-0525.

Angular Dependence of Quantum Oscillations, Magnetoresistance, and Magnetic Field Induced Phase Transitions in Quasi-Two-Dimensional Organic Molecular Conductors

Athas, G.J., Boston Univ., Physics Dept.
Brooks, J.S., FSU Physics Dept./NHMFL
Tanaka, Y., Electrotechnical Lab., Japan
Kinoshita, T., Electrotechnical Lab., Japan
Kinoshita, N., Electrotechnical Lab., Japan
Tokumoto, M., Electrotechnical Lab., Japan
Anzai, H., Himeji Institute of Technology, Japan

The Fermi surface (FS) topology of the Quasi-Two-Dimensional (Q2D) organic conductor family a-$(ET)_2MHg(SCN)_4$ [alpha- bis(ethylenedithio) tetrathiafulvalene-M (= potassium, rubidium, thallium, or ammonium) - mercury -thiocyanate] has been systematically studied in order to understand the different electronic ground-states and associated mechanisms in these isostructural materials.[1-3] The ammonium salt undergoes a superconducting transition at ~ 1 K, while the remaining three salts enter a unique Low Temperature State (LTS) below a characteristic temperature T_{DW}. Here a Peierls-like transition into either a Spin or Charge Density Wave (SDW or CDW) has been proposed to describe the LTS. Unlike the insulating state expected for a SDW or CDW, the FS reconstructs at T_{DW}, leaving the LTS metallic. This is due to the presence of two bands: the open orbit band is unstable at T_{DW} and becomes gapped, but the closed orbit band remains in a reconstructed topology. Therefore magneto-quantum oscillations are accessible in the LTS, and a thorough study of the magnetoresistance and Shubnikov-de Haas oscillations as a function of magnetic field strength and orientation has been applied. From these measurements we have determined the topological Fermi surface changes that occur in the formation of the LTS, mechanisms involving magneto transport in the LTS, and the nature of the LTS (SDW vs. CDW).

The experimental and theoretical results of this work[3] suggest that in the LTS the Fermi surface has hexagonal symmetry, and exhibits magnetic breakdown effects that are strongly influenced by magnetic field orientation. At special angles magnetic breakdown is suppressed, revealing dramatic changes in the DC and quantum oscillatory magnetotransport properties. A model, distinct from that proposed by others, is presented to describe the behavior. Additionally, the LTS state can be suppressed completely by an isotropic magnetic field (> 23 tesla), which is most consistent with the destruction of a CDW ground state in high magnetic field. Finally, the strong hysteresis associated with the magnetic field induced DW to metal transition, along with the observation of quantum oscillations from both the metallic and LTS structure lead us to propose a domain scheme for magnetic fields near the hysteretic region.

This research is supported by NSF-DMR-95-10427.

References:

1 Athas, G.J., Ph.D. Thesis, Boston University 1996.

2 Athas, G.J., et al., Phys. Rev. B (R.C.) 50, 17713-17716 (1994).

3 Athas, G.J., et al., to be published.

SdH Oscillations, Fermi Surface, and Phase Transitions in the Low Dimensional Conductor h-Mo_4O_{11}

Brooks, J.S., FSU Physics Dept./NHMFL
Fisk, Z., FSU Physics Dept./NHMFL
Uji, S., FSU Physics Dept./NHMFL
Terashima, T., National Research Institute for Metals, Tsukuba, Japan
Aoki, H., National Research Institute for Metals, Tsukuba, Japan
Valfells, S., Boston Univ., Physics Dept.
Sandhu, P.S., Boston Univ., Physics Dept.
Hill, S., NHMFL
Sarrao, J., NHMFL
Goettee, J.D., LANL

Low fields: At low magnetic fields, Shubnikov-de Haas (SdH) measurements (H < 14 T) have been performed to investigate the Fermi surface (FS) of the low dimensional conductor h-Mo_4O_{11}. This compound shows two CDW transitions at ~100K and 30 K, but remains metallic down to 50 mK. When H is perpendicular to the conduction plane (H//a), we can observe the large magnetoresistance with the SdH oscillations up to 10 K. The six different SdH oscillations with very low frequencies (F = 2.5 - 20.4 T) are evident in the Fourier transform spectra. The mass of each oscillation is measured to be $0.03m_o$ to $0.09m_o$. Judging from the relation of the frequency and the mass, the four fundamental oscillations (F = 2.5 T, 5.2 T, 7.7 T, and 20.4 T) are determined. The angular dependence of the frequencies suggests that all the FS's are cylindrical. The characteristic peaks observed in the angular dependent magnetoresistance exhibit that there are open orbits along the a-axis, which is consistent with the SdH results.

High fields: The low dimensional conductor h-Mo4O11 has very small cylindrical Fermi surfaces. Below the second CDW transition temperature (~30 K). The four fundamental oscillations (F = 2.5 T, 5.2 T, 7.7 T, and 20.4 T) have been found. The small FS's are caused by the imperfect nesting of the original FS's. When H is applied perpendicular to the conduction plane (H//a), the resistance shows

the SdH oscillations with the low frequencies (F < 21 T, ~0.2% of the original Brillouin zone) below ~15 T and then a steep increase at ~18 T (Hc). Above 30 T, the resistance saturates and the new SdH oscillations appear with the high frequencies (F = ~160 T and ~650 T). Hc increases as the temperature increases or as the field is tilted from the a-axis to the conduction plane. The observation of the high frequency SdH oscillations suggests that the nesting of the FS is removed by the high magnetic field. The steep increase of the resistance at ~18 T is presently being considered in terms of the quantum limit in the small FS's in the low field region and the instability of the CDW state at the high fields.

This research is supported by NSF-DMR-95-10427.

Alteration of Density Wave and Superconducting Behavior in Quasi-Two Dimensional Organic Conductors Under Uniaxial Stress

Campos, C.E., Boston Univ., Physics Dept.
Brooks, J.S., FSU Physics Dept./NHMFL
van Bentum, P.J.M., High Field Magnet Lab. and Research Institute for Materials, Univ. of Nijmegen, The Netherlands
Perenboom, A.A.J., High Field Magnet Lab. and Research Institute for Materials, Univ. of Nijmegen, The Netherlands
Sandhu, P.S., Boston Univ., Physics Dept.
Valfells, S., Boston Univ., Physics Dept.
Tanaka, Y., Electrotechnical Lab., Japan
Kinoshita, T., Electrotechnical Lab., Japan
Kinoshita, N., Electrotechnical Lab., Japan
Tokumoto, M., Electrotechnical Lab., Japan
Anzai, H., Himeji Institute of Technology, Japan

Superconductivity[1] has been induced with cross-molecular plane (b-axis) uniaxial stress in the density wave organic salt a-(BEDT-TTF)$_2$KHg(SCN)$_4$. The appearance of superconductivity, together with the associated rise in the carrier's effective mass, cannot be explained by a simple band effect; rather, electron-phonon and/or electron-electron interactions must play a predominant role. A new sample preparation method was devised to allow the measurement of resistance in these fragile crystals at stresses above 4 kbar. a-(BEDT-TTF)$_2$KHg(SCN)$_4$ belongs to the a-(BEDT-TTF)$_2$MHg(SCN)$_4$ (M = K, Rb, Tl, and NH_4) isostructural family of quasi-two dimensional organic salts. Under ambient conditions, the M = NH_4 salt is a superconductor below 1.1 K whereas the other three members have a density wave ground state below 10 K. Measurements of the low temperature magnetoresistance of the M = K salt indicate that the density wave state is quickly suppressed by 1.5 kbar, the point at which superconductivity (T_c = 1 K) appears. Similar measurements for the M = NH_4 salt showed that T_c rises to 3.5 K at 4 kbar. Thus it is shown that uniaxial stress effectively unifies the ground state behavior in this family of organic conductors. Analysis of the Shubnikov-de Haas oscillations revealed that the frequency of the hole orbits decreases linearly with stress in agreement with an expansion of the in-plane unit cell due to Poisson's effect, and there is a correlation between the real space area of the closed hole orbits and T_c for both materials under uniaxial stress or hydrostatic pressure. Also, for the M = K salt, a slow oscillation appears above 0.9 kbar, a sign that the nesting conditions of the open orbits changes dramatically with stress.

Preliminary investigations[2,3] of the effects of stress on the quasi-two dimensional superconductor k-(BEDT-TTF)$_2$Cu(NCS)$_2$ and quasi-one dimensional spin density wave insulator (TMTSF)$_2$PF$_6$ were also conducted. For k-(BEDT-TTF)$_2$Cu(NCS)$_2$ stress across the molecular planes (a-axis direction) reduced T_c rapidly and increased the frequency of the Shubnikov-de Haas oscillations. Both these results contradict the expectations based on a simple in-plane expansion due to Poisson's effect. For (TMTSF)$_2$PF$_6$ stress along the c-axis reduced the magnitude of the spin density wave particle excitation gap but did not reduce the metal-insulator transition temperature appreciably, which is inconsistent with the standard mean-field behavior.

This research is supported by NSF-DMR-95-10427.

References:

1 Campos, C.E., et al., Phys. Rev. B, 52, R7014 (1995).

2 Campos C.E., et al., Ph.D. thesis, Boston University, 1995.

3 Campos, E.C., et al., Physica B, 221, 293 (1995).

Electron-Electron Interactions and Precursor Effects in Q1D Conductors

Gor'kov, L.P., NHMFL

Peculiar properties of highly anisotropic Q1D materials, such as the Bechgaard salts, can be successfully interpreted in terms of interactions between electrons belonging to the two open Fermi surface sheets with approximate nesting features. However, a number of recent experimental results (Centre d'Orsay) may mean that this model needs some improvement. Experimentally, strong deviations from the Fermi liquid predictions have been seen in these materials, such as, huge magnetoresistance at rather high temperatures, deviations from the T^2-law in the temperature dependence of resistivity and, for the NMR-relaxation rate, deviations from the Korringa behavior. The effects are extended over a rather wide temperature range (~30 K).

It is shown[1] that the very same model displays some "precursor" features-the enhancement of various scattering processes, when the material under consideration is close enough to some instability (such as spin density wave, usually at T~10 K). This precursor behavior has not been noticed in the literature before. Its existence, in fact, extends the above non-Fermi liquid-like anomalies well beyond the vicinity of the mean field transitions, characteristic for the Bechgaard salts, where the critical fluctuations would become important. In Reference 1, implications of the mechanism were considered for the anomalous magnetoresistance. It remains to be seen that same effects may explain all the unusual features mentioned above.

Reference:

1 Gor'kov, L.P. "Precursor Effects and Anomalous Magnetoresistance in the Bechgaard Salts," Europhys. Lett., 31, 46 (1995).

High Field Investigation of $(TMTSF)_2PF_6$ at High Pressure

Hannahs, S.T., NHMFL
Immer, C., NHMFL
Tozer, S.W., NHMFL
Kang, W., Univ. of Chicago, Physics Dept.

We have measured the transport properties of the organic conductor tetramethyltetra-selenafulvalene at a range of pressures and magnetic fields. We have shown that near the pressure where the organic insulator to an Integer Quantum Hall Effect (IQHE) semi-metal, there is an existence of a mixed state. In this mixed state the SDW is partially suppressed. Transport measurements were made in BeCu piston hydrostatic clamps in fields up to 30 tesla. At low temperatures, varying the magnetic field shows anomalous hall resistance indicating a minimum in the carrier concentration. This minimum develops strongly at low temperatures. The magneto-resistance shows a change from a linear dependence on field to a quadratic dependence as the sample is cooled through a transition temperature of about 2 K.

The $(TMTSF)_2PF_6$ also was measured in diamond anvil pressure cells at the Los Alamos Pulsed Field Facility. At higher pressures the IQHE leads to an insulating state at very high fields. For a related compound $(TMTSF)_2ClO_4$, there exist sub-phases within this high field state.[1] A search for these sub-phases was conducted. The existence of such phases and their relationship to the symmetry of the anions in the molecular conductor are of considerable current theoretical interest.

Reference:

[1] McKernan, S.K., et al., Phys. Rev. Lett., 63, 1630-1633 (21 August 1995).

High Frequency, High Magnetic Field, Studies of the Complex Conductivity in the Organic Superconductor k-(BEDT-TTF)$_2$Cu(NCS)$_2$

Hill, S.O., NHMFL
Seeger, L., NHMFL
Brooks, J.S., FSU Physics Dept./NHMFL

Using a millimeter-wave vector network analyzer, we measure changes in the phase and amplitude of microwave radiation (35 - 150 GHz) reflected from a resonant cavity containing a single k-(BEDT-TTF)$_2$Cu(NCS)$_2$ crystal; these measurements have been carried out in magnetic fields of up to 30 T and in the temperature range 0.4 to 4.2 K. The resulting data can be related to changes in the real and imaginary components of the complex conductivity in the material under investigation. Quantum oscillations are clearly observed and are compared with conventional Shubnikov-de Haas oscillations seen in DC transport measurements. Particularly striking is the temperature and magnetic field evolution of the oscillations caused by the magnetic breakdown effect which differ markedly from DC measurements. The possibility of observing cyclotron resonance is also possible, and results in two independent estimates of the carrier effective masses from a single measurement. This technique highlights a new and exciting means for studying changes in the electronic properties of molecular metals in high and ultra-high magnetic fields.

This research is supported by NSF-DMR-95-10427.

A Study of the Molecular Metal (BEDO-TTF)$_2$ReO$_4$H$_2$O in a High Magnetic Field

Ivanov, S.A., Clark Univ., Physics Dept.
Agosta, C.C., Clark Univ., Physics Dept.
Howe, D.A., Clark Univ., Physics Dept.
Immer, C., NHMFL
Hannahs, S.T., NHMFL

We have done a series of magnetoresistance and penetration depth measurements on the title compound in magnetic fields up to 30 tesla (to 0.5 K) and 18 tesla (to 25 mK).

The BEDO-TTF molecule was first synthesized by T. Suzuki et al.[1] by replacing the four outer sulfur atoms of BEDT-TTF by oxygens. Although the BEDT-TTF molecule has been used in a number of superconducting compounds, BEDO-TTF has yielded significantly fewer superconductors, (BEDO-TTF)$_2$ReO$_4$H$_2$O being one of them.

The best (BEDO-TTF)$_2$ReO$_4$H$_2$O samples have a superconducting transition starting at T = 3.5 K[1]. Room temperature Fermi surface calculations predict electron and hole pockets of about 1.7% and 3.4%[1] of the First Brillouin Zone (FBZ). Experimental results, on the other hand, give sizes of about 0.8% and 1.7%[1] of the FBZ. Resistance measurements as a function of temperature show two transitions between room temperature and 4 K, which should be taken into account to explain the discrepancies between the band structure calculations and experimental results.

We have attempted to determine the superconducting phase diagram and to clarify the Fermi surface. Figure 1 shows the field dependence of resistance at T = 25 mK. Two sets of oscillations with frequencies of 38 and 74 tesla are clearly seen. The presence of additional unexplained harmonic content is clear at higher fields, for example, peaks at about 12.5 and 15 tesla. Magnetoresistance measurements in a hydrostatic pressure cell were also performed using a 28 tesla magnet. Preliminary results show a 168% change in the Fermi energy by increasing the pressure to 15 k bar.

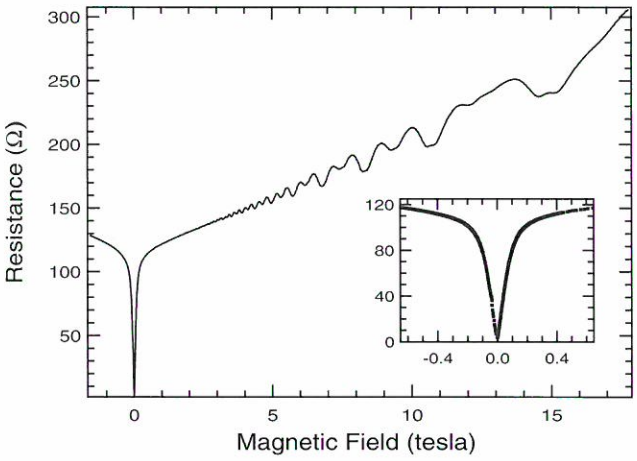

Figure 1. Magnetoresistance of $(BEDO\text{-}TTF)_2ReO_4H_2O$ at 25 mK. Inset shows the expanded view revealing a very broad superconducting transition.

References:

1 Suzuki, T., et al., J. Am Chem. Soc., 111, (1989) 3108.

2 Buravov, L.I., et al., J. Phys. I France, 2, (1992) 529.

3 Kahlich, S., et al., Phys. B, 94, 39 (1994).

4 Kovalev, A.E., et al., JETP Lett., 59, 560 (1994).

Angular Dependence of the Fermi Surface of a Molecular Metal to 50 Tesla

Mielke, C.H., Clark Univ., Physics Dept.
Agosta, C.C., Clark Univ., Physics Dept.
Goettee, J.D., NHMFL/Los Alamos
Lacerda, A., NHMFL/Los Alamos

Pulsed field studies to 50 tesla (T) of the angular dependent magnetoresistance of a layered molecular conductor were performed at the pulsed field facility at Los Alamos. The molecular based superconductors and metals of the organic family based on the BEDT-TTF molecule have produced the highest temperature organic superconductors as well as some of the most interesting quantum oscillations of all of the organics. The angular dependence of $(BEDT\text{-}TTF)_2$ TlHg $(SCN)_4$ is especially interesting due to the presence of a magnetic phase transition to a metallic state that occurs near 27 T at 450 mK. Giant Shubnikov deHaas (SdH) oscillations have recently[1] been observed above this magnetic transition. The angular dependence of the effect has been studied by use of a non-metallic rotational probe designed to operate at 400 mK in the 50 T pulsed field apparatus.

A series of 50 T experiments were performed at angles from 0 to 56 degrees between conducting planes and the magnetic field. It is interesting to note that there was little angular dependence associated with the 27 T magnetic transition as can be seen from Figure 1. Dramatic changes in SdH oscillations were observed at different angular orientations. The flattened oscillations that occur at the 10 and 25 degree orientations indicate the high harmonic content of the magnetoresistance. The presence of beats at 35 degrees and then a reappearance near 48 degrees helps clarify the degree of warping of the 2D Fermi surface. The sharp dips in magnetoresistance that occur near 50 degrees are qualitatively similar to those reported earlier[2] in studies performed in a hybrid DC magnet.

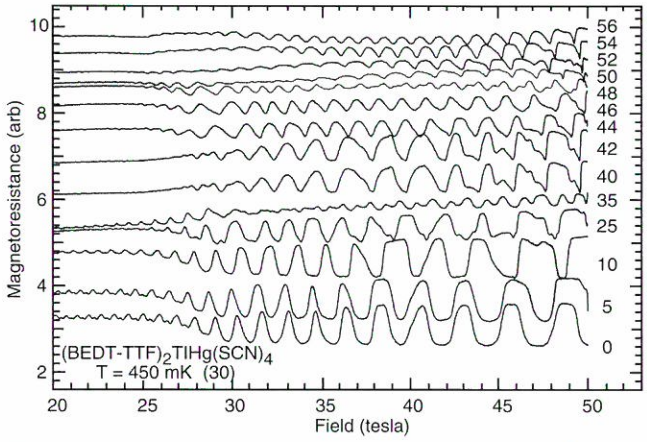

Figure 1. Magnetoresistance of $(BEDT\text{-}TTF)_2TlHg(SCN)_4$ at various field orientations.

References:

1 Agosta, C.C., et al., 11th Int. Conf. on High Magnetic Fields in Semiconductor Physics, p. 726 (1994).

2 Agosta, C.C., et al., Solid State Comm., 92, 939 (1994).

dHvA and SdH Study of (BEDT-TTF)$_2$TlHg(SeCN)$_4$

Naughton, M.J., SUNY Buffalo, Physics Dept.
Laukhin, V.N.,* SUNY Buffalo and Institute of Chemical Physics in Chernogoloka, Russia
Lee, I.J., SUNY Buffalo, Physics Dept.
Petrov, D., SUNY Buffalo, Physics Dept.
Kushch, N., ICP–Chernogolvka
Chaparala, M., NHMFL

We have studied Landau quantization phenomena in the so-called "Tl-Se" ET salt as functions of field, temperature and crystal orientation. Torque and magnetotransport were measured simultaneously, on what appears to have been a particularly high quality sample. We find that if we use the common analysis formulation for magneto-oscillatory phenomena, due to Lifshitz and Kosevich, we obtain dramatic variations of the cyclotron effective mass parameter with magnetic field, with orientation in field, and with measured quantity. For small tilt angles away from the normal to the quasi-2D layers, $m^*_{[SdH]}$ increases linearly with field, reaching 150% of its low field value at 17 T, while $m^*_{[dHvA]}$ is field-independent. At large tilt angles (~50°), both mass determinations decrease in field, though at different rates. We observe near perfect sawtooth torque oscillations at high angles, with extremely large harmonic content (40 harmonics! of the fundamental 650 T orbit via FFT), simultaneous to peculiar resistivity oscillations. The torque interaction phenomenon may play a role in the large angle data, although the absolute magnetization is small compared to the separation of oscillations in field. In addition, a smaller 47 T orbit was seen in both quantities, amounting to of order 1% of the 1st BZ. This orbit is not yet accounted for in band structure calculations. The disagreement between cyclotron mass determinations from susceptibility and conductivity remains to be explained. A more general problem is the fact that for such highly two-dimensional systems, the L-K procedure is probably invalid. Theoretical work addressing this problem will be required before proper interpretation of Landau quantization results on 2D metals will be possible.

This research is supported by the National Science Foundation and the National Academy of Sciences.

* Present, temporary affiliation is Institut de Ciencia de Materials de Barcelona, Bellaterra, Spain.

The Effect of Pressure and Uniaxial Stress on the Electronic Structure a-(BEDT-TTF)$_2$KHg(SCN)$_4$ and k-(BEDT-TTF)$_2$Cu(NCS)$_2$

Sandhu, P.S., Boston University, Physics Dept.
Campos, C.E., Boston University, Physics Dept.
Brooks, J.S., FSU Physics Dept./NHMFL
Ziman, T., Universite Paul Sabatier, Toulouse, France

We have performed extended Huckel tight-binding calculations to model the effects of pressure and uniaxial stress on the electronic band structure of the anisotropic organic metals a-(BEDT-TTF)$_2$KHg(SCN)$_4$ [a] and k-(BEDT-TTF)$_2$Cu(NCS)$_2$ [b]. The calculated changes in the Fermi surface topology are in excellent agreement with the experimental values determined from Shubnikov-de Haas measurements. In [a] the area of the closed orbits increases with pressure and decreases with uniaxial stress, while in [b] the closed orbits increase both with pressure and stress. We also report predictions of the effects of uniaxial stress in the perpendicular directions and discuss the behavior of the effective mass and magnetic breakdown probability.

This research is supported by NSF-DMR-95-10427.

^{77}Se NMR in the Spin Density Wave State of $(TMTSF)_2PF_6$

Valfells, S., Boston Univ., Physics Dept.
Brooks, J.S., FSU Physics Dept./NHMFL
Moulton, W.G., FSU, Physics Dept.
Kuhns, P.L., NHMFL
Kleinhammes, A., NHMFL
Anzai, H., Himeji Inst. of Tech., Japan
Takasaki, S., Himeji Inst. of Tech., Japan
Yamada, J., Himeji Inst. of Tech., Japan

We have measured the NMR linewidth, T_1 and T_2 of the ^{77}Se nuclei in the quasi-1D conductor $(TMTSF)_2PF_6$ above and below the spin density wave transition temperature, T_{SDW} = 12 K, at ambient pressure. For this purpose, an NMR probe capable of working in the high field resistive magnets at the NHMFL has been developed, and the data described here has been taken at 17.5 tesla. We observe four distinct lines at $T>T_{SDW}$ attributable to four non-equivalent selenium sites and shifted by $\Delta w/w \cong 0.7$, 1.9, 3.8 and 4.5 $x10^4$, respectively; they broaden to form a single, broad (about 900~kHz) line below T_{SDW}. The data, however, show no evidence of additional phase transitions at $T<T_{SDW}$ as previously reported by other workers[1] who have studied the proton line. Work is currently underway to resolve this finding, which may involve a fundamental difference in the behavior of the proton and selenium signals. This difference may be due to their relative symmetry and position with respect to the molecular orbital.

This research is supported by NSF-DMR-95-10427.

Reference:

1 Takahashi, T., et al., Synth. Met., 41-43 (1991) 3985-3988.

Temperature Dependence of the Integer Quantum Hall Effect in $(TMTSF)_2PF_6$

Valfells, S., Boston Univ., Physics Dept.
Wang, Z., Boston Univ., Physics Dept.
Brooks, J.S., FSU Physics Dept./NHMFL
Anzai, H., Himeji Inst. of Tech., Japan
Takasaki, A., Himeji Inst. of Tech., Japan
Yamada, J., Himeji Inst. of Tech., Japan
Tokumoto, M., Electrotechnical Lab. Japan

We have studied the temperature dependence of the integer quantized Hall transitions in the molecular crystal $(TMTSF)_2PF_6$. We find that they do not exhibit the universal scaling characteristics of the integer quantum Hall effect found in semiconducting devices: the slope, dr_{xy}/dB of the r_{xy} risers, and the width, $\Delta(1/B)$ of the r_{xy} peaks do not scale with temperature by a simple power law. Rather, we discuss this result[1] in terms of the spin density wave gap and the order parameter of the system. Specifically, in the limit of low temperatures these parameters are limited by the residual resistivity. For temperatures approaching the spin density wave transition, however, these parameters are described best as a function of the square of the BCS-like order parameter.

This research is supported by NSF-DMR-95-10427.

Reference:

1 Valfells, S., et al., to be published.

Investigation of Field Induced Phase Transitions in Quasi-One-Dimensional Inorganic Halide-Bridged Metal Linear Chain by Magneto-Raman Spectroscopy

Wei, X., LANL
Donohoe, R.J., LANL

The study of the low-dimensional materials is a key field in contemporary science from both the perspectives of understanding fundamental interactions (of electrons, phonons, spins, etc.) and prospect of applications. In particular, the quasi-one-dimensional inorganic halide-bridged metal

linear chain (M-X, M=Pt, Pd, Ni; X=Cl, Br, I) materials have attracted considerable attention. The ground state of an M-X chain can be characterized as a commensurate charge (or spin) density wave (CDW or SDW), depending upon the competition of electron-electron and electron-phonon interactions within M-X, which are sensitive to tuning by chemical substitution, pressure, doping, or magnetic field. There are important similarities in their physics to that of the high-temperature superconducting compounds.[1]

Recently, dc magnetization measurements on Pt-I, which has a weak CDW ground state, revealed a magnetic-field-induced strong diamagnetic transition (up to 70% of complete diamagnetism, the "Meisner effect") at fields above 6 tesla.[2] Whether this phase transition leads to superconductivity in Pt-I is not clear at the present time, in part as a result of the difficulty in measuring its resistivity.

To further study the spin-correlation in Pt-I under magnetic field, we plan to conduct magneto-Raman measurements on Pt-I at NHMFL/LANL, to examine whether there is any field-induced SDW phase before the diamagnetic phase transition, by detecting the inelastic light scattering signal of SDW's elementary excitations, magnons.

The preliminary data that we took in our first experiment at NHMFL during 9/18/95-9/28/95 do not reveal any signal due to magnons. However, intensity of the normal Pt-I Raman signal (ν_1 mode) changes with magnetic field H. Figure 1 illustrates the ν_1 mode Raman signal of Pt-I at fields of 0 and 18 tesla, respectively, and Figure 2 shows its relative intensity as a function of magnetic field. Because ν_1 mode is not expected to be detected if the bulk undergoes phase transition to superconductivity, our preliminary data are in agreement with the experimental results of Reference 2.

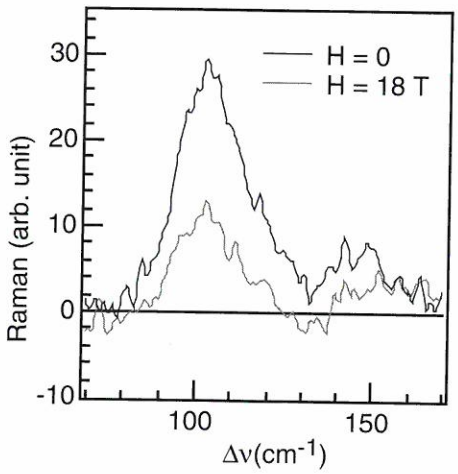

Figure 1. Raman spectra of Pt-I under H.

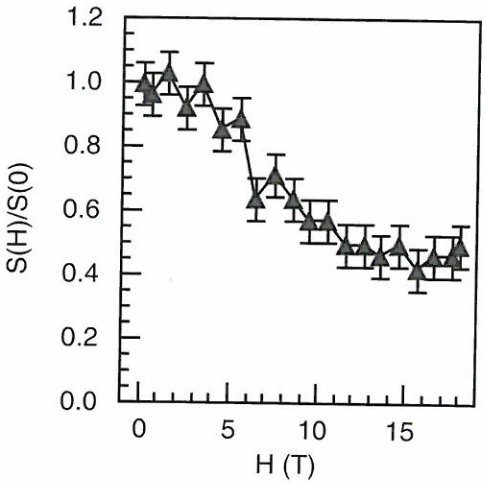

Figure 2. Relative Raman intensity vs. H.

References:

1 Bishop, A.R., et al., L. A. Science, 21, 133 (1993).

2 M. Haruki et al., Phys. Rev. B, 43, 6273 (1991).

Gauge Fluctuations in Composite Fermion Metals

Bonesteel, N.E., NHMFL
Nayak, C., Princeton Univ., Physics Dept.
McDonald, I., Penn. State Univ., Physics Dept.
Melik-Alaverdian, V., NHMFL

The aim of this research is to better understand the experimental consequences of the gauge theory of the $\nu = 1/2$ composite fermion metal first developed by Halperin, Lee, and Read.[1] For example, a symmetrically doped double layer electron system with total Landau level filling fraction $\nu = 1/m$ decouples into two even denominator $\nu = 1/2m$ composite fermion "metals" when the layer spacing is large. Out-of-phase fluctuations of the statistical gauge fields in this system mediate a singular attractive interlayer pairing interaction.[2] Because the metallic "normal" state of this system is not a Landau Fermi liquid it is not obvious that this pairing interaction leads to a superconducting instability. A strong-coupling analysis was performed which showed that the out-of-phase gauge fluctuations acting alone indeed lead to a pairing instability. It was also shown that the pair-breaking effects of the less singular in-phase gauge fluctuations reduce the gap at zero temperature but do not eliminate the instability. We therefore concluded that a double-layer composite fermion metal is *always* unstable to the formation of a paired quantum Hall state, regardless of layer spacing.[3] The experimental observation of this paired state would provide a striking confirmation of the gauge theory description of the $\nu = 1/2$ state proposed by Halperin, Lee, and Read. The connection between this paired state and the experimentally observed $\nu = 1/m$ double-layer quantum hall states is the subject of ongoing investigation.

References:

1 Halperin, B.I., et al., Phys. Rev. B, 47, 7312 (1993).

2 Bonesteel, N.E., Phys. Rev. B, 48, 11484 (1993).

3 Bonesteel, N.E., et al., Preprint.

Numerical Studies of Composite Fermions in the Fractional Quantum Hall Effect

Bonesteel, N.E., NHMFL
Melik-Alaverdian, V., NHMFL

The aim of this research is to develop new numerical tools for making *quantitative* calculations based on the composite fermion theory. Current projects include:

Landau Level Mixing Effects. We have recently developed numerical tools for studying the effect of Landau level mixing on FQHE states.[1,2] Our results have led to new insights into the effect of Landau level mixing on the various excitations in the FQHE as well as its relation to the so-called "finite thickness" correction.

Monte Carlo Comparison of Trial Quasielectron Wave Functions. For the truncated pseudopotential (V_1) model the excitation energy of the $\nu = 1/3$ composite-fermion based quasielectron wave function proposed by Jain has recently been shown to be ~ 20% lower, and consequently significantly closer to the exact quasielectron excitation energy, than that of the quasielectron wave function originally proposed by Laughlin.[3,4] This result was obtained by extrapolating results for finite systems, containing up to 10 electrons, to the thermodynamic limit. It

was also observed that the energy difference between the two wave functions was strongly dependent on system size. Motivated by these observations we have been carrying out variational Monte Carlo calculations in order to compare the excitation energies of these two trial wave functions for larger system sizes and for the physically relevant case of long-range Coulomb interactions.

Spin in the QHE. According to "one-electron" theory the gap in the integer QHE is the energy required to promote an electron from the highest filled Landau level to the lowest empty Landau level. In *n*-type GaAs the Zeeman splitting is a factor of 50 smaller than the cyclotron energy. Thus in the absence of electron correlations the energy gap for odd integer QHE states would be the Zeeman energy required to flip a spin. If this were true then in the limit of zero Zeeman splitting the gaps for odd integer QHEs would collapse leaving only even integer QHEs. Recently, it has been shown that the conventional one-electron theory of the integer QHE is incorrect; electron-electron interactions are crucial for the integer QHE, just as they are crucial for the fractional QHE.[5] Specifically, it was shown in Reference 5 that due to Coulomb repulsion the odd integer QHE persists even in the limit of zero Zeeman splitting. The gap is then set be the typical Coulomb energy $e^2/\varepsilon l_0$ — the *exchange energy* required to flip a spin. In addition, for certain parameters the lowest lying excitations were not flipped spins but rather extended objects called "skyrmions." Recently, Barrett et al.[6] have observed these skyrmions for the $\nu = 1$ QHE by measuring the Knight shift in a multiple GaAs-AlGaAs quantum well structure. Similar experiments are being prepared at the NHMFL by Prof. C. Bowers and collaborators at the University of Florida at Gainesville.

The aim of our theoretical research on skyrmions is to perform realistic calculations of the excitation energy, stability and size of the skyrmion in both the integer and fractional QHE. To do this we are using the same Monte Carlo techniques we have used successfully to study composite fermions. This work is still at an early stage.

References:

1 Bonesteel, N.E., Phys. Rev. B, 51, 9917 (1995).

2 Melik-Alaverdian, V., et al., Phys. Rev. B, 52, 17032 (1995).

3 Girlich, U., et al., Phys. Rev. B, 49, 17488 (1994).

4 Kasner, M., et al., Phys. Rev. B, 48, 11435 (1993).

5 Sondhi, S., et al., Phys. Rev. B, 97, 16419 (1993).

6 Barrett, S.E., et al., Phys. Rev. Lett., 74, 5112 (1995).

NMR Detected Optical Dynamic Nuclear Polarization Studies of ^{69}Ga in GaAs and ^{115}In in InP

Bowers, C.R., UF, Chemistry Dept.
Kuhns, P.L., NHMFL
Kleinhammes, A., NHMFL
Schmiedel, T., NHMFL
Sloan, S.M., UF, Chemistry Dept.
Chabrier, P., UF, Chemistry Dept.
Moulton, W.G., NHMFL/FSU Physics Dept.

Nuclear Magnetic Resonance has proved to be a very valuable local probe to study the dynamics of electronic interactions in many systems of interest to condensed matter physicists. Unfortunately it suffers from inherently low sensitivity, requiring on the order of 10^{18} nuclei at temperatures near 300 K for adequate signal to noise. This is due to the low value of local moments and the resulting small thermal population difference. In appropriate systems this can be enhanced by 4 to 5 orders of magnitude by optical pumping, as discovered by Lampel nearly 30 years ago.[1] This enhancement comes about by the Overhauser cross relaxation between nuclei and optically oriented conduction electrons trapped at point defects. At low temperatures, in the range of a few Kelvin, the nuclear spin-lattice relaxation can be dominated by hyperfine coupling to the electrons, yielding large nuclear polarizations when

the electron spin states are defined by optical pumping. Most of the previous work in optical dynamic nuclear polarization (ODNP) has utilized optical detection, which limits the magnetic field range to below about 0.2 T. In this work we utilize NMR detection and carry out our studies at fields to 20 T.

Studies of the NMR signal produced by ODNP ^{69}Ga in GaAs and ^{115}In InP were made from 1.5 K to 4.2 K in fields up to 24 T in the resistive magnets at the NHMFL. The procedure was to set the NMR frequency and field for the NMR probe, optically pump at any set field, and return to the NMR probe field in a time short compared to the spin lattice relaxation time and measure the polarization by the integrated intensity of the NMR line. This was made possible by the rapid sweep time of the magnets, typically 0.4 T/s. An example of the ^{69}Ga signal with and without optical pumping is shown in Figure 1a. Unpolarized laser radiation was used in the initial experiments. By scanning the laser wavelength, the band gap was observed in the NMR signal intensity, with no enhancement below the gap, and enhancement of several orders of magnitude above the gap. Studies of the pumping efficiency as a function of field show a monotonic increase to about 5 T, and then a gradual decrease to 20 T as can be seen in Figure 1b. A model for this behavior has been proposed. Studies using polarized pumping light are in progress.

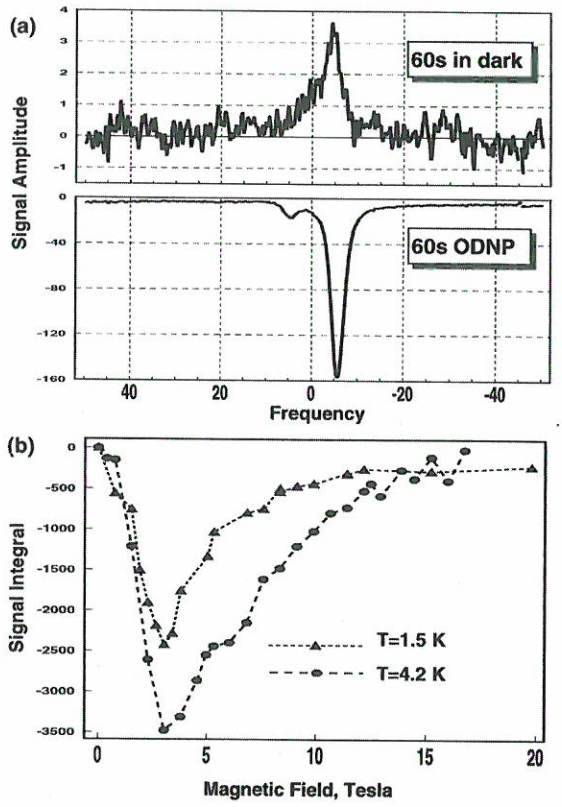

Figure 1. (a) NMR spectra of ^{69}Ga in semi-insulating GaAs substrate after 60 seconds with (bottom) and without (top) optical irradiation. Note that the ODNP signal is both emissive and enhanced with respect to the "dark" signal. (b) Field dependence of the ODNP effect in the same sample at two different temperatures.

Reference:

1 Lampel, G., Phys. Rev. Lett., 20, 491 (1968).

The Spin of Composite Fermions

Du, R.R., Univ. of Utah, Physics Dept.
Yeh, A.S., Princeton Univ., Elect. Eng.
Störmer, H.L., AT&T Bell Laboratories
Tsui, D.C., Princeton Univ., Elect. Eng.
Pfeiffer, L.N., AT&T Bell Laboratories
West, K.W., AT&T Bell Laboratories

The composite fermion model[1-2] provides an elegant description of certain sequences of states in the fractional quantum Hall effect (FQHE). The model incorporates the Coulomb interaction between carriers in high magnetic fields with the adiabatic attachment of an even number of magnetic flux quanta to each electron. This attachment gives rise to new particles, named composite fermions (CFs). At even denominator Landau level filling factors ν, the attached flux and the external flux cancel exactly, and the CFs appear to move in a vanishing magnetic field. In other external fields, this cancellation is not exact, and the CFs experience some non-zero residual field and hence, Landau quantization of CFs. This gives rise to the characteristic transport features of the FQHE. In this sense, the FQHE states of the electrons are equivalent to the integral quantum Hall effect (IQHE) states of the CFs.

The CF model has been very successful in interpreting the series of FQHE states near the even denominator fraction $\nu = 1/2$. Activation energy and Shubnikov-de Haas measurements[3-6] allow the

semiclassical determination of the effective mass, while geometrical resonance experiments[7-9] have demonstrated the existence of a well-defined Fermi wave vector and semiclassical trajectories. While considering other properties of the CF, questions about its spin and g factor naturally arise. Since a CF consists of one electron and several flux quanta, one may expect the electron spin to carry over. However, the size of the Zeeman splitting is unclear; in two-dimensional systems, it depends on the filling factor through exchange interaction.

We tackle these questions by examining the FQHE near $\nu = 3/2$, where spin effects are known to be significant. Our experimental results[10] on a GaAs-AlGaAs heterostructure find a beautifully simple interpretation of the FQHE states in terms of CFs carrying a spin. At any given FQHE state, the CFs fill an exact multiple of spin-split CF Landau levels; the CF Fermi energy resides in the gap; and one observes the characteristic R_{xx} minimum. By tilting the sample in field, one can force the spin splitting (found to be proportional to the total field) and the Landau level splitting (determined by the perpendicular component of the field) to shift with respect to each other. At very specific angles, when a spin level of one CF Landau level coincides with the spin level of another CF Landau level at the CF Fermi energy, what was formerly a gap disappears, leading to a maximum in R_{xx}. Then, by explicitly computing the CF energy levels from our results, it is straightforward to deduce the spin polarizations of the CF system at any filling fraction and Zeeman energy. Finally, the g factor of the CF is found to be largely the g factor of the electron.

References:

1 Jain, J.K., Phys. Rev. Lett., 63, 199 (1989); Phys. Rev. B 40, 8097 (1989); 41, 7653 (1990).

2 Halperin, B.I., et al., Phys. Rev. B, 47, 7312 (1993).

3 Du, R.R., et al., Solid State Commun. 90, 71 (1994).

4 Leadley, D.R., et al., Phys. Rev. Lett., 72, 1906 (1994).

5 Manoharan, H.C., et al., Phys. Rev. Lett., 73, 3270 (1994).

6 Du, R.R., et al., Phys. Rev. Lett., 73, 3274 (1994).

7 Willett, R.L., et al., Phys. Rev. Lett., 71, 3846 (1993).

8 Kang, W., et al., Phys. Rev. Lett., 71 3850 (1993).

9 Goldman, V.J., et al., Phys. Rev. Lett., 72, 2065 (1994).

10 Du, R.R., et al., Phys. Rev. Lett., 75, 3926 (1995).

High Field Transport Measurements on III-V Compounds

Geerts, W.J.M.A., NHMFL/UF Dept. of Materials Science

MacKenzie, J.D., NHMFL/UF Dept. of Materials Science

Pearton, S.J., NHMFL/UF Dept. of Materials Science

Abernathy, C.R., NHMFL/UF Dept. of Materials Science

Schmiedel, T., NHMFL

Introduction: Although GaN/InGaN are successfully applied in commercial blue LEDs, the theoretical understanding of their transport properties is still unclear: possible deep levels, the role of defects, the compensation and/or the presence of impurity bands make the interpretation of transport data difficult. We conducted research on the magneto-transport properties of GaN, InN, and InGaN as a function of the temperatures in high fields. Some preliminary results are reported here.

Experimental procedure: The samples were made by MOMBE.[1] The GaN was p-doped with carbon ($p \sim 10^{17}$ cm^{-3}). The InN and InGaN samples were not intentionally doped but contained a background n-doping of respectively 10^{19} and 10^{20} electrons/cm^3. The transport properties were determined by Van der Pauw geometry Hall/ resistivity measurements using annealed alloyed

HgIn contacts. The low field (0.62 tesla) electrical properties were determined as a function of the temperature (8-300 K). Additional high field (0-30 tesla) measurements were performed at 4, 77, and 300 K.

Experimental results and discussion: For the InN and InGaN samples, both the resistivity and the Hall voltage appeared to be constant over the investigated temperature range 8-300 K, is an indication for impurity band conduction. The high field measurements revealed a positive magnetoresistance coefficient and a positive magneto-Hall coefficient for the InN that could be caused by inhomogenities. The InGaN had a negative magnetoresistance relating to spin dependent scattering on unpaired electrons. At low temperature (4 K) its resistance saturated for fields of 12 Tesla. Above 17 tesla a peculiar hysteresis was observed in the resistivity results. For the GaN sample, the Hall and resistance curves versus temperature showed a maximum and a minimum respectively that suggests a multiband conduction. At low temperature a large positive magnetoresistance was observed due to magnetic field confinement of the impurity wave-functions.

Planned investigations: The temperature range will be extended to 1.8-400 K to determine the location of the impurity bands. A study of the high field anomaly of InGaN and determination of the effective mass of GaN via the Mott transition are also planned.

Reference:

1 Abernathy, C.R., et al., Appl. Phys. Lett., 66, 1632 (1995).

Magneto-Optical Studies on ZnSe/GaAs Single Quantum Well Structures

Haetty, J., SUNY at Buffalo, Physics Dept.
Yu, W.Y., SUNY at Buffalo, Physics Dept.
Petrou, A., SUNY at Buffalo, Physics Dept.
Schmiedel, T., NHMFL
Furdyna, J.K., Univ. of Notre Dame, Physics Dept.

We have carried out reflectivity and optical absorption studies of ZnSe/GaAs and ZnMnSe/GaAs heterostructures in the vicinity of the fundamental bandgap. The experiments were carried out at 4.2 K and in magnetic fields up to 30 tesla. Optical absorption experiments were carried out on samples in which the GaAs substrate was removed by chemical etching. Magnetic fields were applied perpendicular to the layers of the structure. Below, we summarize the results from some of the heterostructures that were studied.

Sample 1: ZnSe/GaAs/ZnSe (10 nm/10 nm/10 nm) single quantum well.

The reflectivity spectrum reveals a sharp feature at 1515 meV and a broader one at 1522.5 meV. They are attributed to the bulk exciton from the buffer and the e_1h_1 exciton from the quantum well, respectively. This interpretation was verified by the experiments carried out in the presence of a magnetic field. When we plot the exciton energies as function of applied field, for sample 1, we see the diamagnetic shifts of both the bulk and the e_1h_1 excitons. In addition, we observe the magneto-excitons[1,2] associated with both types of transitions.

Sample 2: ZnMnSe/GaAs/ZnMnSe (20 nm/6 nm/20 nm) single quantum well.

In addition to the strong GaAs buffer bulk exciton, we observe also the e_1h_1 exciton associated with the quantum well at 1532 meV. The latter appears in the optical absorption spectra. The above interpretation was verified by the high magnetic field reflectivity data.

It appears that the suggestion by Ramesh, et al.,[5] that the conduction band offset is small, is true. The mystery remains that the ZnSe-on-GaAs conduction band offset was reported to be between 300 and 400 meV by Olego.[4] It is possible that the GaAs-on-ZnSe interface is different, which would result in asymmetric confinement potentials for electrons and holes. A recent study[3] indicates that the band offsets depend on the growth conditions. For example, valence band offsets of 600 meV were obtained for Se-rich interface terminations. This would make the ZnSe/GaAs a uniquely flexible semiconductor system for device applications. The

conclusion of this preliminary study is that the MBE growth of high optical quality GaAs/ZnSe and GaAs/ZnMnSe heterostructures is feasible, and that this system offers the possibility for electro-optical applications in the yellow.

References:

1 Duggan, G., Phys. Rev. B37, 2759 (1988).

2 Dutta, M., et al., Phys. Rev. B42, 1474 (1990).

3 Franciosi, A., Bull. Am. Phys. Soc. 40, 562 (1995).

4 Olego, D.J., Phys. Rev. B39, 12743 (1989).

5 Ramesh, S., et al., J. of Crystal Growth, 115, 333 (1991).

Electron Dynamics in Spacially Varying Magnetic Fields

Hu, J., NHMFL
Schrieffer, J.R., NHMFL

We have studied the problem of an electron moving in (1) a periodic magnetic field

$$\vec{B}(\vec{r}) = \left(B_o + B_1 cos(\frac{2p}{a} x) \right) \hat{e}_z,$$

where a is the periodicity of the field and (2) $\vec{B}(\vec{r}) = (B_1 x / L)\hat{e}_z$, i.e., grad B = constant.

1. Choosing the Landau gauge $\vec{A} = (0, B_0 x + (B_1 a / 2\pi)\sin(2\pi x / a), 0)$, Schrödinger's equation can be reduced to a one-dimensional problem:

$$-\frac{\hbar^2}{2m} \cdot \frac{d^2\psi(x)}{dx^2} + V(k_y, x)\psi(x) = E(k_y)\psi(x)$$

with

$$V(x) = \frac{\hbar^2 Q^2}{2m} \left(\frac{k_y}{Q} + \frac{Qx}{(Q\ell_0)^2} + \frac{\sin(Qx)}{(Q\ell_1)^2} \right)^2$$

where $Q = 2\pi / a$, $\ell_0^2 = \hbar / eB_0$ and $\ell_1^2 = \hbar / eB_1$. The system size is given by $L_x = N_x a$ and $L_y = N_y a$. The wave functions and energies are numerically calculated to high accuracy for both the $B_0 = 0$ and $B_0 \neq 0$ cases. Instead of degenerate Landau levels, the energy spectrum forms a magnetic band structure consisting of a set of "Landau bands," which are a periodic function of k_y with period a / ℓ_0^2. The calculated density of states shows interesting behavior. We study the de Haas-van Alphen effect and cyclotron resonance for the dynamics of electrons in the periodic magnetic field and discuss the effects of the periodic field component on other interesting properties of electrons in an otherwise uniform magnetic field.

2. Since $\vec{A} = B_1 x^2 / 2L$ in this case, the effective potential is a quartic oscillator $V(x) = (\hbar^2 / 2ml_1^2)(k_y l_1 + x^2 / l_1 L)^2$ versus the harmonic oscillator corresponding to B = constant (Landau levels). For negative k_y, V has double minima at $\pm l_1 \sqrt{k_y L}$, and the energy spectrum has low lying states which form pairs of bonding and antibonding states in the two wells, split in energy by a weak tunneling between the minima. Magneto optical absorption has been calculated for this case. We are discussing methods of physically realizing these field configurations, using microfabrication and/or laser interferometry for Case 1 (with S. von Molnár) and multipole magnets for Case 2 (with H. Schneider-Muntau).

Interlayer Coherence in Double-Layer Quantum Dots

Hu, J., NHMFL
Dagotto, E., NHMFL
MacDonald, A.H., Indiana Univ., Physics Dept.

There has been considerable interest in the double layer system[1] as well as the system with small number of electrons confined into a single quasi-two dimensional quantum dot[2] in the presence of a magnetic field. Advances in

nanofabrication technology have made it possible to realize these artificial systems. Recent experimental and theoretical[1] studies of a double layer two-dimensional electron system in a high magnetic field have shown a rich variety of new incompressible states related to the quantum Hall effect due to the spontaneous interlayer coherence, such as the existence of an incompressible quantum Hall state at a filling factor of individual layers $\nu = 1/2$ in the absence of interlayer tunneling. On the other hand, the work done in single quantum dot system in strong magnetic field has shown other interesting effects, for example the stability of the maximum-density-droplet (MDD) state which is the ground state in the absence of electron-electron interactions and the low-lying edge excitations and electron-hole excitations associated with the MDD state.[3] In this work, we combine these two systems to study double-layer quantum dot system[4] in the strong magnetic field and the role of the interlayer coherence in stabilizing the "maximum density droplet" state. We construct the phase diagram in terms of the interlayer distance and confinement potential in which the MDD state is stable. In the stable region of MDD state, we study the collective excitations of double-layer quantum dot systems using the equation of motion approach by Hartree-Fock approximation.

References:

1 Girvin, S.M., et al, *Novel Quantum Liquids in Low-Dimensional Semiconductor Structures,*" edited by Das Sarma, S., and Pinczuk, A., (Wiley, New York, 1995), and reference there in.

2 Chakraborty, T., *Comments Condensed Matter,* Phys., 16 35 (1992).

3 MacDonald, A.H., et al., Aust. J. Phys., 46, 345 (1993).

4 Palacios, J.J., et al., Phys. Rev. B, 51, 1769 (1995).

Is Collapse of Spin Splitting in the Quantum Hall Effect a Phase Transition?

Jiang, H.W., Univ. of California, Los Angeles, Physics Dept.

Wong, L.W., Univ. of California, Los Angeles, Physics Dept.

Palm, E., NHMFL

The collapse of the spin splitting in the quantum Hall effect (QHE) at low-magnetic field is a well-known experimental effect. While it is conventionally believed that the "collapse" is the result of a finite temperature that "smears" the resolution of the two levels, a recent experiment[1] suggests a very abrupt termination might actually be taking place, indicative of a critical point. The question of whether or not there is a phase transition from a spin-split QHE to a spin-degenerate QHE is crucial in establishing the topology of a global phase diagram in the QHE. With a view toward resolving this issue, two theoretical models have been proposed.[2,3] At the NHMFL, we have conducted a sequence of experiments with a gated high-mobility GaAs/AlGaAs heterostructure to systematically determine the nature of this phenomena. The difference in filling factors of the spin-split peaks, $\delta\nu_N = \nu_{N\uparrow} - \nu_{N\downarrow}$, is measured as a function of density n, the effective disorder, for five spin-split Landau levels with index N = 1,2,3,4 and 5. We find that $\delta\nu_N$ goes continuously from one to zero and collapses into a single curve when it is plotted as a function of $(n-n_c)/n_c$ as shown in the figure. By continuously tilting the plane of the two-dimensional electron gas with respect to the direction of the magnetic field, we have observed the broadening of the transition with increasing Zeeman energy. Our data presents experimental evidence that in the limit of zero Zeeman energy, this collapse of spin-split Landau levels can be described as a continuous phase transition.

This research is supported by NSF under grant number DMR-93-13786.

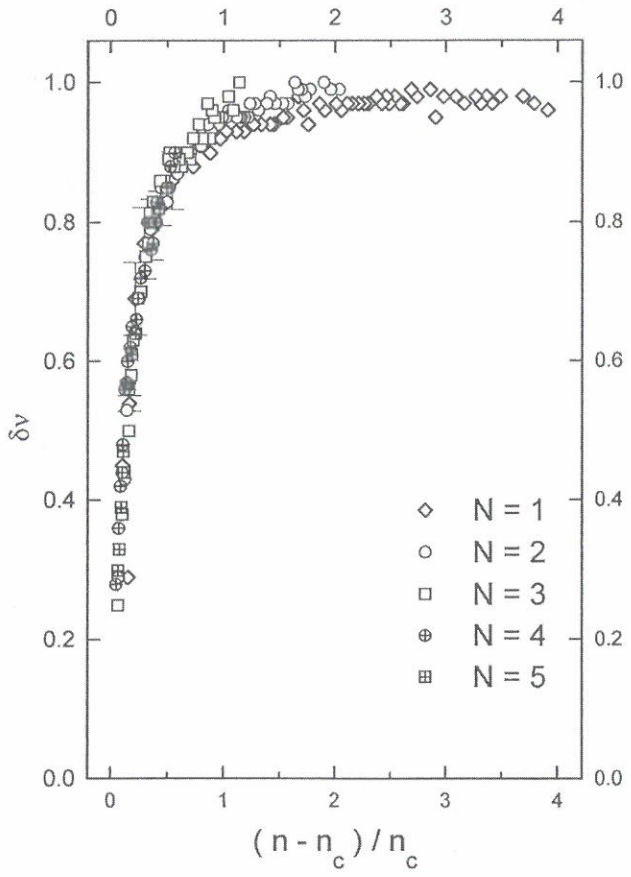

Figure 1. $\delta\nu_N$ is plotted against the dimensionless parameter $(n-n_c)/n_c$ for five spin-split Landau levels, N = 1, 2, 3, 4, and 5.

References:

1 Glozman, I., et al., Phys. Rev. Lett., 74, 594 (1995).

2 Fogler, M.M., et al., preprint.

3 Tikofsky, A.M., et al., preprint.

Optical Determination of the Effective Mass and Binding Energy for a $Si_{0.83}Ge_{0.17}$/Si Quantum Well

Jones, E.D., Sandia National Laboratories
Kurtz, S.R., Sandia National Laboratories
Schmiedel, T., NHMFL
Houghton, D.C., National Research Council, Canada
Lee, K.-S., Electronics and Telecommunications Research Institute, S. Korea
Lee, H., Sandia National Laboratories and Kyunghee University, Phys. Dept., S. Korea

The purpose of this magnetoluminescence study of biaxially compressed $Si_{0.83}Ge_{0.17}$ grown on Si is to determine the effective mass of heavy holes by measuring the diamagnetic shift of interband transitions. This report is a continuation of *1994 NHMFL Annual Report* (page 59). Our study reports the determination of the effective heavy hole mass of undoped SiGe/Si quantum well using magnetoluminescence and helps to clarify the scattered values measured by other techniques.[1,2]

We have performed 1.8 K high field magnetoluminescence measurements, up to a maximum field of 27 T, on a high quality undoped $Si_{0.83}Ge_{0.17}$ quantum well grown by molecular beam epitaxy (MBE). We observe several features at zero field such as a no-phonon (NP) peak at (1.0532±0.0004) eV, the transverse acoustic (TA) phonon at 1.0373 eV, the Si-Si two transverse optic (2TO) phonon at 1.0334 eV, and a Si-Si TO peak at (0.9959±0.0006) eV. The diamagnetic shift of the $Si_{0.83}Ge_{0.17}$ no-phonon and TO phonon peaks due to two dimensional excitons is about 1.7 meV at 27 T for both 20 Wcm^{-2} and 50 Wcm^{-2} laser power densities.

The diamagnetic shift of a ground state exciton of a quantum well can be estimated using a variational calculation. Lee and others[3] modified perturbation approach can fit diamagnetic shifts to arbitrary magnetic field strengths. Using a standard trial wave function that is a product of a hydrogenic and a harmonic oscillator wave function, we fit the diamagnetic shift and get a binding energy (14.8 ± 0.1 meV) and reduced mass (0.165 ± 0.01 m_0), independent of laser power.

Unlike GaAs or InGaAs, the electrons in a $Si_{1-x}Ge_x$ quantum well thermalize to the Δ point of the Brillouin zone for $x \leq 0.15$. Depending on whether there is a compressive or tensile strain, the ground state is Δ_x and Δ_y or Δ_z, respectively. With field direction along the growth direction, the in-plane electron masses are a mixture of m_t and m_l for a compressive strain. For the values of electron masses of the strained $Si_{0.83}Ge_{0.17}$ quantum well, we use the values, $m_l = 0.91m_0$ and $m_t = 0.20\ m_0$ of bulk $Si_{0.83}Ge_{0.17}$ calculated by Rieger and Vogl.[4] Because the $Si_{0.83}Ge_{0.17}$ quantum well is

compressively strained, we use an average value of in-plane electron masses of m_l and m_t. As an *Ansatz*, we use the cyclotron mass value as an average electron mass value even though the cyclotron mass is justified for free carriers. The in-plane cyclotron mass (which is coincidentally equal to density of states mass) of quasi-2 D system of electrons is given by $\langle m_e \rangle = \sqrt{m_t m_l} = 0.47\ m_0$. From the reduced mass, using $m = [1/\langle m_e \rangle + 1/m_{hh}]^{-1}$, we get $m_{hh} = 0.27 m_0$. The mass value is consistent with magneto-transport values reported by Whall et al.[2] using low density carriers. Therefore, our optical data show that the larger values of effective heavy hole masses reported by Cheng et al.[1] may indeed be due to non-parabolicity at high carrier densities.

Acknowledgment: This work was supported by U.S. DOE contract, DE-AC04-94AL85000 and a portion of this work was performed at the NHMFL.

References:

1 Cheng, J.-P., et al., Appl. Phys. Lett., 64, 1681, (1994).

2 Whall, T.E., et al., Appl. Phys. Lett., 65, 3362, (1994).

3 Lee, K.-S., et al., Phys. Rev. B46, 10269, (1992).

4 Rieger, M.M., et al., Phys. Rev. B48, 14276, (1993) and references therein.

miniature diamond anvil cell. At all pressures, the 0_0 Landau level transition was linear in magnetic field, but there is some evidence of a slope change for fields of about 25 T. The pressure coefficients of the bandgap energy, 0.9-1.0 meV/GPa, fall nicely within the range observed for III-V materials. We also observed the Γ-X pressure induced transition between the InGaAs Γ-point and the GaAs barrier X-point at the highest pressures. From these measurements, the pressure coefficients of the conduction and valence-band masses can be determined and used to refine the ab-initio band structure calculations and provide a better understanding of these low dimensional systems.

Future measurements will use pressure and magnetic field in order to determine the source of luminescence in large-bandgap materials.

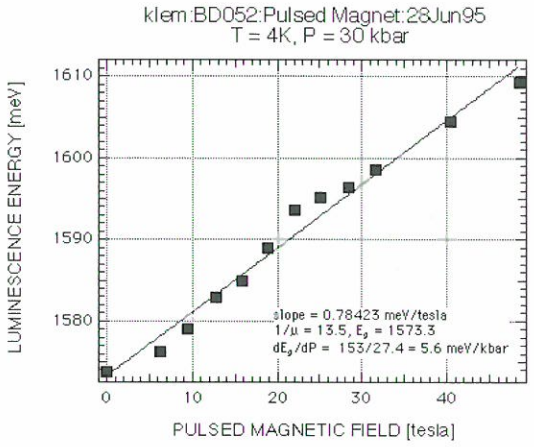

Figure 1. Pressure dependent magnetoluminescence of semiconductor quantum wells.

Pressure Dependent Magnetoluminescence of Semiconductor Quantum Wells

Jones, E.D., Sandia National Laboratory
Perry, C.H., Northeastern Univ., Physics Dept.
Tozer, S.W., NHMFL/FSU
Kim, Y., Northeastern Univ., Physics Dept.
Rickel, D.G., NHMFL/LANL

The low temperature pressure dependent magnetoluminescence of an InGaAs/GaAs (20%) n-type strained single quantum well has been studied in DC fields of 18 T as well as pulsed fields to 60 T. Landau level shifts were measured at 4 and 77 K and to pressures of 4 GPa using a

Study of Two-Dimensional Electron System Under Hydrostatic Pressure

Kang, W., Univ. of Chicago, Physics Dept.
Young, J.B., Univ. of Chicago, Physics Dept.
Hannahs, S.T., NHMFL
Campman, K., Univ. of California, Santa Barbara, Dept. of Elect. and Comp. Eng.
Gossard, A., Univ. of California, Santa Barbara, Dept. of Elect. and Comp. Eng.

The fractional quantum Hall effect is a prototypical example of strong electron correlation effect in a two-dimensional electron system at low temperature and high magnetic field.[1,2] When all

electrons reside in the lowest Landau level, the kinetic energy is quenched and the Coulomb interaction dominates the collective dynamics. The bulk Landee γ-factor in GaAs, however, is rather small ($\gamma = -0.44$) and spin fluctuations become an important dynamical degree of freedom in the system.[3] The Landau levels are split into up and down spin levels, and the composite fermion metal state at half-filling becomes fully spin-polarized at high magnetic field.[4,5]

Application of large hydrostatic pressure alters the band parameters in GaAs and has been shown to decrease the γ-factor. In fact, it may be possible to obtain zero γ-factor with application of sufficiently high enough pressure. With the quenching of the Zeeman energy in high magnetic field, such a system possesses a full spin degree of freedom. We have presently made magnetotransport study of two-dimensional electron system up to 12 kbar of pressure, up to 20 tesla of magnetic field, and down to 30 milliKelvin in temperature. Initial results are consistent with the reduction of the γ-factor within increasing pressure. We also observe a fairly dramatic decrease in the sample density and mobility under increasing pressure. This may be explained in part from application of pressure modifying the GaAs band parameters. Extension of the investigation to higher pressure is currently under progress.

References:

1 Prange, R.E. and Girvin, S.M., editors, The Quantum Hall Effect, (Springer-Verlag, New York, 1990).

2 Chakraborty, T. and Pietilainen, P., The Fractional Quantum Hall Effect, (Springer-Verlag, New York, 1988).

3 Halperin, B.I., Helv. Phys. Acta, 56, 75 (1983).

4 Willett, R.L., et al., Phys. Rev. Lett., 71, 3846 (1993).

5 Kang, W., et al., Phys. Rev. Lett., 71, 3850 (1993).

$\nu = 2/3$ Quantum Hall Effect in a Bilayer Electron System in Tilted Magnetic Fields

Lay, T.S., Princeton Univ., Elect. Eng.
Shayegan, M., Princeton Univ., Elect. Eng.

Bilayer electron systems (BLES's) realized in wide single quantum wells exhibit novel quantum Hall effect (QHE) phase transitions arising from interlayer and intralayer interactions.[1,2] The experiments so far were performed in perpendicular magnetic fields by changing areal density (N_s) via gate bias. The in-plane field, which can modify the charge distribution, and the interlayer correlation strength of the electron layers[3] can serve as additional means to examine the origin of correlated QHE in BLES's. Experiments have in fact already revealed an unexpected in-plane-field-driven QHE phase transition at filling factor $\nu = 1$ in double-quantum-well systems.[4]

We have carried out an experimental study of the $\nu = 2/3$ QHE in a BLES in a 74-nm wide well with fixed $N_s = 9.8 \times 10^{10}$ cm^{-2} in tilted magnetic fields. At different angles (θ) between the sample normal and the field directions, we determine the $\nu = 2/3$ energy gap (Δ) from the temperature activated magnetoresistance data. As we increase θ, Δ starts to decrease and reaches a minimum at a critical $\theta \approx 30^{\circ}$. As θ is further increased, the gap increases and exceeds the gap at zero in-plane field. This is similar to the behavior observed in the same system as the $\nu = 2/3$ QHE makes a one-component to two-component phase transition with increasing N_s at zero in-plane field.[1] The data manifest the same transition, here driven by the in-plane component of magnetic field.

References:

1 Suen, Y.W., et al., Phys. Rev. Lett. 72, 3405 (1994).

2 Lay, T.S., et al., Phys. Rev. B 50, 17725 (1994).

3 Hu, J., et al., Phys. Rev. B 46, 12554 (1992).

4 Murphy, S.Q., et al., Phys. Rev. Lett. 72, 728 (1994).

Optical Determination of the Carrier Effective Masses of (In,Ga)As/AlAs/GaAs Quantum Wells

Lee, K.-S., Electronics and Communications Research Institute, Taejon, Korea
Perry, C.H., Northeastern Univ., Physics Dept., and NHMFL–LANL
Kim, Y., Northeastern Univ., Physics Dept.
Rickel, D.G., NHMFL–LANL

In the presence of a magnetic field applied in the direction parallel to the growth axis, the transition energy of the exciton ground state shows diamagnetic shift, while exciton excited states such as 2s, 3s, and 4s can be observed in absorption-type experiments. The diamagnetic shift of the exciton ground state is especially useful as a probe of the exciton localization.

In this study we have carried out the magnetophotoluminescence investigations on a series of $In_xGa_{1-x}As/GaAs$ quantum well with 0, 1, or 2 layers of AlAs sandwiched between an InGaAs quantum well and GaAs barrier layers. The influence of the quantum well parameters, such as well width, indium composition, and thickness of AlAs interfacial layers, on the exciton properties such as exciton binding energy and effective mass, were investigated in the presence of a magnetic field up to B = 47 T. We observed that deposition of 1 or 2 monolayers of AlAs gives considerable effects on both the exciton transition energy at zero B-field and the diamagnetic shift in the presence of a magnetic field. In the theoretical analysis, considering m*, the exciton reduced mass, as an adjustable parameter, the diamagnetic shift of exciton state is fitted by a variational method using two variational parameters. This allowed us to determine the reduced mass of the exciton ground state in quantum wells. For instance, for x = 0.14 and well width of 6.2, 11.4, and 21.6 nm with 0(1) AlAs interfacial layer, we find that m*/m0 ~ 0.050(0.057), 0.046(0.050), and 0.044(0.046), respectively. The heavy-hole in-plane mass also can be obtained by calculating the dependence of the electron mass on quantum well parameters in the two-band effective mass approximation.

This work has been supported by the Ministry of Information and Communications, Korea, the NSF Cooperative Agreement #DMR 90-16241, the State of Florida, and the U.S. Department of Energy.

Dual Current Studies of Breakdown of Quantum Hall Effects

Mani, R.G., Max-Planck-Institut für Festkorperforschung, Stuttgart, Germany
von Klitzing, K.,Max-Planck-Institut für Festkorperforschung, Stuttgart, Germany
Ploog, K., Paul-Drude-Institut, Berlin, Germany

The so-called breakdown of quantum Hall effect [1-3] is a topic of practical importance because the phenomenon places some constraint in measurements of von Klitzing's constant for metrological applications. Typically, in such applications, more resolution is better and, therefore, measurements are carried out at a high current in order to realize a large Hall voltage. Experimental studies have shown, however, that increasing the current brings with it a narrowing of the quantum Hall plateaus, beginning at the wings of the plateaus due to the appearance of finite R_{xx}, such that the plateaus vanish altogether at a sufficiently high current. Thus, increasing the applied current increases the magnitude of the Hall voltage and, at the same time, reduces monotonically the magnetic field (or filling factor) interval over which a given plateau occurs. The latter feature is undesirable because it is the stabilization of the Hall resistance at the quantized value over a wide range of filling factors (in the vicinity of integral filling factors) that makes quantum Hall effects a valuable resistance standard.

There have been many approaches to understand this effect[3] but a satisfactory explanation has remained elusive because the critical current (and derived critical current densities) for breakdown depend in a non-trivial way on a host of experimental variables including, for example, magnitude and type of disorder, sample dimensions, and possible inhomogeneous current distribution. One hopes that a better understanding of the phenomenon might ultimately

lead to some solutions that help control breakdown, which might prove useful for improving resolution in high precision determinations of von Klitzing's constant.

Recently, we have reported on a novel Hall measurement technique based on applying two (or more) currents to a doubly (or multiply) connected "anti-Hall bar within a Hall bar" geometry which makes possible the realization of two (or more) simultaneous Hall effects in a single specimen. In these studies, we have examined questions relating to the current distribution and have demonstrated, for example, that the Hall voltage on a boundary depends exclusively on the current injected via the same boundary, under a variety of conditions.[4-7]

In this work, we explore whether the isolation observed between the "interior" and "exterior" Hall effects in the "anti-Hall bar within a Hall bar" configuration, is maintained to the high currents that induce breakdown, and whether the breakdown properties might be modified by controlling the current distribution within the specimen, either by current compensation or by multi-port injection or by a combination of techniques. Measurements carried out thus far have yielded some insight into the role of geometrical factors influencing this phenomenon, and suggest the possibility of boosting, in-situ, the quantized Hall voltage above values obtained in the standard Hall bar type measurement.

References:

1 Prange, R.E. and Girvin, S.M.,eds., The Quantum Hall Effect, (Springer, New York, 1987).

2 Ebert, G., et al., J. Phys. C 16, 5441 (1983).

3 Balaban, N.Q., et al., Phys. Rev. Lett. 71, 1443 (1993).

4 Mani, R.G., et al., Z. Phys. B 92, 335 (1993); Appl. Phys. Lett. 64, 1262 (1994); Appl. Phys. Lett. 64 3121 (1994); unpublished.

5 Mani, R.G., et al., Phys. Rev. B 51, 2584 (1995).

6 Mani, R.G., et al., in 11th Intíl. Conf. High Magnetic Fields in the Physics of Semiconductors, ed. D. Heiman (World Scientific, Singapore, 1995), p. 146.

7 Mani, R.G., et al., Appl. Phys. Lett. 67, 2223 (1995).

Magnetophotoluminescence Oscillations of a Modulation-Doped (Al-Ga) As/GaAs Single Heterojunction

Perry, C.H., Northeastern Univ., Physics Dept. and NHMFL–LANL

Kim, Y., Northeastern Univ., Physics Dept.

Rickel, D.G., NHMFL–LANL

Lee, K.-S., Electronics and Telecommunications Research Institute, Taejon, Korea

We report low temperature photoluminescence studies of a modulation-doped (Al,Ga)As-GaAs single heterojunction. In the presence of a magnetic field applied parallel to the growth direction, the luminescence spectra associated with the two-dimensional electron gas showed pronounced peaks that displayed both energy and intensity oscillations. These oscillations were approximately periodic with inverse magnetic field. Similar observations have been reported by others in related materials.[1,2] We infer from our data that the photogenerated electron gas at zero magnetic field causes the second subband to be occupied. Self-consistent Landau-level calculations indicate that the population of the second subband undergoes nearly periodic oscillations proportional to 1/B. The calculated results are in qualitative agreement with our experimental data.

Work at NHMFL-LANL is supported through the NSF Cooperative Agreement # DMR 90-16241, the State of Florida, and the U.S. Department of Energy.

References:

1 Perry, C.H., et al., Application of Magnetic Fields in Semiconductor Physics, ed. G. Landwehr (Springer, Heidelberg), 1989, p. 202.

2 Kukushkin, I.V., et al., Phys. Rev. Lett., 72,736 (1994).

Photoluminescence Studies of Silicon Delta-Doped GaAs in Pulsed Magnetic Fields

Perry, C.H., Northeastern Univ., Physics Dept., and NHMFL–LANL
Kim, Y., Northeastern Univ., Physics Dept.
Rickel, D.G., NHMFL–LANL
Lee, K.-S., Electronics and Communications Research Institute, Taejon, Korea

We report magneto-photoluminescence (MPL) studies of Si delta-doped GaAs in pulsed magnetic fields up to 50 tesla (T) at 4.2 K. This work was based upon some earlier MPL measurements to 15 T by Perry et al.[1] where a series of samples with 2DEG doping densities in the range of (0.8-3.2)x10^{12} cm^{-2} were examined in perpendicular and parallel fields. In this work we studied two samples: One was a single δ-layer (#2764) with an areal electron density of 1.2 x 10^{12} cm^{-2}; the δ-layer profile was ~17 nm. The second sample (#2769) consisted of two Si δ-doped layers with a δ-layer profile of ~10 nm. At B=0, two major excitonic recombination peaks were recorded at 1.515 eV (D(0)-X) and 1.440-1.495 eV (D(X)-B(A)), respectively. Both features displayed magneto-excitonic structure but with slightly different directional behavior with field. For B+ to the doped GaAs layer, the two peaks showed only a slight energy dependence with field. For B//, the D(0)-X exciton showed a factor of fifty increase in intensity before saturating at about 40 T. We believe that this large increase is due to the additional confinement of the holes and greater overlap of the electron and holes wave functions imposed by the parallel B field. In contrast, the intensity of the FX-B(A) peak was practically field independent.

For the double Si δ-doped n-GaAs layer (Sample #1769), peaks corresponding to F-X and D(0)-X excitons were observed. Each peak could be resolved into two peaks with increasing field, possibly due to spin splitting. The energy dependence for the F-X and D(0)-X peaks showed a small anisotropy in the slopes for B// and B+ which is indicative of the influence of the 2-D layers. However, the large intensity changes seen in B// fields in the single δ layer were not observed in this sample.

Work at the NHMFL is supported through the NSF Cooperative Agreement # DMR 90-16241, the State of Florida, and the U.S. Department of Energy.

Reference:

1 Perry, C.H., et al., Surf. Sci., 196, 677, (1988).

Optically Detected Cyclotron Resonance in Semiconductor Heterostructures

Schmiedel, T., NHMFL
Wang, Y.J., NHMFL
Salib, M., SUNY at Buffalo, Physics Dept.
Yu, W.Y., SUNY at Buffalo, Physics Dept.
Petrou, A., SUNY at Buffalo, Physics Dept.

We have carried out optically detected cyclotron resonance (ODCR) experiments on II-VI and III-V semiconductor nanostructures in the recently developed ODCR facility at NHMFL. The first system we studied was a 1 monolayer ZnTe/CdTe quantum well structure using the 118 μm and 163 μm lines of an optically pumped FIR laser. The luminescence was excited using the 488 nm line of an Argon-ion laser. By monitoring the intensity of the band-edge luminescence we detected the cyclotron resonance due to electrons in these structures. The resonance is broad (as shown in Figure 1) and yields electron effective mass values between those of the ZnTe barriers (the sharp resonance of negative sign indicated on Figure 1) and the CdTe wells. The measured effective masses can be used as a probe of the electron wavefunction penetration into the CdTe barriers. It is expected that the future investigation of this and related systems at NHMFL will provide the much needed high field information to combine with the low field data taken at SUNY Buffalo. Such a collaborative effort will serve to clarify many of the issues related to electron mass behavior and confinements effects in wide-gap monolayer quantum well. The data will be presented at the 1996 APS March Meeting in St. Louis.

The second system studied was n-type modulation doped GaAs/AlAs quantum wells. The electron cyclotron resonance in these structures consists of two components on either side of the resonant field observed in undoped samples. The splitting has been attributed to many body interactions. This work has been instrumental in providing a new opportunity for the investigation of II-VI n-type modulation doped heterostructures for which the large electron effective masses require the high fields only accessible at NHMFL. We consider the analysis of both the III-V data taken earlier this year and the data to be taken on the II-VI structures to be a very vital part in the interpretations of many body effects in two-dimensional electron gas systems.

We have also investigated the modulation of reflectivity (rather than PL signal) from bulk GaAs by the FIR laser. Strong cyclotron resonance signals have been observed in this experiment, which allows the study of cyclotron and impurity resonances in samples that show weak luminescence signals. To our knowledge this is the first of such attempts at this detection technique for ODCR making the Tallahassee facility one of the prime locations to perform such measurements.

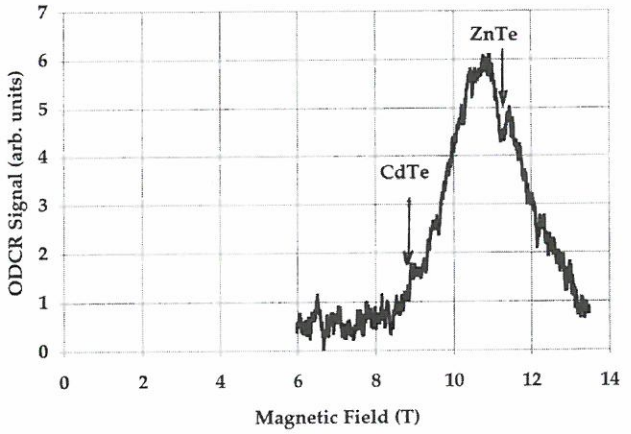

Figure 1. ODCR signal for a ZnTe/CdTe monolayer quantum well.

Magneto-Studies of GaN and AlGaN

Wang, Y.J., NHMFL
Kaplan, R., Naval Research Laboratory
Ng, H.K., Martech/FSU
Doverspike, K., Naval Research Laboratory
Gaskill, D.K., Naval Research Laboratory
Ikedo, T., Meijo Univ., Dept. of E.E., Nagoyo, Japan
Amano, H., Meijo Univ., Dept. of E.E. Nagoyo, Japan
Akasaki, I., Meijo Univ., Dept. of E.E., Nagoyo, Japan

Magneto-optical measurements have been performed on free and bound electrons in GaN films and GaN/AlGaN heterojunctions. Cyclotron resonance studies of the two-dimensional electron gas in $GaN/Al_xGa_{1-x}N$ heterojunctions have yielded $m^* = 0.23m$, x-dependent scattering times consistent with values from transport measurements, and an apparent unexplained level crossing at 70 cm^{-1}. Infrared absorption of doped GaN films has shown that the binding energy of Si donors, 29.0 meV, is much smaller than that of residual donors, in agreement with transport measurements, thus suggesting donor spectroscopy as a useful technique for defect/impurity qualitative analysis. The Zeeman effect of the donor spectra has been used to determine the GaN low frequency dielectric constant, $\varepsilon_o = 10.4$.

Resonant Electron-Phonon Interaction with AlAs-like LO Phonons

Wang, Y.J., NHMFL
McCombe, B.D., SUNY at Buffalo, Physics Dept.

Electron cyclotron resonance (CR) vs. magnetic filed has been studied at 4.2 K in two modulation-doped (Si) multiple-quantum-well samples (1.5 and 2.8 x $10^{11}cm^{-2}$/well) throughout the resonant magnetopolaron region and beyond (up to 30 T). The transmission results for both samples show large CR splittings in the GaAs reststrahlen region with sublinear behavior for the lower branch occurring well below the optical phonon energies and upper branch that approaches the LO phonon energy from above as the filed is decreased. These large splittings appear to be due to so-called dielectric anomalies. However, a much weaker, but nevertheless clear, anomaly splitting into two branches is observed at energies well above the GaAs reststrahlen region (280 cm). The minimum separation between the branches at 27.5 T is approximately 8 cm for the low density sample; it is not resolved for the high density sample. This splitting is attributed to a resonant polaron interaction with the AlAs-like LO modes in the barriers.

MAGNETISM & MAGNETIC MATERIALS

Magnetization Process in Intermetallic Compounds

Bruck, E., Van der Waals-Zeeman Institute, Univ. of Amsterdam
de Boer, F.R., Van der Waals-Zeeman Institute, Univ. of Amsterdam

We have performed high field magnetization measurements at 4.0 K in magnetic fields up to 57 T on the compounds $ErCo_{10}Si_2$, $TmCo_{10}Si_2$, $ErCo_{10}Mo_2$, $GdCo_9Si_2$, $TbCo_9Si_2$, and MnPt ($Al_{1-x}Ga_x$) with x = 0, 0.05, 0.1, 0.15, 0.2, by means of induction measurements with a pickup coil compensated for induction due to the change of magnetic fields.

The samples consist of small powder particles with diameters # 40 mm, which may be considered as single-crystals. In the case of $ErCo_{10}Si_2$, $TmCo_{10}Si_2$, and $ErCo_{10}Mo_2$, these small crystals were emerged in stycast, and hardening of the stycast took place at room temperatures in an applied magnetic field of 1.3 tesla (T) resulting in a preferential orientation of the crystallites along the easy-magnetization direction. The other samples where measured as loose powders with some admixture of isolating non-magnetic material of the same grain-size to avoid the generation of eddy currents during the field sweeps.

The magnetization curves on the samples fixed in stycast thus represent the magnetization along a predefined direction, while in the case of the loose powders moment rotation also will result in rotation of the powder particles resulting in a parallel alignment of the applied magnetic field and the magnetization direction during the whole measurement. Figure 1 shows the magnetization of $ErCo_{10}Si_2$ measured with the field applied parallel and perpendicular to the alignment direction. The various transitions are due to anisotropy within the R and T sublattices.

Finally, the compound MnPtAl is known to exhibit a metamagnetic transition at 28 T. This transition from an antiferromagnetic ordered state to a field-induced ferromagnetic state is accompanied by a drastic reduction of the resistivity of this compound. Chemical substitution of Al by Ga is expected to reduce the antiferromagnetic

exchange between the Mn moments and thus to reduce the transition fields. Samples with 5, 10, 15, and 20 percent Ga substitutions were prepared, and the field of the metamagnetic transitions were studied. The magnetization curves measured on these compounds are strongly affected by additional induction due to eddy currents as these compounds have a very low electrical resistivity (on the order of a few mWcm). Nonetheless it was possible to measure the reduction of the field of the metamagnetic transition due to the Ga substitutions. We find a reduction of approximately one tesla per percent of Ga on the Al sublattice.

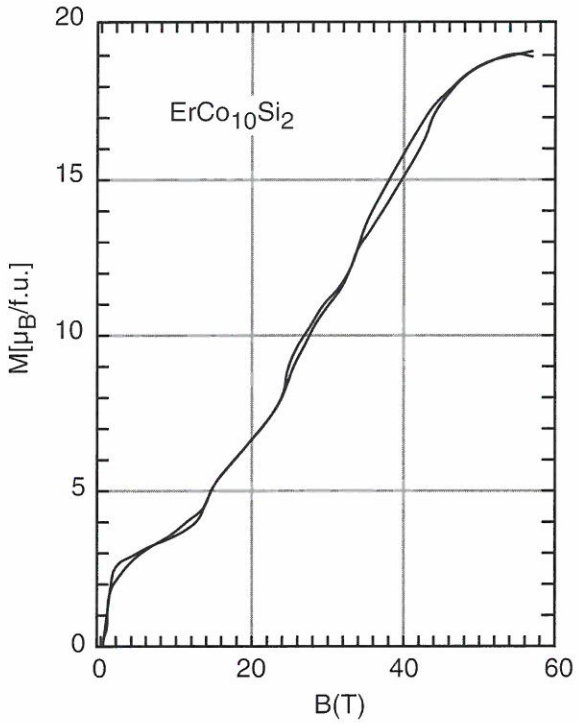

Figure 1. Magnetization of $ErCo_{10}Si_2$ at 4 K.

Angular Dependence of Upper Metamagnetic Transition in $HoNi_2B_2C$

Canfield, P.C., Ames Lab. and Iowa State Univ., Physics Dept.
Cho, B.K., Iowa State Univ., Physics Dept.
Lacerda, A., NHMFL/Los Alamos

The RNi_2B_2C family of magnetic superconductors has generated renewed interest in the interplay between superconductivity and local moment magnetic order. Initial studies have revealed anisotropic $H_{C2}(T)$ and M-T phase diagrams at low temperatures. In the case of $HoNi_2B_2C$, the M(H) isotherms at 2 K show up to three metamagnetic phase transitions, with the critical fields varying as a function of the angle of applied field in the tetragonal a-b plane. The upper transition ranges from below 20 kG to over the 55 kG that our QD SQUID can provide. In order to follow this transition to higher fields, and to see if there were further, as of yet undiscovered transitions, we measured M(H) isotherms for a variety of alignments of applied field in the 180 kG continuous magnet at NHMFL/Los Alamos. The data we obtained has allowed us to determine the angular dependence of the upper transition. This data, in combination with our data on the lower two transitions, is currently being written up for submission to Phys. Rev. B. The detailed nature of our data has inspired theoretical work by V. Pokrovsky at Texas A&M. Pokrovsky is finishing up work that models the angular dependencies that we have found and is also in the process submitting a paper to Phys. Rev. In the next year we anticipate returning to NHMFL/Los Alamos to study R = Er and Dy members of this series and see if similar effects are seen in other members of the series.

Magnetic Thin Films and Multilayers

Childress, J.R., UF, CoE Mat. Sci.
Caballero, J., UF, CoE Mat. Sci.
Park, Y.D., UF, CoE Mat. Sci.
Cabbibo, A., UF, CoE Mat. Sci.
Pearton, S.J., UF, CoE Mat. Sci.
Rehn, F., AT&T Bell Laboratories

We have begun a program aimed at fabricating ultra-thin multilayer magnetic films and other magnetic nanostructures. Materials are fabricated using a four-source sputtering system equipped with a computer controlled, rotating substrate holder with temperature control between 100 and 800 K. Additionally, a load-lock entry chambers allows rapid substrate changes without breaking the vacuum. Control of gas parameters and sputtering power allows deposition of metals at rates below 0.01 nm/sec. Together with computer control of

individual source shutters, this allows continuous films to be deposited reliably with thicknesses down to 0.5–1 nm. Characterization is performed by x-ray diffraction, atomic force microscopy, and a SQUID magnetometer (2–400 K, 5.5 T) with AC susceptibility and magnetoresistance capability.

We have begun magnetic and transport studies of *NiMnSb Heusler alloy films*. Heusler alloys are ternary alloys, including those of the type XMnSb where X=Ni, Pt, Co. In these alloys, Mn carries a large magnetic moment, through which the alloy is ferromagnetic. Heusler alloys have attracted particular attention in the last few years because of the discovery of a very large polar magneto-optic Kerr effect in PtMnSb. Band structure calculations have shown that the unique magnetic and magneto-optical properties exhibited by some of the Heusler alloys with the $C1_b$ crystal structure (NiMnSb, PtMnSb) are due to their half-metallic character, i.e., they are metallic for one spin sub-band, and semiconducting for the other spin sub-band. Such compounds have been given the name of "half-metallic ferromagnets." The remarkable aspect in this case is that the conduction electrons are 100% spin-polarized. Therefore Heusler alloys of this type appear as ideal candidates for giant magnetoresistance (GMR) studies in multilayered structures. Up to now, very few studies have been carried out on Heusler alloy thin-films and have focused on their intriguing magneto-optical properties. Much work is needed, however, to control the deposition of thin Heusler alloy films, due to their complicated crystal structure and structurally-sensitive band structure. The use of perfectly spin-polarized ferromagnetic alloys in GMR structures results in the maximum GMR effect while removing the *interface* as the most efficient source of spin-dependent conduction. Additionally, and independently of GMR effects, the availability of thin-film electron "polarizers" would allow the embodiment of other future magnetoelectronic thin-film devices based on spin-polarized conduction. By depositing 100 nm to 200 nm thick films and using rapid thermal annealing under inert atmosphere up to 800 K, we have successfully synthesized this alloy in the correct stochiometry and identified temperature ranges in which the formation of the $C1_b$ structure. Magnetic characterization of the films show square hysteresis loops with room-temperature coercive fields of about 50 Oe, which is very promising for application of these films to spin-valve structures. Magnetotransport evaluation is underway through a collaboration with Université Paris-Sud in France. We expect to be able to reproduce these results *in situ* using our new heating substrate stage and be able to refine the stochiometry by using multiple sputtering sources. It will then be possible to fabricate multilayer structures with unique magnetotransport characteristics.

We have deposited Fe contacts onto high-mobility GaAs field-effect transistor (FET) structures, with the goal to fabricate spin-sensitive devices whose resistance depends on the relative magnetic orientation of the contacts, and with gate-activated current modulation. The contact regions were etched to expose the 2-D electron gas region, and 100 nm-thick contacts were deposited by sputtering. Initial characterization show that Fe has made contact to the device, but that the ohmic behavior needed is not achieved. Future work will include a two-layer contact process to ensure ohmic behavior at the metal/2DEG interface while retaining spin polarization.

Strongly Disordered Heisenberg Spin-1 Chains: Vanadium Warwickites

Continentino, M.A., IF-UFF/Brazil and NHMFL/Tallahassee
Fernandes, J.C., IF-UFF/Brazil
Guimaraes, R.B., IF-UFF/Brazil
Boechat, B., IF-UFF/Brazil
Borges, H., DF-PUC/Brazil
Valarelli, J.V., IG-USP/Brazil
Silva, P.R.J., CBPF/Brazil
Haanappel, E.G., NHMFL/Los Alamos
Lacerda, A., NHMFL/Los Alamos

One-dimensional magnetic materials have attracted a lot of attention in the last years due to their interesting properties. In the case of spin-1/2 chains our previous study of the titanium

warwickite, $MgTiBO_4$, has shown that this intrinsically disordered material can be very well described by a random exchange Heisenberg antiferromagnetic chain (REHAC) model. The disorder arises from the random occupation of the sites in the ribbons by the Mg and the magnetic transition metal ions. In fact this system is the first inorganic material to exhibit the unusual properties as predicted by the REHAC model[1]. More recently we have investigated a related system, namely the vanadium warwickite $MgVBO_4$. In this case the V^{+++} ion has a spin S = 1 that makes it particularly interesting. Susceptibility and high magnetic field (up to 50 tesla) magnetization measurements down to low temperatures (T = 1.8 K) have provided strong evidence that the disorder intrinsic to the warwickite structure destroys the Haldane gap and that this spin-1 material has a magnetic behavior similar to that of the spin-1/2 titanium warwickite.

Reference:

1 Fernandes, J. A., et al., Phys. Rev., B50, 16754 (1994).

High Field Optical Studies of Spin Distributions in Magnetic Heterostructures

Crooker, S.A., Univ. of California, Santa Barbara, Physics Dept.
Awschalom, D.D., Univ. of California, Santa Barbara, Physics Dept.
Flack, F., Pennsylvania State Univ., Physics Dept.
Samarth, N., Pennsylvania State Univ., Physics Dept.
Schmiedel, T., NHMFL

Epitaxially-grown monolayer and sub-monolayer planes of magnetic MnSe allow for the tailoring and study of two-dimensional magnetic spin distributions in II-VI semiconductors. Beginning with a single isolated Mn^{2+} spin in a II-VI semiconductor host (i.e., in the limit of small fractional monolayer coverages), the magnetic response is that of a nearly ideal spin-5/2 paramagnet with Brillouin-type magnetization. As the fractional monolayer coverage is increased and more spins are "sprinkled" onto the plane, neighboring local Mn^{2+} moments interact via a strong superexchange coupling and form antiferromagnetically-locked clusters of spins of increasing size and complexity. These clusters give rise to new features in the magnetization at high fields, including the presence of magnetization "steps" associated with the re-orientation of locked clusters at fields commensurate with exchange energies involved.

Recently developed "digital" magnetic heterostructures[1] in which discrete ultrathin planes of the magnetic semiconductor MnSe are incorporated into ZnSe/ZnCdSe quantum wells, have been studied at the NHMFL in photoluminescence in magnetic fields up to 30 tesla. The samples consist of single 12 nm quantum wells containing layers of MnSe of thickness 1/8 monolayer up to 3 monolayers. At low temperatures (500 mK), any free Mn spins are completely saturated with the application of a few tesla, and the response of the system at higher fields is then due entirely to the response of the antiferromagnetically-locked spin clusters. Sheet magnetizations are inferred from the Zeeman shift of the luminescence and reveal the existence of a magnetization step at 19 tesla that broadens as the fractional monolayer coverage is increased. Additionally, changes in the linewidth and intensity of the luminescence peak correlate with the observed magnetization steps and lend insight into the local magnetic landscape being sampled by the luminescing exciton.

Reference:

1 Crooker, S.A., et al., Physical Review Letters, 75, 505 (1995).

An Anomalous Low Dimensional System: A Study of Magnetism and Electrical Conductivity in $Na_2Ru_4O_{9-\delta}$

Crow, J.E., NHMFL
Cao, G., NHMFL
McCall, S., FSU, Physics Dept.
Shepard, M., FSU, Physics Dept.
Henning, P., FSU, Physics Dept.

The magnetic susceptibility $\chi_{||}(H||b)$, $\chi_{\perp}(H\perp b)$ ($2<T<700K$) and electrical resistivity ρ (T) ($2<T<300K$) of single crystals $Na_2Ru_4O_{9-\delta}$ ($\delta>0$) with various oxygen content were measured. The crystal structure of this compound is monoclinic with single, double, and triple chains along the b-axis. The most striking feature of this compound is the drastically large anisotropy reflected in resistivity which exhibits metallic behavior along the chains and semiconducting behavior perpendicular to the chains. The resistivity ratio for these two directions ρ_{Trans}/ρ_{Long} is larger than 10^5. This ratio is exceptionally large, indicating that the anisotropy of the bandwidth is substantial. Consistently, the magnetic susceptibility also suggests occurrence of low dimensional behavior with a maximum in the vicinity of 70 K. It is remarkable that, after reduction of oxygen content in the system, the magnetic susceptibility undergoes a drastic change, whereas the electrical resistivity along the b-axis is altered only slightly. It is argued that the different sensitivity to oxygen content reflected in magnetic and transport properties suggests decoupling of spin and charge and may be attributed to the complexity of the crystal structure. The striking observations presented here may suggest a one dimensional system that possesses unique physical properties.

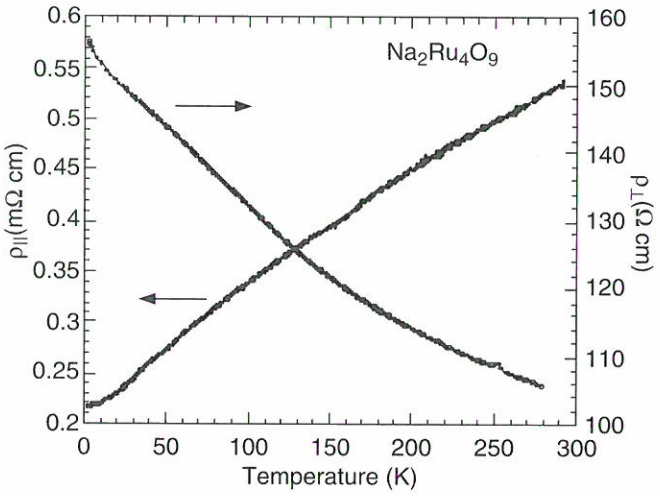

Figure 1. Resistivity vs. temperature for directions parallel and perpendicular to chains.

Magnetic and Electrical Properties of $SrPb_{1-x}Ru_xO_3$ and $CaSn_{1-x}Ru_xO_3$

Crow, J.E., NHMFL
Cao, G., NHMFL
McCall, S., FSU, Physics Dept.
Bolivar, J., FSU, Physics Dept.
Shepard, M., FSU, Physics Dept.
Freibert, F., FSU, Physics Dept.

$SrRuO_3$, $SrPbO_3$, $CaRuO_3$, and $CaSnO_3$ are all perovskites with an orthorhombic distortion. $SrPbO_3$ is a paramagnetic semiconductor, and $SrPb_{1-x}Ru_xO_3$ is a ferromagnetic metal with T_C=160 K. On the substitution of Ru by Pb in $SrPb_{1-x}Ru_xO_3$, there appears to exist a critical concentration of Ru in the vicinity of x=0.15 where the lattice parameters and physical properties undergo a drastic change. Particularly, a ferromagnetic-like ordering develops at 200 K when x>0.15. Although the magnitude of magnetic moment changes with Pb concentration, the ordering temperature seems to be insensitive to the Ru doping up to x=0.70. The small size of the remnant moment compared to the paramagnetic moment suggests that this magnetic behavior, when x<0.70, may be attributed to weak itinerant ferromagnetism. The electrical conductivity, in addition, increases significantly when x is larger than x=0.15. On the other hand, $CaRuO_3$ is a paramagnetic conductor, and $CaSnO_3$ a paramagnetic insulator. When doped with Ru, $CaSn_{1-x}Ru_xO_3$ becomes antiferromagnetic and more metallic. In the vicinity of x=0.65, the resistivity displays a linear T dependence above 50 K, and a saturation at lower temperatures, indicating a metal-insulator transition.

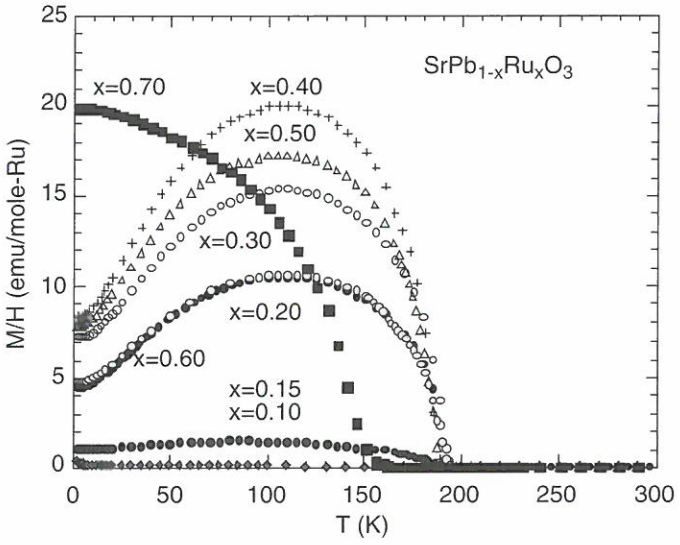

Figure 1. Magnetic susceptibility M/H vs. temperature for $SrPb_{1-x}Ru_xO_3$.

Magnetic and Transport Properties of Na Doped $SrRuO_3$ and $CaRuO_3$ Perovskites

Crow, J.E., NHMFL
Cao, G., NHMFL
Shepard, M., FSU, Physics Dept.
McCall, S., FSU, Physics Dept.
Freibert, F., FSU, Physics Dept.

The magnetic susceptibility χ (T) for 2<T<400 K and electrical resistivity ρ (T) for 2<T<300K of Na doped $SrRuO_3$ and $CaRuO_3$ single crystals have been studied. These two perovskites are orthorhombic with space group Pbnm. While both of them exhibit metallic conductivity, $SrRuO_3$ is a ferromagnet with T_C = 160 K, whereas $CaRuO_3$ is a paramagnet. When slightly Na doped with Na (<12%), $SrRuO_3$ drastically becomes an insulator with a depressed T_c. In contrast, similarly doped $CaRuO_3$ remains metallic with the appearance of antiferromagnetism below 70 K. This dramatically different dependence between magnetic and transport properties of $CaRuO_3$and $SrRuO_3$ on Na doping reflects different mechanisms involved in these two systems that govern magnetic coupling and conduction electron scattering.

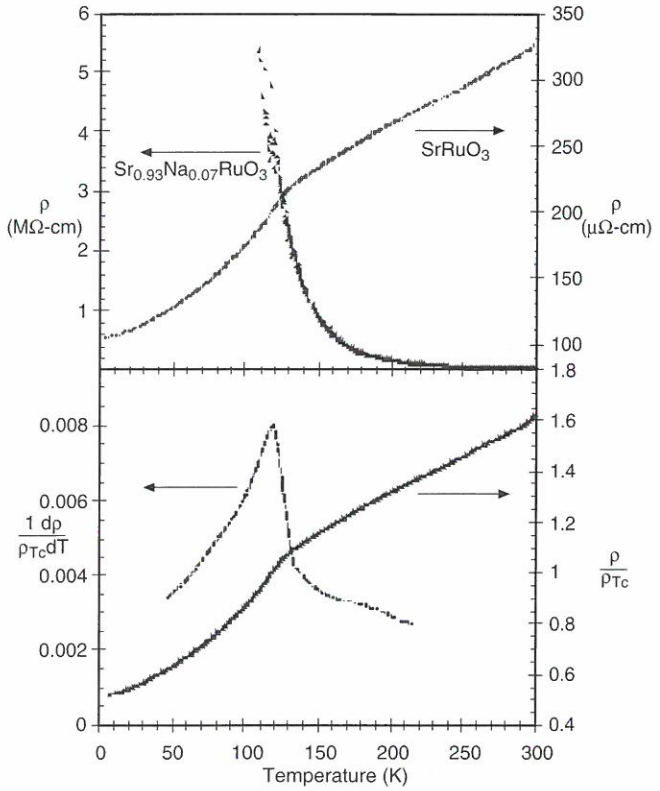

Figure 1. (Top) Resistivity vs. temperature for $SrRuO_3$ and $Sr_{0.88}Na_{0.12}RuO_3$ single crystals. (Bottom) Normalized resistivity and its derivative vs. temperature for $SrRuO_3$ single crystal.

Spin Dynamics of Hole Doped $Y_{2-x}Ca_xBaNiO_5$

Dagotto, E., FSU Physics Dept./NHMFL/ MARTECH
Riera, J., Inst. de Fisica de Rosario, Argentina
Sandvik, A., NHMFL
Moreo, A., FSU Physics Dept./NHMFL/ MARTECH

We propose an electronic model for the recently discovered hole doped compound $Y_{2-x}Ca_xBaNiO_5$. From a multiband Hamiltonian with oxygen and nickel orbitals, a one band model is discussed. Holes are described using Zhang-Rice-like S=1/2 states at the nickels propagating on a S=1 spin chain. Using numerical techniques to calculate the dynamical spin structure factor *S(q, ω)* in a realistic regime of couplings, spectral weight in the Haldane gap is observed in agreement with neutron scattering data. Low energy states with S=3/2 also appear in the model. Several predictions are made to test these ideas. The case of static defects relevant for Zn-doped chains is also discussed.

High Field EPR of Linear Chain Heisenberg Anti-Ferromagnets

Dalal, N., Univ. of West Virginia, Chemistry Dept.
Singh, K., Univ. of West Virginia, Chemistry Dept.
Hassan, A., NHMFL
Krzystek, J., NHMFL
Pardi, L., NHMFL
Brunel, L.C., NHMFL

Peroxychromates, represented by the general formula M_3CrO_8, where M is the monovalent alkali ion (Li, Na, K, Rb or Cs), are one of the rare examples of highly-correlated-electronic S=1/2 systems with the unpaired spin occupying the metal 3d1 orbital. Our group has recently succeeded in growing single crystals of all five compounds in this series, as well as some mixed lattices. Their preliminary magnetic susceptibility data on pure lattices indicate that these materials might constitute a new class of linear chain Heisenberg anti-ferromagnets with very small single-ion anisotropy. These conclusions were supported by low frequency (X- and Q-band) EPR linewidth data. However, heat capacity data indicate that each material undergoes at least two closely-spaced phase transitions in the liquid helium temperature range. Perhaps, equally interesting was the observation that in the liquid helium range, the measured specific heat was among the highest known for such materials. Because of these interesting properties and the fact that these materials have the simplest 3d1 electronic ground state, we have undertaken a systematic investigation of these materials by very high field (330 GHz) EPR spectroscopy utilizing Dr. Brunel's recently developed high field EMR spectrometer. This was the second example of the high resolution obtained in the 11–12 tesla field range. Figure 1 shows a comparison of the low field (9.5 GHz, 0,33 tesla, Figure 1a) and the high field (330 GHz, 11-12 tesla, Figure 1b) data. Clearly, there is much higher resolution evident in the higher field data (Figure 1b).While we have not yet succeeded in understanding the nature of the elementary excitations underlying the new peaks in the higher-field data, measured spectra demonstrate the impressive increase in the spectral content and resolution with the newly operational high-field EMR spectrometer.

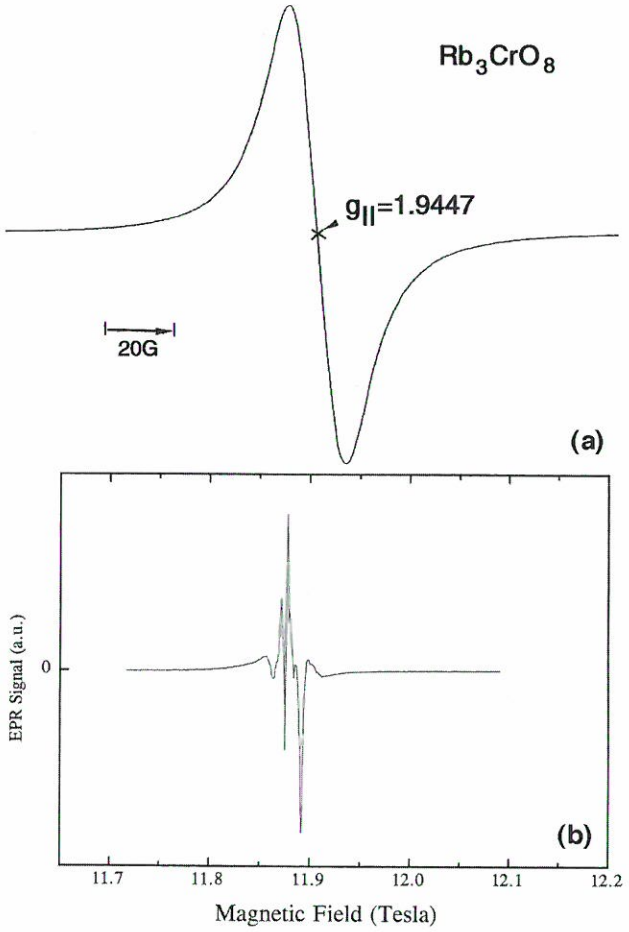

Figure 1. EPR spectrum for Rb_3CrO_8. (a) Recorded at 9 GHz. (b) Recorded at 330 GHz.

Influence of Next-Nearest-Neighbor Electron Hopping on the Static and Dynamical Properties of the 2D Hubbard Model

Duffy, D., FSU Physics Dept./NHMFL
Moreo, A., Physics, FSU/NHMFL/MARTECH

Comparing experimental data for high T_c cuprate superconductors with numerical results for electronic models, it is becoming apparent that a hopping along the plaquette diagonals has to be included to obtain quantitative agreement. However, the values for t´ discussed in the literature were obtained comparing theoretical results in the weak coupling limit with photoemission data and band structure calculations. The goal of this paper

is to study how t' gets renormalized as the interaction between electrons, U, increases. For this purpose, the effect of adding a bare diagonal hopping t' to the two dimensional Hubbard model Hamiltonian is investigated using numerical techniques. Spin-spin correlations, $n(k)$, $\langle n \rangle$ *vs* μ, and local magnetic moments are studied for several values of U/t and the electronic density. The spectral function $A(k,\omega)$ is also discussed. We introduce a new criterion to determine probable locations of Fermi surfaces at zero temperature. In general, we conclude that it is very dangerous to extract a bare parameter of the Hamiltonian t' from PES data where renormalized parameters play the important role.

Torque Anisotropy of Ferritin Films

Gider, S., Univ. of California, Santa Barbara, Physics Dept.
Awschalom, D.D., Univ. of California, Santa Barbara, Physics Dept.
Chaparala, M., NHMFL

The ferritin protein can serve as a host for a variety of nanometer scale magnets. Natural ferritin contains a ferrihydrite core of up to 4500 ferric ions within a 7.5 nm protein shell, among the smallest known magnetic particles. This core is believed to be antiferromagnetic, but evidence is largely indirect because the particles are superparamagnetic at temperatures where one would expect the Néel point (240 K) and hence, the magnetization cannot be followed through the transition. The ordering may be studied in high fields at low temperatures, however, where the moments are blocked. In initial force measurements with a cantilever magnetometer, the magnetization was found to be sensitive to the orientation of the film, most likely due to strain developed in the drying of the ferritin. A more intriguing possibility is that the proteins self-assemble into a crystalline structure akin to the manner in which opals form in nature. To study the anisotropy directly, we have performed torque measurements on ferritin films, also with a cantilever magnetometer. These measurements confirm that the easy axis of magnetization is parallel to the film, suggesting that the source of the anisotropy is strain. Angle dependent measurements further imply that the anisotropy is not simply uniaxial, but unidirectional, as the torque curve goes through only one maximum in a 180° rotation. An unexpected result was hysteresis in the torque curve, which could be due to the different roles of surface and bulk spins coupled by an anisotropic exchange.

Critical Field of Oriented Single Crystals of TMNIN

Granroth, G.E., UF, Dept. of Physics
Meisel, M.W., UF, Dept. of Physics
Chou, L.-K. , UF, Dept. of Chemistry
Talham, D.R., UF, Dept. of Chemistry
Chaparala, M., NHMFL

We have performed a variety of measurements[1-5] on the Haldane gap material $(CH_3)_4N[Ni(NO_2)_3]$, commonly known as TMNIN[6]. A major accomplishment of our work has been to synthesize large single crystals that have been used in our magnetization and electron spin resonance (ESR) studies. With these large single crystals, we made the first unambiguous identification of the crystal structure of TMNIN[1,2], improving upon the work of others[6]. The crystal structure of TMNIN is quite unique since the chains consist of alternate Ni ions that are chemically distinct, with one Ni being octahedrally coordinated with six nitrite nitrogens while the other Ni is octahedrally coordinated with six nitrite oxygens. The crystal structure allows one to estimate that the single-ion anisotropy (D) in this material is exceedingly small when compared to J $\approx$ 10 K, where J is the nearest neighbor interaction energy. Our susceptibility measurements, parallel and perpendicular to the chain axis, are nearly orientation independent, providing circumstantial experimental evidence that D $\approx$ 0 [1,2]. More definitive evidence is provided by our magnetization measurements performed below 60 mK, i.e. at temperatures well below the Haldane gap energy of approximately 3 K. This work, performed at the NHMFL–Tallahassee utilizing a cantilever force magnetometer[7], measured the

anisotropy of the Haldane critical field and, within the theoretical description of Golinelli, Jolicœur, and Lacaze[8], provide an upper bound of $D < 0.03$ K. The crucial unsettling issue is that this D value may be incompatible with the ESR data. The frequency vs. magnetic field energy level diagrams obtained on powdered samples by us[5] and others[9] may be explained, at least in part, by $D \approx 2.7$ K. Our ESR work on our single crystals[5] is consistent with the powdered results. Assuming that the small D value is intrinsic to TMNIN, alternative explanations are needed to understand the ESR data. One possibility is that the ESR spectra reveal some resonances that arise from splittings of higher energy levels. In this picture, some of the previously unexplained states might be identified. A second possibility is that the ESR spectra have coupled to some in-gap states. Further studies are needed to clarify this point. This work was supported, in part, by an individual research grant, NSF DMR-9200671 (GEG and MWM).

References:

1 Chou, L.-K., et al., Physica B, 194-196, (1994) 311.

2 Chou, L.-K., et al., Chem. Mater., 6, (1994) 2051.

3 Granroth, G.E., et al., Physica B, 211, (1995) 208.

4 Granroth, G.E., et al., PPHMF-II, Tallahassee, FL, May 1995, to be published.

5 Koido, N., et al., J. Magn. Magn. Mater., 140-144, (1995) 1639; and in preparation.

6 Gadet, V., et. al., Phys. Rev. B, 44, (1991) 705.

7 Chaparala, M., et al., AIP Conf. Proc., 273, (1992) 407.

8 Golinelli. O., et al., J. Phys. Condens. Matter, 5, (1993) 7847.

9 Sieling, M., et al., J. Magn. Magn. Mater., 140-144, (1995) 1637.

De Haas-van Alphen Effect and Fermi Surface of a Quasicrystal

Haanappel, E.G., NHMFL/LANL
Mueller, F.M., LANL, STC
Rabson, D.A., LANL, T-11

We have extended our earlier measurements of the magnetization, the magnetoresistance, and the de Haas-van Alphen effect on the icosahedral quasicrystal $Al_{70}Pd_{21.5}Mn_{8.5}$. The zero-field resistivity of the material was weakly temperature dependent with a residual resistance ratio of 1.04. The resistivity of the material is 1.25 mΩcm. The magnetization of $Al_{70}Pd_{21.5}Mn_{8.5}$ was measured in a 5 T superconducting magnet using a SQUID magnetometer. The magnetization, which was measured with the field parallel to a fivefold axis and also parallel to a twofold axis, showed a 3% anisotropy.

We studied the de Haas-van Alphen effect at temperatures close to 400 mK and at the highest attainable fields. We observed two well-defined frequencies when the magnetic field was parallel to a fivefold axis, but a very rich spectrum of frequencies with the field parallel to a twofold axis. These frequencies are shown in Figure 1 and were reproducible in different field pulses. The frequencies were several kiloteslas, much larger than the expected Fermi surface. We believe that they arise from magnetic breakdown, tunneling between the disjoint parts of the Fermi surface in adjacent quasicrystal Brillouin zones. This allows us to describe the effective gap structure of the material. From the temperature dependence of the effect we conclude that the carriers have large masses of the order 25–50 m_e.

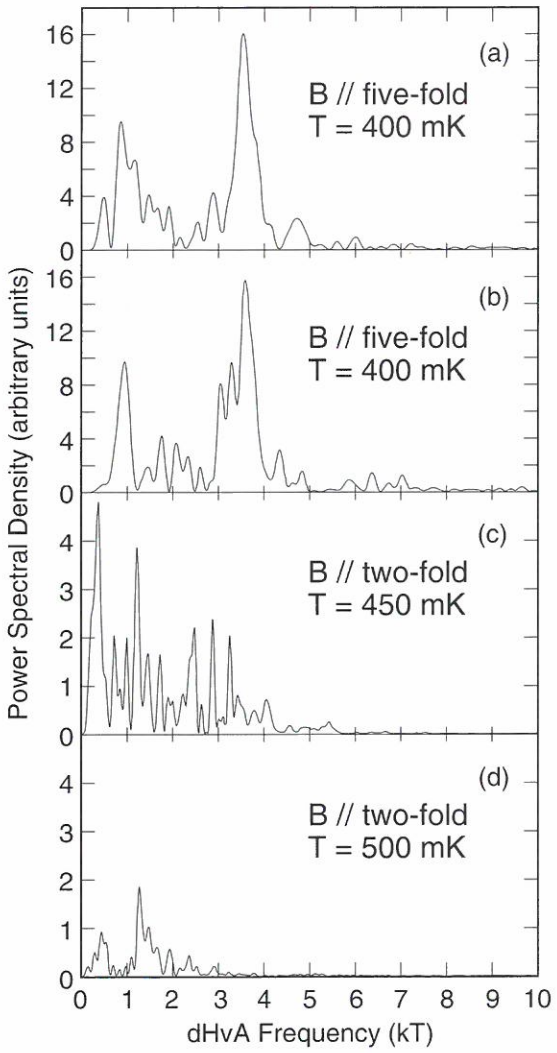

Figure 1. De Haas-van Alphen spectra of $Al_{70}Pd_{21.5}Mn_{8.5}$ for two field directions. The magnetic field was between 40 T and 50 T. For each field direction two measurements are shown. The spectra are similar for equal temperatures. On increasing the temperature the height of the peaks decreases.

Antiferromagnetically Induced Photoemission Band in the Cuprates

Haas, S., FSU Physics Dept./NHMFL/SCRI
Moreo, A., FSU Physics Dept./NHMFL
Dagotto, E., FSU Physics Dept./NHMFL

Strong antiferromagnetic (AF) correlations in models of high critical temperature (high-T_c) cuprates produce quasiparticle-like features in photoemission (PES) calculations above the Fermi momentum $\mathbf{P}_F$ corresponding to weakly interacting electrons. This effect, discussed before by Kampf and Schrieffer (Phys. Rev., B 41, 6399 (1990)), is analyzed here using computational techniques in strong coupling. It is concluded that weight above $\mathbf{P}_F$ should be observable in PES data for underdoped compounds, while in the overdoped regime it will be hidden in the experimental background. At optimal doping the signal is weak. The order of magnitude of our results is compatible with experimental data by Aebi et al. (Phys. Rev. Lett., 72, 2757 (1994)) for Bi2212.

Predictions for Neutron Scattering and Photoemission Experiments on $CuGeO_3$

Haas, S., FSU Physics Dept./NHMFL/SCRI
Dagotto, E., FSU Physics Dept./NHMFL

Applying numerical techniques to a model recently proposed for the one dimensional (1D) spin-Peierls compound $CuGeO_3$, we calculate dynamical properties that can be directly compared with inelastic neutron scattering (INS) data and angle-resolved photoemission (ARPES) experiments. The momentum and energy dependence of the dynamical structure factor $S(q,\omega)$ are discussed, as well as the static structure factor $S(q)$. The latter is shown to be specially useful to estimate the strength of the spin interaction beyond nearest neighbors. The spectral function $A(q,\omega)$ calculated from the one particle Green's function at half-filling is shown at several values of the hole hopping amplitude t. The results have some unique features characteristic of one dimensional systems including small weight near the Fermi energy. The presence of "shadow bands" induced by short distance antiferromagnetic (AF) correlations is predicted to appear in ARPES experiments for $CuGeO_3$ and also for Sr_2CuO_3.

High Field Magnetoresistance Up to 30 Tesla in Manganese Perovskites

Hwang, H.Y., AT&T Bell Labs and Princeton Univ., Physics Dept.
Cheong, S.-W., AT&T Bell Labs
Tozer, S.W., NHMFL
Batlogg, B., AT&T Bell Laboratories

There is renewed interest in manganese perovskites due to the large negative magnetoresistance exhibited near the ferromagnetic ordering of Mn spins, which is accompanied by a large increase in electrical conductivity. Recently, there have been a number of conflicting reports on the magnetic field dependence of the magnetoresistance in the low temperature ferromagnetic metallic regime. In order to address this issue, we have measured the magnetoresistance up to 30 tesla for a wide range of compositions and temperatures in both single crystal and polycrystalline form. The magnetoresistance is markedly different in the two types of samples. With decreasing temperature, the magnetoresistance of the single crystal samples diminishes to a very small value, extrapolating to zero magnetoresistance at zero temperature. The polycrystalline samples exhibit a nonvanishing magnetoresistance at low temperatures, indicating that the magnetoresistance is dominated by nonintrinsic scattering, perhaps involving the grain boundaries. Quite remarkably, there is no evidence for a saturation of the magnetoresistance up to 30 tesla.

We have also conducted some preliminary experiments to examine the effects of applying large external pressures on the magnetotransport properties of manganese perovskites using diamond anvil cells. The extreme strain sensitivity of these materials makes it quite difficult to observe the true intrinsic properties using this quasi-hydrostatic technique, and we plan to continue this study in the coming year.

Metastability and Temporal Dependence in the Dilute Antiferromagnet $Fe_xZn_{1-x}F_2$ at High Fields

Montenegro, F.C., Departamento de Fisica, UFPE – Brazil
Lima, K.A., Departamento de Fisica, UFPE – Brazil
Torikachvili, M.S., San Diego State Univ., Physics Dept.
Lacerda, A., NHMFL/Los Alamos

The strongly anisotropic diluted antiferromagnet (AF) $Fe_xZn_{1-x}F_2$ has been studied by vibration sample magnetization technique at magnetic fields to 18 T, for x=0.41 and 0.56. In this present work, we have investigated the magnetic behavior for concentration of Zn ranging from 0.4 to 0.6, where we were be able to access the upper part of the phase diagram (H, T) with the application of intense magnetic fields available at the NHMFL–Los Alamos. As shown in Figure 1, no spin-flop phase was found in these samples in the following field and temperature intervals: $0 < H < 18$ T and $4\ K < T < 50$ K. The stability of the antiferromagnetic phase has been studied by temporal dependence of the magnetization and the unstable regions have been mapped in the (H, T) diagram. A glassy phase appears in the upper part of the (H, T) diagram as also observed[1] in a sample of $Fe_{0.31}Zn_{0.69}F_2$. For samples with higher concentrations of magnetic ions this phase appears at stronger fields. Based on these results we were able to determine quantitatively the evolution of the phase diagram of this compound for $x < 0.6$. The next step will be the study of the spin-flop phase, which appears for $x > 0.6$. Stronger magnetic fields are requested for this purpose. These next experiments are planned to be performed in the pulsed magnetic fields (to 60 T) available at the NHMFL–Los Alamos.

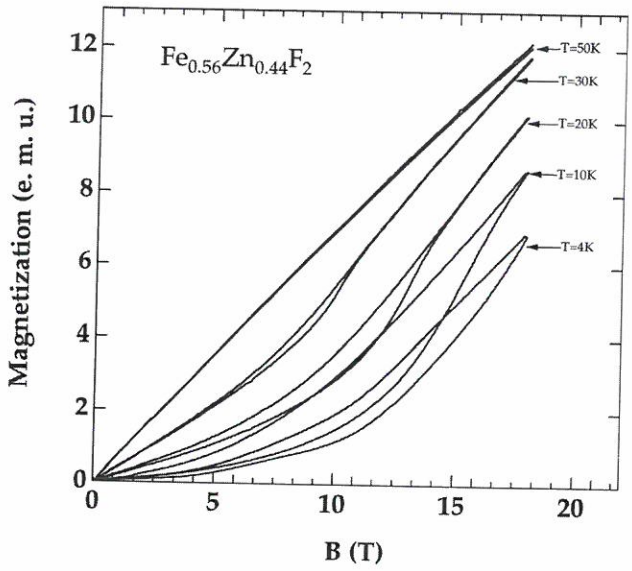

Figure 1. Magnetization as a function of magnetic field of $Fe_{0.56}Zn_{0.44}F_2$.

Reference:

1 Montenegro, F. C., et al., Phys. Rev., B44, 2155 (1991).

Quasiparticle Dispersion of the t-J and Hubbard Models

Moreo, A., FSU Physics Dept./NHMFL
Haas, S., FSU Physics Dept./NHMFL/SCRI
Sandvik, A., NHMFL
Dagotto, E., FSU Physics Dept./NHMFL

The spectral weight $A(\mathbf{p},\omega)$ of the two dimensional *t–J* and Hubbard models has been calculated using exact diagonalization and quantum Monte Carlo techniques, at several densities $0.5 \leq \langle n \rangle \leq 1.0$. The photoemission ($\omega < 0$) region contains two dominant distinct features, namely a low-energy quasiparticle peak with bandwidth of order J, and a broad valence band peak at energies of order t. This behavior *persists* away from half-filling, as long as the antiferromagnetic (AF) correlations are robust. The results give support to theories of the copper oxide materials based on the behavior of holes in antiferromagnets, and it also provides theoretical guidance for the interpretation of experimental photoemission data for the cuprates.

An Infrared Investigation of the Broken Symmetry Ground State in $GeCuO_3$

Musfeldt, J.L., State University of New York at Binghamton, Chemistry Dept.
Wang, Y.J., NHMFL

We have made infrared transmittance measurements of a high-quality single crystal sample of $GeCuO_3$[1,2] as a function of temperature and a magnetic field. We have observed and characterized strong changes at 311 cm^{-1}, which seem to be related to a magnetic excitation of the low-temperature broken-symmetry state. Overall, our explorations of the various phase boundaries of the *H*-T phase diagram indicate most of the spin-lattice coupling is either very weak or takes place at lower energy scales than are probed in this experiment, in striking contrast to the more well-studied organic spin-Peierls systems.[3]

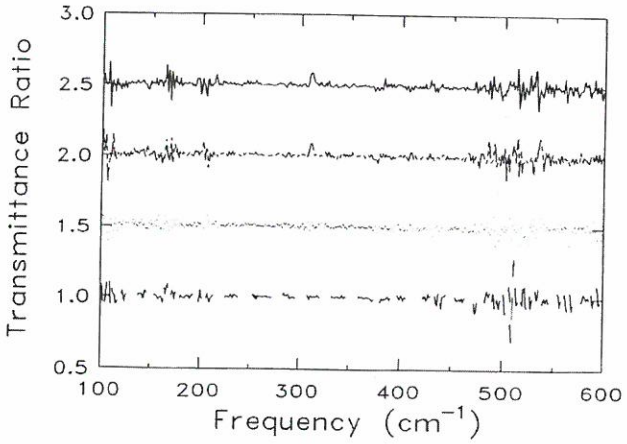

Figure 1. Transmittance ratios of $GeCuO_3$ in the far-infrared at 6 K. Solid line: 18 T/0 T; double-dashed line: 15 T/0 T; dotted line: 11 T/0 T; dashed curve: 6 T/0 T. The curves have been off-set for clarity.

References:

1 Hase, M., et. al., Phys. Rev. Lett., 70, 3651 (1994).

2 Hase, M., et. al., Phys. Rev. B., 48, 9616 (1994).

3 Musfeldt, J.L., et. al., unpublished results.

Characterization of Molecular Based Magnetic Materials by Neutron Scattering Techniques

Pardi, L., NHMFL
Gatteschi, D., Univ. of Florence, Italy
Sessoli, R., Univ. of Florence, Italy
Caneschi, A., Univ. of Florence, Italy
Gillon, B., Laboratoire Leon Brillouin, CEA-CNRS, France
Hennion, M., Laboratoire Leon Brillouin, CEA-CNRS, France
Mirabeau, I., Laboratoire Leon Brillouin, CEA-CNRS, France.
Kahn, O., Univ. of Bordeaux, France
Brunel, L.C., NHMFL

Polarized Neutron Diffraction (PND) have been used to investigate the spin density distribution in one organic radical[1] and in a copper dimer.[2] The Triazole–Nitronyl–Nitroxide of formula:

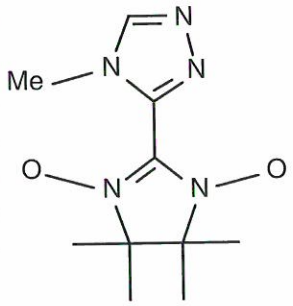

presents interesting magnetic properties: first it is the combination of two different organic moieties, the triazole part which, as a ligand, plays an important role in the area of spin transition and the nitronyl nitroxide part which is one of the building block of the novel class of molecular magnetic materials, second in the solid state exhibits intermolecular ferromagnetic interactions, and weak ferromagnetism below 0.6 K. The PND experiment, carried out on the polarized diffractometer 5C1 of the reactor Orphée (Laboratoire Leon Brillouin), put in evidence a large negative spin density, of the order of -0.07(2) B.M., on the nitrogen atom in position 2 of the triazole ring. This negative spin density is compared with the positive spin densities of the order of 0.24 B.M., present on the N - O group of the nitronyl - nitroxide. Ferromagnetic interactions between the radicals can be attributed to McConnel mechanism, involving the positive spin densities on the nitroxide group.

In the copper compound $Cu_2(t\text{-}bupy)_4(N_3)_2(ClO_4)_2$ two azido N_3 group bridge in an end-on fashion two copper(II) ions. The ground state of the dimer is a spin triplet with a gap of 105 cm^{-1}, as shown by EPR and magnetic measurements. PND technique showed surprising results concerning the spin density on the bridging nitrogen atom of the azide molecule. The results are in contradiction with the suggested exchange mechanism, showing a weak negative spin density on the terminal atom of the azido bridge, and virtually no spin density on the bridging nitrogen.

Inelastic Neutron Scattering (INS) and Neutron Diffraction techniques were used to investigate the magnetic excitation in an energy range up to 3 THz, and the spin correlation respectively, in a manganese cluster containing 8 Mn(III) and 4 Mn(IV) ions.[3] These experiments were carried out on the G6 spectrometer (diffraction) and 4F1 and 1T three axis spectrometers of the reactor Orphée. The results of this study put in evidence some inconsistency of the model that was developed to account for the magnetic and relaxation properties of this system.[4,5] In particular while the low energy excitation of the low temperature spectrum is in agreement with the pervious results obtained by High Field EMR spectroscopy[6] and is exactly predictable on a theoretical basis, the range of energy excitations between 1.0 and 2.5 THz is not fully understood.

References:

1 Pey, Y., et al., Adv. Mater. 6, 681(1994); Pey, Y., et al., to be published.

2 Aebersold, M.A., et al., to be published.

3 Hennion, M., et al., to be published, see also 27th Annual Southeastern Magnetic Resonance Conference.

4 Sessoli, R., et al., J. Am. Chem. Soc. 115, 1804 (1993).

5 Politi, R., et al., Phys. Rev. 75, 537 (1995).

6 Caneschi, D., et al., J. Am. Chem. Soc. 115, 1805 (1993).

Electron Correlations, Magnetism, and Structure of Small Clusters

Pastor, G.M., NHMFL
Mühlschlegel, B., Univ. of Cologne, Germany

The electronic, magnetic and structural properties of small clusters were studied in the framework of the single-band Hubbard Hamiltonian. Various ground-state and excited-state many-body properties were calculated exactly by means of Lanczos' numerical diagonalization method. A full geometry optimization was performed for $N \leq 8$ atoms by considering *all* possible non-equivalent cluster structures with fixed nearest-neighbor bond-lengths. The most stable structure and the corresponding total spin S were obtained rigorously as a function of the Coulomb-interaction strength U/t and number of electrons ν. The resulting interplay between electron correlations, magnetism and cluster structure was analyzed and the main trends as a function of N, U/t and n were derived. The stability of cluster ferromagnetism was studied from two complementary points of view. First, for $N \leq 8$ and $\nu = N+1$, we determined exactly the stability of the ferromagnetic ground-state with respect to electronic excitations and structural changes. It was shown that in small clusters the structural changes can be as important to the temperature dependence of the magnetization as the purely electronic excitations. Secondly, we determined the stability of the saturated ferromagnetic state with respect to single spin-flips as a function of the band filling ν/N. In this case a few selected larger clusters $(7 \leq N \leq 43)$ in the strongly correlated limit $(U/t \rightarrow +\infty)$ were considered. It was shown that the ν/N -dependence of the spin-flip energy $\Delta\varepsilon_{sf}$ shows interesting electronic-shell-like oscillations, which reflect the characteristics of the single-particle energy-level structure and its dependence on the symmetry and size of the cluster. Relevant extensions, such as considering a continuos distance dependence of the hopping integrals or several-band models, have been analyzed and are currently in progress.[1]

Reference:

1 Pastor, G.M., et al., Phys. Rev. B (1995) to be published.

Magnetic Anisotropy of Low-Dimensional Transition-Metal Systems

Pastor, G.M., NHMFL
Dorantes-Dávila, J., Universidad Autónoma de San Luis Potosí, Mexico
Dagotto, E., NHMFL

The magnetic anisotropy properties of several low-dimensional transition metal systems were studied in the framework of a d-electron tight-binding-like Hamiltonian that takes into account hopping, Coulomb, and spin-orbit interactions on an equal electronic level as well as the dipole-dipole energy contributions. The system-specific electronic structure was determined by calculating the spin-polarized electron-density distribution self-consistently. The magnetic anisotropy energy (MAE) was obtained in a non-perturbative fashion as difference between electronic energies.

The magnetic anisotropy energy (MAE) and related electronic properties of 3d transition-metal (TM) clusters were determined by calculating self-consistently the effects of the spin-orbit coupling on the spin-polarized charge distribution and on the electronic spectrum for different orientations of the magnetization. The MAE shows a complicated, non-perturbative behavior as a function of cluster size, structure, bond-length and d-band filling. In agreement with experiment, the MAE of small clusters is found to be considerably larger than in the corresponding crystals, often even larger than in thin films. Remarkably, the in-plane anisotropy can be of the same order of magnitude as the off-plane anisotropy.

The in-plane and off-plane magnetic anisotropy of bcc (110) transition-metal ultrathin films was determined self-consistently in order to characterize the MAE surface of these low-symmetry films. The MAE's were found to be very sensitive to the d-band filling, the exchange splitting and the film thickness. In particular we found alternations of the

easy and hard axes as a function of n_d as well as transitions from uniaxial to triaxial MAE surfaces. Remarkably, the in-plane anisotropy of (110) films is of the same order of magnitude as the off-plane anisotropy, which should be detectable experimentally.

The role of interlayer packing on the magneto-anisotropic behavior of close-packed (111) ultra-thin films was determined by considering fcc- and hcp-like films having up to 4 layers. For Fe, Co and Ni, we performed self-consistent calculations as a function of d-band filling and of film thickness, from which the MAE was obtained. The role of the self-consistent determination of spin-polarized charge redistribution on the MAE was quantified by comparison with simpler constant-exchange-splitting calculations. The magneto-anisotropic properties of (111) close-packed fcc- and hcp-like films were analyzed and compared with available experimental information.

Magnetic Properties of the Hubbard Model on Arbitrary Finite Graphs

Pastor, G.M., NHMFL
Dagotto, E., NHMFL

The magnetic properties of the Hubbard model were investigated on arbitrary finite graphs, i.e., by considering all possible forms of the kinetic-energy operator with nearest-neighbors hoppings. The ground-state correlation functions and total spin were determined numerically for ($N \leq 8$) sites by using the Lanczos method. For bipartite graphs ($N \leq 8$) at half-band filling one finds that the total spin S is independent of the strength of the interaction U/t. $S = |N_A - N_B|/2$, where N_A and N_B are the number of atoms in each sublattice ($N_A + N_B = N$). This coincides with the predictions of a theorem demonstrated by Lieb for N even. Our results suggest that the theorem could be possibly extended to all N. For non-bipartite graphs a much more complicated behavior is observed. In fact, depending on the graph, transitions to both higher and, less frequently, lower S are found as U/t increases. Simple predictions of the ground-state spin in terms of the graph connectivities seem difficult to find even in the limit of very strong correlations. Extensions of this work away from half-band filling, in particular by comparison with similar studies on the t-J model are currently in progress.

Short-Range Magnetic Order in Fe and Ni Clusters

Pastor, G.M., NHMFL
Dorantes-Dávila, J., Universidad Autónoma de San Luis Potosí, Mexico

A simple relation was derived between the low- and high-temperature values of the magnetization per atom of a N-atom cluster [$\bar{\mu}_N(T=0)$ and $\bar{\mu}_N(T>T_c)$]. Taking into account the degree of short-range magnetic order (SRMO) within the cluster, the experimental results for $\bar{\mu}_N(T=0)$ and $\bar{\mu}_N(T>T_c)$ of Fe_N and Ni_N were shown to be in agreement with model-independent predictions. The degree of SRMO retrieved in this way for the clusters is quantitatively similar to the one known from bulk and surface studies. A clear evidence for the existence of SRMO in small transition-metal clusters above $T_c(N)$ has been thus provided. Consequently, SRMO should play a significant role in the whole finite-temperature behavior of magnetic TM clusters and it should be considered in the interpretation of experiments as well as in future theoretical developments.[1]

Reference:

1 Pastor, G.M., et al., Phys. Rev. B, 52, 13799 (1995).

High Field Magnetization Studies of U_2T_2X Single Crystals

Prokes, K., Van der Waals-Zeeman Institute, Univ. of Amsterdam
de Boer, F.R., Van der Waals-Zeeman Institute, Univ. of Amsterdam
Havela, L., Charles Univ., The Czech Republic, Dept. of Metal Physics
Sechovsky, V., Charles Univ., The Czech Republic, Dept. of Metal Physics
Pereire, L.C., European Commission, Institute for Transuranium Elements, Germany
Nakotte, H., LANSCE-LANL
Haanappel, E.G., NHMFL/Los Alamos
Lacerda, A., NHMFL/Los Alamos

Recently, a new large isostructural group of tetragonal (U_3Si_2-type structure) U compounds with stoichiometry U_2T_2X (T = late transition metal, X = p-metal) was discovered showing the development of magnetic properties with respect to the constituent elements. This points to the importance of hybridization of f-electronic states with the d- and p- states of the surrounding ligands, which is also responsible for huge magnetic anisotropy fields, typically hundreds or thousands of tesla (T), which force the moments to lie in particular crystallographic directions. An initial antiferromagnetic ground state of the ordered samples can be changed upon application of rather high magnetic fields through metamagnetic transitions. At present, several single crystals prepared by the mineralization method became available. The most interesting sample, U_2Pd_2In, as one of them, orders antiferromagnetically below 37 K and exhibits metamagnetic transition at 25 to 30 T depending on orientation with respect to applied field (Figure 1). No transition could be found when applying the magnetic field parallel to the c-axis in magnetic fields to 55 T. Initial diffraction studies performed at Manuel Lujan Jr. Neutron Scattering Center (MLNSC), formerly Los Alamos Neutron Scattering Center (LANSCE), determined the noncollinear moment arrangement (moments perpendicular to the c-axis). Subsequent theoretical work in Germany, published in Phys. Rev. Letters[1], reproduced the experimental results and in addition showed the in-plane anisotropy to be much larger than the normal uniaxial anisotropy. Our experimental result is readily understood in terms of the previous results as an antiferromagnetic dimer, in which one uranium moment flips against the exchange field, with no change in the magnetic anisotropy. The second system studied, U_2Ru_2Sn, which can be classified as a spin fluctuating system (close to magnetic ordering) exhibits no metamagnetic transition up to 55 T. In this particular case, weaker anisotropy has been observed.

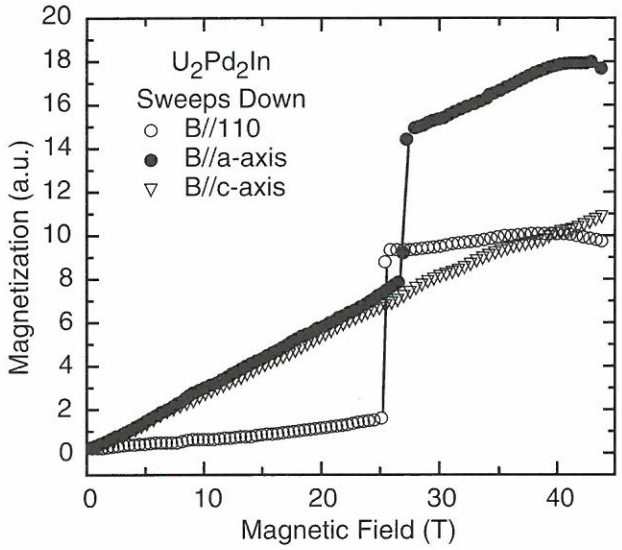

Figure 1. Magnetization of U_2T_2X at 4 K.

Reference:

1 Sandratskii, L.M., et al., Phys. Rev. Lett., 75, 946 (1995).

Quantum Monte Carlo Calculations of NMR-Rates in Low-Dimensional Quantum Antiferromagnets

Sandvik, A., NHMFL
Dagotto, E., NHMFL
Scalapino, D.J., Univ. of California, Santa Barbara, Physics Dept.

We have used a quantum Monte Carlo technique and a maximum entropy analytic continuation method to compute the spin-lattice relaxation rate $1/T_1$ and the spin-echo decay rate $1/T_{2G}$ for the S = 1/2 antiferromagnetic Heisenberg

model in several geometries.[1-4] Our goal in these studies have been to verify theoretical results and establish their limits of validity, as well as to obtain results useful for direct comparisons with experiments. For the linear chain, we have shown that the possibility of observing the expected asymptotic low-temperature forms depends strongly on details of the nuclear hyperfine form factor.[2] If the form factor has significant weight at long wavelengths, the contributions to $1/T_1$ from uniform magnetization fluctuations are important and the temperature dependence at high temperatures is significantly different from theoretical predictions including only the contributions from the staggered magnetization fluctuations. The temperature dependence of $1/T_{2G}$ is also affected. Results obtained for the 2-leg ladder model have been compared to recent experiments on $SrCu_2O_3$.[4] We have proposed a reason for the discrepancy reported for the size of the spin gap in this compound as obtained from susceptibility and $1/T_1$ measurements. We argue that the correct gap is obtained from the susceptibility, and that the theoretical form used to extract the gap from $1/T_1$ is not accurate in the temperature regime accessible experimentally. We find that the experimental results for the susceptibility, $1/T_1$ and $1/T_{2G}$ can all be accounted for reasonably well within a ladder model with equal chain and rung couplings of strength $J \approx 850K$. Results for $1/T_1$ and $1/T_{2G}$ calculated for a two-dimensional model are in good agreement with experiments on La_2CuO_4.[1] Studies of a bilayer model indicate that even a quite weak coupling between the planes pushes the system significantly deeper inside the renormalized classical regime, with consequences for many experimentally observable quantities. In particular, we propose that measurements of $1/T_{2G}$ at high temperatures would be useful for extracting the strength of the intrabilayer coupling J_2 in bilayer cuprates such as $YBa_2Cu_3O_6$.[3]

References:

1 Sandvik, A.W., et al., Phys. Rev. B, 51, 9403 (1995).

2 Sandvik, A.W., Phys. Rev. B, 52, R9831 (1995).

3 Sandvik, A.W., et al., Phys. Rev. B, accepted.

4 Sandvik, A.W., et al., Phys. Rev. B, accepted.

Magnetoluminescence Study of $Zn_{1-x}Mn_xSe$ Epilayers at High Magnetic Fields

Schmiedel, T., NHMFL
Lee, S., Univ. of Notre Dame, Physics Dept.
Dobrowolska, M., Univ. of Notre Dame, Physics Dept.
Furdyna, J.K., Univ. of Notre Dame, Physics Dept.

Despite intense studies of ZnMnSe as a representative wide gap II-VI DMS system for more than 10 years, some of its fundamental magneto-optical properties are still not fully understood. In this report we present a comprehensive magneto-photoluminescence study of a series of $Zn_{1-x}Mn_xSe$ epitaxially grown layers with a Mn concentration ranging from $0<x<0.25$, which provides significant insight into the magneto-optical behavior of this material for higher Mn concentrations.

The photoluminescence measurements were performed using the 364 nm Argon laser line at a temperature of 1.8 K, and at fields up to 30 T. Figure 1a and 1b show the dependence of the excitonic luminescence peak energy on the magnetic field for various Mn concentrations x. In the presence of even moderate magnetic fields (< 10 T), the PL peak exhibits a giant red shift. In addition, the intensity of the emission increases by a factor of about 10.

The red shift reflects the value $\langle S_z \rangle$ of the thermally averaged spin of the Mn ions. It is well known that for low temperatures and low Mn concentrations ($x < 0.05$), the red shift (and thus also $\langle S_z \rangle$) saturates beyond 5 T. We, on the other hand, record a continued red shift for Mn concentration $x > 0.15$ and fields up to 30 T without signs of saturation.

This behavior can be understood in a picture of a DMS alloy consisting of isolated Mn spins, as well as Mn spin pairs and larger clusters, which

necessarily form for higher concentrations x. This exchange coupled Mn spin sublattice undergoes a transformation when the magnetic field increases. As expected, the single Mn spins are aligned into saturation. However, at higher fields, the pairs and larger clusters undergo an internal spin reconfiguration. For example, in the 6 level d-spin system of Mn, the pairs are initially spin compensated <-5/2, +5/2>. With increasing field, a gradual quantized realignment of the spins turns them successively into 3/2, 1/2, -1/2, etc. positions, causing a net magnetization of the pairs at higher fields. A similar behavior is expected for larger clusters, which becomes more important as x increases, and eventually dominates the observed behavior for x > 0.15. This increased spin contribution leads to a non-saturation behavior of the Zeeman splitting as seen in Figure 1b.

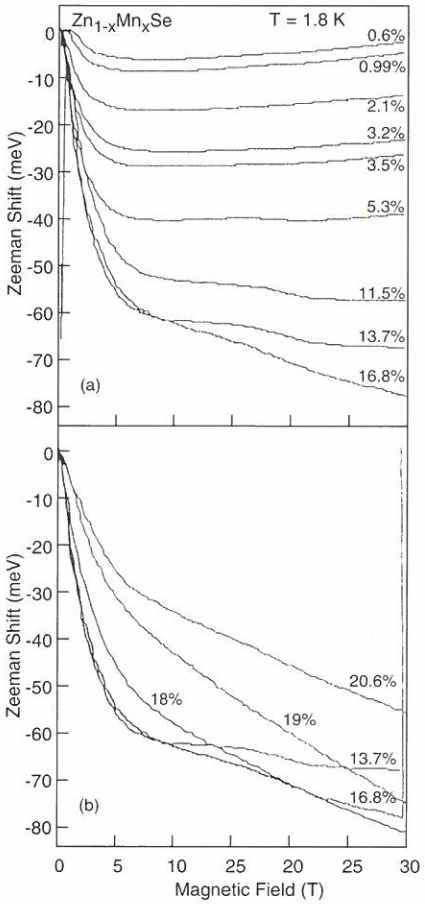

Figure 1. Zeeman Shift for $Zn_{1-x}Mn_xSe$ of different Mn concentrations.

The breakup of Mn spin pairs and clusters has its distinct signature in the observed change in slope of the Zeeman splitting at 15 T (Figure 1a). This agrees well with the known behavior of AF pairs, which give rise to magnetization steps in DMSs. This is observed for $0.05 < x < 0.15$, but for higher x these steps gradually wash out and finally give way to the continuous non-saturating increase in the magnetization $\langle S_z \rangle$ seen for $x > 0.15$ (Figure 1b). This increase is expected in $Zn_{1-x}Mn_xSe$ to continue up to nearly 100 T.

Fermion Spectral Function in Antiferromagnetic Spin Fluctuation Systems

Schrieffer, J.R., FSU Physics Dept./NHMFL
Kampf, A.P., Institute for Theoretische Physik, Universität zu Köln, Germany

We have extended our earlier calculations[1] of the one hole spectral function within the one loop approximation for the two dimensional one band Hubbard and spin fermion models, using a spin susceptibility χ which is peaked at wavevector $Q = (\pi, \pi)$ and having a characteristic spin fluctuation frequency ω_o. Finite concentration hole doping has been investigated, with the spin correlation length varying from the lattice spacing to size large compared to this length. One of the key results of this work is the understanding of the origin of the central peak of the spectral function, which for the undoped crystal above the Néel temperature occurs midway between the SDW valence and conduction band edges. In essence, the central peak arises from motional averaging the phase of the SDW which leads to a very weak scattering potential for the hole energies less than the spin fluctuation energy ω_o, while the full potential enters in determining the spectrum of hole or electron states whose energies are large compared to ω_o.[2] This effect is analogous to anomalous dispersion of electromagnetic modes that occurs in solids having a large dielectric constant ε at low frequency and a small value of ε at high frequency. In the present problem, the role of ε is played by $(1-\Sigma/\omega)^2$ where Σ is the electron self energy. The central peak can be viewed as the Landau quasi particle peak continued into the strong spin fluctuation phase.

References:

1 Kampf, A.P., et al., Phys. Rev. B, 42, 7967 (1990).

2 Kampf, A.P., et al., Physical Phenomena in High Magnetic Fields II, to be published by World Scientific Press, (1996).

High Field Magnetization of a $NdCu_2$ Single Crystal in the Paramagnetic Region

Svoboda, P., Charles University, The Czech Republic, Dept. of Metal Physics
Divis, M., Charles University, The Czech Republic, Dept. of Metal Physics
Sechovsky, V., Charles University, The Czech Republic, Dept. of Metal Physics
Nakotte, H., LANSCE-LANL
Lacerda, A., NHMFL/Los Alamos
Onuki, Y., University of Osaka, Japan
Sugawara, H., Tokyo University, Japan

$NdCu_2$ crystallizes in the orthorhombic $CeCu_2$ structure and orders antiferromagnetically below $T_N = 6.3$ K.[1] For this compound, the relatively weak antiferromagnetic exchange is dominated by orthorhombic crystal field (CF). Therefore, $NdCu_2$ is a model system for extracting the importance of crystal fields in these kinds of materials. Inelastic-neutron-scattering experiments showed that the CF splits the ground state multiplet $^4I_{9/2}$ of Nd^{3+} into five Kramers doublets and the energy of first excited doublet is 33 K.[2] The magnetocrystalline anisotropy of $NdCu_2$ is the dominated by the population of these doublets. The temperature dependences of magnetic susceptibilities measured along the principal crystallographic axes show changes in the magnetocrystalline anisotropy around 15 K and around 80 K. Changes in the anisotropy are also found in magnetization measurements below T_N, which reveal a crossing of the magnetizations for fields applied along the a and b-axis.[3] The observed susceptibility and magnetization behavior can be qualitatively described by a set of crystal-field parameters as given in references 2 and 3. A quantitative comparison of the measured and calculated magnetizations, however, is hampered due to exchange interactions in the magnetically-ordered region. Therefore, we performed magnetization measurements in the paramagnetic region, where the effect of exchange interactions should be considerably smaller. We have measured magnetic response with field applied along principal crystallographic directions at 10, 20, 50, 80, and 100 K using the 20 T superconducting magnet at the Pulsed Field Facility at Los Alamos National Laboratory. As expected from susceptibility measurements, we find that, compared to the other two directions, the b-axis magnetization is the highest at 10 K, while it is the lowest at 100 K. Our comprehensive set of high-field magnetization curves in paramagnetic region is a very sensitive test of validity of our crystal-field parameters. Such analysis is presently underway and the results of our calculation will be used as an independent test of new inelastic-neutron-scattering results obtained on a single crystal of $NdCu_2$.

References:

1 Hashimoto, Y., J. Sci. Hiroshima Univ., A43, 157 (1979).

2 Gratz, E., et al., J. Phys. Condens. Matter, 3, 9297 (1991).

3 Svoboda, P., et al., Physica B, 211, 172 (1995).

Usefulness Of Cernox™ Sensors for Low Temperature Thermometry in Magnetic Fields to 20 Tesla

Brandt, B.L., NHMFL
Liu, D., FSU, Physics Dept.
Courts, S.S., Lake Shore Cryotronics

The increasing use of higher field magnets for laboratory research has increased the need for temperature sensors that give accurate, repeatable measurements in magnetic fields ≤20 T. An ideal sensor would be independent of magnetic field. The next best alternative would have field dependence that is small and correctable by a method that is independent of the manufacturing process. Considerable research aimed at developing sensors has been done and several commercially available sensors have been characterized.[1] CERNOX™ zirconium oxy-nitride film sensors (CXRT) from Lake Shore Cryotronics were found in preliminary studies to have lower magnetoresistance than comparable sensors, so we decided to do a more thorough series of measurements in magnetic fields up to 20 T at temperatures between 1.5 and 320 K. The cryostat and methods used were the same as for a previous study of carbon-glass (CGRT) sensors.[1]

Average longitudinal magnetoresistance data $\{\Delta R/R_o=[R(B)-R(O)]/[R(O)]\}$ at selected temperatures are shown in Figure 1 for seven of the CERNOX units. The magnetoresistance behavior is similar to that of carbon and carbon-glass, exhibiting both positive and negative values in different temperature and field regions.

Researchers measuring temperatures in high magnetic fields are interested in not only the relative change in resistance of a temperature sensor, but also the apparent or equivalent temperature change. Equivalent percentage temperature errors are approximately given by $\Delta T/T = (\Delta R/R_o)/S_d$, where $S_d = (T/R)(dR/dT)$ is the dimensionless sensitivity measured at the temperature corresponding to R_o. A sensor with a low $\Delta R/R$ may nevertheless have a large apparent temperature error if the dimensionless sensitivity is low. Figure 2 shows a comparison of the CXRT average values of $\Delta T/T$ with comparable values for CGRTs for two values of the magnetic field. It is clear that the CXRT has less magnetoresistive temperature error for most of the temperature range studied. However there was more variation of the magnetoresistive behavior from batch to batch the CXRTs than in CGRTs; perhaps because the process of manufacturing CXRTs is newer and not fully understood. Also, fewer different models of CGRTs were included in the earlier study. Future work with more sensors from different batches will show the circumstances under which correction of CXRTs is reliable. We will also consider the orientation dependence of the magnetoresistance and extend the data to higher magnetic fields.

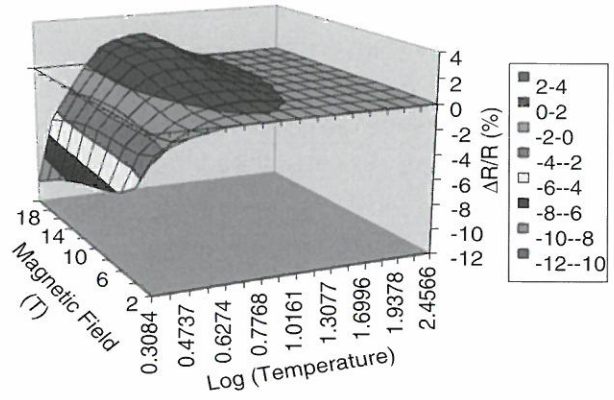

Figure 1. $\Delta R/R_o$ (%) for seven CERNOX sensors displayed as a function of the magnetic field and the log of the temperature.

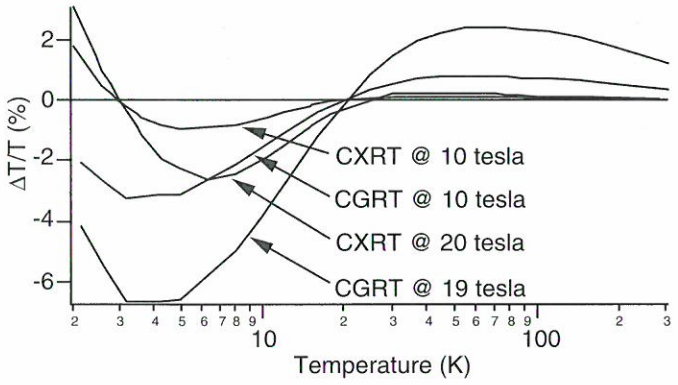

Figure 2. Comparison of temperature errors due to magnetoresistance of CERNOX and carbon-glass sensors. ΔT/T (%) is shown as function of temperature for large and intermediate fields.

Reference:

1 Sample, et al., Low-temperature thermometry in high magnetic fields, V. Carbon-glass resistors, Rev. Sci. Instrum. 53:1129 (1982).

Anomalous Magneto-Transport Near Metal-Insulator Transitions

Dobrosavljevic, V., NHMFL
Sarachik, M., City College of CUNY
Bogdanovic, S., City College of CUNY
Dai, P., City College of CUNY

Uncompensated doped semiconductors such as Si:P or Si:B have long been used as prototypical systems for the study of metal to insulator transitions (MIT). Nevertheless, many properties of these systems have proved to be puzzling, and difficult to understand or even analyze in conventional terms. In particular, temperature and concentration dependence of the conductivity seems difficult to fit into standard scaling formulations of the MIT.

Interestingly, application of strong magnetic fields (0-9 tesla) has recently been shown to provide important clues as to the origin of these anomalies. Detailed experimental studies of the low temperature (50-500 mK) magneto-transport have been carried out in Si:B, displaying remarkable scaling behavior.[1,2] These results, together with an appropriate theoretical interpretation, demonstrated that the *amplitude* of the magneto-conductance displays a dramatic *decrease* in the vicinity of the MIT. Theoretically, this amplitude measures the spin-dependent part of the effective electron-electron interaction.

Very recently, we have formulated[3] a simple phenomenological description of this behavior. A "minimum model" has been presented that, while adopting a standard scaling description, at the same time is consistent with the experimental findings. Our results show that in the considered case, the rapid decrease of the magnetoconductance induces *corrections to scaling* that cannot be ignored. We propose that this behavior could very well be at the source of most of the observed anomalies, and also suggest ways to test these ideas in other systems.

References:

1 Bogdanovic, S., et al., Phys. Rev. Lett., 74, 2543, (1995).

2 Bogdanovic, S., et al., to be published.

3 Dobrosavljevic, V., et al., unpublished.

Glassy Behavior of Disordered Interacting Electrons

Dobrosavljevic, V., NHMFL
Horbach, M., Rutgers Univ., Physics Dept.

Very generally, the interplay of electronic correlations and disorder is believed to be the driving force behind metal-insulator transitions observed in a wide range of materials. However, while the electronic repulsion favors *uniform* spatial ordering, disorder due to impurities breaks translational invariance and leads to inhomogeneities. As a result, the electronic correlations and disorder can be thought as *competing* forces—leading to *frustration,* similarly as in spin glasses. One thus anticipates the existence of many low-lying metastable states, and possibly glassy freezing at low temperatures. In contrast to spin glasses where *spin* degrees of freedom were found to freeze in complex patterns, in the present case, it is the *charge* degrees of freedom that are expected to display glassy behavior.

In this project, we have set out to study the role of such glassy freezing as a possible driving force for the metal-insulator transitions. The simplest model that contains the relevant physics is given by a single-band model of *spinless* electrons characterized by a hopping element t, nearest-neighbor repulsion V, and random site energies ε_i ("random t – V model"). On general grounds, one anticipates that electron localization will occur for sufficiently small values of the quantum hopping t. To investigate this behavior, we have concentrated our analysis on the classical limit $t \rightarrow 0$, which still represents a nontrivial problem due to competing electronic repulsion and disorder. Interestingly, in this limit the problem can be mapped onto the well-known *random-field Ising model* (RFIM), by introducing pseudo-spin variables $S_i = 2n_i - 1 = \pm 1$, instead the occupation numbers $n_i = 0,1$. The electronic repulsion V is then replaced by an antiferromagnetic interaction $J = \frac{1}{4}V$, and the random site energies ε_i by random magnetic fields h_i.

A powerful tool for analyzing the behavior of strongly correlated disordered electrons,[1] as well as glassy systems[2] is the dynamical mean-field approach based on taking the large dimensionality limit ($d \rightarrow \infty$). We have investigated[3] the existence of a low temperature glassy phase in the RFIM by using a standard replica approach, and performing a 1/d expansion. It is well known that a glassy phase is not found in the mean-field ($d = \infty$) limit. However, to next order in 1/d, a replica symmetry breaking instability emerges at low temperatures, that can be interpreted as an onset of ergodicity breaking, i.e., glassy behavior. Our results demonstrate that the critical temperature $T_g(H_{rf})$ decreases very slowly, ~$1/H_{rf}$, as the random field strength H_{rf} is increased. In the electronic language, T_g is the temperature below which the electronic density *freezes* in a nonuniform fashion, leading to strongly enhanced *effective* strength of disorder seen by the itinerant electrons. If this effect is sufficiently pronounced away from the classical limit, the discovered renormalization of disorder could be considered as a possible driving force for the metal-insulator transition. In the coming period, we will extend our approach to the quantum regime ($t \neq 0$), and examine the melting of this *electron glass* by quantum fluctuations.

References:

1 Dobrosavljevic, V., et al., Phys. Rev. Lett., 71, 3218 (1993).

2 Sompolinsky, H., et al., Phys. Rev. Lett., 41, 359 (1981).

3 Dobrosavljevic, V., et al., unpublished.

Multiple Echoes in Solid Hydrogen at High Nuclear Spin Polarizations

Kisvarsanyi, Erika G., UF Physics Dept.
Sullivan, N.S., NHMFL/UF Physics Dept.

NMR multiple echoes can occur in solids if the non-linear components of the equations of motion for the nuclear magnetization are sufficiently strong. In principle they can be observed in any material but in practice have only been observed in solid ^{3}He [1,2] for which the high particle-particle exchange rates result in increases of the nuclear spin-spin relaxation time T_2 by almost three orders of magnitude above the rigid lattice values. We are particularly interested in the possibility of observing multiple spin echoes in solid hydrogen in order to test for the existence of quantum tunneling in the solid hydrogens. The current theoretical understanding of tunneling in solid ^{3}He leads to multiple particle exchange effects and these are predicted to lead to observable tunneling rates in solid H_2. Observation of these rates or new limitations on the rates for solid H_2 would provide a crucial test of the understanding of tunneling in quantum solids in general.

In the formation of the NMR solid echoes using two $\pi/2$ pulses, the first pulse creates a transverse magnetization M_t that precesses about the direction of the local applied magnetic field. A second pulse converts the transverse magnetization into a longitudinal magnetization $M_z(t)$ that will have a spatial variation that will carry a *fingerprint* of the

The design chosen for the spectrometer uses two junction field effect transistors (JFETs), one operating as a source follower with the RF tank circuit as input, and the second as a common gate amplifier providing RF feedback to the tank circuit. The non-linearity of the amplifying stage and the feedback is adjusted to provide marginal oscillation and thus realize the high sensitivity of the Pound-Watkins marginal oscillator.[2] The critical feature of this design is the choice of field effect transistors that must operate with high transconductance at low gate cut-off voltages in very high magnetic fields. It is also important to use electronic components in the circuit construction with low magnetic susceptibility ($< 5.\ 10^{-4}$ cm^3/gm.) in order to not seriously distort the magnetic field at the experimental site. We selected the JFET J300 series[3] because of the planar geometry of the device and examined the variation of the conductance with orientation in an applied magnetic field. We observed that the high transconductance of these devices could be maintained for the correct orientation, with more than 80% of the zero field transconductance realized at 30 T. For orientations perpendicular to the 30 T applied field the conductance dropped to 15% of the zero field value. The field dependence at fixed angle was observed to be non-linear and further studies are needed to have a complete picture of the field dependence resulting from the geometry of the internal structure of the device.

This work was supported by a grant from the National Science Foundation DMR-9216785.

References:

* NHMFL Minority Fellow, 1995.

1 Andersen, P.M., et al., Rev. Sci. Instr., 63, 157 (1992).

2 Pound, R.V., et al., Rev. Sci. Instr. 21, 219 (1950).

3 Motorola Inc. Semiconductor Products, Phoenix, AZ.

Improved Penning Ion Traps

Marshall, A.G., NHMFL/FSU, Chemistry Dept.
Guan, S., NHMFL/FSU, Chemistry Dept.
Huang, Y., NHMFL

Fourier transform ion cyclotron resonance (FT-ICR) mass spectrometry requires that ions be confined in a Penning trap, consisting of a spatically uniform magnetic field, B, and the electrostatic potential shown in Figure 1 (top). However, optimal excitation and detection of such ions requires the rf potential of Figure 1 (bottom); moreover, "shrink-wrapping" of ions to form a compact ion packet requires the rf potential of Figure 1 (middle). If the

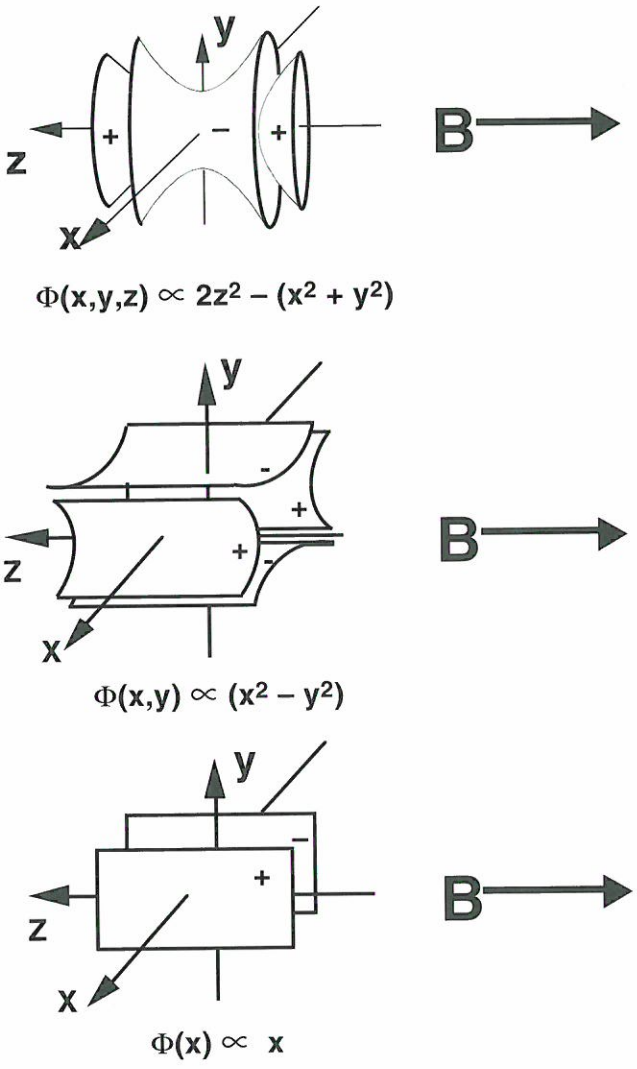

Figure 1. Electric isopotential surfaces. Top: 3D axial quadrupolar; Middle: 2D azimuthal quadrupolar; Bottom: 1D dipolar.

trap is to be constructed with continuous conductive surfaces, then none of the trap shapes of Figure 1 can satisfy all three requirements. As a result, dozens of compromise Penning trap designs have evolved.[1]

In 1995, we showed that by suitable segmentation of such a trap,[1-3] with appropriate voltages applied to each of the segments, it is in fact possible to approach closely all three of the desired potentials with a *single* geometric configuration. Figure 2 shows our "matrix-shimmed" Penning trap.[1] Numerical simulations confirm that it provides highly accurate potentials of the three types shown in Figure 1, and experimental construction of a prototype is under way.

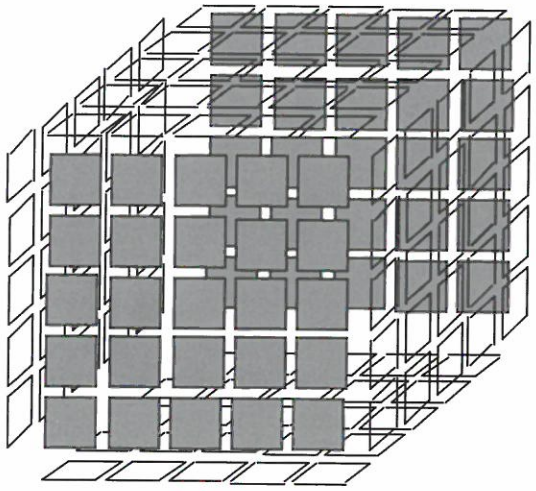

Figure 2. Matrix-shimmed segmented cubic Penning ion trap. This trap can produce any or all of the potentials shown in Figure 1.

References:

1 Guan, S., et al., Int. J. Mass Spectrom. Ion Proc., 146/147, 261-296 (1995).

2 Guan, S., et al., Rev. Sci. Instrum., 66, 63-66 (1995).

3 Guan, S., et al., J. Mass Spectrom., 30, 0000-0000 (1995).

New Techniques for Ion Injection into a Penning Ion Trap

Marshall, A.G., NHMFL/FSU, Chemistry Dept.
Guan, S., NHMFL/FSU, Chemistry Dept.
Marto, J.A., NHMFL/Ohio State Univ., Chemistry Dept.
Limbach, P.A., Ohio State Univ., Chemistry Dept.
May, M.A., Ohio State Univ., Chemistry Dept.

Some of the best methods for generating molecular or quasimolecular ions require atmospheric pressure, whereas Fourier transform ion cyclotron resonance mass spectrometry (FT-ICR MS) is optimally performed at a pressure of 10^{-8} torr or less. Injection of ions into a region of strong magnetic field requires that ions be accelerated (and later decelerated) and/or kept tightly focused along the B-axis to defeat the "magnetic mirror" effect. Prior ion injectors have been based on rf-only quadrupole or octupole ion guides (Figure 1, middle diagrams), electrostatic einzel lenses, or a lens-less supersonic ion beam. In 1995, we reviewed various ion injection methods.[1]

We also presented the first detailed analysis of ion trajectories through a wire-in-cylinder ion guide (Figure 1, top).[2] Based on our numerical simulations, this device promises to transmit ions up to very high mass-to-charge ratio ($m/z = 10{,}000$), with relatively low accelerating potential (~25 V), and wide entry angle (30°) through a strong magnetic field gradient, without significant ion loss. A prototype ion guide of this type has been built, and is currently being installed.

In an entirely different approach, we showed that ions moving at constant speed parallel to the axis of a stack of statically charged rings of alternating charge sign (Figure 1, bottom) encounter an effectively static "pseudopotential" much like that in a more conventional multiple ion guide.[3] The main difference is that the radial pseudopotential in the stacked-ring guide varies as exp(r), whereas the radial pseudopotential in a quadrupole or octupole ion guide varies as r^2 or r^4,

respectively. Thus, the stacked-ring guide is more like a mechanical "pipe" in which ions move relatively freely until they nearly hit the walls. Our simulations show that the stacked-ring ion guide should also transmit ions of a wide range of mass or energy, with the advantage of simple and inexpensive construction (e.g., a stack of drilled pennies should work).

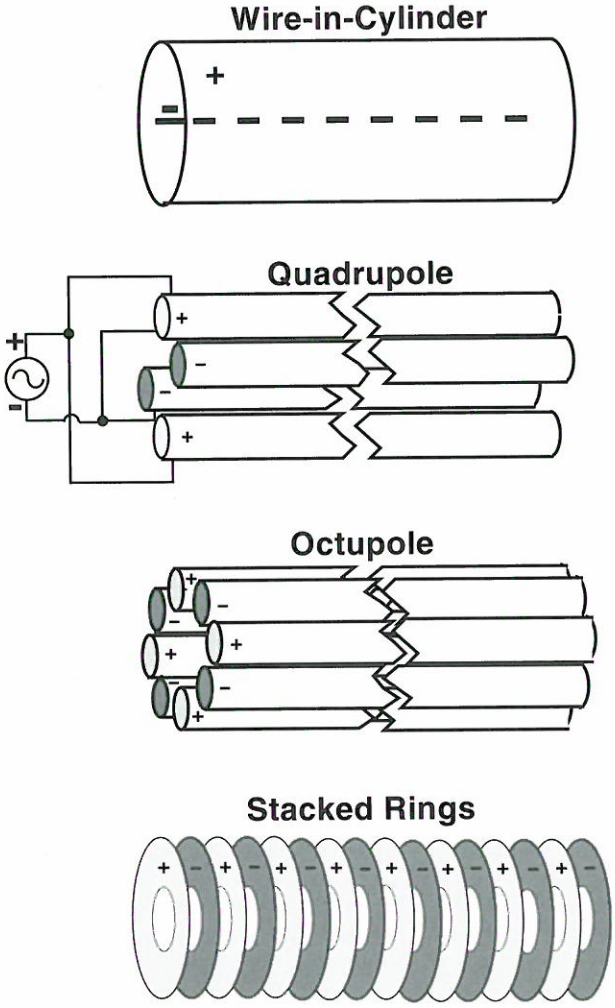

Figure 1. Various ion guides for injection of ions from an external ion source, through a strong magnetic field gradient, into a Penning trap at high magnetic field.

References:

1 Marshall, A.G., et al., Nucl. Instr. and Meth. A., 363, 397-405 (1995).

2 Marto, J.A., et al., J. Am. Soc. Mass Spectrom. 6, 936-946 (1995).

3 Guan, S., et al., J. Amer. Soc. Mass Spectrom. 6, 0000-0000 (1995).

Line Shape Variations of a Spin 1/2 Nucleus Coupled to a Quadrupolar Spin Subjected to RF Irradiation

Murali, N., NHMFL
Rao, B.D.N., IUPUI, Physics Dept.

We have investigated line-shape variations in the multiplet structure of a spin 1/2 nucleus I (^{13}C) scalar coupled to a quadrupolar spin S (^{2}H) as a function of the strength of continuous-wave radio frequency (rf) field applied in the vicinity of the S spin resonance and of the relaxation times of the latter. These line shapes were simulated using an exact theoretical treatment based on the solution of the complete density matrix equations (including both coherent and incoherent parts) in the presence of rf irradiation of spin S. The rf field strength of the irradiation was varied over a wide range and the two cases of (i) complete and (ii) incomplete "washing out" of the spin coupling between the nuclei were separately considered. The simulations illustrate the dependence of the spectrum of spin I on various parameters such as the value of the scalar coupling constant, the quadrupolar relaxation times, and the irradiation strength in any experimental context (Figure 1). In addition, a simpler theory for the case of completely washed out scalar coupling in which the scalar interaction is treated exclusively as a relaxation process has been explored.

by the Lorentz force per unit length acting on the ring, L^i and the spring forces per unit length due to the radial links to the adjoining rings, $\frac{F_{i-1}}{b_{i-1}}$ and $\frac{F_{i+1}}{b_{i+1}}$. Where

$$F_{i-1} = c_{i-1}\,[u^{(i-1)}(\theta_{i-1}) - u^{(i)}(\theta_{i-1})]$$

$$F_{i+1} = c_{i+1}\,[u^{(i+1)}(\theta_{i+1}) - u^{(i)}(\theta_{i+1})]$$

$b_{i\pm1}$ = width of the connection between rings i and $i \pm 1$

$\theta_{i\pm1}$ = angular position of link between rings i and $i\pm1$

$c_{i\pm1}$ = stiffness of link between rings i and $i\pm1$.

Making the appropriate substitutions and integrations, we see

$$p_k^{(i)} = \frac{2}{\pi}\frac{m}{k}\left\{\frac{c_{i-1}}{b_{i-1}}\sin\left(\frac{kb_{i-1}}{2r_i}\right)\sum_{n=0}^{\infty}\left[u_n^{(i-1)} - u_n^{(i+1)}\right] + \frac{c_{i+1}}{b_{i+1}}\sin\left(\frac{kb_{i+1}}{2r_i}\right)\sum_{n=0}^{\infty}(-1)^{\frac{n+k}{m}}\left[u_n^{(i+1)} - u_n^{i}\right]\right\} + \left(\frac{EA_i}{r_i^2} + \frac{EI_i}{r_i^4}\right)u_k^{(i)}$$

where i is an even number and a radial link between rings one and two lies at 0° and m is the number of links per ring. By symmetry we see that only the integer multiples of m are non-zero in both p and u. If we truncate the series we can then get a diagonally-dominant set of equations that can be solved to give u. We can then compute stresses and use this for magnet design.

Preliminary results agree well with ANSYS calculations and are orders of magnitude faster to generate.

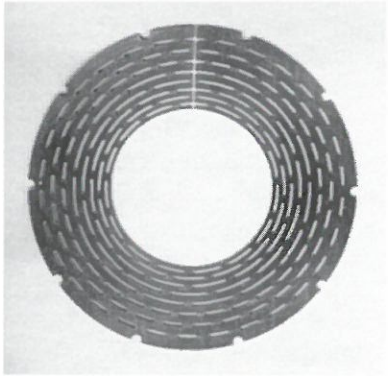

Figure 1. Compliant Bitter disk for 34 T magnet.

The Uniformity of CuAg Sheet

Bird, M.D., NHMFL
Summers, L.T., NHMFL
Garmestani, H., NHMFL/FSU-FAMU CoE

A copper-silver alloy was recently developed at the National Research Institute for Metals in Tsukuba, Japan and is available in sheet form from an industrial supplier. This material has a combination of high strength and high electrical conductivity that is unmatched by any other known alloy. Consequently it shows great promise for fabrication of Bitter disks.

We recently obtained 500 pieces of material 158 * 635 * 0.40 mm and have investigated the uniformity of the material. The measured thickness of the material was $0.415^{+0.012}_{-0.029}$ mm. Three dogbone tensile specimens were made parallel and perpendicular to the rolling direction of the material. The tensile and yield stresses were measured and are reported in Table 1. We see 16% and 13% variations in yield and ultimate strengths between the two directions.

Table 1. Yield and ultimate strength of 0.4 mm CuAg sheet.

Specimen	Yield Strength (MPa)	Ultimate Strength (MPa)
Parallel 1	760	910
Parallel 2	786	913
Parallel 3	799	933
Average	782	919
Perpendicular 1	930	1044
Perpendicular 2	898	1039
Perpendicular 3	900	1042
Average	909	1042

Three sets of fatigue tests were performed using specimens both parallel and perpendicular to the rolling direction. The first one used photochemically machined (PCM) modified dogbone specimens that were cyclically loaded to 833 MPa. The second test used the same geometry and load but the parts were cut using computer

numerically controlled (CNC) milling. The third test used CNC machined specimens that were loaded to 694 MPa. Cycles to failure are presented in Table 2. It is important to note that two of the PCM parts failed at a very low number of cycles. These specimens did not show uniform hole size, rather the holes varied in width by about 10%.

Table 2. Fatigue life of 0.4 mm CuAg sheet.

Sheet Orientation	Cycles to Failure		
	PCM	CNC1	CNC2
Parallel	24	3358	11541
Parallel	48	4023	15002
Parallel	9129	——	12531
Average	3067	3690	13024
Perpendicular	5043	6500	14455
Perpendicular	5501	4555	16746
Perpendicular	4052	9231	17588
Average	4865	6762	16230

When real Bitter disks were fabricated, it was seen that the holes do not etch uniformly as shown in Figure 1. The cause of this non-uniformity is being investigated. Non-uniform Ag concentrations could easily explain the thickness variation, the etch rate variation, and the resulting fatigue life variation.

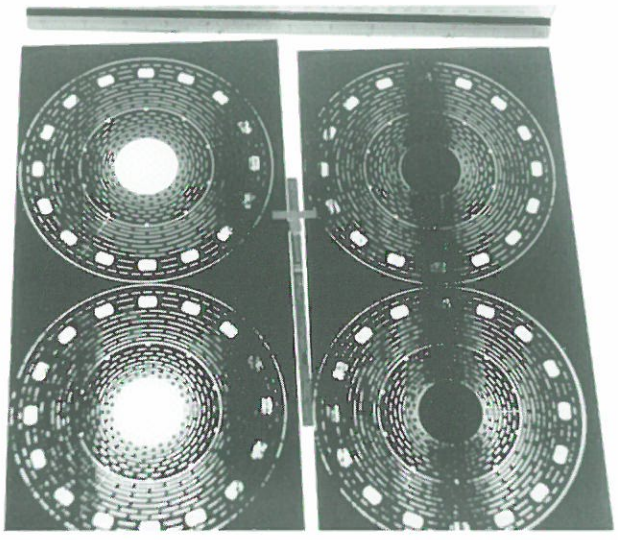

Figure 1. Non-uniform etching of CuAg sheet.

Design and Analysis of High Homogeneity Resistive Magnets

Eyssa, Y.M., NHMFL
Bird, M.D., NHMFL
Gao, B.J., NHMFL
Schneider-Muntau, H.J., NHMFL

The NHMFL will design and construct a 25 T, 50 mm bore resistive magnet with a spatial uniformity better than 1 ppm over a 10 mm diameter sphere. It will be the world's highest field magnet for magnetic resonance spectroscopy: nuclear magnetic resonance (NMR), electron paramagnetic resonance (EPR), and ion cyclotron resonance (ICR).

As a first step in designing high homogeneity magnets, we have modified our 27 T, 3-coil, 32 mm bore, 600 ppm (10 mm DSV) first resistive magnet to 24.6 T, 30 ppm simply by having a split of 51.5 mm at the midplane of the middle coil. The field uniformity is limited by the stray field from the current leads and bussing. In the proposed 25 T, 50 mm bore magnet we will adopt a magnetic, thermal and mechanical design that should result in a 1 ppm field uniformity. To reduce the current leads stray field, we will bring the current leads from and to the power supply terminal to the housing as close to each other as possible. The bussing connection between the three concentric coils will be axisymmetric. We are designing each stack to have a high uniformity by itself to increase the acceptable tolerances in centering the midplane of all the stacks. This is not the optimum way to generate the maximum possible field, but it eliminates one critical tolerance from the manufacturing process which is difficult to control after installation. The high uniformity of each coil is accomplished by axial current density grading of each coil. Figure 1 shows the expected uniformity of the three coils.

Another factor that affects the uniformity is the current distribution in Bitter disks. Because of the presence of cooling holes, tierod holes, and non uniform conductivity due to the temperature distribution, the current density deviates from the ideal 1/r distribution. Preliminary analysis shows

the importance of accounting for the actual current distribution in calculating field homogeneity.

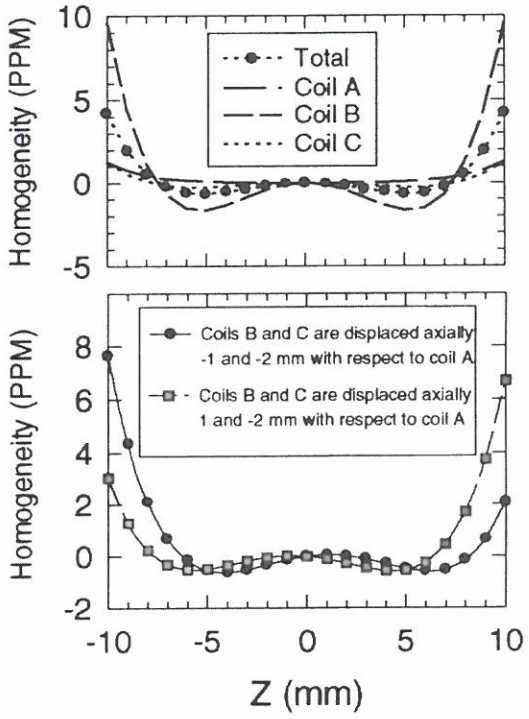

Figure 1. Computed uniformity of the three coils of the 25 T NMR resistive magnet showing insensitivity to midplane positioning.

General Solution for Stresses in a Compliant Florida-Bitter Disk

Eyssa, Y.M., NHMFL

A compliant "Florida-Bitter" disk has staggered elongated cooling holes. This design is chosen to reduce the effective modulus in the radial direction resulting in much lower stresses at the inner radius. In the derivation below, we assume zero axial stress at midplane, homogeneous and orthotropic material. These assumptions result in simple analytical equations for the hoop and radial stresses. The equation relating the stresses and the strains in the radial and tangential directions are:

$$\varepsilon_\theta = \frac{u}{r} = \frac{\sigma_\theta}{E_\theta} - \nu_{r\theta}\frac{\sigma_r}{E_r} \quad , \qquad (1)$$

$$\varepsilon_r = \frac{du}{dr} = -\nu_{\theta r}\frac{\sigma_\theta}{E_\theta} + \frac{\sigma_r}{E_r}$$

where, $\frac{E_\theta}{E_r} = k^2$, $\frac{\nu_{r\theta}}{E_r} = \frac{\nu_{\theta r}}{E_\theta}$ (2)

E is Young's modulus, ν is Poisson's ratio and u is the radial displacement. k is a measure of compliance. As k approaches infinity, the stresses in the hoop direction approaches the case of mechanically independent rings. As k approaches unity the stresses follow the well known formula, in Montgomery's Book "Solenoid Magnet Design." We should note here that the relation between the Poisson ratio in the two directions follows the relation between the modulii in equation 2 above,

$$\frac{E_\theta}{E_r} = \frac{E}{E_r} = \frac{\nu_{\theta r}}{\nu_{r\theta}} = \frac{\nu}{\nu'} = k^2 \qquad (3)$$

where ν and ν' are the disc material original and reduced Poisson's ratios. Inverting equation 1 yields:

$$\sigma_\theta = \frac{k^2 E}{k^2 - \nu'^2}\frac{u}{r} + \frac{\nu' E}{k^2 - \nu'^2}\frac{du}{dr} \quad , \qquad (4)$$

$$\sigma_r = \frac{\nu' E}{k^2 - \nu'^2}\frac{u}{r} + \frac{E}{k^2 - \nu'^2}\frac{du}{dr}$$

The force balance equation is,

$$-\sigma_\theta + \frac{d}{dr}(r\sigma_r) = -j.B.r = -j_o a_1 B \qquad (5)$$

In Bitter coils J and B are,

$$j(r) = j_o\frac{a_1}{r} \; , \; j_o \approx \frac{I}{\lambda\, b\, a_1 \ln(a_2/a_1)} \; , \qquad (6)$$

$$B(r) = B_1 - \Delta B\frac{\ln(r/a_1)}{\ln(a_2/a_1)} \; , \; \Delta B = B_1 - B_2$$

where B_1 and B_2 are the axial midplane field at the inner radius a_1 and the outer radius a_2. I is the current. b is the disk thickness. λ is a space factor. Substituting equations (4) and (6) in (5) yields,

$$-k^2\frac{u}{r} + \frac{d}{dr}\left(r\frac{du}{dr}\right) = -\frac{j_o a_1 (k^2 - \nu'^2)}{E}\left(B_1 - \Delta B\frac{\ln(r/a_1)}{\ln(a_2/a_1)}\right) \qquad (7)$$

Similar to the derivation by Markiewicz et al. [NHMFL-IR-93-788], the solution for equation 7 is:

$$\frac{u}{r} = D_1 r^{k-1} + D_2 r^{-k-1} + \frac{j_o a_1 (k^2 - \nu'^2)}{E(k^2-1)} \left[B_1 - \frac{2\Delta B}{(k^2-1)\ln\alpha} - \frac{\Delta B}{\ln\alpha} \ln\left(\frac{r}{a_1}\right) \right], \quad (8)$$

$$\frac{du}{dr} = kD_1 r^{k-1} - kD_2 r^{-k-1} + \frac{j_o a_1 (k^2 - \nu'^2)}{E(k^2-1)} \left[B_1 - \frac{2\Delta B}{(k^2-1)\ln\alpha} - \frac{\Delta B}{\ln\alpha} \left(\ln\frac{r}{a_1} + 1\right) \right]$$

$D_{1,2}$ must be chosen to satisfy $\sigma_r = 0$ at a_1 and a_2.

$$D_1 = -\frac{j_o a_1 (k-\nu')}{E(k^2-1)} \left\{ \frac{a_2^{k+1} - a_1^{k+1}}{a_2^{2k} - a_1^{2k}} \left[(\nu'+1) \left(B_1 - \frac{2\Delta B}{(k^2-1)\ln\alpha} \right) - \frac{\Delta B}{\ln\alpha} \right] - \frac{a_2^{k+1}}{a_2^{2k} - a_1^{2k}} (\nu'+1)\Delta B \right\} \quad (9)$$

$$D_2 = +\frac{j_o a_1 (k-\nu')}{E(k^2-1)} \left\{ \frac{a_2^{k+1} - a_1^{k+1}}{a_2^{2k} - a_1^{2k}} \left[(\nu'+1) \left(B_1 - \frac{2\Delta B}{(k^2-1)\ln\alpha} \right) - \frac{\Delta B}{\ln\alpha} \right] - \frac{a_2^{-k+1}}{a_2^{-2k} - a_1^{-2k}} (\nu'+1)\Delta B \right\}$$

Substituting equations (8) and (9) in (4) yields both the radial and axial stresses as function of the radius.

As shown in Figure 1, there can be significant reduction in stresses at the inner surface due to disk compliance. The degree of compliance depends on the staggered cooling hole arrangement. Finite element and other simple analytical models show that k^2 values ranging between 20 to a 100 are easily obtainable in Florida-Bitter disk design. The desired general solution represents a powerful tool in our optimization codes for resistive magnets.

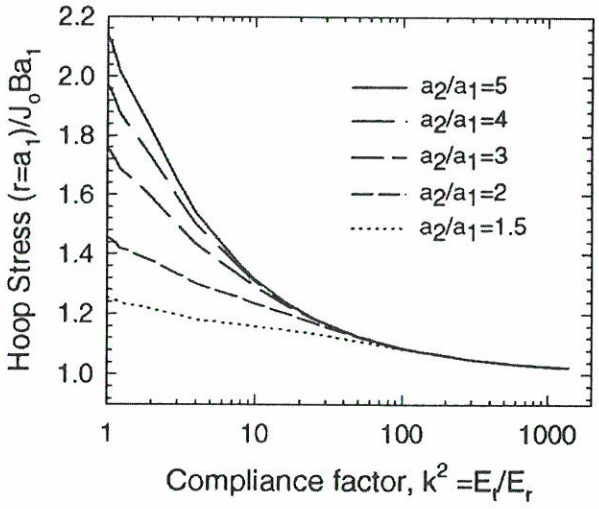

Figure 1. Stress reduction as function of disk compliance for different aspect ratios. Analysis is for B_1=30 T and j_0=500 A/mm^2.

A New Concept in Bitter Disk Design

Gao, B.J., NHMFL
Schneider-Muntau, H.J., NHMFL
Eyssa, Y.M., NHMFL
Bird, M.D., NHMFL

A new concept in cooling hole design in Bitter disks that allows for much higher power density and results in considerably lower hoop stresses has been developed and successfully tested at the NHMFL in Tallahassee, FL. The new cooling hole shape allows for extreme power densities (up to 12 W/mm^3) at a moderate heat flux of only 5 W/mm^2. The new concept also reduces the hoop stress by about 30-50% by making a Bitter disk compliant in the radial direction through staggering small width and closely spaced elongated cooling holes. Finally, the design is optimized for equal temperature.

A Bitter coil is constructed of perforated copper disks and insulators that are stacked to form a thick monolayer winding. High pressure cooling water is pumped axially through cooling holes that are aligned carefully to ensure sufficient and uniform heat removal. The copper disks have a current distribution that is inversely proportional to the radius. This configuration uses power more efficiently than uniform current density magnets and is much easier to cool.

Figure 1 shows successive stages in cooling hole development developed in magnet laboratories around the world. The maximum stress occurs at the inner radius because, due to the Lorentz force distribution, the outer part would like to strain more than the inner part.

Figure 2 shows a new concept in cooling hole distribution (staggered cooling holes) that would make the radial modulus very small. As a result there is a significant reduction in stresses at the inner radius. We will refer to that design as "Florida-Bitter." We have constructed coil A of our 30 T magnet using Florida-Bitter discs. Finite element analysis (Figure 3) shows a significant reduction in stresses using the Florida disk compared with non-staggered cooling pattern (aligned cooling holes).

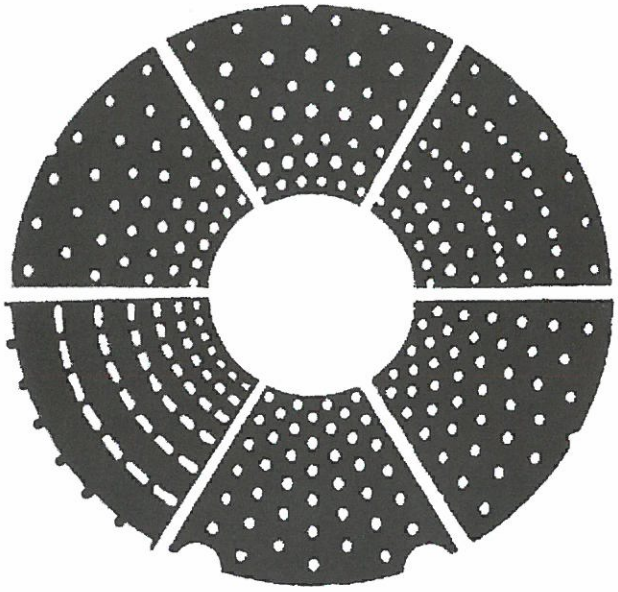

Figure 1. Successive stages in cooling hole developments.

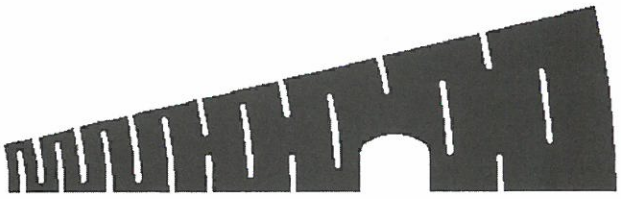

Figure 2. "Florida-Bitter" staggered cooling hole pattern and elongated tie rod developed at NHMFL.

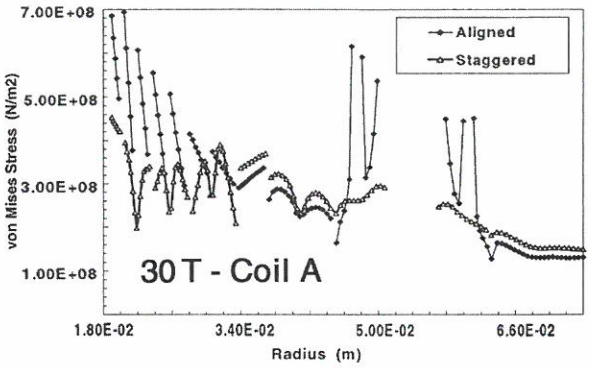

Figure 3. Finite element analysis comparison between stress distribution of a Bitter plate with aligned and staggered cooling hole distribution. There is a significant reduction in stresses at the inner radius as well as peak stresses at cooling holes.

Flow Simulation Code Development

Prestemon, S., NHMFL/FAMU-FSU CoE

The development of a code for the simulation of 3D turbulent fluid flow in the cooling channels of resistive magnets continues. Based on results achieved using optimized compact schemes, we have decided to use fully spectral methods for the code. Although spectral methods demand more computational time, they are more accurate and more stable than compact schemes.

There are two main difficulties associated with the flow problem. (1) The geometry is complex: our goal is to impose roughness conditions like those created during the construction of the magnets. The simulation will therefore require multiple domains connected via interfaces. (2) The Reynolds number associated with the flow is large, around 25000, and therefore requires large eddy simulations (LES).

Spectral methods outperform finite difference methods in simple geometries due to their high resolution. Their stability is also exceptional. Stability is difficult to achieve in high order finite difference schemes, particularly for high Reynolds number flows.

Through domain decomposition we expect to reduce the complex geometry to a set of simple geometric problems. In each domain, a relatively small number of collocation points will be needed.

This is an ideal situation for spectral methods: the calculation of the derivative of a 1D function is an $O(n^2)$ operation for spectral methods, as compared to an $O(n)$ operation for finite differences. The difference is not large for small values of n yet the difference in resolution can be extraordinary. Figure 1 shows streamlines near the entrance of a 2D confined backstep flow. There is regular periodic shedding of vortices. Low order finite differences would yield a laminar time invariant solution at this Reynolds number (Re=500). Yet the resolution of the flow shown in Figure 1 is only 30x30. Thus for a relatively low number of discretization points, spectral methods are capable of capturing the dynamics of a flow that would not have been discerned with basic finite differences.

Currently, the code is being written in cylindrical coordinates and a third periodic dimension is being added using Fourier modes. A major concern during the code development is future implementation on vector and parallel architectures. Here again, spectral methods are the preferred choice, in that they are ideally suited for parallelization.

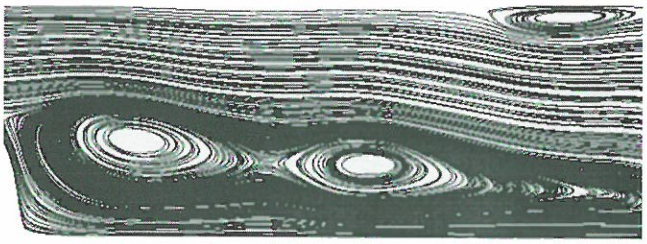

Figure 1. Streamlines of confined backstep flow. The flow enters from the upper left. The low pressure behind the step sets up eddies, which upon formation are advected downstream.

MAGNET SCIENCE AND TECHNOLOGY
Large Superconducting Magnet Systems

Program Overview

J.R. Miller

The technologies required for very large superconducting magnet systems, which we may define somewhat arbitrarily as those with stored energies exceeding some tens of megajoules, differ in many ways from those that work quite satisfactorily in smaller magnets. Stability, protection, and mechanical structures become increasingly prominent issues, which lead to even stronger emphasis on technologies that can be proved in a program of development and testing at the component level.

In our program of development for large superconducting magnet systems at the NHMFL, we are at present focused primarily on the technologies for hybrid magnet systems, with the 45-T Hybrid Project clearly at the forefront in the near term. The technologies being developed, however, are broadly applicable, and our work has led to involvement over the past year with several groups outside the NHMFL, e.g., with Babcock and Wilcox for developmental tests of a 20-kA class, cryogenic current lead with HTS element; with Princeton Plasma Physics Laboratory for review and analysis of magnet systems for the proposed TPX fusion machine; and with the Westinghouse Science and Technology Center for cryogenic electrical testing of a model coil (also for the TPX project).

Representative of our efforts, we include here a brief report on the status of the 45-T Hybrid Project and several research reports of more general interest.

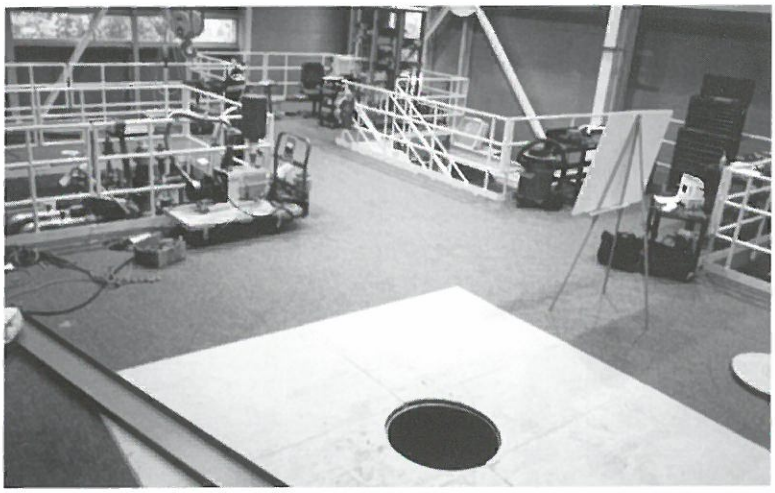

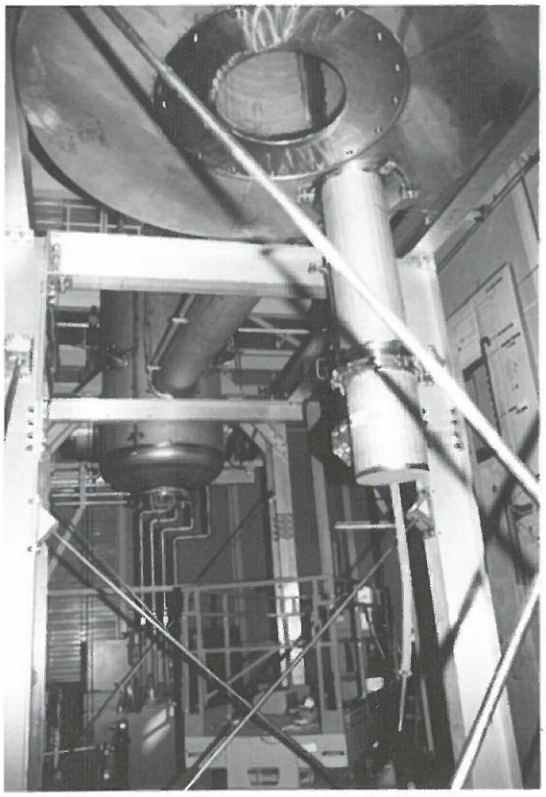

Easy, unobstructed access to the hybrid magnet from above and beneath was one of the design goals for the hybrid magnet.

Status of the 45-T Hybrid Project

The cable-in-conduit conductors (CICCs) for the three superconducting coils of the 45-T Hybrid use special conduit alloys, and in 1995, a great deal of effort was needed to overcome these problems. In one case, the 316LN for the coil-C conductor (NbTi) was not processed correctly, leaving some of it unusable. In another, it was clearly demonstrated that the Incoloy 908 chosen for the two Nb_3Sn coils was incompatible with the manufacturing processes for those coils because of a high potential for SAGBO cracking during heat treatment. In both cases, these issues have now been resolved. For coil C, it was possible to use 304L for some of the conductor in areas where the greater strength of the 316LN was not required. For the Nb_3Sn coils, a modified version of 316LN was identified that would have sufficient strength and would not be susceptible to degradation during the heat treatment. The use of 316LN with the Nb_3Sn conductors will tend to suppress the critical-current performance, but we have evidence that this can be partially or fully offset by changes to the heat treatment schedule, and a test program is in place to quantify the necessary changes.

Other accomplishments on the 45-T Hybrid Project have been significant. They are summarized briefly by major task as follows.

Superconducting Outsert

- Production of all Nb_3Sn wire was completed. All lots exceeded all critical performance specifications and were of uniform quality.
- Cables of the Nb_3Sn wire, in lengths significantly exceeding the minimum requirements for both Nb_3Sn coils, were completed and delivered to the jacketing vendor.
- Tests on samples of jacketed cable indicate that coupling losses within the allowables can be achieved for normal operation (including an insert trip).

- The conductor jacketing line was fully developed and proved on both dummy and real conductors. The combined total produced thus far exceeds 7 km.
- Detailed manufacturing and quality-assurance plans have been developed and instituted for fabrication of both the conductors and windings of the two Nb_3Sn coils.
- Using our full-scale, half-length model of coil A, we demonstrated our ability to make in-situ repairs to the conductor (prior to heat treatment) by partially unwinding, repairing, and rewinding. Then, we demonstrated our ability to achieve and maintain the required temperature uniformity over the coil during the prescribed heat-treatment schedule to form Nb_3Sn.
- Further development of the termination and joining process for the Nb_3Sn coils has revealed adequate performance and repeatability as well as margin for improvement.
- The facilities for vacuum-pressure impregnation of the Nb_3Sn coils (mixing tank, impregnation/curing tank, and pumping systems to outgas and transfer the resin) have been designed and fabricated.
- The design and structural analysis of the outsert magnet vessel was completed, reviewed, and approved. A vendor for the vessel was selected and fabrication is underway.
- The superconducting bus system and vapor-cooled leads (VCLs), which had been installed in the outsert cryostat during its manufacture, were tested as part of the initial cryostat acceptance tests.

Outsert Cryogenics

- The outsert cryostat, which was fabricated in industry, was delivered, installed in the NHMFL Operations Building, and connected to the rest of the cryogenic system.
- Initial tests of the cryostat, the first time that all components of the cryosystem had been operated as a combined unit, were completed in early June. The tests included parallel operation of the two refrigerator units (including all four compressors, the two cold boxes, and the two He-II refrigeration loops). A dummy load in the cryostat was cooled to 1.8 K and heat loads were measured.
- Some difficulties were encountered with balance between the two refrigerator units during the June tests, and system modifications to correct the situation (additional valves) have been implemented. Although only one refrigerator will be required for the steady operation of the 45-T Hybrid, it is desirable to use two for more rapid cooldown or to recover from an upset.
- During initial tests, the heat load to the 1.8-K space of the cryostat was higher than expected. Based on post-test analyses, potential contributors have been identified, adjustments have been made, and follow-up testing has been planned.
- A number of more routine measures were implemented to improve the overall reliability of the cryogenic plant, additional features have been added to the general instrumentation and controls system to simplify cryosystem operation, and a second full-system test is ready to begin.

Outsert Power and Protection

- Installation of all power-circuit components was completed, including the 11-kA, ±25-V power supply, the remote zero-flux current transductor, the high-voltage current interrupters, the emergency discharge resistor, and the interconnecting buswork.

- The power supply was tested to full current and voltage using an in-house-fabricated, 250-kW, water-cooled resistor.
- Tests of the power-circuit components revealed the potential for spontaneous opening of the current interrupters at less than the full design current of the outsert magnet, which turned out to be the result of normal operation of the over-current-limit feature of these units. This feature is neither used nor desirable in the present system and has been disabled. Also, the physical opening of the interrupters was observed to be nearly an order of magnitude slower than expected. This was subsequently corrected by a modification of the control circuits to bring the opening times for all interrupters below 100 ms.
- Controls for the power supply have been partially integrated into the general instrumentation and controls system, which will be exercised during upcoming tests of the cryosystem to check subsystem compatibilities and for further testing of the VCLs and superconducting bus system.

Systems Integration and Test

- All major site preparations are complete with the exception of piping and buswork for the resistive insert. The design for these is complete and components are on order. The plan is to assemble the piping system when the resistive insert housing is delivered to the NHMFL in February 1996.
- The general instrumentation and controls system is partially complete. Further development is planned in conjunction with continued testing of the cryo and power subsystems.

AC Losses in Superconducting Nb_3Sn and NbTi CICCs

Bonito Oliva, A., NHMFL
Baudouy, B.J.P., NHMFL
Miller, J.R., NHMFL
Van Sciver, S.W., NHMFL/FAMU–FSU CoE

AC loss measurements and calculations on large scale Cable-in-Conduit Conductors (CICC's) have been carried out to support the NHMFL Hybrid magnet development effort. Tests were conducted using the Test of AC losses (TACL) facility that consists of a 7 T superconducting dipole magnet with insulated insert cryostat operating at 1.8 K.[1,2] In the test configuration, the dipole magnet produces a magnetic field perpendicular to the conductor axis and no transport current is present in the sample. The losses are determined by measuring the enthalpy increase in the He II bath containing the conductor.

In order to predict the losses in the conductor, it is necessary to know the coupling time constant and the effective conductor radius. In our analysis, we have determined the time constant of the samples by measuring the losses produced during a slow ramp field variation. We also have carried out loss measurements at higher rates of variation using an exponential decay of the external field. From these measurements, we have been able to determine the effective radius and penetration field of the conductors.

Four different conductor samples were manufactured for these tests. Three of them used a Nb_3Sn conductor, while the last one was a hybrid prototype NbTi conductor supplied by MIT. In order to investigate the impact of cable void fraction and strand surface condition on the AC loss in the Nb_3Sn conductor, different sample preparations and jacket materials were used. Table 1 details the sample description.

Linear ramp tests were only performed on Samples 2, 3, and 4. Sample 1 losses were lower than the sensitivity of our measurement system. The sample losses were then fit to the expression,

$$Q_{sample} = Q_{hyst} + n\frac{\Delta B_{ext}}{\mu_o}\frac{\theta}{T}\left(1-\frac{\theta}{T}\left(1-e^{-\theta/T}\right)\right)$$

where T is the ramp time, q the conductor time constant and Q_{hyst} the hysteresis loss calculated for the filaments are adjustable. The values for these quantities are also listed in Table 1.

References:

1 Baudouy, B.J.P., et al., New Calorimetric AC Loss Measurement Technique involving Superfluid Helium, Advances in Cryog. Engn., Vol. 41 (to be published).

2 Baudouy, B.J.P. et al., AC Loss Measurement of the 45-T Hybrid CIC Conductor, IEEE Trans. on Appl. Supercon 30, 4, 1563 (1994).

Table 1. Dimensions of test samples.

	Sample #1	Sample #2	Sample #3	Sample #4
Strand f (mm)	0.5	0.5	0.5	0.81
Copper Fraction	0.83	0.83	0.83	0.80
Cable Pattern	5x3x3x3	5x3x3x3	5x3x3x3	5x5x5x3
Jacket Mat'l	316L	Incoly 908	316L	316 LN
Strand Surface	Mobil 1	none	none	none
Outer Dimen.	16.4x13.2	16.3x13.6	16.4x13.2	15.8x13.7
Void Fraction	0.41	0.36	0.41	0.45
Time Const. (ms)	3	206	112	16

Development and Testing of Joints for the Nb_3Sn Coils of the 45-T Hybrid

Miller, J.R., NHMFL
Kenney, W.J., NHMFL
Miller, G.E., NHMFL
Painter, T.A., NHMFL

The 45-T Hybrid requires joints of very low resistance between cable-in-conduit conductors (CICCs). At the normal operating current of 10 kA, 1-W dissipation has been budgeted for the cryogenic heat-load in joints associated with the two Nb_3Sn coils and 1-W in those for the NbTi coil. There are five joints associated with the two Nb_3Sn coils., two connecting Nb_3Sn conductors to NbTi conductors and three others joining Nb_3Sn conductors. Two configurations are used: "praying hands," where conductor ends come together from the same direction, and "shaking hands," where they approach from opposite directions. The goal of this work has been to develop and prove a reliable process for all the joints associated with the Nb_3Sn coils.

A common feature of all the joints in this study is that they begin with the CICCs terminated in copper blocks approximately 600-mm length x 25-mm square. The cable end, which is sealed inside the copper block, must be cleaned, fluxed, and solder filled without its direct exposure. Although this feature complicates the process, it protects the fragile Nb_3Sn cable strands from damage by handling. The cleaning solution is a mix of acetic acid, phosphoric acid, and fuming nitric acid in a ratio of 94:3:3. A standard "stainless-steel" flux is used, which is based on hydrochloric acid with zinc chloride added to improve wetting. The terminations are filled with 95Sn-5Ag solder and subsequently joined with 60Sn-40Pb solder to preclude remelting the solder in the terminations.

For the first round of proof tests, the four joints described in Table I were assembled in a configuration that allowed simultaneous testing. They were tested at 4.2 K, zero background field, and up to 5 kA transport current (limited by the

test facility). Figure 1 shows the results graphically. To meet the 1-W dissipation limit in the Hybrid, the mean zero-field resistance must be less than about 0.5 nΩ (2.5 mV at 5 kA). Joints 1 and 3 are well below this level, while joints 2 and 4 are well above. Joint quality apparently does not correlate with joint or conductor type. When sectioned, all joints revealed excessive flux residue trapped inside the terminations. Another round of joints are being prepared in a manner to eliminate this problem.

Table 1. Description of joints tested.

Joint #	Joint Type	Conductor Types
1	Praying hands	NbTi/Nb_3Sn
2	Praying hands	Nb_3Sn/Nb_3Sn
3	Shaking hands	Nb_3Sn/Nb_3Sn
4	Shaking hands	Nb_3Sn/NbTi

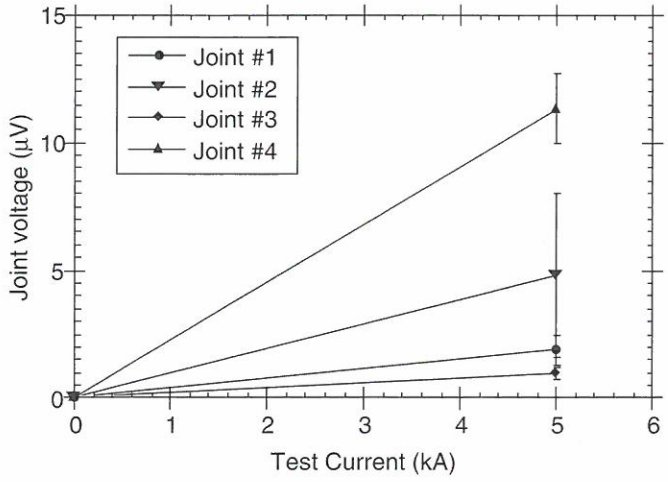

Figure 1. Voltage vs. current recorded during proof tests of joints.

Developmental Testing of Seals Between He I and He II

Miller, J.R., NHMFL
Miller, G.E., NHMFL
Windham, C.L., NHMFL

Several components in the supply cryostat for the 45-T Hybrid are designed for easy removal and employ a feed-through/seal between the He I and He II spaces comprising a conical plug fitting into a conical seat of stainless steel. In cases where the plug must be electrically insulating, G-10 was used. In other cases, stainless steel was used, allowing more precise fit up and minimizing leaks due to distortion during cooldown. Also, if the option of cold extraction of a component is to be retained, mating surfaces of the seal must be left dry. Others will be coated with a sealant. This report describes tests of an experimental model comparing plug types and surface conditions.

The test model consisted of a conical seat with mating plug separating two chambers. One chamber was pressurized with He gas (typically to about 2 bar) while the other was pumped using a vacuum pump with known pumping speed vs. inlet pressure. Tests were performed near LN_2 temperature, and the effective area A_{eff} of the leak was estimated using the formula,

$$A_{eff} = \left[\frac{f \dot{m}^2 L \langle P_{wet} \rangle}{8 \langle \rho \rangle (p_{high} - p_{low})} \right]^{1/3}.$$

The mass flow rate $\dot{m}$ was determined from pump inlet pressure and pumping speed, the length L of the leak was taken as the shortest path along the face of the plug, the mean wetted perimeter $\langle P_{wet} \rangle$ was taken as twice its mean circumference, and the friction factor f was taken as the laminar-flow value. The mean density $\langle \rho \rangle$ was approximated according to the ideal-gas law by using the average of pressures p_{high} and p_{low} on either side of the seal and the measured temperature T_{plug} of the seal. Values of A_{eff} determined in this manner were used to estimate heat leaks between He I and He II spaces according to the relation,

$$\dot{Q} = A_{eff} \cdot 10^4 \cdot \left[\frac{X(T_{res}) - X(T_\lambda)}{L} \right]^{1/3.4}.$$

Use of T_λ in the equation implies the assumption that the end of the leak in the He I reservoir is just at the lambda temperature. The empirically determined value for $X(T_\lambda)$ is 0, and for a temperature in the reservoir T_{res} = 1.8 K, $X(T_{res})$ is approximately 3750 mm. Table 1 summarizes the measurements and analysis of leaks in several plug/sealant combinations.

Table 1. Measured flow rates, derived flow cross-sections, and projected heat leaks for leaks in various plug/sealant combinations.

Plug/Sealant	Seal temp. during test (K)	Measured pressure drop (kPa)	Measured mass flow (g/s)	Derived flow cross section (mm^2)	Projected heat flow at He II (mW)
G-10/vacuum grease	98	233	.0374	4.25	121
G-10/Sealant 738	106	223	.0405	4.65	132
G-10/Grease 111	113	207	.0351	4.84	137
Steel/unlapped & greased	77	226	.0105	2.54	72
Steel/lapped & ungreased	287	220	.0331	7.63	217

MAGNET SCIENCE AND TECHNOLOGY
High Field Magnetic Resonance Systems

Program Overview

W.D. Markiewicz

There has been a strong movement in the application of high-current-density, epoxy-impregnated magnet technology to higher field magnets and, of special interest, to much larger high field magnets than have been attempted previously. This trend is seen, for example, in the very high field NMR spectrometer magnets that have been initiated by a number of laboratories in recent years. The reason for the present efforts to extend adiabatic superconducting magnet technology to these systems is one of economic feasibility. The cost of these magnets is becoming high, but an adiabatically stable design should be significantly less expensive that any alternative. The challenge for magnet science and technology is to develop the technology to allow these magnets to be made successfully. The objective of the NHMFL program is to develop suitable technology through the design and fabrication of a number of advanced high field magnets, including a 25 tesla high resolution NMR magnet, a 12 tesla research imaging magnet system for installation in the University of Florida Brain Institute, and a high field FT–ICR magnet.

The 25 tesla high resolution NMR magnet is a long range objective of the High Field Magnetic Resonance Systems activity. A superconducting magnet at this field level will utilize an innermost coil section containing HTS conductor. In recognition of this fact, the achievement of the 25 tesla long range objective is seen to rest on two major programs, the one being the development of a suitable HTS conductor and associated magnet technology, the other being the development and demonstration of the remainder of the magnet which itself represents a very large and ambitious high field magnet. The 900 MHz magnet is the objective of this second program.

The 900 MHz magnet system will be produced in a collaboration between the NHMFL and U.S. industry. The major responsibility of the magnet will be shared between the lab and Intermagnetics General Corporation. The division of responsibility will be as follows, where the organization with primary responsibility for each activity is indicated.

- engineering design NHMFL
- manufacturing design IGC
- conductor To Be Determined
- Nb_3Sn coil fabrication NHMFL
- NbTi coil fabrication IGC
- magnet assembly NHMFL
- cryostat To Be Determined

The activity of this past year was devoted to development of technology as identified in the Benchmark Design and to the preparation of the facility required at the NHMFL.

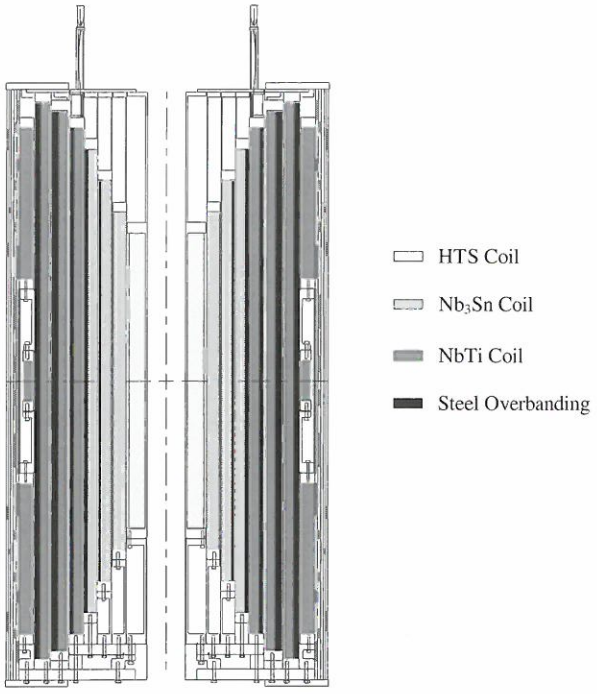

25 tesla, 1.066 GHz magnet.

Facilities Development

The facilities consist of a full capability for winding, heat treatment, and epoxy impregnation of coils the size required for the 900 MHz magnet. In addition to the fabrication facilities, various test capabilities were established within the laboratory this year. A number of short sample test probes were fabricated and evaluated for testing large Nb_3Sn conductors to high fields in the user facility. A facility for the testing of superconducting persistent joints was established, consisting of background field magnet, probes, electronics and software for data acquisition.

Magnet Technology Development

A very large number of epoxy compositions were formulated to find tough, crack-free epoxies suitable in their properties for impregnation of wire wound coils. This work has resulted in the selection of the system designated as *NHMFL 138* for 900 MHz magnet program. A number of small coils were prepared to examine issues of epoxy impregnation of windings, including cloth wetting, the extent of fill, and bonding to conductors. Somewhat larger coils were specifically prepared to study the radial impregnation that will be required for the NbTi coils. Observations made from the radial impregnation coils lead to the view that more control was required of the radial impregnation process than provided for by the random spacings provided by a tightly wound with Formvar insulated conductor. As a result, the development of a wire configuration to provide a degree of radial porosity was initiated and such conductor will be incorporated in upcoming coil impregnation tests. Other models and small coils were fabricated to evaluate the Free Supported Lead concept, which relies on an epoxy-fiber structural extension of the winding pack for lead support. A number of small superconducting test coils were initiated to demonstrate the concepts and provide training in coil fabrication.

Testing was done to establish the mechanical properties of both NbTi and Nb_3Sn conductors. The relationship between the conductor yield stress and the area reduction in the final conductor processing will be examined. Nb_3Sn conductor has decidedly non-linear stress strain characteristics. Measurements on representative conductors have forced a recognition of just how mechanically soft these materials are, and have motivated the examination of the possibility of using a high strength Nb_3Sn in the first 900 MHz magnet. The mechanical properties of samples modeling the NbTi windings were measured. The measurements also gave the shear strength of the interface between the windings and the external reinforcement, a value that is of some importance given the role of the reinforcement in the design. Models

of the Nb_3Sn windings are presently being prepared for similar tests, the fixtures having been prepared. Concern for the softness and yielding of the Nb_3Sn has lead to the examination of detailed stress in and around the conductors in the windings. The development of high strength Nb_3Sn conductor has been in progress for some time, and it may be possible to move from development to application of these conductors in the 900 MHz. The NHMFL has opened a dialogue with the Bochvar Institute, which has resulted in the production of samples of copper-niobium strengthened Nb_3Sn conductor for testing.

The quench protection system concept for the 900 MHz relies on heaters imbedded within the epoxy on the outer surface of the coil windings. The limits of energy deposition into these heaters before damage to the surrounding epoxy has begun to be understood on the basis of measurements on a heater test coil. Further testing will be done on a coil that has been prepared using the recent epoxy formulation and the latest heater design geometry and surface preparation.

An extensive set of measurements of the available critical current density in bronze process Nb_3Sn conductors of a size suitable for the 900 MHz magnet have been made. At the time that the Benchmark Design was prepared, the selected conductor critical current density was a target, somewhat high, but recognizing the development activities underway to improve current density in bronze process conductors. The recent measurements confirm the commercial availability of the current density assumed in the Benchmark Design. The data base for low temperature properties was also extended.

Compressive Shear Measurements of NbTi Coil Composites

Dixon, I.R., NHMFL
Walsh, R.P., NHMFL
Markiewicz, W.D., NHMFL

As part of the materials characterization of the 900 MHz magnet, the shear strength of superconducting composites is measured. Since shear strength is influenced by normal stress, a bi-axial strength test is employed. The compression/shear tests use special fixtures that support and load samples in compression and shear. The fixtures, shown in Figure 1, are three components attached in series with the load path. There are two symmetric end components and one center component. They are cylindrical in shape and have mating surfaces that are machined at an angle. The mating surfaces have at their centers a recess where specimens are inserted. The test loads two samples simultaneously. A compressive force applied to the fixtures is transmitted through the specimens contained within the recesses. The applied load may be resolved into a shear force along the plane of the mating surface and a compressive force normal to the mating surface. The resultant forces are a function of the fixture angle.

The NbTi composite samples consisted of multiple NbTi and E-glass cloth layers, impregnated with epoxy. Fixtures of various angles were used in the tests at 77 K and 4.2 K. The results of the tests are plotted in Figure 2. Curves for the average strength at each fixture angle are shown for each temperature. The shear strength increases significantly with an increase in compressive stress. Thus a radially compressive load within the windings is advantageous for a greater shear strength capability. In addition, an increase in average strength is shown to exist at lower temperature for higher fixture angles. The maximum operational stress analyzed to exist within the largest NbTi coil is illustrated in Figure 2. The compressive shear results show there is a large margin from the operational load.

The mode of failure in all samples was debonding of the Formvar insulation from the conductor. The insulation and epoxy-glass attached very well thus making the weakest bond occur at the interface of the conductor and Formvar. At low compressive loads failure typically occurred in a clean manner shearing the glue line materials from a single face of the fracture surface. At high compressive loads, the attachment of glue line

materials occurred in a more sporadic nature where both fracture surfaces contained random pieces of cloth, epoxy, and Formvar.

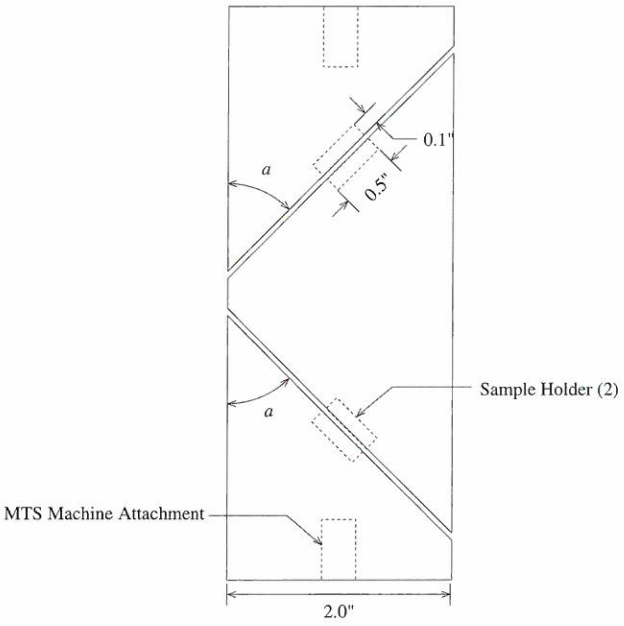

Figure 1. Schematic of compression/shear test fixture.

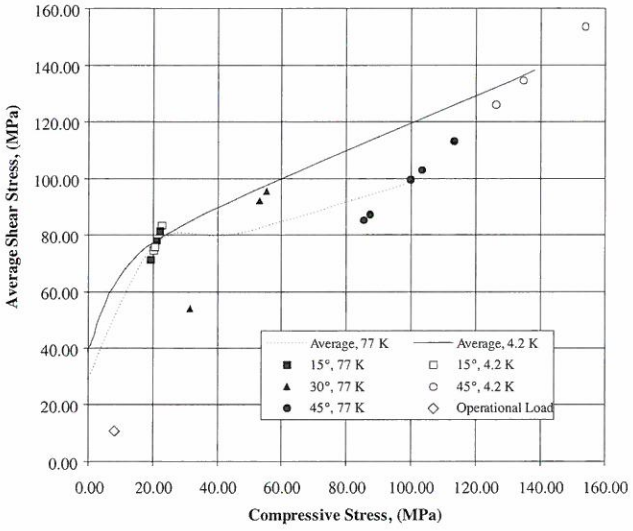

Figure 2. Compressive/shear failure strengths of NbTi composites at 77 K and 4.2 K with 900 MHz magnet coil operational load.

Micro-Stress Analysis of Composite Winding Bundle

Dixon, I.R., NHMFL
Markiewicz, W.D., NHMFL

An investigation into the stress distribution through the material components of a winding composite is conducted to evaluate the need for high strength conductors in the 900 MHz magnet. The windings of an epoxy impregnated magnet are a composite material consisting of epoxy-glass insulation and conductor. The copper stabilizer and bronze in a Nb_3Sn conductor is likely to yield during operation of the magnet, which results in a low effective modulus. The extent of the deformation from yielding and the redistribution of stress into the barrier, filaments, and insulation are studied in detail by performing a local stress analysis of the winding composite.

A local stress analysis is performed in a neighborhood consisting of nine conductor cells using axisymmetric finite elements. The material regions and configuration of the cells are shown in Figure 1. In each cell, five distinct regions exist. Each conductor has a surrounding epoxy-glass insulation layer. The outer portion of the conductor is the copper stabilizer. A thin barrier separates the stabilizer from the central region. The central region is modeled as two components with bronze surrounding Nb_3Sn. Inelastic material properties are used to describe the yielding behavior of the copper and bronze components.

A global stress analysis of an entire coil with averaged properties is first performed to determine the boundary conditions around the neighborhood of the local analysis. The normal and shear stress are applied to the boundary of the local model and the Lorentz forces are applied to the Nb_3Sn. There is an initial stress distribution in the conductor resulting from the cooling of the composite conductor from the heat treatment reaction temperature. For the present analysis, a precompression of the filaments is assumed, and by force equilibrium the initial strain state in the copper and bronze is determined.

It is observed that the copper and bronze are initially loaded in tension, reducing the applied strain required to induce yielding. The load is redistributed into the barrier, filaments and the epoxy-glass insulation. The final operating stress levels in the barrier and filaments are reduced by the compressive prestress. Figure 2 contains a typical stress distribution through the center of a conductor and insulation. Although yielding occurs, the deformations appear small. Further analysis will compare the behavior of conventional conductors with conductors that employ a quantity of copper-niobium in the stabilizer for strengthening.

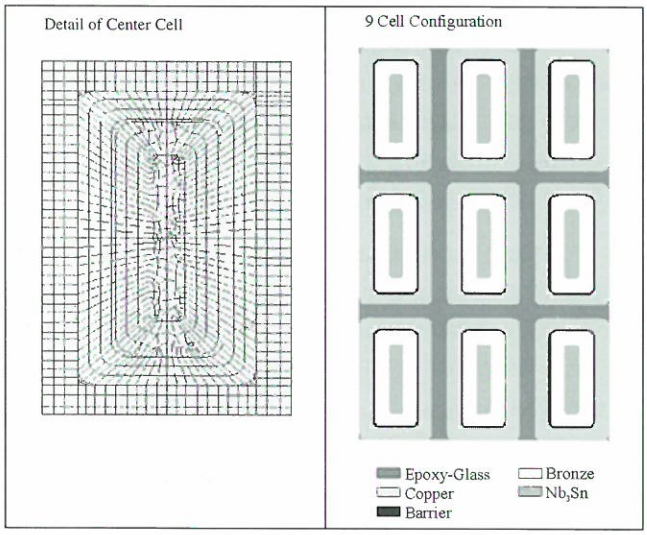

Figure 1. Finite element model of conductor cells.

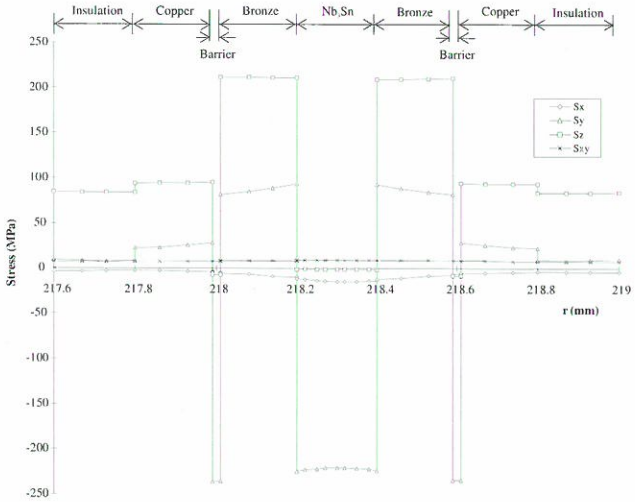

Figure 2. Stress distribution through mid-plane of center conductor cell.

Cu/SS Wires as Reinforcement and Quench-back Protection for Epoxy Impregnated Magnets

Eyssa, Y.M., NHMFL
Markiewicz, W.D., NHMFL

Cu/SS wires that are used in pulse magnets as alternative to other conductors such as CuAg or CuNb have shown to have excellent thermal and mechanical properties. It was found that the rule of mixtures holds very well in predicting their properties. As a result it is expected that wires that have 10% Cu and 90% SS will keep the SS high modulus and high strength properties that is needed as reinforcement for high field NMR magnets. The 10% copper, however, will improve the conductivity of this reinforcement that it can act as quench-back circuit in case of a quench. In this study we simulated a quench of a high field (20 T) magnet system and varied the Cu/SS ratio.

The Cu/SS reinforcement windings A, B and C shown in Figure 1 are short circuited during a quench when the voltage across their protection diodes exceeds the specified conducting voltage. The reinforcements act as quench-back circuits when they are shorted by the protection diodes. The presence of the protection diodes prevent eddy current heating in the reinforcement during the slow charging process.

We have varied the copper to SS ratio from 0.0 to 0.1 to examine the quench-back effect. In this example, we eliminate all other quenching mechanism such as AC loss heating or quench heaters. The 9-coil superconducting wires are wired so that they are two circuits. The reason is that we wanted to avoid large current transfer between many coupled circuits that could have resulted in windings quenching due to the current exceeding the critical current. Windings 7, 8, and 9 have no reinforcements, so protection heaters are used for them.

The quench simulation started by a normal zone in coil #1. In case of all SS reinforcements, coils 4, 5, and 6 did not quench because the current in the quench-back circuits is too small to induce a quench-back. In case of 5% and 10% Cu ratios,

the Cu/SS reinforcements acted as quench-back circuit with the higher ratio resulting in a faster quench. Figure 2 shows the analysis for 10% Cu in the reinforcement.

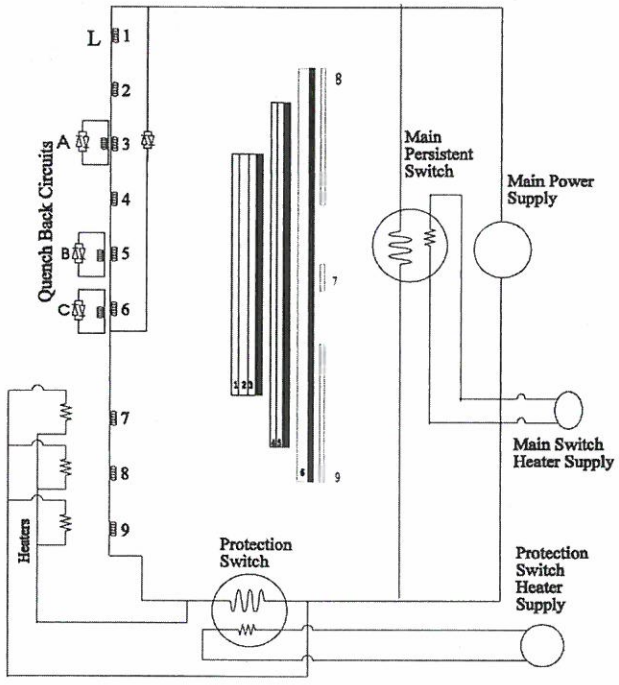

Figure 1. Quench simulation: coils 1-6 are protected by quench-back reinforcement circuits.

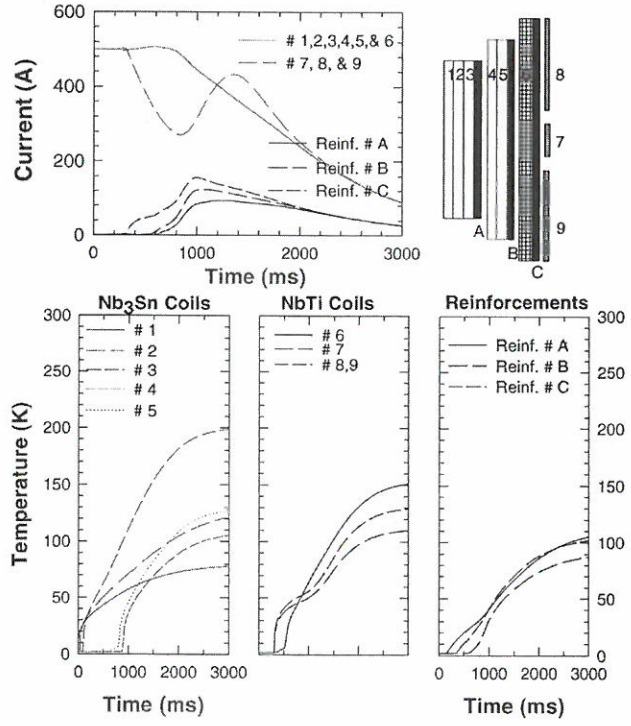

Figure 2. Quench-back analysis using reinforcement of Cu/SS with Cu to SS ratio =0.1.

J_c(B,T) Testing of Large Nb_3Sn Conductors

Markiewicz, W.D., NHMFL
Bonney, L.A., NHMFL
Swenson, C.A., NHMFL
Pickard, K.W., NHMFL

A short sample test capability for large Nb_3Sn strand conductors has been assembled and is being used to meet conductor characterization requirements of the 900 MHz magnet program. The conductors for the 900 MHz magnet are relatively large monolithic strand. Critical current values are required up to 1000 A, extending to high fields and at temperatures of 4.2 K and 1.8 K. The tests are performed in the 50 mm warm bore, 20 tesla magnets in the user facility, with a large helium capacity insert cryostat, using a new high current sample holder.

The sample preparation and mounting procedures are fairly conventional, using a method that appears most suitable for the size of conductor being tested. Helical samples are mounted for heat treatment on stainless steel grooved fixtures. Given the high currents involved, the samples are transferred to the sample holder instead of mounting the entire heat treatment fixture to avoid mechanical contacts. Following developments introduced for the ITER program, a shunt of the alloy Ti-6V-4Al is used to give a better match to the thermal contraction of the conductor than that for stainless steel. The sample is mounted in a dip solder process. The lack of wetting of the shunt with solder leaves the sample free over the shunt region. The sample is tested with the Lorentz force directed inward to eliminate additional mechanical strain on the sample.

The probe assembly may be connected to the house vacuum system in order to reduce the temperature of bath in the cryostat. The probe is fitted with a thin film resistance thermometer to provide temperature readings which are relatively independent of field. Temperatures down to 1.8 K are achieved with house vacuum. Temperature stability can be adequately maintained with manual trimming of valves during a trace.

One meter samples of conductor are mounted, with voltage taps in the central 27 cm. A sensitivity of 0.1 μV/cm is easily obtained.

A variety of Nb_3Sn conductor has been tested in the facility as part of the conductor qualification program for the 900 MHz magnet. The measurements will form the basis of the procurement specification for the 900 MHz magnet conductor. For selected samples, there is good agreement with data taken in other laboratories. The measurements have extended the available data on critical current density at low temperatures, as shown in Figure 1.

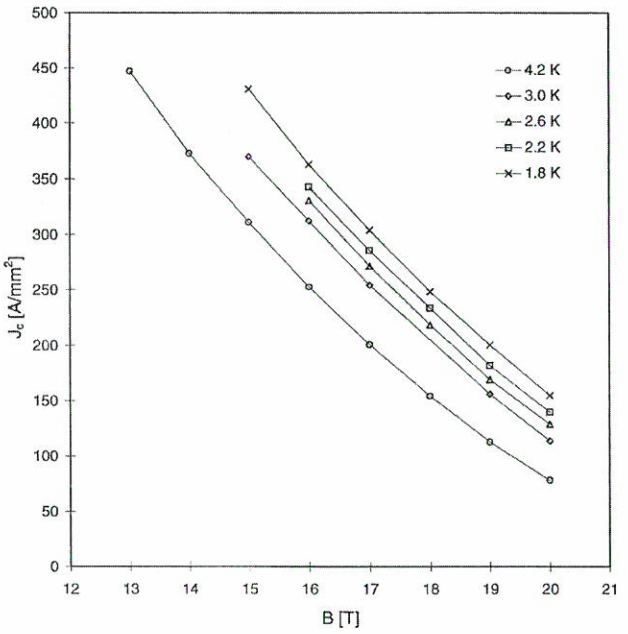

Figure 1. Critical current density versus field and temperature for bronze process Nb_3Sn conductor, 0.1 μV/cm sensitivity.

Tough Epoxy for High Field Magnet Application

Markiewicz, W.D., NHMFL
Brennan, A.B., UF, Materials Science Engineering

Tough epoxy is especially desirable for adiabatically stable, epoxy impregnated wire wound magnets. Tough epoxy suitable for magnet application based on high molecular weight additives to amine cured epoxy was demonstrated some time ago. Amine cured epoxy historically has shortcomings associated with high viscosity and short pot life, but some practical systems were identified. Unfortunately, a key component in earlier tough epoxies, DDM, was declared to be a carcinogen and is no longer available. Motivated by the lack of a satisfactory epoxy, a program was initiated to formulate a tough epoxy with properties compatible with coil impregnation based on material with safe handling characteristics. The requirements were:

- viscosity < 2 poise
- pot life > 5 hours
- TSR > 25 cycles
- cure < 100 C
- non-toxic materials.

The approach taken was to work from the experience base of the widely used DGEBA resin and the earlier results showing the influence of high molecular weight curing agents. A survey was conducted to identify candidate curing agents and alternative resins based on viscosity and reactivity. Areas of composition space with potentially interesting properties were defined and systematically examined. Samples were prepared to allow testing of compressive modulus and thermal shock, often with a number of different cure schedules. It was observed that the addition of increasing quantities of high molecular weight and flexibilizing components could provide epoxy systems with good thermal shock resistance (TSR), but would quickly soften the cured epoxy to the point where there was concern for using such a system in a Nb_3Sn magnet winding. The compressive modulus in composition space as a function of two curing agents is shown in Figure 1. A minimum room temperature compressive modulus of 1 GPa was imposed as a constraint. Epoxies have now been identified which significantly exceed the initial specifications. The viscosity profile of one such system, NHMFL 138, is compared in Figure 2 to an anhydride cured system with characteristically low viscosity. While the viscosity profiles are comparable, NHMFL 138 is fully tough in comparison with the anhydride cured system which is known to be quite brittle.

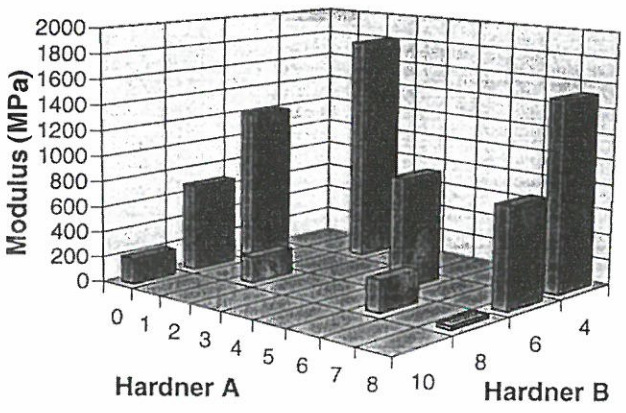

Figure 1. Room temperature compressive modulus as a function of curing agent content in % equivalent molar fraction.

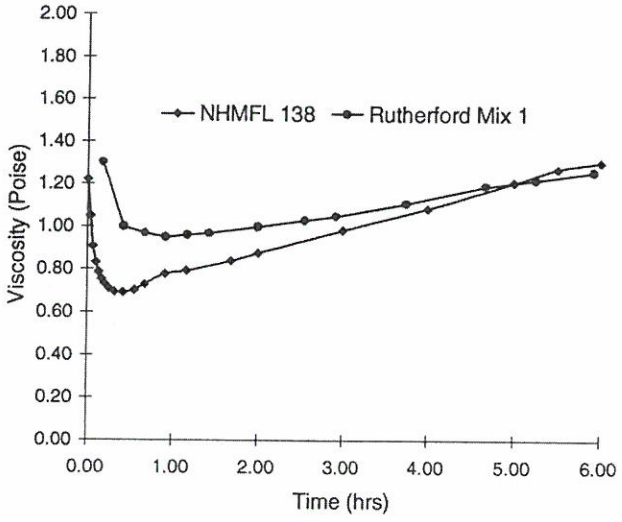

Figure 2. Comparison of viscosity between NHMFL 138 and Rutherford Mix 1.

Superconducting Joint Testing

Swenson, C.A., NHMFL
Pickard, K.W., NHMFL
Markiewicz, W.D., NHMFL

The 900 MHz magnet design is a series of ten nested Nb_3Sn and NbTi solenoid coils. The magnet requires persistent superconducting joints between and within these coils. Coil conductors are large rectangular monoliths designed to operate at 350 A. The field decay requirements for high resolution NMR limit the allowable joint resistance to the order of 10^{-11} Ω. Joints must also operate at the highest possible fields to limit the length and complexity of lead runs from magnet coils. Persistent joints are therefore an essential aspect of the magnet technology.

Joint development for the 900 MHz magnet encompasses the following persistent joint configurations:

Nb_3Sn-Nb_3Sn	Joints within Nb_3Sn coils
Nb_3Sn-NbTi-Nb_3Sn	Joints between Nb_3Sn coils
NbTi-Nb_3Sn	Nb_3Sn and NbTi coils
NbTi-NbTi	Joints within NbTi coils
NbTi-NbTi	Joints between NbTi coils

The standard measurement practice is to make a sensitive four wire DC resistance measurement. The current range required for characterization is 0-600 A. Voltage signals are at the nanovolt level. Measurements are complicated by thermal emfs and inductive pickup noise from power supplies.

The joint test equipment has been constructed. Test probes have operated at 800 A in a 5 tesla background field. Joint voltage measurements are made with a Keithley 2001 voltmeter equipped with a Keithley 1801 nanovolt pre-amp. The joint power supply operates in a step and hold mode during testing.

Measurements have been made on NbTi joints to evaluate the sensitivity of the test apparatus. Presently, measurement sensitivity is on the order of $2x10^{-11}$ Ω at 500 A. The joint measurement sensitivity sets an upper bound to our ability to estimate the field decay rates in the 900 MHz. A measurement sensitivity of $2x10^{-11}$ Ω corresponds to a field decay fraction on the order of 10^{-9} per 1 hour. The present sensitivity is acceptable for development and characterization of joint manufacturing methods. Joint work is in process, and there is a continuing effort underway to improve measurement sensitivity.

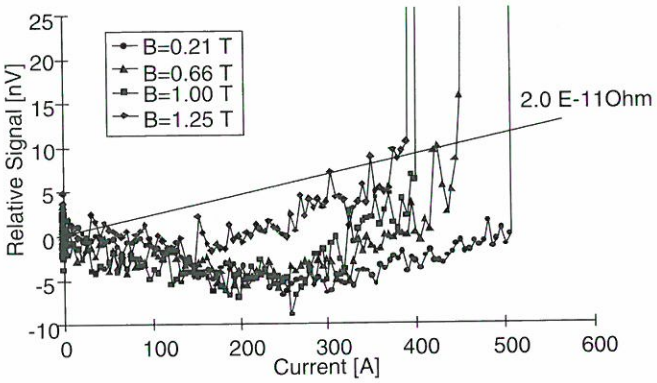

Figure 1. Composite V vs. I traces for test joint # 36C. Measurements were made at 4.2 K.

Stress Analysis of a Superconducting Solenoid Using Green's Function Solution

Vaghar, M.R., NHMFL/UF
Garmestani, H., FAMU-FSU CoE/MARTECH
Markiewicz, W.D., NHMFL
Schneider-Muntau, H.J., NHMFL

The analytic solution to the stress distribution throughout the windings of a solenoid is made difficult by the shear stress components. At present, calculations may be performed by a lengthy series approximation or use of finite element techniques. It is the purpose of this work to develop a full stress analysis using the Lorentz body force distribution directly.

For an axisymmetric distribution of magnetic body forces $\mathbf{X}(r,z)$ acting in the interior of an elastic, isotropic magnet with inside radius of a_1, outside radius of a_2 and length of $2L$, the displacement vector $\mathbf{u}(r,z)$, in cylindrical coordinates is represented by,

$$(\lambda+\mu)\nabla(\nabla\bullet\mathbf{u})+\mu\nabla^2\mathbf{u}+\mathbf{X}=0 \qquad (1)$$

where λ and μ are elastic constants. From Helmholtz theorem, any displacement vector satisfying Eq. (1) may be given by the following expression

$$\mathbf{u}=\nabla\phi+\nabla\times\mathbf{V} \qquad (2)$$

where $\Phi(r,z)$ is a scalar potential and $\mathbf{V}(r,z)$ is a vector potential such that $\nabla\bullet\mathbf{V}=0$. The potential functions ϕ and $\mathbf{V}$ can be any independent functions and since they give one more freedom than needed to determine the three components of displacement vector, it is admissible to represent these functions as follows

$$\phi=\frac{1}{\lambda+2\mu}\nabla\bullet\Psi \qquad \mathbf{V}=-\frac{1}{\mu}\nabla\times\Psi \qquad (3)$$

where components of Ψ are stress functions. Substituting Eqs. (3) and (2) into Eq. (1) yields to

$$\nabla^4\Psi+\mathbf{X}=0. \qquad (4)$$

Solutions to Eq. (4) can be obtained by a variety of methods. The present work provides the solution using the Green's function method. The advantage of this method is that the solution can be obtained for any complex body forces (even for discrete ones) without changing the formulation.

$$\psi_i=\int_{a_1}^{a_2}\int_{-L}^{L}G_i(r',z',r,z)X_i(r',z')dz'dr' \qquad i=1,3 \quad (5)$$

where $G_1(r',z',r,z)$ *and* $G_3(r',z',r,z)$ are the Green's functions in radial and axial directions

$$G_1(r',z',r,z)=-\sum_{i=1}^{\infty}\sum_{j=1}^{\infty}\frac{G^i_{1z}(z',z)G^j_{1r}(r',r)}{L\left[k_{1j}^2+\left(\frac{2i-1}{2L}\pi\right)^2\right]^2}$$
$$G_3(r',z',r,z)=-\sum_{i=1}^{\infty}\sum_{j=1}^{\infty}\frac{G^i_{3z}(z',z)G^j_{3r}(r',r)}{L\left[k_{0j}^2+\left(\frac{i}{L}\pi\right)^2\right]^2} \qquad (6)$$

$$G^i_{\eta z}(z',z)=\begin{cases}\cos\left(\frac{2i-1}{2L}\pi z'\right)\cos\left(\frac{2i-1}{2L}\pi z\right) & \eta=1\\ \sin\left(\frac{i}{L}\pi z'\right)\sin\left(\frac{i}{L}\pi z\right) & \eta=3\end{cases} \qquad (7)$$

$$G^j_{\eta r}(r',r)=r'\left[\frac{J_n(k_{nj}r')J_n(k_{nj}r)}{\int_{a_1}^{a_2}\rho^2J_n^2(k_{nj}\rho)d\rho}+\frac{Y_n(k_{nj}r')Y_n(k_{nj}r)}{\int_{a_1}^{a_2}\rho^2Y_n^2(k_{nj}\rho)d\rho}\right] \qquad (8)$$

where $n=1$ for $\eta=1$, $n=0$ for $\eta=3$ and k_{nj} $(n=0,\ 1)$ is the jth root of the following characteristic equation.

$$J_n(\sqrt{\kappa}a_1)Y_n(\sqrt{\kappa}a_2) - J_n(\sqrt{\kappa}a_2)Y_n(\sqrt{\kappa}a_1) = 0 \quad (9)$$

Note that $\psi_2=0$, since no magnetic body force in tangential direction is present.

In general, the solution to the radial, axial and shear stresses obtained from stress functions will not be satisfied at their respective boundaries. Therefore other solutions must be found that satisfy these new boundary conditions. However, these solutions are sought to satisfy only the homogeneous form (without body forces) of Eq. (4) and can be found by using the Fourier Bessel (Hankel) transformation. The final solution to the problem will then be the superposition of all solutions.

MAGNET SCIENCE AND TECHNOLOGY
Pulse Magnets

Program Overview

P. Pernambuco-Wise

The Pulse Magnet Group is responsible for the development of new higher field and increased capability magnets and for provision of all capacitor energized coils for the NHMFL User Facility at Los Alamos. With three separate experimental stations available, the demand for replacement magnets has increased substantially. The group vigorously pursues a development program that aims to produce ever higher fields and capabilities. A major component of this is the fabrication of small evaluation magnets designed to test new conductors, reinforcements, and insulator schemes. An important finding arising from these test magnets will lead to a cooperation with the Aerospace Department of the Georgia Institute of Science and Technology on cryogenic properties of carbon fiber composite materials.

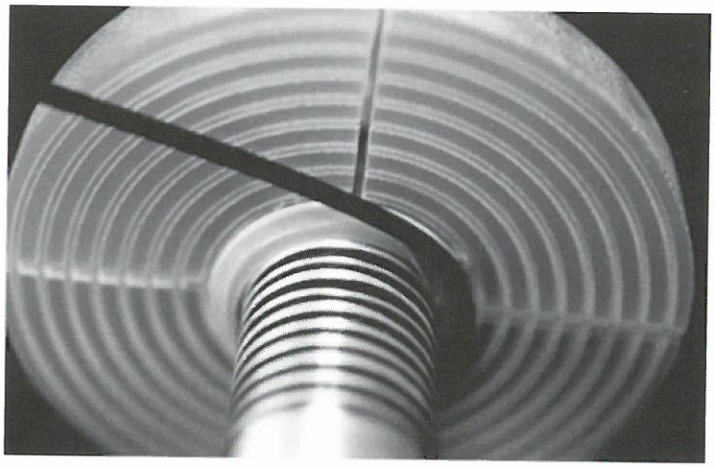

(Top) Winding of a 50T pulse magnet.

(Left) Two people can comfortably fit inside the ninth coil of the NHMFL 60 tesla quasi-continuous magnet now being assembled at Los Alamos. Equally pleased with the accommodations are Don Parkin, Co-Principal Investigator, on the left and James Sims, the principal design engineer, on the right. This will be the first magnet of its kind in the United States and the most powerful in the world, requiring a power supply of 400 MW.

In the last 12 months, twenty magnets of all descriptions have been produced. Of these, one of the most exciting is the 40 T long pulse magnet that will substantially increase user facility capabilities and provide a very desirable staging magnet for the 60 T long pulse magnet being constructed at Los Alamos.

To aid with magnet design, a sophisticated multi-method, coil optimization program package has been assembled that allows multiple section solenoids, multiple conductor, and reinforcement schemes. This capability saves a great deal of time when computing magnet designs utilizing new materials.

As well as taking part in several international conferences and workshops, the pulse group also has supported local education efforts by taking part in school mentoring programs.

At the Los Alamos facility of the NHMFL, the work on the generator driven 60 T magnet has continued and is close to completion. During the past year the 60 T long pulse coils were fabricated, the major design completed, and fabrication begun on the frame, dewar, magnet power busbar, and liquid nitrogen handling systems that support, hold, and service the coils. The current or near term status of the coils is detailed below:

- coils 1-4 received and passed acceptance tests at Los Alamos
- coils 5 &7 completed, passed acceptance tests at vendor (Everson Electric Co. of Bethlehem, PA), and shipped to Los Alamos
- coils 6 & 9 impregnated in shells, passed acceptance tests at vendor and in final machining
- coil 8 impregnated in shell
- all coils are expected at Los Alamos by the end of 1995.

Four of the coils in the set weigh more than a ton. The coils are wound of large cross-section, aluminum oxide dispersion strengthened copper conductor with strength three times that of common structural steel. During fabrication, winding tension was required to be maintained at all times including during conductor splicing and lead attachment operations. Tough, high strength stainless steel external shells were accurately fitted to the coils for reinforcement. Problems with tooling, conductor materials, manufacturing procedures, and quality control were encountered and addressed. The delivery of the 60 T long pulse coils will mean that the NHMFL has a pulsed coil set of a strength, size, and energy capacity that is unmatched in the world.

Simulated Annealing Optimization Codes for Pulse Magnet Design

Gilmore, P., NHMFL
Pernambuco-Wise, P., NHMFL
Eyssa, Y.M., NHMFL

To optimize a magnet design the scientist must utilize the variables at his disposal to balance specific user criteria against the physical limitations of the available magnet materials. Typical variables are the height of the magnet, the number of layers and the voltage across the capacitor bank. Lorentz forces and energy dissipation within the coil result in a set of nonlinear constraints that must be satisfied if the design parameters are to be fulfilled. Mathematically the problem may be formulated as follows:

$$\min_{x \in Q} f(x) = -B(x) + r \sum_{i=1}^{m} \alpha_i \left(\frac{g_i(x) - b_i + |g_i(x) - b_i|}{2} \right)^2 \quad (1)$$

In equation (1) x is the n-vector of magnet design variables, each having lower and upper bounds, forming the hyper-box Q. In (1), the function to be minimized $f(x)$, is the sum of the negative of the magnetic field produced by a given

design and quadratic penalty functions for each nonlinear constraint. At the NHMFL a technique called Ensemble Based Simulated Annealing (EBSA) is used to solve the pulse magnet design optimization problem. The simulated annealing algorithm is given below.

1. *Given* $f:Q \rightarrow R$, $x_0 \in Q$, T_{min}, T_{max}, δT, $L>0$ *and* $K>0$, *set* $T=T_{max}$ *and* $l=0$:
2. *Generate* $x_t \in N(x_k)$ *and* $r \in [0,1]$
3. *Set* $k=k+1$
4. $x_k = \begin{cases} x_t & \text{if } f(x_t) < f(x_k) \text{ or } r < \exp(-\Delta f / T) \\ x_{k-1} & \text{otherwise} \end{cases}$
5. *If* $x_k \neq x_{k-1}$, *set* $l=l+1$
6. *If* $l<L$ *and* $k<K$ *go to 2*
7. *Set* $T=T*\delta T$.
   If $T<T_{min}$ *terminate, otherwise go to 2*

In line (1) of the above algorithm $N(y)$ indicates a neighborhood around y, currently a sequence of decreasing ϵ-boxes is being used. The method of implementation is thus: given an initial neighborhood radius, perform a simulated annealing optimization; when the optimization is complete, reduce the radius ϵ, repeat. This process continues until ϵ is sufficiently small.

As the name suggests, EBSA uses more than one simulated annealing sequence. Typically each uses a fast cooling schedule i.e. small T_{max}, big T_{min}, small δT, and small K. A useful feature is that more than one computer can be simultaneously used to perform a single device optimization thus significantly reducing running time.

The pulse magnet design optimization problem is a complicated one containing nonlinear constraints, many local minima, and both continuous and discreet variables. The variant of EBSA developed at the NHMFL has been very successful in solving these problems, putting the NHMFL at the forefront of not only pulse magnet design but numerical optimization also.

Design and Construction of a 40 T Long Pulse, High Homogeneity Magnet

Pernambuco-Wise, P., NHMFL
Gilmore, P., NHMFL
Lesch, B., NHMFL

The standard pulse magnets available at the Los Alamos user facility provide fields in the 50 to 60 T regime over a time frame of approximately 40 ms. While this is a suitable pulse shape for most experiments, samples with high conductivity may experience induced eddy currents (proportional to $(dB/dt)^2$) that are large enough to render measurements difficult or impossible. Other physical phenomena have an associated relaxation time that requires experimental measurement over a long time frame, thus the usual user magnet may not be suitable for the task.

A long pulse magnet has been designed and built by the Tallahassee Pulse group with input from the CNRS Magnet Laboratory of Toulouse, France. This magnet will reach a peak field of 40 T with a rise time of 100 ms and an overall pulse time of 500 ms, in a 77 K bore of 24 mm. Such long pulse times create significant problems that must be addressed with careful design as well as giving rise to new construction and winding techniques that must be learned.

To have a long pulse time, the inductance of the magnet must be made high by winding many more turns than in a conventional pulse solenoid. This makes the coil much larger physically requiring an extensive support and mounting superstructure. A larger coil requires more energy to operate, thus the LANL capacitor bank has been upgraded from 1.1 MJ to 1.6 MJ. One advantage that arises from a longer coil is that the homogeneity can be much improved; this magnet has the greatest field uniformity of any pulse magnet built so far for the NHMFL. A long pulse requires that the conductor used have a very high conductivity so as to avoid excessive joule heating. High conductivity materials are also in general very weak and internal reinforcement of the conductor to offset the Lorentz forces is not possible on a layer by layer basis due to the lowering of the conductor filling

factor and consequent decrease of the maximum field. Instead a thick external steel shell must be used. This again adds to the mass of the finished magnet; the finished coil exceeds 145 Kg.

Magnets produced in the Toulouse facility have a lifetime of between 250 to 300 pulses. This limitation arises because the severe plastic elongation of the conductor during use—often by as much as 25%. Repetitive cycling causes small cracks to develop in the wire insulation leading to electrical shorts and consequent magnet failure. Because of the high use that the NHMFL magnets receive, a redesign of the basic solenoid was necessary. Three thin layers of S2 glass fiber were introduced to provide internal reinforcement of the inner magnet layers without excessive lowering of the filling factor. This improvement lowers plastic elongation by a factor of approximately 4, and it is hoped will lead to a much improved lifetime. The addition of S2 fiber makes this coil a true hybrid of the internally reinforced Leuven and externally reinforced Toulouse technologies and will be the first of its kind in operation when commissioned in December of 1995. It will add significantly to the capabilities of the NHMFL Pulse Magnet User Facility.

Results of Systematic Failure Testing of Internally Reinforced Pulse Magnets

Pernambuco-Wise, P., NHMFL
Gilmore, P., NHMFL
Lesch, B., NHMFL

To obtain the highest routine fields for the NHMFL Pulse Magnet User Facility, internally reinforced coils of the type pioneered in Leuven are used. These magnets utilize a medium strength, medium conductivity material together with an interlayer S2 glass fiber composite reinforcement material to offset the immense Lorentz forces generated during a magnetic field pulse. The disadvantage of this design is that the coil's mechanical properties are extremely difficult to model accurately, being a complicated system of interdependent, anisotropic materials some of which are still in the experimental development stage and have yet to be fully characterized in the range of temperatures and conditions that the magnet will see during its lifetime.

Small, easy and cheap to produce test magnets have been built and purposely taken to failure fields so as to test computer modeling and provide information that can be applied to future user coils. This is the first such systematic study of the processes of magnet training, aging and failure that has been performed. In the first experiment, eight coils were manufactured and six of these tested to failure to ascertain reproducibility, an important factor in the production of magnets for the user facility.

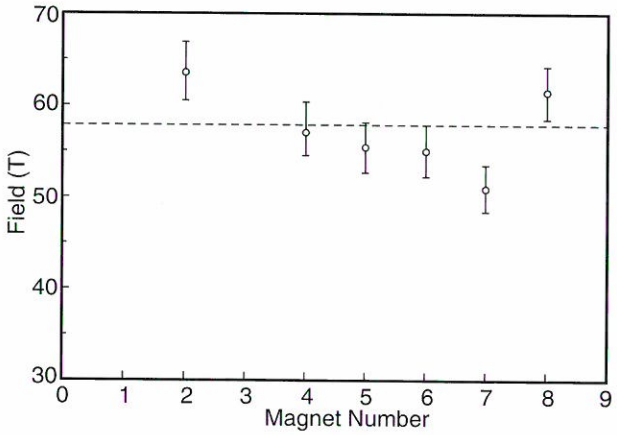

Figure 1. Maximum fields reached for test magnets.

The field measured by a pickup coil at the magnet center at failure is shown in the figure. The lowest field point is from a coil that had not been previously pulsed giving an indication that gradual 'training' of a magnet to high field may have a positive influence on the maximum attainable field. The average field of the remaining five coils was 58 T, which compares well to the value of 59 T calculated from thermo-mechanical codes written at the NHMFL. The reproducibility of magnets is about 7%. This value indicates that the substantial effort placed in quality control of the various construction stages is justified and yields extremely reliable magnets and also indicating that the

CICC's, such as those used for the NHMFL Hybrid Magnet, require structural steels with high strength and high fracture toughness at cryogenic temperatures. Traditional stainless steels, such has 304LN and 316LN, are typically used for such applications. Selection of steels for the Hybrid Magnet, however, is complicated by the requirements for a very high yield strength (>950 MPa with a K_{Ic}>100 MPa) coupled with the need to process the Nb_3Sn superconductor at temperatures near 700° C.

With sufficient addition of soluble nitrogen, the yield strength of 300 series stainless steels approaches 1000 MPa.[1] Heat treating stainless steels in the sensitization regime (550-800° C), however, produces Cr carbides, generally of the $M_{23}C_6$ type. These carbides form intergranularly and have been shown to significantly reduce the low temperature fracture toughness.[2-5] Chemistry modifications, outside of the commercial specifications for 316LN, that rely on reductions in C content and additions of C getters such as Nb have proved beneficial in reducing grain boundary sensitization during prolonged heat treatments in the sensitization regime.[2,3,5,6]

For the Hybrid Magnet conduit we have partly specified a stainless steel chemistry based on empirical NIST data that predicts the yield strength as a function of chemistry and grain size. The 4 K yield strength is given by[7]

$$\sigma_y(\text{MPa}) = -689 + 2510[\text{N}] + 790d^{-1/2} + 436[\text{Mo}] + 78.1[\text{Ni}] - 30[\text{Mo}][\text{Ni}]$$

where,

[X] = concentration of element in wt. %
d = grain size in μm.

For sensitization resistance, the chemistry was specified on the basis of work by Reed, Muster, and Shimada, which suggests a C content of less than 0.01 wt. % Nb content of 0.05 wt. % and a N content > 0.16 wt. %.[2,3,5,6]

We have measured the 4 K mechanical properties of the as received strip. The results of these tests appear in Table 1. Testing of weld metal and aged weld and base metal is in progress.

Table 1. Results of measurements of the mechanical properties of the NHMFL Hybrid Magnet conduit steel.

Test Temp K	Orientation	Yield Strength MPa	Tensile Strength MPa	Elongation %
295	long.	438	760	41
4	long.	1289	1648	29
4	trans.	1292	1645	34

References:

1 Simon, N.J., et al., National Bureau of Standards, Structural Materials for Superconducting Magnets, I. AISI 316 Stainless Steel, (1982).

2 Kübler, J., et al., Advances in Cryogenic Engineering, 38, 191-198 (1992).

3 Muster, W. J., et al., Cryogenics, 30, 799-802 (1990).

4 Nohara, K., et al., in Austenitic Steels at Low Temperatures, R. P. Reed, T. Horiuchi, Eds. (Plenum Press, New York, 1983) pp. 117-133.

5 Reed, R. P., et al., Advances in Cryogenic Engineering, 38, 45-54 (1992).

6 Shimada, M., et al., Advance in Cryogenic Engineering, 34, 131-139 (1988).

7 Simon, R. P. R. Nancy J., in Materials Studies for Magnetic Fusion Energy Applications at Low Temperatures-XI R. P. Reed, Ed. (National Bureau of Standards, Boulder, CO, 1988), vol. XI, pp. 71-87.

The Effect of Load Controlled Fatigue at Liquid Helium Temperatures on the Electrical Resistivity of High Purity Aluminum

Summers, L.T., NHMFL
Walsh, R.P., NHMFL
Nilles, M., Babcock and Wilcox Naval Nuclear Fuel Division

Cryoconductors, such as high purity Al and Cu, have been proposed for use in magnet applications as either protection circuits for superconducting

cables or as the primary conductor in resistive magnet designs. In support of Superconducting Magnetic Energy Storage (SMES) we are investigating the effects of cyclic strain on the 4 K electrical resistivity of high purity aluminum.

The samples used in this study are of a dog-bone shape of high purity Al that are mounted to a high strength Al backing plate. Current leads and voltage taps are provided to inject current and measure the voltage drop across the specimen gage length.

The specimens were tested in the 100 kN mechanical test facility. Samples were cooled to 4 K and the initial unstrained electrical resistivity was measured. The samples were then pulled in tension to a strain of 0.25%, the load recorded. Cyclic straining in load control was conducted using an R ratio of 0.1 and a peak load corresponding to the 0.25% strain load. The electrical resistivity was measured at specified hold points during the test.

The electrical resistivity as a function of the number of load cycles is shown in Figure 1. The force-strain curve for the composite sample is shown in Figure 2.

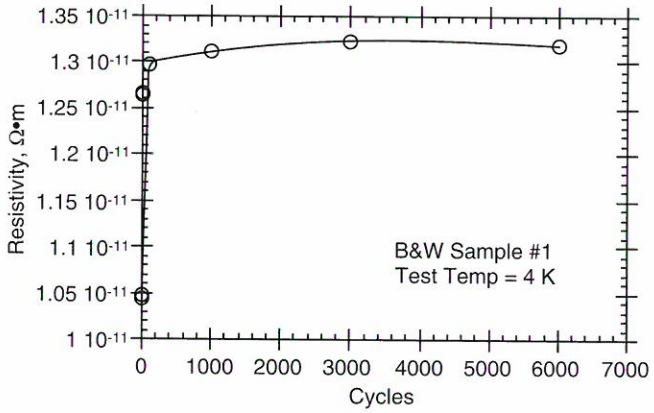

Figure 1. Electrical resistivity as a function of cyclic loading.

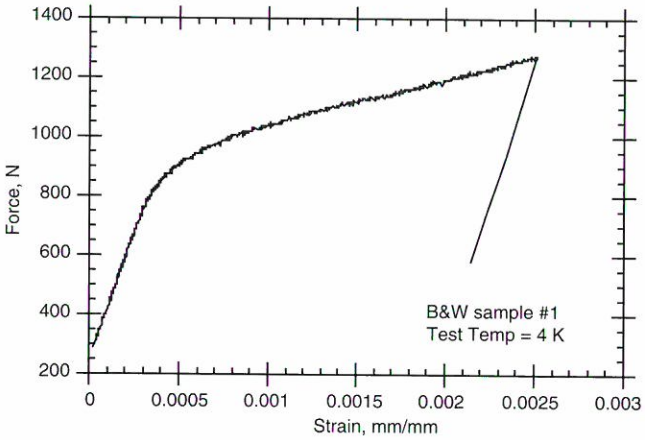

Figure 2. The force-strain curve of the composite (high purity Al and backing plate) test sample.

Design and Construction of a Facility for the Studies of the Effect of Mechanical Strain on the Transport Current of Large Cabled Superconductors —Facilities Development

Summers, L.T., NHMFL
Walsh, R.P., NHMFL
Miller, J.R., NHMFL

A new and major addition has been made to the Materials Development and Characterization Laboratory. This facility is designed to provide researchers and magnet designers with the capability to make electrical and mechanical tests of large samples in high magnetic fields.

The system consists of a 12 T split-solenoid superconducting magnet (see Figure 1). The magnet has a bore diameter of 150 mm and a radial access port of 30 x 70 mm, thus allowing tests of large conductors or mechanical test specimens. Operating currents for powering samples are as high as 10 kA, with higher currents possible by replacement of the existing vapor cooled leads.

The magnet cryostat is designed to accept a 250 kN capacity tensile test machine that sits on riser legs attached to the cryostat's top flange. Force transmission is accomplished using a pull rod that penetrates the top flange and connects to a specimen nominally located in the radial access port. The bottom end of the specimen can be attached to remotely operated grips fixed to the cryostat floor. Loads are returned to the cross head via the cryostat inner wall.

The facility will initially be used for studies of superconducting materials. In the case of materials such as Nb_3SN, the limiting transport current density is a strong function of the strain state. For single wires and tapes the strain effects have been extensively studied and have been found to predictable using scaling laws.[1,2] The complex geometry of cabled conductors, such as those for the NHMFL Hybrid, and their uncertain strain state make it difficult to predict the critical current using existing scaling laws. This facility is designed expressly to provide researchers with an experimental platform for investigation of such configurations.

The first series of tests to be conducted in the new facility will be an evaluation of Hybrid Cable-In-Conduit Conductors (CICC's). The samples for this testing will consist of pairs of CICC's connected electrically in series (mechanically in parallel) by a joint located in the low field region at the bottom of the radial access port. A series of samples covering a range of helium void fractions will be evaluated in early 1996.

This new facility also can be reconfigured to allow mechanical testing of relatively large samples in field. Reorientation the magnet so that the bore is vertical, provides researchers with a 150 mm diameter, 4 K test space that can accommodate any one of a number of ASTM standard test specimens. Possible uses of the facility in this configuration include mechanical tests of metastable materials that exhibit both field induced phase transformations.

Presently, the 12 T magnet has been delivered and successfully operated to full field. The tensile test machine has been fabricated and installed and the completed system is undergoing performance trials.

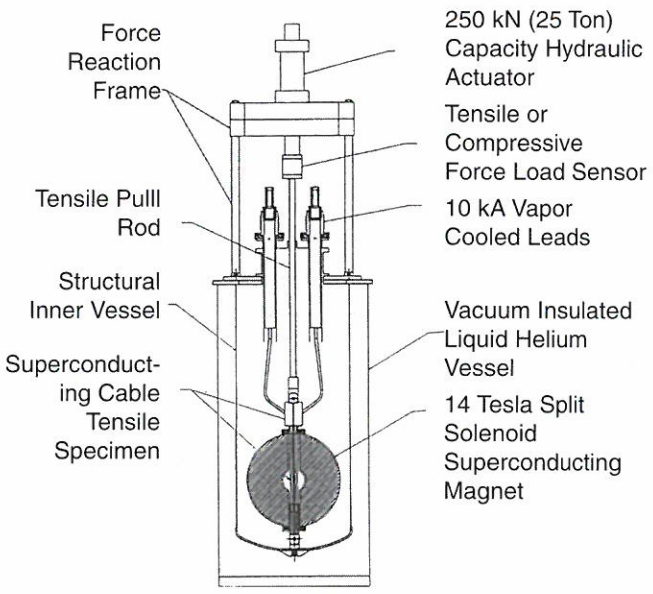

Figure 1. A cross-section view of the large conductor mechanical-electrical test facility.

References:

1 Ekin, J. W., Cryogenics, 20, 611-624 (1980).

2 Summers, L.T., et al., IEEE Transactions On Magnetics, 27, 2041-2044 (1991).

MAGNET SCIENCE AND TECHNOLOGY
High Strength Conductors

Program Overview

T.S.E. Summers

The choice of conductor materials for pulse and resistive magnet applications is influenced by many interrelated factors. The conductor must have high strength to resist the Lorentz forces produced by the magnetic field, and it must have good conductivity and a high heat capacity to minimize heating of the magnet. Factors such as ductility, fatigue resistance and the size and shape of the conductor are important as well. In pulse magnets, the conductor is used in wire form, and current designs require a 2x3 mm rectangular cross section. Cross sections as large as 4x6 mm may be required in future designs, however. The resistive Bitter magnets are made from conductors in strip or sheet form with a thickness of 0.4 or 0.7 mm.

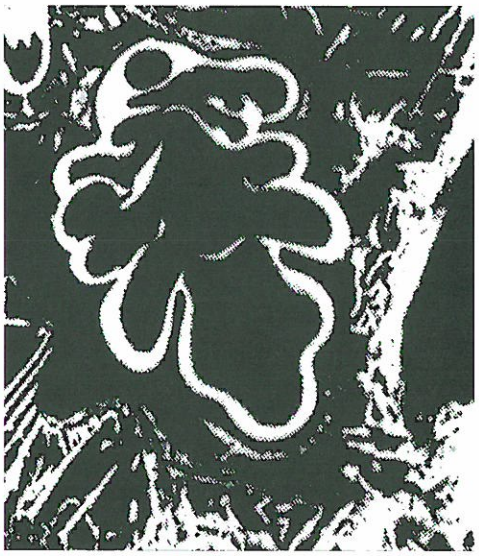

SEM micrograph of as-cast Cu-Nb.

The current goals of this program are to produce conductors with a strength on the order of 1.2-1.5 GPa and a conductivity better than about 50-60% IACS (International Annealed Copper Standard). Since strength is generally inversely related to conductivity and ductility, however, obtaining high values of all the above properties in the same material is not a trivial problem. The conductor materials currently being investigated may be divided into two broad categories: microcomposites and macrocomposites.

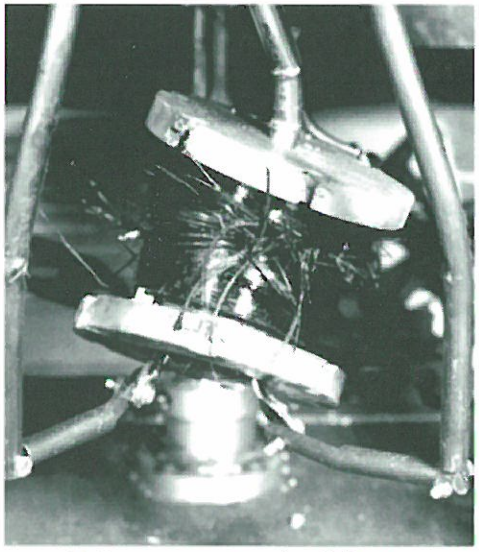

Pulse magnet tested to failure.

The microcomposites are two-phase materials that develop a filamentary microstructure when heavily deformed by a process such as wire drawing or rolling. This fine filamentary structure provides high levels of strengthening, but because the filaments are aligned with the wire axis and because the phases comprising the filaments are relatively pure, strengthening is not accompanied by an unacceptable decrease in conductivity. Emphasis is placed on Cu-based systems because of the high conductivity of Cu, and those alloys currently under investigation are Cu-Nb, Cu-Ag and Cu-Nb-Ag.

The main problem associated with the microcomposites does not actually involve the ability to achieve high strength. High strengths are easily achieved with large amounts of deformation. Limits associated with practical ingot sizes and drawability, however, restrict the final wire size to diameters that are much too small for pulse magnets. The Bitter magnets currently utilize Cu-Ag strip, but further strengthening must be provided without a decrease in the strip thickness. The microcomposite research has therefore focused on processing techniques that produce strengthening without excessively decreasing the billet cross section.

Because the strength of the microcomposites is due to the fine filamentary structure that develops during deformation, high strength can be achieved with less deformation if the microstructure of the starting material is refined. Melt spinning is a method by which as-cast material is produced in ribbon form with extremely rapid cooling rates that result in very fine as-cast structures. Cu-Ag ribbons have been successfully produced at UF* and at the NHMFL, LANL. Consolidating these ribbons into a wire form that can be drawn is currently being investigated. Another method by which as-cast material is refined is through directional solidification. This process has the added advantage that the structure produced is aligned with the ingot axis. Testing of wires produced in this way is currently in progress at UF.**

A preliminary investigation[1] of equal channel angular extrusion (ECAE) that is a shear deformation process currently being developed at Texas A&M was concluded. This study was carried out at both Texas A&M*** and the NHMFL, Tallahassee to determine if the ECAE process could be used to refine the starting microstructure so that less wire drawing would be needed to produce high-strength wires. The results of this study are promising and are given in a research report that follows.

Electrodeposition of alternating layers of copper and silver as a means of producing high-strength, isotropic strip material for Bitter magnets is also under investigation at UF.[1] Submicron-layered composites have been successfully produced, and the mechanical and electrical properties of this material are currently being investigated.

Silver has a higher solubility than niobium in copper. This fact causes precipitation to play a role in the strength of Cu-Ag alloys as was pointed out by Sakai,[2] and intermediate heat treatments during wire drawing or rolling have a dramatic effect on the final properties of Cu-Ag conductors. The precipitation reactions occurring during these heat treatments are as yet not well understood. The results of investigations of these precipitation reactions are given in two research reports. In addition, a heat treatment optimization study[3] is also discussed in a research report.

The macrocomposites use pure Cu for good conductivity and reinforce it with steel for high strength. Since steels have very poor conductivity, the overall conductivity goes approximately as the volume fraction of Cu in the wire. This conductivity is lower than that obtained with the microcomposites at room temperature but, because of the high resistance ratio of pure Cu, is higher at 77 K. In addition, the high heat capacity of steel is expected to help reduce magnet heating. Two steel reinforcing materials are currently under investigation: pearlitic steel, which is known to have high strength with large amounts of deformation, and the 300 series austenitic stainless steels, which have a good combination of strength and ductility even at low temperatures. One 2x3 wire produced at Supercon, Inc. using Cu clad with approximately 40% 316 stainless steel had 800-MPa strength at room temperature. This stainless steel, however, is known to be stable with respect to deformation and consequently does not work harden excessively. A similar wire with the much less stable 304 stainless steel is currently being produced.

References:

1 Summers, T.S.E., et al., Adv. Cryo. Eng., vol. 42, in press, (1996).

2 Sakai, Y., et al., IEEE Trans. Magnetics, 28:887, (1992).

3 Sakai, Y. and Schneider-Muntau, H., to be published.

* This work was funded by the NHMFL, to be conducted by Prof. F. Ebrahimi at UF.

** This work was funded by the NHMFL, to be conducted by Prof. M. Kaufman at UF.

***This work was funded by the NHMFL, to be conducted by Prof. K.T. Hartwig and Dr. V. Segal at Texas A&M.

Microstructure and Conductivity of Cu-Ag

Heringhaus, F., NHMFL/Institut für Metallkunde und Metallphysik, RWTH Technical University, Aachen, Germany
Leffers, R., Institut für Metallkunde und Metallphysik, RWTH Technical University, Aachen, Germany
Raabe, D., Institut für Metallkunde und Metallphysik, RWTH Technical University, Aachen, Germany
Gottstein, G., Institut für Metallkunde und Metallphysik, RWTH Technical University, Aachen, Germany

In a broad range of compositions copper-silver alloys are being applied or have potential applicability for both Bitter magnets and pulse magnets. For a better understanding of the materials behavior and for further optimization of the processing and the final properties, investigations of the microstructure and properties of the following materials have been carried out: (a) Cu, (b) Cu with maximum soluble Ag (4.9 at %Ag), (c) eutectic Cu-Ag (59.6 at %Ag), (d) Ag with maximum soluble Cu (14.1 at %Cu), and (e) Ag. Of primary interest, with respect to the eutectic composition, is the correlation of the deformation-induced changes in the microstructure and the properties. The eutectic composition solidifies in a lamellae structure which refines during deformation. Figure 1 depicts the resistivity of eutectic Cu-Ag as a function of the lamellae thickness. The lamellae thickness was investigated by means of scanning and transmission electron microscopy (SEM and TEM) and is averaged for Cu and Ag according to their volume percentage. The strong increase of the resistivity with very thin lamellae can be understood in terms of the restriction of the conducting volume for each lamellae and an increased interface scattering. The interfacial spacing between Cu and Ag reaches the order of magnitude of the mean free path of the conduction electrons. Due to the temperature dependence of the mean free path, low temperature measurements show a much stronger increase of the resistivity with decreasing interfacial spacing (Figure 2). On the other hand, the strong interface contribution to the overall resistivity leads to a fairly low magnetoresistivity (5% @ 4.2 K in 27 tesla) as compared to pure Cu and Ag (>100%). With respect to the investigation of the precipitation process in compositions (b) and (d), studies of the dissolution of the second phase atoms in the matrix, optimizing the initial state, and the effect of pre-deformation on precipitation kinetics have been carried out. The latter has to be accompanied by further TEM investigations.

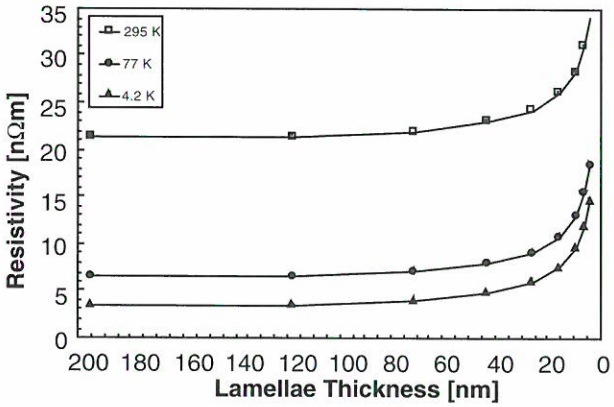

Figure 1. Resistivity vs. lamellae thickness for eutectic Cu-Ag.

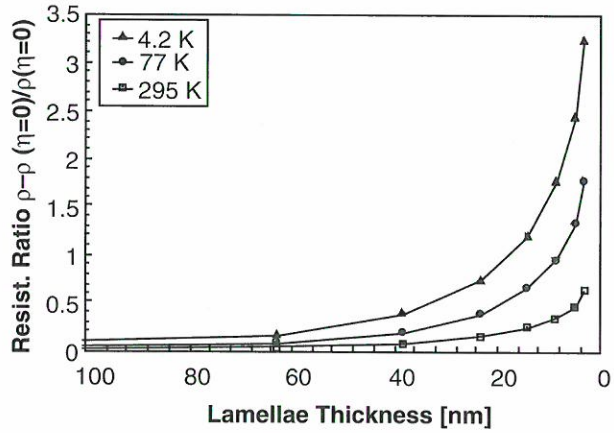

Figure 2. Resistivity ratio vs. lamellae thickness for eutectic Cu-Ag.

Hydrostatic Extrusion of CuNb Spark Eroded Powder

Hill, M.A., LANL
Bingert, J.F., LANL
Bingert, S.A., LANL
Spada, F.E., Center for Magnetic Recording Research, Univ. of CA, San Diego
Berkowitz, A.E., Center for Magnetic Recording Research, Univ. of CA, San Diego

High strength, high conductivity copper-niobium wire is a promising conductor wire for use in pulsed high field magnets. A peak field of 68 T has been achieved by Foner using copper-niobium as the conductor.[1] Due to the high melting point of niobium, it is difficult to produce an ingot with a fine, homogeneous structure. One possibility for reducing the scale of the cast structure, improving the homogeneity of the ingot, and enhancing the strength at a given level of deformation strain is to use rapid solidification techniques, such as powder processing, to fabricate the Cu-Nb ingot. Both melt spinning and gas atomization of Cu-Nb are difficult due to problems associated with thermal shock of components, such as crucibles and stopper rods. Spark erosion provides a method for powder production without the use of components that may crack under thermal stresses. Spark erosion also has been shown to have the fastest quench rates of any powder production technology.[2]

A Cu-10 vol.% Nb ingot was double consumable arc melted. The starting elemental charge was C10100 copper and 99.9 percent niobium. This material was then extruded and drawn into hexagonal shaped wire. The hexes were bundled in a copper can that was subsequently hot isostatically pressed. The total reduction in area for the rod was 93% or a strain of 2.6. This rod was then machined into electrodes and charged for production of spark eroded powder.

The spark erosion process involves spark discharges among pieces of material placed in a dielectric fluid. Localized melting or vaporization of the material results from this spark discharge. When molten droplets freeze or vapor condenses and freezes, powder particles form. These powders are quenched rapidly since they are quenched *in situ*. Cu-Nb was initially prepared in dodecane-pentane, but niobium carbides were found in the powder when x-rayed. Cu-Nb was then spark eroded in liquid nitrogen; niobium nitride contamination was discovered, however, using x-ray diffraction. The Cu-Nb powder, which was eventually consolidated, was prepared in liquid argon. Some CuO was noted in the powder using x-ray diffraction.

The average particle size of the powder is less than 10 microns. The consolidated rod has not been characterized for mechanical and electrical properties. Metallographically, the rod appears fully dense.

References:

1 Foner, S., Appl. Phys. Lett., vol. 49, pp. 982-983, 1986.

2 Berkowitz, A.E., et al., J. Mater. Res. 2 (2), Mar./Apr. 1987, p. 277.

Hydrostatic Extrusion of Rapidly Solidified Copper-Silver Melt Spun Ribbon

Hill, M.A., LANL
Bingert, J.F., LANL
Bingert, S.A., LANL
Thoma, D.J., LANL

Rapidly solidified ribbon of Cu-16 at % Ag was cold pressed and hydrostatically extruded into rod. The consolidated rod was tested for both mechanical and electrical properties. A significant increase in strength and conductivity was noted in the hydrostatically extruded ribbon when compared with conventionally processed Cu-Ag rod.

With melt spinning, the starting microstructure of the Cu-Ag was refined to 1 μm, as compared to 10-20 μm achieved with continuous casting by Sakai, et al.[1] This refinement of the microstructure is important since it relates to an increase in strength. By die pressing the ribbon, a density of 95% was achieved. The material was extruded cold in the hydrostatic extrusion press. Adiabatic heat generation associated with deformation work increases the actual billet temperature during

extrusion. An estimate of this temperature change following the method of Laue and Stenger[2], for R = 4, gives ΔT = 160 K and an exit temperature of 185°C. Hydrostatic extrusion offers the benefit of obtaining higher reductions in area at lower temperatures for a given amount of press capacity, when compared with conventional extrusion. Hydrostatic extrusion is especially appropriate for processing composites since the reduction of container and die friction contributes to more uniform material flow. The starting diameter of the extrusion was 9.5 mm and the final diameter was 2.5 mm. This reduction was achieved in two passes. The reduction in area associated with the extrusion is 93%, which translates to a strain of 2.6.

Optical metallography of the transverse section of the extrusion shows a composite that consists of an 84% copper-silver core surrounded by 16% pure copper, previously in the form of a can. The material appears to be fully dense. Using high resolution scanning electron microscopy, one hundred nanometer silver filaments were observed in the microstructure of the consolidated rod.

The resistivity of the rod at room temperature is 2.02 μohm-cm or 86% IACS (International Annealed Copper Standard). The resistivity at liquid nitrogen temperature is 0.34 μohm-cm, resulting in a resistivity ratio (ρ_{77K}/ρ_{296K}) of 5.94. Since the operating temperature of the magnet is below room temperature, a high resistivity ratio is desirable. The resistivity ratio of hydrostatically extruded copper-silver compares well with other conductors utilized for high field magnets and is almost twice the resistivity ratio for conventionally processed copper-silver. This high resistivity ratio results from the thick outer layer of copper in the composite.

Yield strength values exceeded those of conventionally processed Cu-Ag (Figure 1). In this study, yield strengths were determined by compression testing due to a lack of material for tensile testing. Tests accomplished by Sakai et al.[1] were done in tension. Previous experience testing CuAg in both tension and compression has shown good agreement as to the yield strength of the material, provided the material is free from defects.

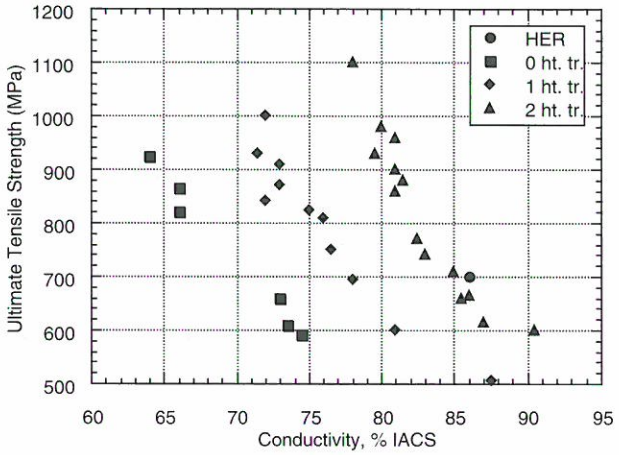

Figure 1. Hydrostatic extrusion of rapidly solidified copper-silver melt spun ribbon as compared to conventionally processed Cu-Ag.

References:

1 Sakai, Y., et al., IEEE Trans. on Magnetics, vol. 28, no. 1, 1992, pp. 888-891.

2 Laue, K., et al., *Extrusion,* ASM, Materials Park, OH, 1981, pp. 27-30.

Ultra-High-Strength, High-Conductivity Cu-Ag Wires

Sakai, Y., NHMFL and NRIM, Japan
Schneider-Muntau, H.J., NHMFL

A new wire fabrication method was developed for Cu-Ag alloys containing 6-24 wt. % Ag in which ultra-high strength and high conductivity are obtained through a combination of cold drawing and intermediate heat treatments. These heat treatments were developed so that high strength could be achieved without the need for large amounts of deformation so that large-cross section conductors could be produced for pulse magnet applications.

Electrolytic copper and 99.96% pure Ag were melted in a Tammann furnace with compositions in the range of 6-24 wt. % Ag. Each charge of about 250 g was melted in an argon atmosphere and then cast into a heated Cu mold where it was held for 1-2 min. before quenching into water. Each ingot, initially 70 mm long and 20 mm in diameter, was turned down to 18.5 mm in diameter before wire

drawing. The wire drawing and heat treatment schedule is given in Table 1 where the draw ratio $\eta=\ln(A_0/A_f)$ is the logarithmic strain. Details of the procedure and results are given elsewhere.[1] Figures 1 and 2 show the results of drawing Cu-24 wt. % Ag. As shown in Figure 1, a strength of 1.45 GPa was achieved with a final drawing reduction of $\eta=5.8$. The room-temperature conductivity of the wires produced is typical for Cu-Ag microcomposite wires.

Table 1. Thermomechanical treatment.

Cold Wire Drawing		Intermediate Heat Treatment	
Draw Ratio, η	**Reduction in Area (%)**	**Temp. (°C)**	**Time (h)**
0.13	12	430	2
0.54	54	430	1
1.02	64	370	1
1.47	77	370	1
2.30	90	330	1
4.6-5.8	-	-	-

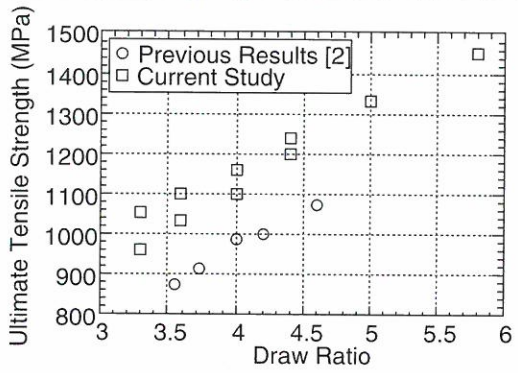

Figure 1. The room temperature strength of wires processed by the procedure given in Table 1.

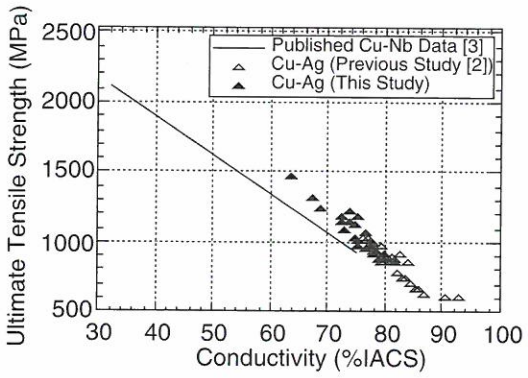

Figure 2. Strength vs. conductivity plot showing typical inverse relationship.

References:

1 Sakai, Y., et al., to be published.

2 Sakai, Y. et al., IEEE Trans. Magnetics, 28:887 (1992).

3 Gielisse, P.J., et al., Deformation-processed high strength high conductivity microcomposite conductors (a review), Vol. 1, NHMFL Internal Report (Sept., 1992).

ECAE-Processed Cu-Nb and Cu-Ag Nanocomposite Wires for Pulse Magnet Applications

Summers, T.S.E., NHMFL/FAMU–FSU CoE
Walsh, R.P., NHMFL
Pernambuco-Wise, P., NHMFL

Equal Channel Angular Extrusion (ECAE) is an innovative processing technique currently under development at Texas A&M University[1-3] that can impart large amounts of deformation to a 25x25x125 mm billet without reducing its cross sectional area. The effect of this processing technique on the microstructure and properties of Cu-18 wt.%Nb and Cu-25 wt.%Ag that was subsequently drawn into wire was investigated[4] as a joint project between the NHMFL, Tallahassee and Texas A&M University.[1]

A billet processed by ECAE is extruded through two identical channels that are at an angle to one another. This extrusion results in a shear strain along the plane of intersection of the two channels. In two-phase materials, this shear strain results in elongation of the phases along the plane of shear. When repeated with the billet in the same orientation for each ECAE pass, the phase alignment becomes finer, more uniform and rotates toward the billet axis.[2,3] Thus, a fine, filamentary structure, which is responsible for the strength of Cu-based microcomposites, evolves without the need of reducing the billet diameter. Since the starting material is much stronger than as-cast material, less wire drawing should be required to produce high strength. Therefore, large-diameter, high-strength wires should be possible.

The results of this study are summarized in Figure 1. As an example of how promising they are, consider a 25-mm diameter ingot of Cu-Ag. Strengthening of such an ingot to almost 1.1 GPa would require 99% reduction resulting in a wire with 2.5-mm diameter. The same strength could be obtained in an ECAE-processed wire with nearly an 8-mm diameter. It is important to note that the Cu-Ag in this study did not receive any heat treatments during wire drawing. With optimized heat treatments, higher strengths and/or wire diameters are expected. Optimization of these heat treatments as well as rolling of ECAE material for resistive magnets is currently under investigation.

The project was a collaborative effort with V. Segal and K.T. Harwig at Texas A&M University.

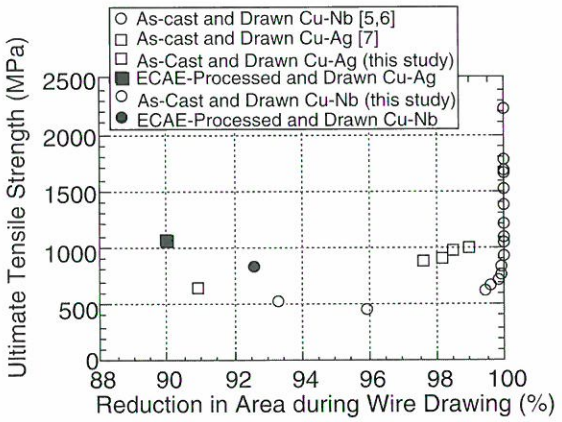

Figure 1. Comparison of ECAE-processed and as-cast drawn wires.

References:

1 Segal, V.M., et al., Russian Metallurgy (Engl. Transl.), 1:115 (1981).

2 Segal, V.M., Mat. Sci. Eng. (in press).

3 Segal, V.M., et al., to be submitted to J. Mat. Sci. Eng.

4 Summers, T.S.E., et al., Adv. Cryo. Eng., vol. 42 (1996), in press.

5 Spitzig, W.A., et al., Acta Metall., 35:2427 (1987).

6 Bevk, J., et al., in *In Situ Composites IV*, F.D. Lamkey, H.E. Cline and M. McLean, eds. Elsevier Science Publishing Co. (1982), p. 121.

7 Sakai, Y., et al., IEEE Trans. Magnetics, 28:887 (1992).

Design and Process of Cu/Steel High Strength High Conductivity Composite with Nb Barrier

Zhou, R., LANL
Smith, J.L., LANL
Embury, J.D., McMaster Univ.
Wood, J.T., McMaster Univ.

The construction of long pulse, high field magnets requires a unique class of materials that have simultaneously high electrical conductivity to avoid resistive heating and high mechanical strength to support the large Lorentz force present in the energized coil. These properties do not generally co-exist in the same material. In the past several years, various high-strength, high-conductivity alloys and composites have been developed. These materials can be divided into two groups. The first consists of so-called microcomposites, such as CuAg and CuNb having ultimate tensile strengths of over 1 GPa and conductivities of the order of 70-80% IACS (International Annealed Copper Standard). The alternative is the macrocomposites, generally stainless steel and copper that have strengths and conductivities proportional to the ratio of the constituent materials. The construction of the 100 tesla pulsed magnet requires further advances in conductor materials. The Cu/carbon steel composite developed at Los Alamos National Laboratory outperforms CuNb, CuAg, and Cu/stainless steel. The major advantage of this type of conductor is that a whole range of mechanical strengths can be obtained simply by varying the ratio of copper and the steel. Another advantage is that it has the full electrical properties of the amount of copper it contains, including its high resistivity ratio between room temperature and liquid-nitrogen temperature.

The composite was made of a carbon steel cylinder filled with an oxygen-free-high-conductivity (OFHC) copper core and jacketed with an OFHC copper can on the outside. Niobium foils were placed between the copper and steel as diffusion barriers to ensure the high conductivity of the copper by preventing the elements in the steel from diffusing into and contaminating the copper during high-temperature extrusion and heat treatment. After evacuation, the assemblage was sealed by electron beam welding followed by extrusion into a rod. Then the rod went through a series of heat treatments called patenting during which an ultra-fine lamellar pearlite formed in the steel. After patenting, the rod was drawn to final sizes by swaging and wire drawing. Figure 1 shows that the ultimate tensile strength of the composite increases with increasing reduction in area. At a reduction in area of 99%, an ultimate tensile strength of 1.67 GPa is achieved. In Figure 2, conductivity of the composite at room temperature is plotted as a function of reduction in area. The conductivity decreases slightly as the reduction in area exceeds 95%. It is worth mentioning that the conductivity of the composite at liquid nitrogen temperature is over 400%, which is much better than that of CuNb or CuAg. It is also relatively easy to scale up the process to large scale production of the composite. In conclusion, we believe that the macro Cu/carbon steel composite is a very promising conductor for the 100 tesla pulsed magnet.

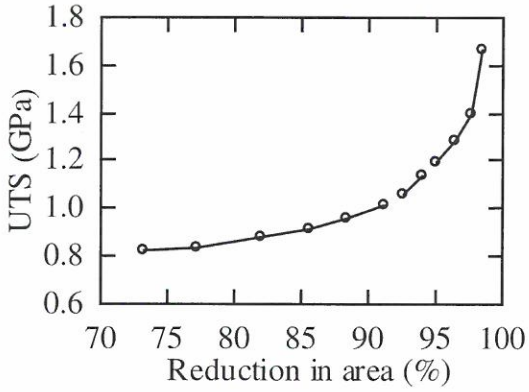

Figure 1. The ultimate tensile strength of the composite plotted as a function of reduction in area.

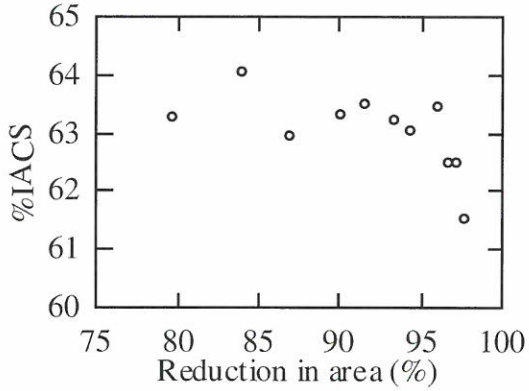

Figure 2. The conductivity at room temperature as a function of reduction in area.

MAGNET SCIENCE AND TECHNOLOGY
High Temperature Superconductors

Program Overview

J. Schwartz and S.W. Van Sciver

Research into high-T_c superconductivity at the NHMFL extends over the broad range of physics and engineering issues that characterize this diverse field. The most recently discovered high-T_c materials system, $HgBa_2Ca_nCu_{n+1}O_x$, has the highest T_c of any superconductor but offers many important challenges. Here we report on fundamental investigations into the nature of the vortex state in this system and on our synthesis and processing investigations. In the more established $Bi_2Sr_2Ca_nCu_{n+1}O_y$ system, we discuss our measurements of the thermal conductivity in high magnetic fields, which addresses both the fundamental magnetic behavior and determines important engineering data for $Bi_2Sr_2Ca_nCu_{n+1}O_y$ magnets.

Furthermore, we discuss engineering studies of high-T_c conductors and magnets. We are using three-dimensional finite element methods to consider the magnetothermal stability and quench propagation in anisotropic, Ag-clad $Bi_2Sr_2Ca_nCu_{n+1}O_y$ conductors operating under a variety of thermal boundary conditions. We are also evaluating alternative winding geometries for toroidal magnets that may significantly reduce the mechanical strain in the brittle oxide superconductor while aligning the transport current parallel to the generated magnetic field, thereby increasing the critical current density. While each individual research summary has specific activities and goals, as a whole they represent a research program aimed at the development of high-T_c applications.

Finally, we summarize progress in the Delta B program, which is principally directed toward development of high field insert coils for low temperature superconducting magnets. The ΔB Program was initially formed to support the 25 T (1.1 GHz) NMR project. This project, which involves the development of spectrometer magnets for chemical and biological investigations, is a two-phase activity with the first consisting of a 900 MHz (B = 21 T) magnet system based on low temperature superconductors (NbTi and Nb_3Sn). At that operating point, the 900 MHz system will be at the limit of LTS conductor technology. The second phase of the 1.1 GHz program involves the development of a 5 T insert coil, using HTS conductor technology, which will replace the inner section of the

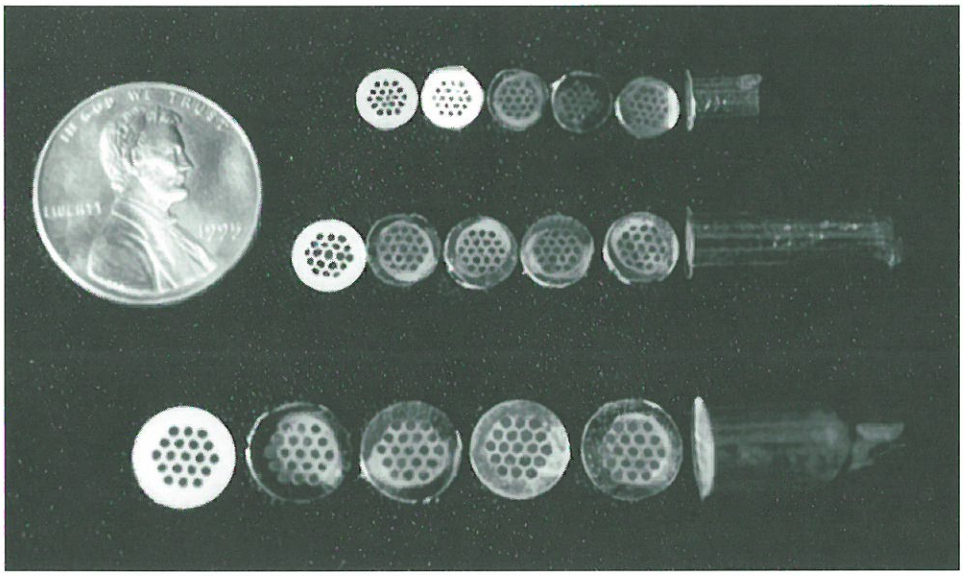

Optical micrographs of 19-filament, multicore, BSCCO wire at different stages of drawing (8.1 mm, 5.9 mm, 5.0 mm from bottom to top). The wire shows high uniformity.

LTS magnet system and thereby produce the desired 25 T, albeit on a somewhat smaller inner diameter. In addition to the 1.1 GHz program, the ΔB Program has recently initiated a design effort toward a 1.5 GHz (B = 35T) solid state NMR system also consisting of an LTS outer section and an HTS insert. This coil would represent the first large scale application of HTS technology in magnet systems.

The ΔB Program supports both of these magnet development activities. The essential approach of the program is to conduct research and development in relevant aspects on HTS magnet technology to advance the state-of-the-art so that the NMR insert coils can be built and reliably operated. Such a broad goal requires a multi-task program directed at the major hurdles to the accomplishing the goals. Since resources are limited, the ΔB Program has focused on specific tasks: HTS conductor development; insulation techniques for HTS coils; joint development in HTS conductors; HTS transport characterization; microstructural characterization; and, Ag-BSCCO magnet design and development.

Force-Reduced Toroidal Magnet Concepts

Amm, B.C., NHMFL
Schwartz, J., NHMFL/FAMU–FSU CoE

Large scale superconducting magnets fabricated from high critical temperature superconductors are limited in part by the large Lorentz forces generated. These forces are generated by the interaction of the electric and magnetic fields in the magnet and dictate the maximum achievable field of the magnet. However, there exists a set of analytical solutions that have no Lorentz forces. Such "force-free" solutions are achieved by selecting a conductor winding path which generates a magnetic field parallel to the current flow. An infinite number of such solutions exists; however, only a handful show any practical applicability due to their complexity.

Depicted in Figure 1 (page 138) are magnetic field isosurfaces and a few magnetic field lines of the chosen ideal force-free solution. With a solution selected, the challenge then becomes one of taking the continuous analytical solution and forming a discretized solution that can be wound into a superconducting magnet without sacrificing the current-magnetic field alignment.

Unfortunately, no useful device can be built force-free. The Virial Theorem, which relates magnetically stored energy to structure strain energy, places a lower limit on the magnet mass required if the device is to store energy; however, it is still conceivable to produce improvements through stress redistribution. Since toroidal magnet designs face their highest stresses in their inner leg, by utilizing a force-free solution in this region, and a more conventional D-shape for the outer portion, a reduction in the overall stress of the structure should be possible. Thus, though the Virial Theorem shows a force-free magnetic to be impossible, the goal is to produce a "force-reduced" magnet design with higher fields and less support structure, thus, an improved cost/benefit ratio.

It has been shown that discretization of the selected ideal aligned field solution is possible, and that the magnetic field of the discretized solution still maintains the general form of the ideal solution. The proposed force-reduced magnet design is shown in Figure 2 (page 138) and has been named the Modified Square Toroid (MST).

The magnetic characteristics of the MST have been calculated and are similar to a conventional toroid. The majority of the magnetic field is in the toroidal direction. The MST also possess a small z field similar to a solenoid. The mechanical behavior of the MST is now being studied. Current work involves refining the finite element model that describes the system to allow a comparison between the force-reduced system and a conventional toroidal array. Proposed factors of merit for such a comparison are the ratio of stored energy to peak stress and peak field to peak stress.

This research is supported by the Department of Energy through the Argonne National Laboratory.

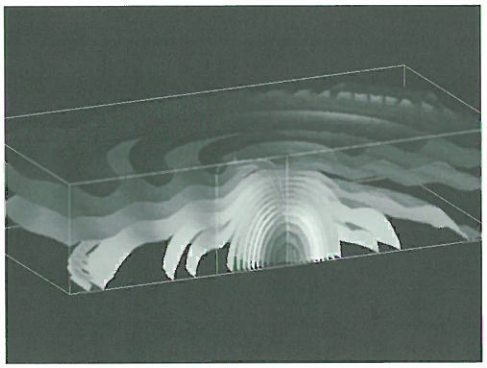

Figure 1. Magnetic field surfaces for a force-free magnetic field.

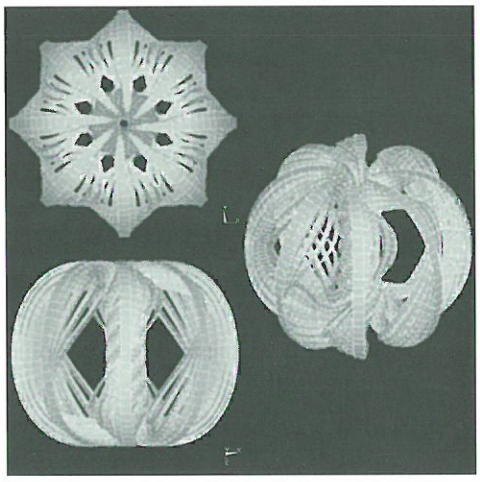

Figure 2. The proposed Modified Square Toroid configuration, based upon a force-free magnetic field in the inner-leg and a conventional D-shaped outer leg.

A New Winding Technology for HTS Coils: The Self Insulating Substrate Tape (SIST)[1]

Belenli, I., NHMFL
Hascicek, Y.S., NHMFL

Technologically significant conductors of High Temperature Superconductors (HTS) are in tape form in most cases. Most often pancake coils are wound from these conductors by using the "wind-and-react" approach, and ceramic based papers or tapes are used for turn-to-turn insulation. The insulation is, of course, taking up the valuable winding space, and currently the thinnest material available is about 0.1 mm in thickness. If the insulation was included within the tape itself and made thinner, this would present several advantages to the present technology. First of all winding will become less laborious and less costly. The saved winding space by using thinner insulation can be used to put more amp turns. We proposed the Self Insulating Substrate Tape (SIST) to be used as substrate for making HTS tape conductors.

Facing sides of two silver tapes are coated with fine alumina or zirconia powder with desired particle size then the tapes are rolled together to produce SIST. This self insulating tape can be used as substrate for dip coating, electropherotic deposition or doctor blade casting of high temperature superconductors.

Both side edges of the self insulating substrate tape are coated with a narrow strip of an appropriate polymer in order to prevent superconducting layers at both sides from making contact. When the superconducting composite tape is annealed before or after winding, the polymer coating will burn off, leaving the edges clean.

Transverse section of the superconducting composite tape made using self insulating substrate tape is shown in Figure 1 (page 139). When this tape is wound into pancake coil, the outer superconducting layer of each tape turn will come into contact with the inner superconducting layer of the next tape turn. These two superconducting layers will form a current turn of the pancake coil. Tape turn units and current turn units of the pancake coil are shown in Figure 2 (page 139).

The inner most and the outer most current turns have one superconducting layer only after winding. These layers do not carry current and connections are made as seen in Figure 3 (page 139).

We have already demonstrated that flexible self insulating substrate tape can be produced. We coated only one side of two silver tapes with alumina based high temperature ceramic. These two tapes are pressed together making good contact and let to dry. More recently a prototype of 5 m long SIST was produced at NHMFL. Collaboration with Oxford Superconducting Technology to fabricate pancake type coils from SIST HTS dip coated conductors is underway.

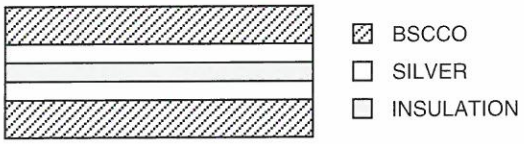

Figure 1. Transverse section of SIST.

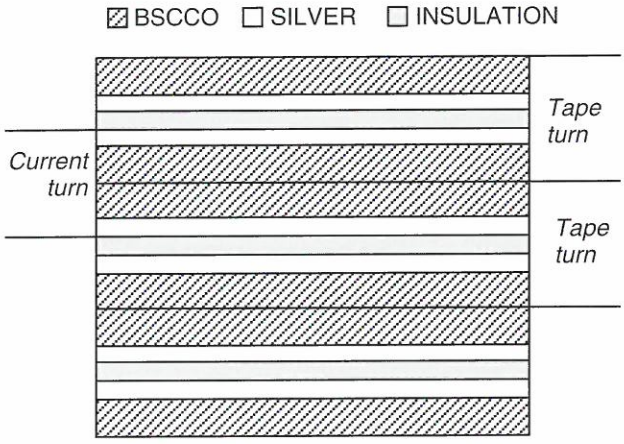

Figure 2. Schematic representation of use of SIST in pancake coils.

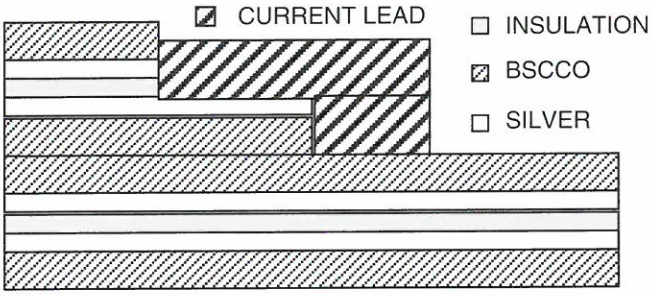

Figure 3. Current lead connection to the pancake coils fabricated using SIST.

Reference:

1 Belenli and Hascicek FSU invention disclosure.

Magnetothermal Stability of High Temperature Superconducting Conductors

Burkhardt, E.E., NHMFL/University of Illinois Urbana, Nuclear Engr. Dept.
Schwartz, J., NHMFL/FAMU–FSU CoE

The stability of superconducting magnets subjected to external thermal disturbances or flux jumps depends on the interplay between the electromagnetic and thermal characteristics of the system. As stability can limit the performance of a superconducting magnet, the stabilities of NbTi and Nb_3Sn conductors have been well studied. Here we investigate the stability of Ag/Bi-Sr-Ca-Cu-O superconducting conductors.

The finite element method (FEM) is used to solve the heat conduction equation at each time step. FEM consists of dividing a section of the tape into small elements and analyzing each element separately. As a result, each element can be considered homogeneous, allowing the analyses of a variety of geometries readily. This numerical analysis is used as a result of the temperature dependence of the material properties of both the superconductor and the stabilizer. To illustrate the FEM approach, the stability of a composite tape with a 2.5:1 Ag/BSCCO ratio is studied. Starting with the tape at steady–state with a current I operating in a magnetic field B, a heat pulse is introduced to raise the local temperature above T_c. The external source must be large enough to raise the temperature such that the critical current, I_c, becomes less than I locally. I_c for the tape is determined by summing I_c over all the BSCCO elements. The current that exceeds I_c contributes to the heat source resistively. After determining the current contributing to the heating, $I_s=I–I_c$, the fraction of I_s in each element, dI, is found via Ohm's law. Using the resistance of each element, dR, the elemental source due to the current is $dQ_s=dI^2dR$. The tape is considered unstable when the temperature rises sufficiently such that the tape remains normal and does not return to the initial state. If a pulse source is used, dQ_s is the only remaining source term after the pulse is finished; however, if a constant heat source is applied, that and dQ_s coexist.

A two-dimensional code has been tested but due to the highly anisotropic behavior of the conductor and the strong temperature dependence of the thermal properties over the relevant temperature range, a three-dimensional analysis is required. The three-dimensional FEM code has been written and is being tested. Issues to be considered are variation of the parameters (e.g. the geometry/cross–section of the tape, the Ag:superconductor ratio, the operating current, etc.), cooling mode (conductive and convective), anisotropy of the Ag in a magnetic

field, inhomogeneity of the Ag, the current density distribution in the BSCCO, and current diffusion from the BSCCO into the Ag. This ongoing effort will model conductors used in coils built by industry and tested by the Navy.

This research is supported by the Advanced Research Projects Agency through the Naval Research Laboratory.

Enhanced Flux Pinning in $Bi_2Sr_2CaCu_2O_{8+x}$ Superconductors with Embedded Carbon Nanotubes

Fossheim, K., The Norwegian Institute of Technology, Univ. of Trondheim/NHMFL
Tuset, E.D., The Norwegian Institute of Technology, Univ. of Trondheim/NHMFL
Ebbesen, T.W., NEC Research Institute
Treacy, M.M.J., NEC Research Institute
Schwartz, J., NHMFL/FAMU–FSU CoE

A new approach toward enhanced flux pinning in high-temperature superconductors with potential for applications has been studied. Carbon nanotubes, with shape and size similar to columnar tracks from heavy ion irradiation, were embedded in $Bi_2Sr_2CaCu_2O_{8+x}$ (Bi-2212) polycrystalline samples to produce strong pinning centers to magnetic vortex lines. The encouraging result is that the doping survived the high temperature heat treatments. The pinning properties for the best case of superconductor-nanotube composite prepared was found to surpass the pure ceramic superconducting matrix.

The $Bi_2Sr_2CaCu_2O_x$ precursor made by Seattle Specialty Ceramics Inc. was first calcinated at 850°C for 6 hours and then mixed with certain wt.% content of nanotubes (NT's). The powder mixture was calcinated in Ar, which reduces the melting temperature to about 806°C This initial treatment in Ar atmosphere led to significant oxygen removal, and oxygen was restored to the superconducting matrix in 30°C temperature intervals in series of samples from 760°C to 890°C. The microstructures of the Bi-NT samples were observed by transmission electron microscopy (TEM) and scanning electron microscopy (SEM). The superconducting properties were studied magnetically by a Quantum Design MPMS5 SQUID magnetometer.

TEM micrographs showed the nanotubes were able to wet with the superconducting matrix. The nanotubes are partially inside grains near the surface and partially sticking out of grains. Improvements in vortex pinning was proved by comparing the magnetic hysteresis and the irreversibility line between optimized Bi-NT and the pure Bi-2212. The best case for Bi-NT in our limited experiments was with 8% of NT heat treated by partial melting in Ar at 806° C. In Figure 1, the magnetic moment per gram versus field at 50 K is plotted. The width of the loop for Bi-NT is much wider than for the pure Bi-2212. Similar data was obtained at other temperatures. In addition, SEM analysis showed the average grain size of the pure Bi-2212 was typically a factor of three larger than those of Bi-NT. Thus we conclude that the J_c for Bi-NT material is approximately one order of magnitude larger than in the pure superconductors.

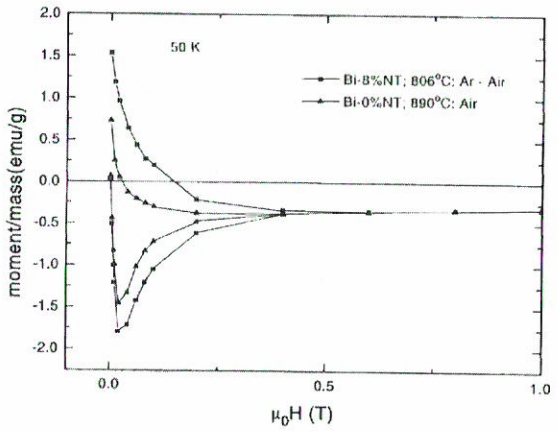

Figure 1. Comparison of magnetic hysteresis at 50 K for the Bi-8%NT and pure Bi-2212.

High Temperature Cryo-Insulation for HTS Coils

Godfrey, M.I., NHMFL
Belenli, I., NHMFL
Hascicek, Y.S., NHMFL

Insulation for HTS coils must comply with processing and fabrication constraints and

requirements, like handling during magnet winding and heat treatment afterwards. For example, the processing of wind-and-react coils involves a heat treatment at around 900°C with the coil already in its final form. Therefore, the insulation must be stable at high temperatures and must also be compatible with a thermal cycle between RT to 900°C, back to RT and numerous cycles between RT and 4.2 K while in actual use.

A ceramics based insulation coating process has been developed at NHMFL for providing turn-to-turn insulation for the HTS coils. The coatings obtained are compatible with both the high temperatures necessary for processing and the cryogenic temperatures needed for operation. The process utilizes zirconia or alumina coatings that are applied by various coating processes to the green HTS tapes and wires before the wind-and-react process. Figure 1 shows a typical SEM micrograph of the insulation layer in a longitudinal section of a PIT Bi-2212/Ag tape conductor. This approach offers the following advantages: (1) the coating thickness is controllable to about 10 microns; (2) the material is compatible with the heat-treatment process for the green tapes; and (3) the dielectric constant of the ceramics used has a very high value, and therefore offers good insulation protection.

A spray coating set-up for about 10 meter lengths of conductor and also a continuous spray coating and curing apparatus in one pass with supply and take-up spools have been designed and built in house. A separate continuos insulation printing set-up has been designed and is being built. This machine will print a continuos uniform or patterned uniform insulating ceramic layer on a tape conductor in one pass.

Several pancake coils were built from HTS tape conductors produced in-house or by our industrial collaborators by using the cryo-compatible high temperature insulation technique. Most of these coils were successful in insulating. One of these coils had a patterned (striped) insulation for possible He force flow operation beyond its critical current.

Several 10 meter long Ag tape pieces have been coated with high temperature cryo-compatible NHMFL insulation and provided to OST to be used in the insulation of pancake coils built from dip coated Bi-2212 conductors. The insulation coating was alumina based and about 50 microns thick. A significant improvement (about 25%) in turn density as compared with using alumina paper insulation was achieved by this collaboration.

Preliminary results indicate that varying thicknesses of alumina and zirconia based insulation layers caused no degradation in short sample J_c of PIT Bi-2212 tape conductors when heat treated at around 890°C necessary or melt texturing the HTS core.

The adhesion of the insulation coating to Ag/BSCCO tapes needs to be evaluated. This may open up the possibility of combining insulation and impregnation in one process. The spray-coating parameters need to be further optimized for the continuous spray coat and cure set-up for tapes and round conductors. In this case sustaining a continuous flow in the spray gun or guns and obtaining uniform coating on a round conductor are areas that need to be addressed. Also, curing in one pass in the curing chamber needs to be optimized. Coating techniques like spray pyrolysis are being considered for much thinner and uniform insulation coatings.

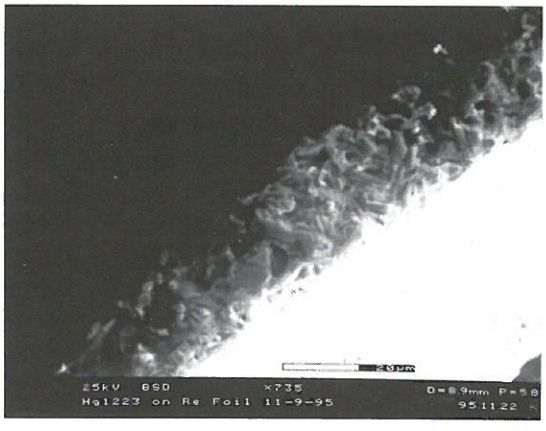

Figure 1. Typical SEM micrograph showing the alumina based insulation layer on one side of the HTS conductor.

Logarithmic Current Density Dependence of the Activation Barrier in Superconducting $HgBa_2CaCu_2O_{6+x}$

Gjolmesli, S., Norwegian Institute of Technology, Univ. of Trondheim, Norway, Division of Physics
Fossheim, K., Norwegian Institute of Technology, Univ. of Trondheim, Norway, Division of Physics
Sun, Y.R., NHMFL
Schwartz, J., NHMFL/FAMU–FSU CoE

The high critical temperature and high irreversibility field of the Hg-Ba-Ca-Cu-O superconductors make them promising for applications. It is expected, however, that the small pinning energies still cause significant magnetic flux motion, producing energy dissipation in the current carrying state. Here we report our studies on magnetic relaxation measurements on grain-aligned $HgBa_2CaCu_2O_{6+x}$ (Hg 1212) with field applied parallel to the c-axis. We found that the activation energy U(j) is well described by $U(j)=U_c\ln(j_c/j)$.

Hg 1212 powder with an average grain size of 3.1×10^{-4} cm was embedded in epoxy and cured in magnetic field of 7 T. The sample was neutron irradiated to a fast fluence of 1.2×10^{17} n/cm^2. Measurements of the magnetic moment were performed on a SQUID magnetometer in the temperature range 5-60 K and at fields of 0.1–4 T.

Figure 1 shows a typical set of magnetic moment, m, versus time, t, in a field of 1 T. To first order, the decays are logarithmic. To obtain the barrier energy we apply the method of Maley et al.[1] By inverting the rate equation, the pinning barrier is U(B,T,m) = T(ln A-ln|dm/dt|). Figure 2 shows the activation energies as a function of m. The data at different temperatures can be aligned by letting ln(A) take the values of 40, 20, 20, 15, and 20, for the fields of 0.1, 0.5, 1, 2, and 4 T respectively. The magnetic relaxation can be solved exactly for this logarithmic barrier with U/T >> 1: $\ln(m) = \text{const} - T/U_c\ln[t/t_0]$. From experimental data of the creep rate $S=d\ln(m)/d\ln(t)=T/U_c$, the characteristic energy U_c is obtained. As assumed, there is no significant temperature dependence of U_c at low temperatures. As T -> 0, the analysis breaks down due to quantum tunneling. At high temperatures, U_c is almost temperature independent. The numerical values for U_c analyzed from the inversion method agree with the data to within 20%.

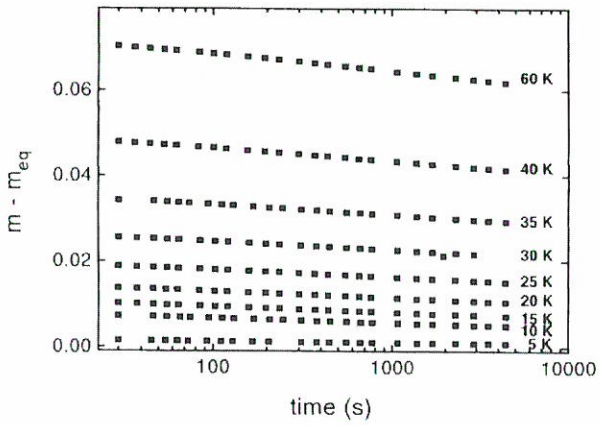

Figure 1. Typical relaxation curves of the non-equilibrium magnetic moment in a field of 1 T, along the c-axis.

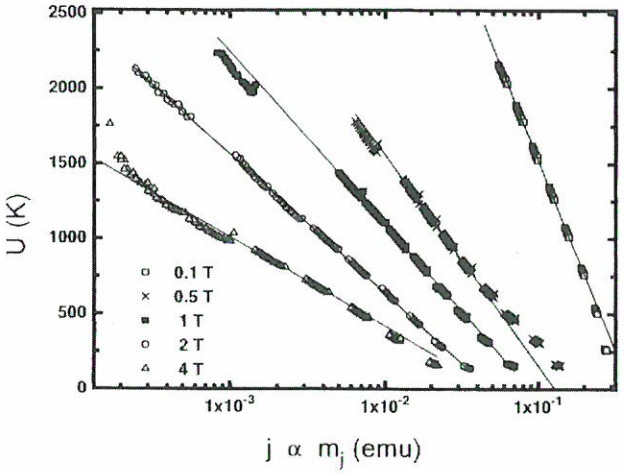

Figure 2. The barrier energy as calculated from equation (1). Each curve consists of data from the temperatures indicated in Figure (1).

Reference:

1 Maley, M.P., et al., Phys. Rev. B, 42, 2639 (1990).

the critical current (J_c) of HTS conductors would degrade by thermal cycling.[1-4] It was shown by the present authors that the J_c of powder in tube processed (PIT) Bi-2223/Ag and Bi-2212/Ag tape and wire conductors did not degrade if the thermal cycling was carried out in helium ambient.[5-7] It is also known that the J_c of some of the HTS coils degrade in time due to aging, thermal cycling environmental effects, or a combination of all or some of the above. The results of thermal cycling between RT and LHe temperature in helium ambient of wound HTS conductors are presented here.

After measuring the virgin $J_c(T)$ profile, a short straight Bi-2223/Ag fully heat treated tape conductor was wound at RT on mandrels of decreasing diameter and thermally cycled at each diameter in helium ambient between RT and 4.2 K. Samples of longitudinal sections of the wound Bi-2223/Ag tape samples were prepared by standard metallographic techniques and examined with Scanning Electron Microscope (SEM).

No degradation in J_c was observed when Bi-2223/Ag and Bi-2212/Ag tape and wire conductors were thermal cycled between RT and liquid helium temperature in He ambient then between RT and liquid nitrogen temperature in air.[7] Figure 1 shows a J_c versus temperature profiles for a Bi-2223/Ag monocore tape sample as it was thermal cycled between RT and LHe temperature at varying strain levels in He ambient. Bending surface strain dependence of J_c of these conductors have been presented elsewhere,[5,6] and is well known. As seen from these curves in Figure 1, however, apart from degradation in J_c due to bend strain, no additional degradation in J_c due to thermal cycling was observed.

SEM micrographs on the longitudinal sections of wound HTS conductors revealed that there are transverse cracks in the oxide core. These cracks initiated at the tension surface of the oxide core and propagated radially. Occasionally small normal cracks (normal to the main radial crack direction) were observed.

Apart from degradation in J_c due to bending, no further degradation occurred by thermal cycling in He ambient. We conclude that degradation of J_c is not an intrinsic property of these composite HTS conductors. Microstructural investigations showed that transverse cracks were present in the oxide core of the wound samples.

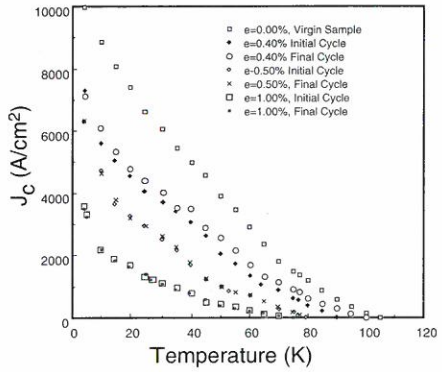

Figure 1. J_c versus temperature profiles for a Bi-2223/Ag wound tape conductor before and after thermal cycling at varying winding radii. Only thermal cycles at three strain levels are shown here for clarity.

References:

1 Ochiai, S., et al., Cryogenics, 31, 954-961 (1991).

2 Jenkins, R.G. et al., Cryogenics, 33, 81-85 (1993).

3 Willis, J.O., et al., HTS Wire Development workshop, US DOE conf-940278, Feb. 16-17, 1994.

4 Huang, S., et al., accepted for publication, Mat. Lett. (1995).

5 Hascicek, Y.S., et al., IEEE Trans. Mag., 30, 2229 (1994).

6 Hascicek, Y.S., et al., Processing of Long Length of Superconductors TMS. pub. Ed Balachandran, Collings and Goyal, p. 262 (1993).

7 Hilton, D.K., et al., IEEE Trans. Appl. Supercon., 5, 3478 (1995).

Magnetothermal Conductivity of Bi-Sr-Ca-Cu-O Superconductors

Nakamae, S., NHMFL
Schwartz, J., NHMFL/FAMU–FSU CoE

The study of the thermal conductivity, κ, of high temperature superconductors can provide a theoretical understanding of the nature of the charge carriers, phonons, and scattering processes between them. From the applications point of view, thermal conductivity determines the growth rate of local hot spots in a superconductor and therefore it is an important parameter in thermal stability analysis. The change in κ of type-II superconductors in the presence of a magnetic field is assumed to be mainly due to their unique vortex line movements. Thus, the magnetothermal conductivity is considered a key factor in understanding the vortex mechanisms.

κ of a Bi-Sr-Ca-Cu-O bulk sample (pellet) has been measured in a magnetic field up to 20 T at 45 K, 60 K, and 70 K. The thermal conductivity decreases with increasing field (see Figure 1). Hysteresis in κ(H), due to the trapped magnetic flux in the sample, was observed.

Single crystal samples will be used for further investigations of vortex behavior of type-II superconductors. These results, coupled with the bulk measurements, will allow the separation of intergranular and intragranular effects. Some of the important parameters of Bi-Sr-Ca-Cu-O, such as the upper and lower critical field values, will also be determined.

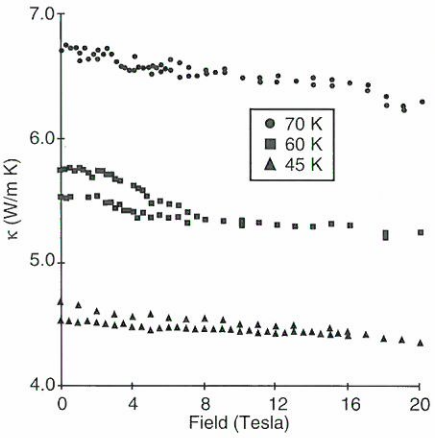

Figure 1. Magnetothermal conductivity of a Bi-Sr-Ca-Cu-O pellet sample.

Effects of Li-doping on Powder-in-Tube $Bi_2Sr_2CaCu_2O_x$ Tapes

Schwartz, J., NHMFL/FAMU–FSU CoE
Wei, W., NHMFL

Li-doping of the 2212 phase reduces the melting temperature, increases the growth kinetics, and increases the critical temperature of the 2212 superconducting phase. There is also evidence that it improves flux pinning at high magnetic fields. Here we investigate the potential of Li-doping the powder-in-tube 2212 tape conductors.

A powder study using a DTA was performed to investigate the difference in melting behavior of the doped and undoped 2212 phase. Instead of one melting peak (at 885°C) for the pure 2212 phase, we observed endotherms (at 780°C and 850°C) for the Li-doped system (see Figure 1). Li-doped tapes were prepared according to the previously described procedure with the heat treatment adjusted according to the melting behavior of the doped powder. J_c of 60,000A/cm^2 (I_c=60A) was obtained at a maximum heat treatment temperature

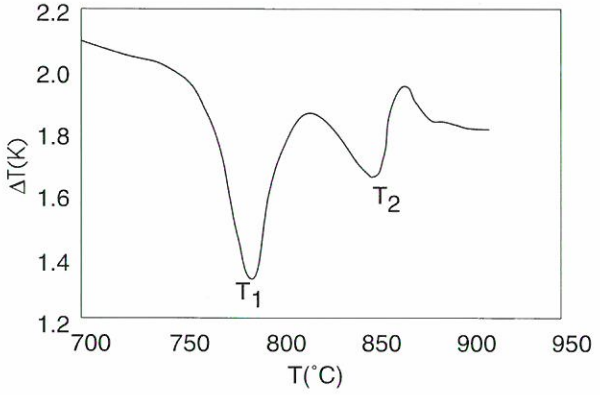

Figure 1. DTA of Li-doped 2212 powders shows that the melting has been shifted to a lower temperature and that two endotherms exist.

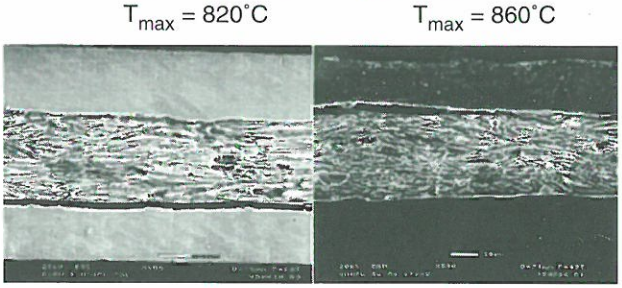

Figure 2. SEM micrographs of Li-doped 2212 tapes, illustrating the large grain sizes that are obtained.

of about 870°C. Microscopy (see Figure 2) of these samples indicated that the 2212 grain size of the doped tapes is significantly larger than in undoped materials. Furthermore, using the x-ray diffraction pole-figure technique, we see that the grain alignment in the doped materials is significantly improved relative to undoped materials (see Figure 3). Although up to now there is no difference in the magnetic field dependence of J_c between doped and undoped tapes, the n-values of the transition ($V \sim I^n$) may have been increased. This requires further investigation.

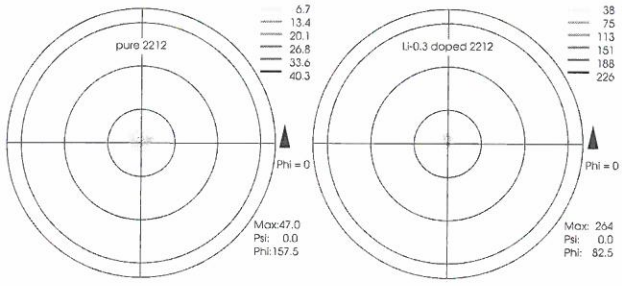

Figure 3. X-ray pole figures of Li-doped and undoped 2212 tapes, showing the enhancements in grain alignment achieved by Li-doping.

Powder-in-Tube $Bi_2Sr_2CaCu_2O_x$ Conductor Development

Schwartz, J., NHMFL/FAMU–FSU CoE
Kessler, J., NHMFL
Wei, W., NHMFL
Fischer, V., NHMFL
Miller, V., NHMFL
Chen, S., NHMFL/FAMU-FSU CoE
Dimapilis, D., NHMFL/FAMU-FSU CoE

The conductor research and development activity is aimed at producing intermediate lengths (40-50 m) of high quality, coil-relevant powder-in-tube $Bi_2Sr_2CaCu_2O_x$ (2212) superconductor for coil engineering studies. Our maximum short sample J_c values for Ag-clad powder-in-tube 2212 at 4.2 K, 0 T is 140kA/cm^2, corresponding to an engineering J_e of 45kA/cm^2. Our primary focus has switched from Ag-clad material to Ag1%Mg clad material to improve the mechanical properties of the conductor. This change significantly impacts the mechanical deformation and heat treatment optimization for high J_c materials.

An important step in powder-in-tube processing is the packing of the tube because trapped impurities can cause bubbling in the tape and destroy its performance. This problem becomes severe if the annealing is performed in flowing oxygen atmosphere, which is required for the highest critical current densities. Thus we developed a powder handling procedure which maintains the powder and tube in a controlled atmosphere until the tube is sealed. Before sealing the packed tube, the entire assembly is annealed in flowing oxygen to purge the tube of any other gases and to remove carbon that may have been absorbed on surfaces. This procedure has significantly reduced bubbling in samples of a few meters in length. We are improving this process to further reduce bubbling of longer samples and in coils.

Ag-sheathed multifilament wires consisting of 19 filaments were drawn to almost 1 mm diameter. Due to differences in the plastic deformation behavior a change in the wire design was necessary when we replaced the Ag sheath by Ag1%Mg sheath. With intermediate annealing to relieve work hardening, we are able to draw AgMg multifilament wire to small diameter. Cross-sections of deformed wires are illustrated in Figure 1. After drawing, the conductor is rolled into tape. To obtain straight tapes, tension controlled take-up and pay-out systems were installed at the rolling mill. Modifications were made to allow the rolling mill to operate at roll temperatures exceeding 500°C, including a 1.5 m long furnace to preheat the conductor. While cold rolling is absolutely necessary to fabricate conductor suitable for pancake coils, the advantages of hot-rolling are being investigated.

Tapes were annealed in a one-step process in flowing oxygen. The samples were furnace-cooled from the peak temperature (partial melting) to 873°C where the recrystallization of the 2212 phase occurs, reducing the generation of non-superconducting phases. The tapes were then slowly cooled to the sintering temperature to enable the growth of large 2212 grains. We also investigated the effect of varying the cooling rate from the peak (partial-melt) temperature to the first solid-state temperature, and found that cooling as

rapidly as possible is required. Lowering the cooling rate decreases J_c. This is particularly disadvantageous for the heat treatment of a complete coil because the large heat capacity does not allow fast cooling rates. Nevertheless, at 10 K/h, J_c reaches again values in the range of 30 kA/cm^2. The magnetic field dependence of J_c is shown in Figure 2 for representative samples. The tape was oriented with the surface perpendicular to the magnetic field.

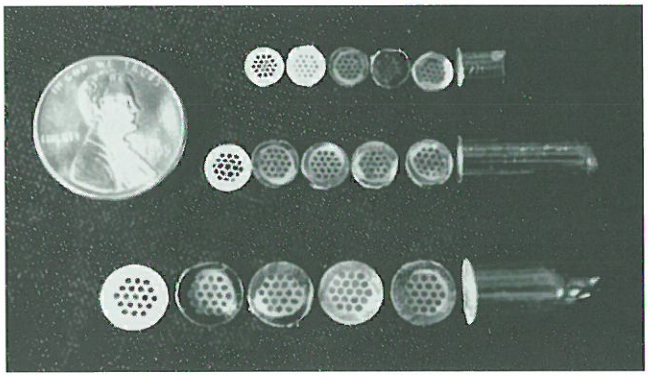

Figure 1. Optical micrographs of multifilamentary conductors during mechanical deformation.

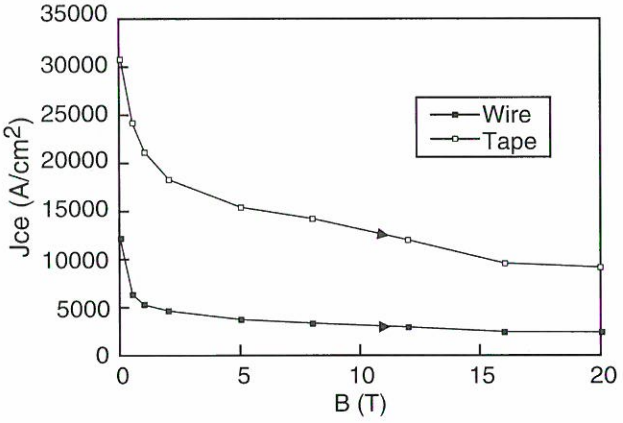

Figure 2. J_{ce} of a tape and a wire versus magnetic field B at 4.2 K. For both J_{ce} at 20 T is about 1/3 of the J_{ce} at 0 T.

Synthesis of Hg-based High Temperature Superconductors

Schwartz, J., NHMFL/FAMU–FSU CoE
Wolters, Ch., NHMFL
Amm, K., NHMFL
Siegel, S., NHMFL

The mercury-based superconductors, $HgBa_2Ca_{n-1}Cu_nO_x$, have set a record of 135 K for the superconducting transition temperature (T_c), with T_c exceeding 150 K under high pressure. Because of these high critical temperatures and irreversibility fields of up to 12 T at 77 K, the Hg-based superconductors are strong candidates for applications at liquid nitrogen temperature.

The main technique for the synthesis of bulk $HgBa_2Ca_{n-1}Cu_nO_x$ is encapsulating and post-annealing. This technique involves numerous critical parameters such as carbon content of the precursor, heating rate, annealing conditions, and Hg vapor pressure. These parameters are controlled by the capsule volume and sample volume fraction in the encapsulation technique, resulting in a limit to the quantity of sample to nominally 100 mg/cm^3. Independent control of temperature and pressure, which is feasible with a two-zone technique developed at the NHMFL, eliminates the volume restriction and allows the preparation of large samples. In addition, the growth kinetics and mechanisms can be investigated by studying the influence of the temperature profile and Hg vapor pressure on the formation of the superconducting phases.

$(Hg,Re)Ba_2Ca_1Cu_2O_y$ and $(Hg,Re)Ba_2Ca_2Cu_3O_y$ superconductors were prepared with high phase purity, starting from carbonates, nitrates, and commercially available precursors. Optimal annealing temperatures were found to be in the range of 900°C to 950°C for the $(Hg,Re)Ba_2Ca_2Cu_3O_y$ phase and below 850°C for the $(Hg,Re)Ba_2Ca_1Cu_2O_y$ phase. The addition of Re was found to have beneficial effects on the phase formation and chemical stability of the superconducting phase. Systematic investigations of samples quenched from various stages of the annealing procedure indicate that crystal growth is assisted on a microscopic length scale by a liquid phase. It was also found that the $(Hg,Re)Ba_2Ca_2Cu_3Oy$ phase forms via the $(Hg,Re)Ba_2Ca_1Cu_2Oy$ phase. The microstructure is dominated by high density island-like areas of several hundred μm diameter, interconnected by low density material. The platelike grains show random orientation and are typically 5 μm thick and up to 100 μm long (see Figure 1).

Since the production of HTS wires, e.g. by the PIT method, requires a compatible metallic sheath material, the preparation of superconductor/metal composites has also been investigated. Studies of the interfacial reactions between $HgBa_2Ca_{n-1}Cu_nO_x$ superconductors and Au and Ag sheaths have been performed in cooperation with the Naval Research Laboratory using hot isostatic pressed samples. While Au did not interfere with the formation of the superconductor, Ag exhibited significant reactions with Hg, severely suppressing superconducting phase formation. To avoid this problem, Ag-$HgBa_2CuO$ composites were reacted in the two-zone assembly. With an abundant source of Hg provided, the superconductor as well as the Ag sheath are saturated and the superconducting phase is successfully formed.

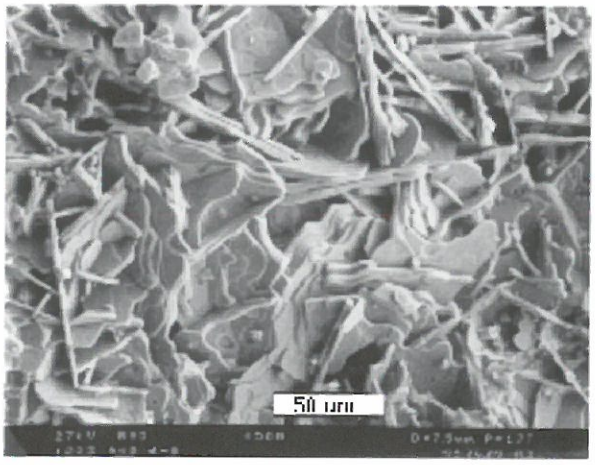

Figure 1. SEM micrograph of $(Hg,Re)Ba_2Ca_2Cu_3O_y$ showing plate-like growth in localized regions but random alignment when averaging over the entire sample.

Development of Joints for HTS Conductors

Shaoff, P., NHMFL/FAMU-FSU CoE
Schwartz, J., NHMFL/FAMU-FSU CoE
Van Sciver, S.W., NHMFL/FAMU-FSU CoE
Hascicek, Y.S., NHMFL
Weijers, H.W., NHMFL

The HTS joint development program has studied a series of joint prototypes utilizing the partial melt BSCCO 2212 PIT reaction process to connect the current paths between superconducting cores of the free ends. It is hoped that these techniques can be successfully upgraded to multifilament conductors.

The cup joint model was the first prototype to be investigated. These joints are made by placing two green BSCCO 2212 monocore tapes into a silver "cup," filling the cup with unreacted powder, pressing the powder into the cup against the tapes, and then running the whole assembly through the heat treatment for monocore tapes. The powder used is of the same stoichiometric composition as that used to produce the PIT conductor. The finished cup joints are bulky and awkward to handle. Using the 1 μV/cm criterion, the straight sample has an I_c of 7.6 A. At this current value the joint, which includes 2 cm of tape, shows a voltage of 1.5 μV. Thus, there appears to be a good chance of developing a joint that will not limit the performance of the coil beyond the restrictions imposed by the straight wire itself.

The second joint type investigated is the wrap joint. It is similar to the cup joint except that it uses a thin silver film to wrap the joint package. The wrap joints are constructed by overlapping the free ends of the green conductor while laying them on a piece of 0.1 mm thick silver foil inside of a press mold. The tapes enter from opposite sides but this geometry can be easily modified. The free space around the conductor is filled with unreacted powder and the interior of the mold is compacted using a uni-axial press. When this compaction is completed, the assembly is removed from the mold, the silver foil is wrapped around the joint, and its edges are sealed. It is then reacted with the same heat treatment as the cup joints. The SEM micrograph in Figure 1 (page 150) shows the cross section of this joint structure.

The wrap joints are less bulky than the cup joints and easier to fabricate. They have excellent transport values relative to a straight sample and a sharper transition than the cup joints. Using the 1 μV/cm criterion, the a typical wrap joint has an I_c of 12.3 A, which outperforms the best equivalent straight sample I_c of 7.7 A. This is probably due to the increased amount of superconductor present in the joint region which allows for an increased amount of Ag to superconductor interface surface area.

The most recently developed wrap joint uses unreacted, binder free, dip-coated BSCCO 2212 conductor instead of the loose powder. This approach makes the joint more compact and easier to manufacture. It also provides a more uniform cross section and grain alignment mechanism by incorporating the dip-coated technology. Initial testing suggests that this modified joint has performance comparable to the powder filled wrap joint design. For example, one wrap joint had a critical current value of 40.5 A, while a straight sample of the same conductor reacted at the same had an I_c of 31.5 A. In addition, there does not appear to be a significant difference in the pattern of applied field behavior between a joint and a straight sample up to 3.0 T.

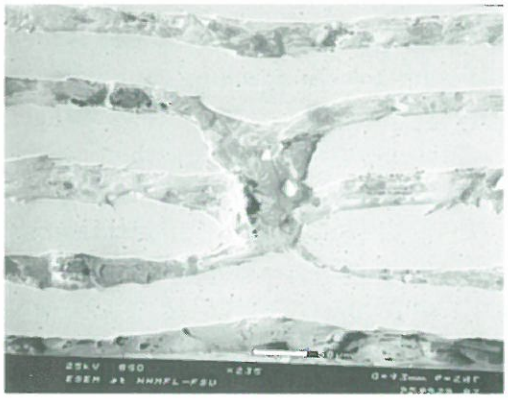

Figure 1. Scanning electron micrograph of an HTS joint.

References:

1 Shoaff, Jr., P.V., et al., HTS Coil and Joint Development for a 5 T NMR Insert Coil, to be published in Advances in Cryogenic Engineering, Vol. 41.

Anisotropy Studies on Aligned $HgBa_2CaCu_2O_{6+\delta}$ Powder

Sun, Y.R., NHMFL
Schwartz, J., NHMFL/FAMU–FSU CoE

All high temperature copper-oxide based superconductors posses layered structures: the CuO_2 (ab) plane, separated by other non-superconducting layers, provides path for loss-free currents. Although experiments via a transport current flowing in the ab-plane explored the behavior of the in-plane critical current, the properties of the out-of-plane critical current remains unclear. Blatter *et al*[1] developed a theory using a scaling approach which allows one to map known results for isotropic superconductors into anisotropic materials in a much simpler way. We studied DC magnetic responses of aligned Hg 1212 powder in the irreversible regime. By applying a magnetic field tilted with respect to the c-axis, both longitudinal and transverse signals were collected, allowing us to detect both in-plane and out-of-plane current. Our scaling analysis shows the current in any direction responds to the effective field $H_{eff} = \varepsilon_\theta H$, where $\varepsilon_\theta = (\cos^2\theta+\varepsilon^2\sin^2\theta)^{1/2}$ and $\varepsilon^2 = m/M$ where m and M are the effective masses for the electron moving within the basal plane and in the c direction, respectively.

The experiments were performed on 0.075 g of neutron irradiated grain-aligned Hg 1212 polycrystalline powder embedded in epoxy. Studies by Scanning Electron Microscopy showed that the particles have even dimensions along and perpendicular to the ab-plane. All measurements were conducted using a commercial SQUID magnetometer.

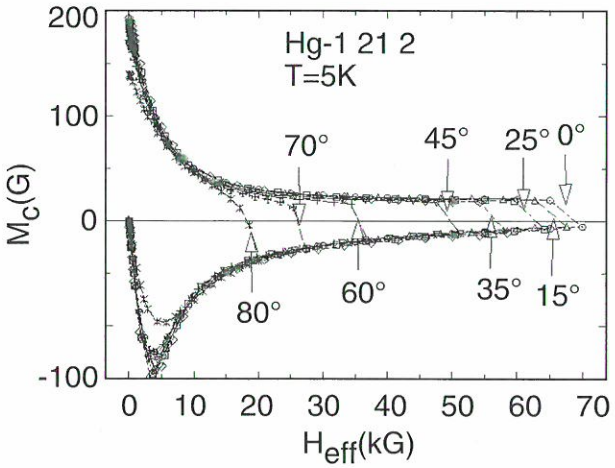

Figure 1. Magnetization M_c versus H_{eff} at T = 5 K with θ = 0–80°; ε = 1/5 is the only required fitting parameter.

While the behavior of the in-plane critical current density $J_c^{\parallel}$ is obtained from the magnetization hysteresis loops $M_c(H)$ along the c-axis, the properties of the out-of-plane critical current density are revealed via analysis of the longitudinal magnetization M_L and the transverse

magnetization M_T. In Figure 1 the magnetization M_c versus H_{eff} at T = 5 K with $\theta = 0 - 80^\circ$ is plotted, where $\varepsilon = 1/5$ was used as a fitting parameter to calculate ε_θ in obtaining the values of H_{eff}. The results clearly indicate that H_{eff}, instead of H, determines the magnetic response and confirms the theoretical prediction. In addition, the figure shows that the dependence $J_c^{\parallel}$ of in-plane J_c on the field orientation is solely through H_{eff}.

Figure 2 shows ΔM_L, scaled by $1/\varepsilon_\theta$, as a function of H_{eff} at T = 5 K with various angles. The results confirm the collective pinning theory for anisotropic materials. The scaling does not work well for $\theta = 80^\circ$ and fails for $\theta = 90^\circ$. The failure of the scaling approach with field aligned closely to the ab-plane has been understood with the two dimensional theory.

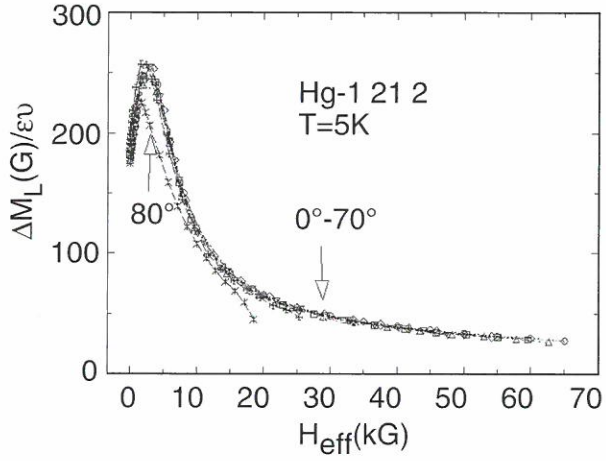

Figure 2. ΔM_L, scaled by $1/\varepsilon_\theta$, as a function of $\varepsilon_\theta H$ at T = 5 K with various angles.

Reference:

1 Blatter, G., et al., Rev. of Mod. Phys., 66, 1125 (1994).

Ag-BSCCO Coil Development and Characterization

Weijers, H.W., NHMFL
Hascicek, Y.S., NHMFL
Godfrey, M.I., NHMFL
Van Sciver, S.W., NHMFL/FAMU–FSU CoE

Several small HTS coils have been constructed with the purpose of both developing magnet fabrication techniques and testing lengths of several meters of NHMFL made conductor. Coil geometries include layer wound solenoids utilizing round wire and ceramic braid as insulator and pancake coils with zirconia powder insulation. Superconducting properties of these coils are variable with maximum currents less than half of the short sample. The coils were very stable and showed a few percent degradation in critical current after repeated quenches. Several tape wound pancakes were extensively tested and shown to have no turn-to-turn shorts. One pancake coil was vacuum impregnated with epoxy. The epoxy fully penetrated our ceramic insulation without doing damage.

To allow a more systematic comparison between coils and coil winding techniques the so called "mini coil" has been defined. The outer dimension of the winding is determined so that it can be tested in the 20 T resistive magnet at the NHMFL. The winding volume allows both pancakes and wire wound coils. A number of standard stainless steel coil formers have been made and the construction of a series of mini coils is currently under way. The mini coils will incorporate standard 1.5 to 3 m lengths of either NHMFL conductor or commercially produced conductor. They will utilize NHMFL insulation and joint technology where appropriate.

Our next step in this program is to build a series of 1-T coils using in house and commercial materials. These coils will be tested in the 20 T Oxford magnet. Studies will include critical current, quench characteristics, and stability.

References:

1 Hazelton, D.W., et al., IEEE. Trans. on Applied Superconductivity 5, 2, 234, June 1995.

2 Van Sciver, S.W., et al., Intern. Workshop on Superconductivity, ISTEC/MRS co-sponsor, June 18-21, 1995.

MAGNET SCIENCE AND TECHNOLOGY
Cryogenics

Program Overview

S.W. Van Sciver

The Cryogenics Program was established to study problems related to applications of superconducting magnets. Our main responsibility is to support the development of magnets for NHMFL facilities such as the NHMFL Hybrid and 1.1 GHz NMR systems. In addition, the Cryogenics Program derives a significant amount of support from outside funding agencies; mainly, the Department of Energy. This work is specifically tied to magnet development for HEP accelerators and magnetic fusion energy systems. We also have a collaboration with Babcock and Wilcox for their magnetic energy storage program.

Our approach is to experimentally and numerically model specific aspects of magnets systems in order to better understand how to design and characterize the performance of complete magnet systems. Research reports in this section describe a number of projects of this type that were completed during the last year. Specific project reports for 1995 include: heat transfer studies in two-phase helium flow; pressure drop and transient heat transfer in cable-in-conduit conductors; boiling heat transfer to He I; and continuous cooling of support structures.

Test of the 10kA current leads of the hybrid magnet.

Heat and Mass Transfer Between Two Saturated He II Baths

Huang, X., NHMFL
Panek, J., NHMFL/FAMU–FSU CoE
Van Sciver, S.W., NHMFL/FAMU–FSU CoE

A new cooling scheme using two-phase vapor/HeII has been proposed for the superconducting magnet strings in the Large Hadron Collider (LHC). The objective is to absorb the heat generated at 1.9 K in the LHC with minimum temperature rise by utilizing the latent heat of liquid He II. Such a cooling scheme, however, suggests two-phase flow and heat transfer in saturated He II over the whole range of vapor quality. Unfortunately, despite preliminary experimental tests performed at CERN demonstrated the feasibility of such a cooling scheme, little has been known about the basic heat transport mechanism in two-phase He II.

To fully understand the basic heat transport mechanism in a two-phase He II system, our efforts in the past year have been directed on the analytic and experimental investigation on the heat and mass transfer between two saturated He II baths. The experimental apparatus used for this study consists of two 1.0 m long stainless steel cans connected with two 10.0 cm long tubes. The upper tube, with a 1.3 mm ID, is filled with saturated helium vapor; the bottom tube, with a 5.0 mm ID, is filled with HeII. Heat deposited in the left can will then be transferred to the right can by mass-transfer process through the top tube and by the counter-flow process through the bottom tube. Because the counter-flow and mass transfer processes are decoupled in this problem, we were able to obtain analytic steady state solution.

We have carried out a series of steady state and transient heat transfer experiments with the system to provide important benchmarks for our analytic models. Figure 1 displays the steady state relationship between the heat input and the temperature difference between the two cans at 2.04 K along with calculations based on our model. Two important conclusions can be drawn from this figure. First, although the upper tube has a flow area about 15 times smaller than that of the bottom tube, the heat transferred by the mass-transfer process through the top tube is still greater than that by the counter-flow process over a majority of the heat input range. This clearly suggests that the mass transfer process is a very effective heat transfer mechanism even in two-phase He II system. Second, the experimental data agree very well with the model prediction especially at power inputs below about 0.7 W. Theoretical analysis is still under way to interpret the dynamic behavior of the system.

In the coming year, our efforts will be focused on the heat transfer aspect of two-phase He II in horizontal channels. The goal is to establish a theoretical model to describe the mechanism governing the heat transport process in two-phase He II, supporting the work with experimental studies. The Liquid Helium Flow Facility (LHFF) will be used to support the experimental studies. The product of this work will be a better understanding of the dynamics of two-phase He II so that the new concept can be confidently employed in future superconducting magnet cooling system designs.

This research is supported by the U. S. DOE-Office of High Energy Physics.

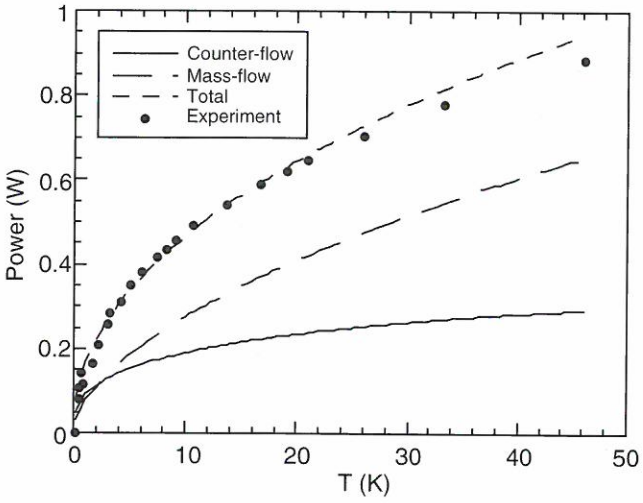

Figure 1. Steady state relationship between the total heat input and the temperature rise between the saturated He II baths at 2.04 K.

Localized Heat Transfer to Vertical Forced Flow Two-Phase Helium

Huang, X., NHMFL
Panek, J., NHMFL/FAMU-FSU CoE
Van Sciver, S.W., NHMFL/FAMU-FSU CoE

Localized heat transfer measurements in vertical two-phase helium are reported. The test loop contains two short heat transfer sections made of 5 mm thick Oxygen Free High Conductivity (OFHC) copper discs. These test sections were installed in a U-shaped vertical flow loop driven by a single-stroke bellows pump. The surface temperature of each test section is measured with two germanium thermometers placed on different radial positions in each test section. With one test section placed on the downflow side and one on the upflow side of the loop, the effect of flow orientation on heat transfer characteristics in vertical two-phase helium flow is investigated. The study includes the effects of system pressure, mass flow rate, and geometry on the heat transfer coefficient, critical heat flux, and recovery heat flux.

The effect of saturated temperature for a fixed flow rate of 0.5 g/s is shown in Figures 1 and 2. The four different temperatures correspond to the following four saturated pressures: 1.0, 0.8, 0.6, and 0.4 atmospheres. For both upward and downward flow, higher saturated temperatures result in higher heat transfer coefficients in the nucleate boiling regime. Little effect of saturation temperature is seen in the film boiling regime, but the downward flow has lower heat transfer coefficients than the upward flow.

A larger effect of flow direction with respect to gravity is observed in the critical heat flux transition from nucleate to film boiling, Figure 3. Low mass flow rates flowing downward result in significantly smaller critical heat fluxes than for upward flow. The recovery heat flux, Figure 4, is also smaller for downward flows at low mass flow rates.

Flow orientation, system saturated temperature, and mass flow rate can have significant effects on heat transfer in vertical channels cooled by He I. Critical and recovery heat flux are also studied under various flow conditions. Further work could expand the envelope of mass flow rates, channel diameters, and system saturated pressures. Another avenue of investigation would be to change the inlet quality of flow to the test section.

This research is supported by the U.S. Department of Energy-Office of High Energy Physics.

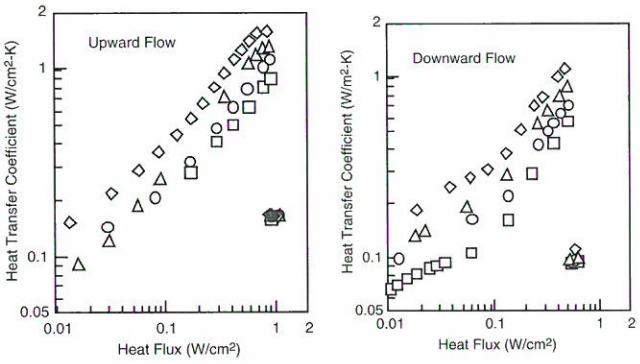

Figures 1 and 2. Heat transfer coefficient as a function of heat flux for different saturated temperatures at a fixed mass flow rate of 0.5 g/s and different flow directions. Square, 4.222 K; circle, 3.993 K; triangle, 3.722 K; diamond, 3.379 K.

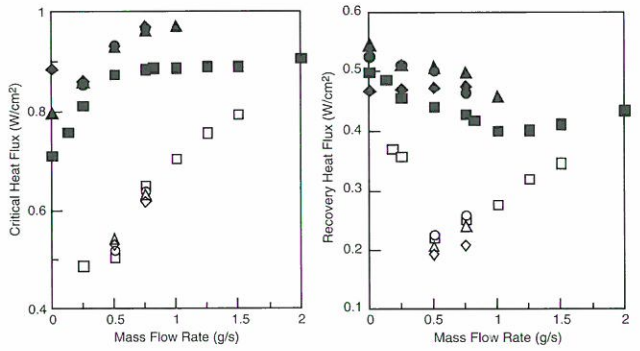

Figures 3 and 4. Critical and recovery heat fluxes as a function of mass flow rate for different temperatures and flow directions. Square, 4.222 K; circle, 3.993 K; triangle, 3.722 K; diamond, 3.379 K. Open symbols are for downward flow, and dark symbols are for upward flow.

Cooling of Mechanical Supports for Superconducting Magnets

Iyengar, K., NHMFL/FAMU-FSU CoE
Van Sciver, S.W., NHMFL/FAMU-FSU CoE

Cryogenic systems operated at low temperatures are supported by structural members that transmit exerted mechanical loads to the ground. The temperature difference across the ends of the support causes a large amount of heat to be conducted from the ground into the cryogenic equipment, via the support. Large amounts of refrigeration power must be expended to remove this heat.

The present research seeks to improve the efficiency of the support cooling process and minimize the refrigeration power requirements. Various methods of cooling the mechanical support have been studied. Discretely cooled supports are cooled by one or more discrete heat-intercepting stations, located at specified axial positions along the length of the support, and maintained at specified temperatures by means of applied refrigeration. Continuously cooled supports are cooled by means of convective heat transfer to a surrounding coolant envelope, consisting of one or more streams of a coolant, flowing counter to the heat flow in the support.

Numerical modeling of the various cooling methods has been undertaken. Optimization of the cooling methods has been performed, so as to minimize the total refrigeration power. The discrete cooling method is optimized in terms of the axial locations and temperatures of the cooling stations. The counter-flow coolant envelope cooling method is optimized in terms of the mass flow rates and the locations and the temperatures of injection of the coolant streams.

A new method of cooling the support has been proposed. In this method, the support is cooled continuously by means of a coolant-carrying tube, wound in a helix around the support. The coolant (such as helium gas) is injected into the helical tube near the cold end of the support, flows within the cooling tube, and exits the tube near the hot end of the support, cooling the support over its length by convective heat transfer. Compared to the envelope cooling method, this method provides a coolant flow-path of increased length, and smaller cross-sectional flow area, resulting in improved heat transfer. Numerical modeling of the helical cooling coil method has been undertaken.

An experimental model of the helical cooling coil method is currently being constructed and will be used to validate the numerical model.

The numerically computed Carnot refrigeration power for various support cooling methods is compared in Figure 1. The support studied here corresponds to the experimental configuration. The perfect envelope corresponds to the assumption of perfect thermal contact between the support and the coolant. The non-dimensional Carnot refrigeration power is plotted as a function of the non-dimensional mass flow rate of the helium gas coolant. The stations refer to the number of discrete cooling stations. The perfect envelope corresponds to the assumption of perfect thermal contact between the support and the coolant. For the imperfect envelope, the heat transfer coefficient between coolant and support is computed. The annulus refers to the radial width of the annular coolant flow channel, in the case of the imperfect envelope.

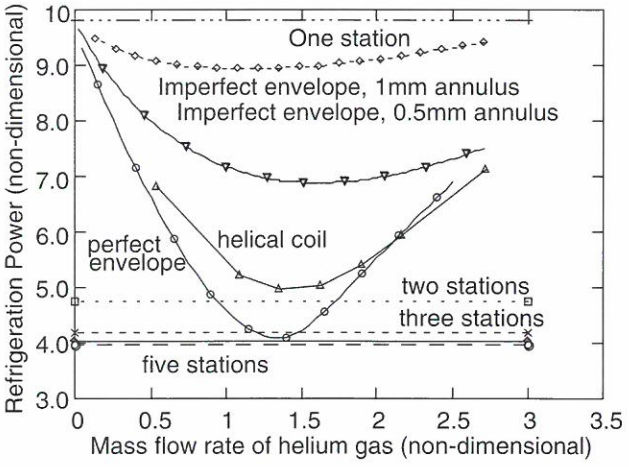

Figure 1. Non-dimensional refrigeration power for various methods of cooling the support.

Pressure Drop and Transient Flow in CIC Conductors

Maekawa, R., NHMFL/Univ. of Wisconsin, Nuclear Engineering
Smith, M.R., NHMFL
Van Sciver, S.W., NHMFL/FAMU–FSU CoE

We have characterized a prototype ITER fusion conductor from CEA/Cadarache for transient flow and pressure drop under an applied heat pulse. This conductor has a hybrid flow geometry composed of an axial cooling channel surrounded by six bundles, with a total of 864 strands. The axial cooling channel provides enhanced cooling over conventional CICC geometries.

A 3 m long sample of the conductor was instrumented at regular intervals along its length for pressure and temperature, as well as overall pressure drop along the conductor. During the initial phase of the experiment, a pitot-static tube, installed at the downstream end of the conductor, recorded the flow in the central channel as a function of the total mass flow in the conductor. Later, an array of thermometers was installed in the central channel to record thermal transients there. All phases of the experiment were carried out in the NHMFL Liquid Helium Flow Facility, and data were recorded as a function of applied flow rate and energy deposited in the conductor by the heat pulse, in both He II and supercritical helium.

Physical dimensions of the conductor cross section, such as flow area wetted perimeter and hydraulic diameter, were derived from image analysis done in collaboration with the University of Wisconsin. These were used first to correlate the pressure drop data in terms of an effective friction factor. Second, the hydraulic diameter was used to model the flow by considering the conductor to be composed of parallel channels with different hydraulic diameters.[1-3] Measured values for flow in the central channel and overall pressure drop compared favorably with the model.

Transient heat pulses were delivered to the conductor with a 4 T pulsed coil installed at the center of the test section. Typical temperature profiles are shown in Figure 1. This inductive heater was powered by a specially constructed 10 kA pulsed power supply, which enabled us to deliver over 2 J/cm^3 to the copper strands. This energy transfer to the strands was calibrated via a series of counterflow experiments completed last year.

Final data characterizing the pressure drop of this conductor were taken in January, with the first phase transient experiment following in February and March. The second phase transient data, with the thermometer array installed in the central channel, were taken in April. Results were summarized in a PhD thesis[3] by Ryuji Maekawa, who graduated in August.

This research is supported by the U.S. Department of Energy-Office of Fusion Energy.

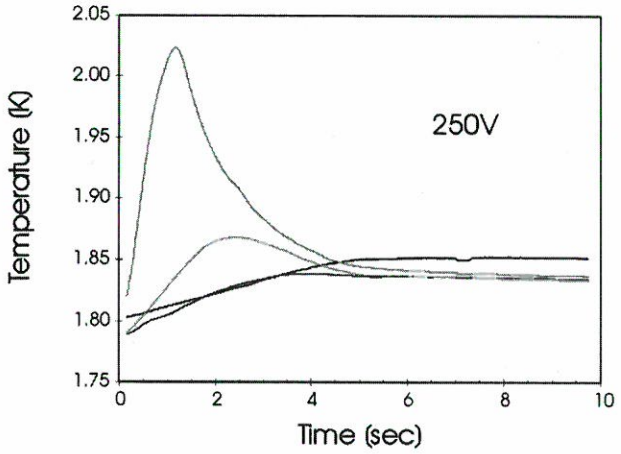

Figure 1. Temperature traces at different points along the central channel following the application of a heat pulse.

References:

1 Katheder, H., A General Formula For Calculation Of The Friction Factor For Cable In Conduit Conductors, The NET team, Internal note N/R/0821/26/A.

2 Maekawa, R., et al., Thermal Hydraulic Characteristics of a Prototype CEA Cable-in-Conduit Conductor, to be published in Advances in Cryogenic Engineering, Volume 41.

3 Maekawa, R., Thermal Hydraulic Characteristics Study of Prototype NET and CEA Cable-in-Conduit Conductors (CICCs), PhD Thesis, University of Wisconsin-Madison, 1995.

FACILITIES & PROGRAMS 2

Chapter Overview

The National High Magnetic Field Laboratory's programs and facilities are distributed over three sites and many disciplines. Everyone—distant and local researchers, magnet designers, and instrumentation specialists—profits from the intellectual cross-fertilization that occurs when so many activities are grouped together.

The General Purpose DC Field Facility in Tallahassee retired its first 27 T, 32 mm bore magnet and replaced it with two 30 T, 32 mm bore magnets in new housings that showed greatly reduced vibrations from the magnet cooling water. The 27 T magnet had run over 1000 hours without showing any signs of functional decay in any of the three coils. The plates from a middle and inner coil from a 27 T magnet were rearranged, and the three coils carefully aligned to produce a 24.5 T, 32 mm bore, higher homogeneity magnet that quickly generated excitement among users interested in using NMR to study high T_c superconductors, quantum wells, and other condensed matter systems.

Multiple units of high demand instrumentation were purchased or built for users of the DC Field Facility, thereby increasing the effectiveness of their use of the magnets and power supplies and increasing the number of samples that could be studied per magnet hour. NHMFL staff responded to user requests for new sample holders to support interesting new techniques. Experience with operating major equipment led to improvements that increased reliability, user friendliness, and/or performance. The User Instrumentation and Electron Magnetic Resonance groups cooperated in the purchase of expensive instruments that could be used for EMR and other measurements of interest to other users.

The Pulsed Field Facility in Los Alamos enlarged its user facilities markedly by establishing, through a sabbatical by Prof. Clive Perry, a spectroscopic capability for photoluminescence and related magneto-optical studies in both pulsed and DC fields. The 50 T and 60 T pulsed magnets based on a design of Prof. Fritz Herlach's group at Leuven continue to provide the working fields, although other designs are being tested. The new instrumentation for these magnets includes magnetization coils from the University of Amsterdam and a sample rotator and ^{3}He cryostat from Clark University. The use of diamond anvil cells in pulsed fields continues to be developed. The single most significant new instrument for the 50 T pulsed fields is the dilution refrigerator commissioned by Oxford Instruments in February. It has a base temperature of 25 mK.

The Ultra-High B/T Facility in Gainesville put its dilution refrigerator into operation during 1995 and tested it down to 4 mK. The $PrNi_5$ demagnetization stage should be in operation by the time this report is available, with the high field magnet installed soon thereafter. The Ultra-High B/T Facility will open to users in early 1996.

Each of the groups that make up the Center for Interdisciplinary Magnetic Resonance (CIMAR) brought new magnet-based instruments on-line in 1995.

- The EMR group succeeded in producing high-frequency (440 GHz) EPR spectra with a newly installed 17 T superconducting spectrometer, and also achieved EPR measurements on a 20 T resistive magnet.

- Wide-line NMR was observed at 25 T on a resistive magnet. Preliminary wide-line NMR spectra were observed at >19 T with a superconducting solenoid.

- The world's first wide-bore 600 MHz (14 T) NMR spectrometer was installed and is now operating with both magnetic resonance micro-imaging and solid-sample magic-angle spinning probes. A unique-design 720 MHz pumped high-resolution NMR magnet was installed and is now in routine operation.

- A new 3 T, 80 cm bore, whole-body system for MRI and MRS was installed in the fall. Already it is giving exquisite head images and angiograms of unrivaled resolution. It was opened by Senator Bob Graham in November and is the first such instrument in the Southeast.

- The world's highest-field FT-ICR magnet (9.4 T superconductive) was installed and preliminary electrospray data have been obtained. A new FT-ICR data system has been developed.

The CIMAR faculty grew with the hiring of several CIMAR-associated postdoctoral fellows. An accelerating R&D effort aims at continued expansion of the CIMAR national user base.

The Isotope Geochemistry Program will get underway in earnest in 1996. An ultra-clean chemistry laboratory was completed in 1995 and new experiments were made possible by the addition of instrumentation and staff.

General Purpose DC Field Facilities-Tallahassee

General Purpose DC Magnets Available in Tallahassee in December, 1995

FIELD (T) BORE (mm)	FIRST USE	NO. IN USE	SUPPORTED RESEARCH
SUPERCONDUCTING			
20, 52 15, 45	3/93 7/95	2 1	Magneto-Optics, ultra-violet through far infrared; Magnetization; Specific heat; Transport; Temperatures from 20 mK to 300 K; Pressure from ambient to 13 GPa.
12, 150	7/95	1	Split coil magnet with 30 X 70 radial access. Stress testing of materials, especially superconducting cable
RESISTIVE			
20, 50 27,32 30,32 24.5, 32[1]	3/94 7/94 3/95 7/95	2 1 2 1	Magneto-Optics, ultra-violet through far infrared; Magnetization; Specific heat; Transport; Temperatures from 0.5K to 300 K; Pressure from ambient to 13 GPa; NMR in highest fields - low resolution

[1]Increased homogeneity (10 ppm over 2 mm DSV) magnet for magnetic resonance experiments.

The general purpose DC resistive magnets in Tallahassee continue to impress users with their reliability and freedom from vibration and power supply electrical noise. The two 30 T magnets in the new housing design came on line this year and have become the new "workhorse" magnets. The first 27 T resistive magnet in the world was retired after 1080 hours of service, and the inner coil was restacked to provide higher field homogeneity for magnetic resonance experiments. This 24.5 T, 32 mm bore magnet is being used for studies of a number of condensed matter systems. It is also helping to guide the design of a future resistive magnet with 1 ppm inhomogeneity. New resistive magnets planned to be completed in 1996 include one of ~34 T and 32 mm bore, one of ~20 T and 200 mm bore, and the 32 mm bore resistive insert for the 45 T hybrid.

Instruments for Users of the General Purpose Magnets

Only a few pieces of major equipment were purchased or developed for the DC High Field Facility during 1995, but considerable effort went into improving the array of available instruments and experimental techniques based on our increasing experience meeting users' needs.

Magneto Optics

A sample holder for doing infrared reflectance measurements in the 20 T superconducting magnet was built for use with the Fourier transform infrared spectrometer by Bradley Love, FSU Physics Graduate

Student; Yong-Jie Wang, NHMFL Postdoctoral Fellow; and Prof. Hon-Kie Ng, FSU Physics. It covers 20-3000 cm^{-1} frequency range and has a stage that rotates one of four samples into the light path. The temperature range is approximately 2 K to 50 K.

An optically pumped far infrared (FIR) laser (Edinburgh FIRL 100) was purchased this year. The laser output covers the wavelength range from about 40 μm to 500 μm with the standard glass cavity, and a few additional lines up to 1000 μm are added if the optional brass cavity is used. The output power for the strongest 118 μm line is over 100 mW. One of the more interesting techniques made possible by the FIR laser is optically detected cyclotron resonance. This is a very powerful technique that relies on the detection of changes in a photoluminescence (or reflectivity) signal while exciting the sample with the FIR laser and sweeping the magnetic field. Cyclotron resonance for both free carriers and impurity related transitions can be observed in any of the resistive magnets.

Recent improvements by Thomas Schmiedel, NHMFL Postdoctoral Fellow, in the visible optics facilities include sample holders and equipment for some new as well as basic techniques. New fiber optic-based sample holders for transmission measurements have been built, and there is a new sample holder with high efficiency direct lens optics for polarized light in conjunction with NMR measurements. A special sample holder for optically detected cyclotron resonance has been successfully tested in luminescence and reflectivity modes. All of these sample holders can be used from 1.8 K to 300 K, and a new double sample holder has been built for use in ^3He to 0.4 K. So far, all sample holders can accommodate samples up to at least 5x5 mm^2. A xenon lamp was purchased for use as an ultraviolet excitation source.

A new HeCd laser (325 nm, 40 mW) and a high efficiency single fiber sample holder have been used to measure changes in the excitonic emission from the GaN band edge. The sample holder provides up to 25 mW of laser light to the sample and allows detection of emissions at wavelengths as low as 335 nm through a sharp-onset long-pass filter.

New data acquisition programs for controlling the magnet, the high resolution spectrometer and CCD detector allow recording of spectra while the magnet is swept. These spectra can then be fed into a peak fitting program to be analyzed immediately after the magnet sweep. Previously users were required to hold the field fixed while a spectrum was recorded, ramp to a new field and repeat the process for the desired field range, so the new software greatly accelerates data acquisition and analysis.

Magnetization

Murali Chaparala, NHMFL Postdoctoral Fellow, has improved the facilities for magnetic measurements by developing stiffer cantilevers for studying strongly magnetic materials by force magnetometry. The magnetization of chrome alum [$KCr(SO_4)_2.12H_2O$], a spin 3/2 paramagnet, measured with this cantilever, shows the expected collapse of the data onto the universal Brillouin curve. A new sample holder for magnetic force measurements permits separation of the torque term from the magnetization signal. A new rotating stage sample holder allows angular dependence measurements in the 50 mm bore resistive magnets. The system has a resolution of 5 millidegrees and is designed for use in a helium three refrigerator in the 50 mm bore resistive magnets. It can be used for temperatures from 0.4 K to 300 K, and is not limited to magnetization measurements.

Two different groups have done simultaneous magnetization and transport measurements with the cantilever beam force magnetometer; measurements that would be very difficult, if not impossible with other methods. Prof. M. J. Naughton et al. used simultaneous deHaas-van Alphen and Shubnikov-deHaas

measurements on a so called "Tl-Se" ET salt as a function of angle to study its Fermi surface. U. Welp et al. looked at flux lattice melting in YBCO using simultaneous magnetic moment and resistivity measurements.

Proposals for a vibrating sample magnetometer to be used in all of the resistive magnets, including the hybrid, were sought and evaluated in 1995. The chosen design is due for delivery in March, 1996.

General Purpose Instrumentation for Use in Resistive Magnets

The improvements to the general purpose instrumentation available to users of the general purpose DC magnets fall into the general category of "more copies of things to serve more users more conveniently." Included were two new dewars (one for 32 mm bore and one for 50 mm bore magnets); three new helium-3 cans, two for the 32 mm bore magnets, one for the 50 mm bores; three new He-4/He-3 gas handling systems (for a total of four); two general purpose vacuum pumps; a high speed turbo pumping station specifically for pumping down the dewars for resistive magnets. A dewar with a larger helium reservoir was purchased to allow longer use between fills when the experiment boiled helium, or other cryogen, at a high rate. A 200 ampere high current probe was built for superconducting wire testing in the new large body dewar. A neon liquifier that works with the high current probe and the large body dewar was built for testing high temperature superconductors. This work, and the work on the dilution refrigerator and other superconducting magnet systems (below) was done by Scott Hannahs, Eric Palm, Tim Murphy, Bobby Pullum, and Chris Immer.

Proposals for a portable, top-loading, dilution refrigerator for use in the hybrid and other resistive magnets were sought and evaluated in the fall of 1995. The new refrigerator is expected to be delivered in July, 1996.

Improvements to the Dilution Refrigerator in the 20 T Superconducting Magnet

The sample rotating probe was rewired with 12 twisted pairs of phosphor bronze wire. These leads have a lower resistance than the original ones, so sample and temperature sensor resistance measurements are simplified, but the wires' high thermal resistance still allows the dilution refrigerator to make the same base temperature.

The original grounded micro-coax on both probes was replaced with isolated micro-coaxial cables that terminate in a standard BNC connector on the probe head. These new connectors also make it possible to expand the number of isolated coax to four in the future if so desired.

Other improvements to the dilution refrigerator include:

- Installed larger, more efficient cold traps to reduce plugging.

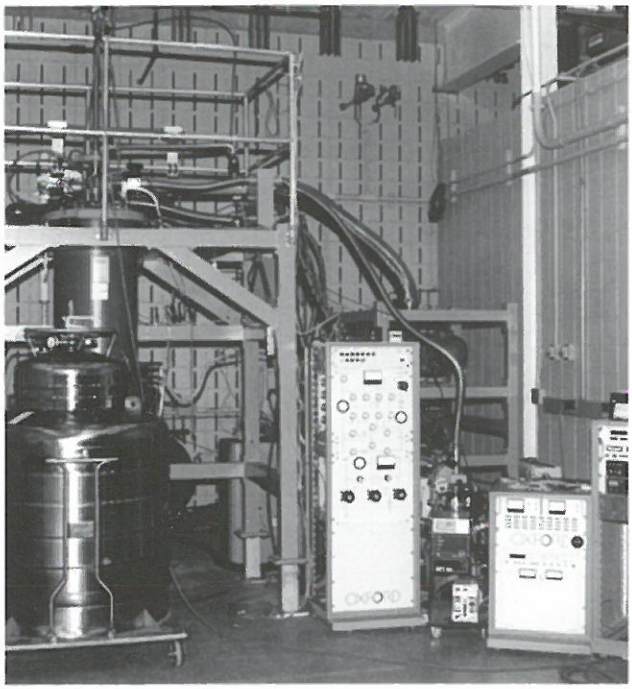

20 T superconducting magnet and dilution refrigerator with 20 mK base temperature.

- Replaced the sealed pump with one that shows when a worn shaft seal is leaking before it causes a problem for the dilution refrigerator.
- Replaced the 1K pump with a larger, higher speed pump that allows probes to be inserted and cooled faster. The new pump also fixes a problem that occurred when the lambda refrigerator was run. The 1K pot would warm because the pump could not keep up with the increased flow of helium from the bath.
- Mapped the cooling power of the dilution refrigerator with different combinations of pumps, and provided a chart for the users.
- Successfully controlled the sample temperature with a standard temperature controller using a heater in close proximity to the thermometer. Sample temperature can now be controlled to within 1% of the set point for set points between 20 mK and 800 mK.
- Replaced the yoke on the rotator with a new stronger material.

Improvements to Other Superconducting Magnet Systems

- The general purpose 20 T superconducting magnet was repaired by Oxford Instruments, tested, and placed back into service.
- A 15 T superconducting magnet donated by IBM was placed into service, and a variable temperature insert and sample holder were built and used in it.

Instruments Developed by NHMFL, Florida State University, and Visiting Scientists

Magnetic Field Modulation Coils

Prof. Roy Goodrich and Donovan Hall, graduate student, of Louisiana State University, collaborated with NHMFL staff to develop a water cooled coil for modulating the magnetic field at the sample for de Haas-van Alphen measurements in the 32 mm bore magnets. The modulation field was 94 mT, peak to peak, at 17 Hz. Future designs will aim for higher amplitude modulation.

NMR Spectrometers for High Field, Low to Medium Resolution Experiments

There are some important problems in condensed matter physics that can be addressed by nuclear magnetic resonance measurements, even in the low homogeneity general purpose magnets. Over the past two and a half years the Condensed Matter NMR group has developed instrumentation for performing NMR in the resistive magnets at the NHMFL at fields up to 30 T and over a temperature range from 1.5 K to 300 K. Experiments have been routinely carried out for the past year in a wide variety of condensed matter systems with collaborators both within the NHMFL and from elsewhere. The principle limitation in this work until August, 1995, was the 100 ppm over 1cm DSV inhomogeneity of the magnets, thus confining the research to systems with very broad NMR lines, such as magnetic systems, or to T_1 measurements.

In August a new magnet developed by the resistive magnet design group was installed. The measured inhomogeneity proved to be about 10 ppm over 2 mm DSV. There are many very interesting systems with natural line widths that exceed this magnet limitation, and several have already been studied with this magnet. Examples of condensed matter physics research currently in progress with the group's collaborators

includes studies of magnetic phase transitions in the cuprates, optically pumped dynamic polarization studies of InP and GaAs detected by NMR, studies of high temperature superconductors, and investigation of the high field spin density wave phases of one and two dimensional organic conductors. Nuclei that have been studied to date include: ^{1}H, ^{2}H, ^{19}F, ^{63}Cu, ^{65}Cu, ^{7}Li, ^{31}P, ^{35}Cl, ^{37}Cl, ^{139}In, ^{77}Se, ^{69}Ga, ^{17}O, ^{27}Al and ^{39}K.

A 15 T at 4.2 K, 17 T at 2.2 K, superconducting magnet, 1ppm homogeneity, has been ordered for condensed matter NMR research, and as a staging magnet for NMR experiments in the medium homogeneity resistive magnet.

Improvements to the Condensed Matter NMR instrumentation were made by Phil Kuhns and Alfred Kleinhammes, NHMFL; and Bill Moulton, FSU Physics.

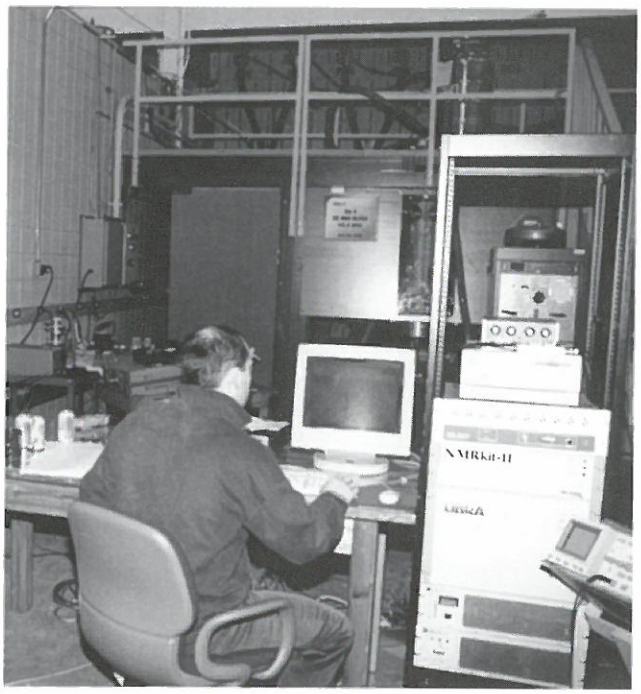

NMR research in a resistive magnet.

High Pressure Research

A high pressure facility has been created to perform both electrical transport and optical measurements over a wide range of temperatures (20 mK to 350 K), sample volumes, and attainable pressures under conditions of both hydrostatic and uniaxial stress. The principal components of this facility were described in the 1994 NHMFL Annual Report. Improvements made by Stan Tozer, NHMFL scientist, in 1995 include:

- Diamond Anvil Cell (DAC) #3, (mass = 1.7 g, sample volume = 0.5 X 0.08 mm^2) has been successfully taken to 2.7 GPa and used to perform electrical transport measurements at this pressure on a single crystal organic conductor. A variable temperature holder for this DAC fits into the sample cryostats used in the DC resistive magnets, and the 50 T, 24 mm and 60 T, 15 mm bore pulsed magnets. The DAC is suspended from the optical fiber that is used for pressure calibration and other optical measurements. There are leads for the diode temperature sensor, heater, dB/dt coil, and up to six leads for the sample.
- DAC #2 has been used successfully in an optical experiment to pressures of 5.7 GPa at liquid helium temperatures. The variable temperature probe for this DAC fits into the sample cryostats used for the DC and pulsed magnets, except for the 15 mm bore pulsed magnets.
- DAC rotators are available for the 20 T DC and 50 T pulsed magnets. Another rotator for the smallest DAC has been designed for the 32 mm bore DC magnets.

The largest of the diamond anvil cells, shown disassembled. The coin diameter is 19 mm.

Materials Testing

A facility for the evaluation of cryogenic materials and magnet components supports measurements of transport currents in superconductors, testing of large scale magnet components, and mechanical properties testing of superconductors, high strength normal conductors, structural alloys, and composites. The activities and accomplishments of this facility are described by Leonard Summers in the Magnet Science and Technology section of the Research Reports.

Infrastructure for Research Support

Mechanical Instruments

The Mechanical Instrumentation Facility has added a high precision Hardinge Lathe for close tolerance machining and micromachining and a computer controlled vertical machining center for machining large components. These machines complete the basic requirements for a well equipped machine shop. Three temporary machinist positions were upgraded, and one new machinist was hired to meet increasing demand.

Electronic Instruments

Staff and minor equipment were added to the Electronic Instrumentation Facility during 1995 to support the increasing demand for new special electronic instruments for NHMFL researchers and to carry out repairs and calibrations as needed.

Computers and Networks

The Computer Support Group continued to expand the telecommunications and computing facilities of the NHMFL as the laboratory expanded. New system security measures were installed to meet the increased complexity of the challenges faced by the networks.

Magnet Systems Available in Los Alamos in December, 1995

FIELD (T) BORE (mm)	FIRST USE	PULSE, rise/duration (ms)	SUPPORTED RESEARCH
PULSED			
50, 24 60, 14 45, 24[1]	12/92 3/93 2/95	6/30 7/35 9/60	Magneto-Optics, ultra-violet through far infrared; Magnetization; Mechanical Properties; Thermal expansion; Specific heat; Transport; Temperatures from 25 mK to 550 K; Pressure from ambient to 5.7 GPa; NMR in highest fields - low resolution
SUPERCONDUCTING, DC			
20, 52	12/92		Same as pulsed fields
9, 32	11/95		Magneto-Optics, ultraviolet to near infrared

[1]Higher homogeneity

20 T Superconducting Magnet Instrumentation

- A probe was constructed that allows photoluminescence measurements from 2.2 K to 250 K.

- A magnetostriction cell design was tested successfully in a prototype. This cell measures either thermal expansion or magnetostriction of a sample of dimensions 0.5 to 4.0 mm. It is a volume magnetostriction cell, so it can be rotated 90 degrees in a magnetic field. The current sensitivity of the prototype is 1 part per billion. This sensitivity is expected to be exceeded with installation of the second version in the 20 T magnet in 1996.

Capacitor Driven Magnet Improvements

- Three independent magnet stations were completed, one of which contains a 50 T, 24 mm bore magnet dedicated to the dilution refrigerator (see below). The remaining two cells are fitted with whatever types of magnets are needed by the scheduled users.

- In response to a user's request, experiments were conducted for the first time in a maximum field gradient which turned out to be 11 T/cm at a field of 28 T, as shown in the figure on page 166.

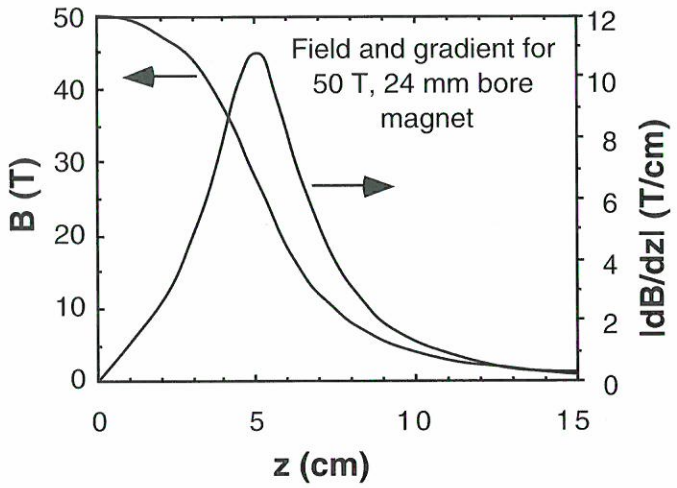

Field, B, and gradient, dB/dz, in a 50 T, 24 mm bore, pulsed magnet.

- A 42 T, long decay magnet has been wound and is expected to be installed in early 1996.

- Oxford Instruments completed commissioning of the dilution refrigerator in February, 1995. The base temperature is 25 mK and temperature recovery following a field pulse occurs within 15 to 20 minutes. (The empty cell warms to approximately 60 mK during a 50 T pulse; any temperature rise in the sample depends on its conductivity and size.) This is possible because the refrigerator contains non-metallic components in key places. This is the lowest temperature ever reached in 50 T fields.

60 T Quasi-Continuous Magnet

Generator Facility, Power Modules, and Control System

Josef Schillig of NHMFL collaborated closely and extensively with ABB on the third design of the power supply transformer. This design passed the short-circuit test in October, 1995, and will be used. Jim Ferner and Heinrich Boenig also monitored the ABB effort closely. Five of these transformers are required for the 60 T quasi-continuous (q-c) magnet.

The current limiting device (CLID) control and protection wiring was completed and the CLID commissioned. Likewise for the load breaker.

About half of the man-machine interface screens for the control system were completed under the direction of Josef Schillig. Progress was also made on the reversing switches, the crowbar switch, the dummy load, and coil monitoring and protection systems.

Magnet Progress

Everson Electric completed fabrication of the 60 T long pulse coils. The major design on the frame, dewar, magnet power busbar, and liquid nitrogen handling systems (which support, hold, and service the coils) was completed by Jim Sims and John Rogers; and fabrication was begun. All nine coils, which were designed by Sims, have arrived and have passed acceptance tests. Four of these weigh more than a ton.

Non-Destructive 100 T Magnet

Preliminary studies by Yehia Eyssa, Paul Pernambuco-Wise, and Heinrich Boenig showed that a 2 MJ capacitor bank is sufficient to provide the energy for a 50 T insert magnet installed in the bore of a 50 T background field to provide a 100 T nondestructive magnet. To provide a large amount of flexibility and some amount of redundancy, the capacitor bank was designed by Boenig as a system containing four independent 600 kJ units. The units have voltage standoff capability to allow all four units to run either in parallel at 6 kV, in series at 24 kV, or in a set of two units in parallel and series at 12 kV. In addition three units can operate in series at 18 kV. This wide combination of voltages allows many different coil types at voltages from 6 to 24 kV to be tested with energies up to 2.4 MJ at 6, 12, and 24 kV.

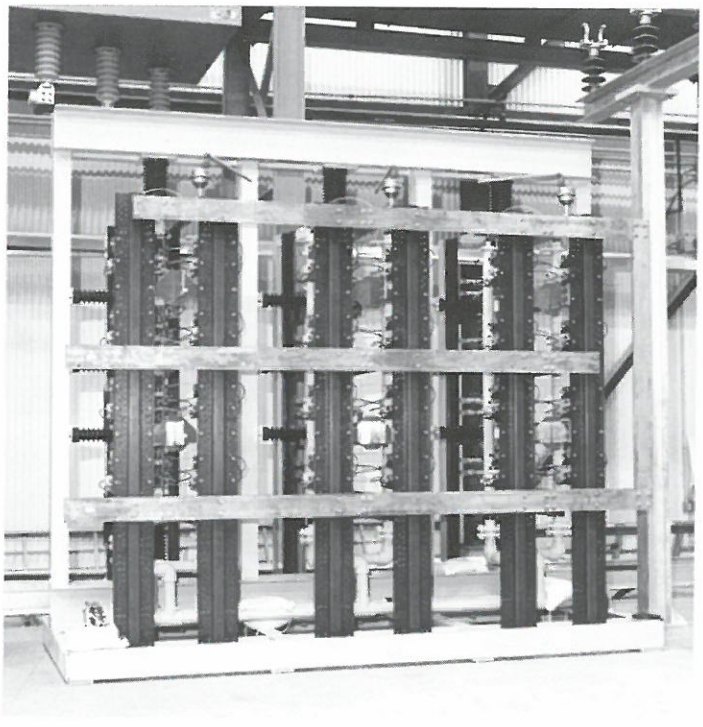

One of five 80 MW rectifier units for the 60 T quasi-continous magnet.

All the capacitors were ordered for the total bank. The capacitors are designed to survive 50,000 full voltage shots. Delivery of the capacitors from Aerovox and the first charging supply from NWL (National Winding Laboratory) are expected at the end of the first quarter in 1996; delivery of the solid state switches from Silicon Power Corp. is expected in the second quarter.

Spectroscopic Facility for the Visible and Near IR Regions

A spectroscopic facility was established through the efforts and supervision of Prof. Clive Perry of Northeastern University. Three spectrometers became operational:

- 0.25 m f/4 Jarrel-Ash monochromator with a thermoelectrically cooled GaAs photomultiplier and a liquid nitrogen cooled Ge photo-detector for operation in the visible and near IR (300-1600 nm).
- 0.6 m f/10 Spex "Triple-Mate" spectrometer with a Photometrics Model 9000 CCD array detector for the 300-1050 nm region.
- 0.28 m f/4 Acton Instruments monochromator with a Princeton Instruments CCD array detector for operation in the 300-1050 nm region.

Fiber optic cables with core sizes from 62.5 to 600 μm connect any spectrometer to sample holders located in either the 20 T superconducting magnet or the 50 T and 60 T pulsed magnets. Low temperature (1.5-4.2 K) facilities are currently available for photoluminescence, reflection or absorption spectroscopy with both perpendicular (Faraday) or parallel (Voigt) magnetic field geometries. Excitation sources consist of a broad band white-light source, a Coherent Radiation Innova Model 310, 8 W multiline Argon laser, and a Mira 900-D femtosecond/picosecond Titanium-Sapphire laser that is tunable from 710-1060 nm. A Pockels cell shutter is used to synchronize the spectroscopic data acquisition with the "flat-top" region of the pulsed magnetic field. All spectrometers, detectors, and pulsed magnet field operation are under computer

control. (Some of the above equipment was acquired by loan; it is being replaced by equivalent NHMFL equipment as funds allow.) An 8.5 T, 30 mm bore superconducting magnet was loaned to NHMFL to use as a staging magnet for optical probe and technique development and for calibration of samples and probes prior to pulsed magnet experiments.

Other Los Alamos National Laboratory Facilities Available to NHMFL Users

Funding was secured by another laboratory program (Pegasus) to design a method for flux compression to 600 T using an existing Los Alamos capacitor bank. If successful, this will be a second potential source of megagauss fields for NHMFL users, in addition to the explosive flux compression.

Arrangements were made through other laboratory programs to pursue a series of explosive flux compression shots in early 1996 using Arzamas generators that potentially can reach 1000 T. These shots will carry experiments suggested by NHMFL users, which NHMFL will assist through its pulsed field facilities and program.

Ultra-High B/T Facility-Gainesville

A special annex facility for studies of materials at ultra-high values of the ratio of magnetic field to temperature (B/T) is being developed as a collaborative effort between the NHMFL and the Microkelvin Laboratory at the University of Florida. This facility will provide users with the ability to carry out experiments that simultaneously require fields up to 20 T and temperatures down to 500 mK. The B/T ratio of 4 x 10^4 T/K will be the highest available anywhere, and will allow users to study new phenomena that require the establishment of high spin polarizations or high magnetizations. Plans for the facility were described in the 1994 Annual Report and are available on the NHMFL World Wide Web Site.

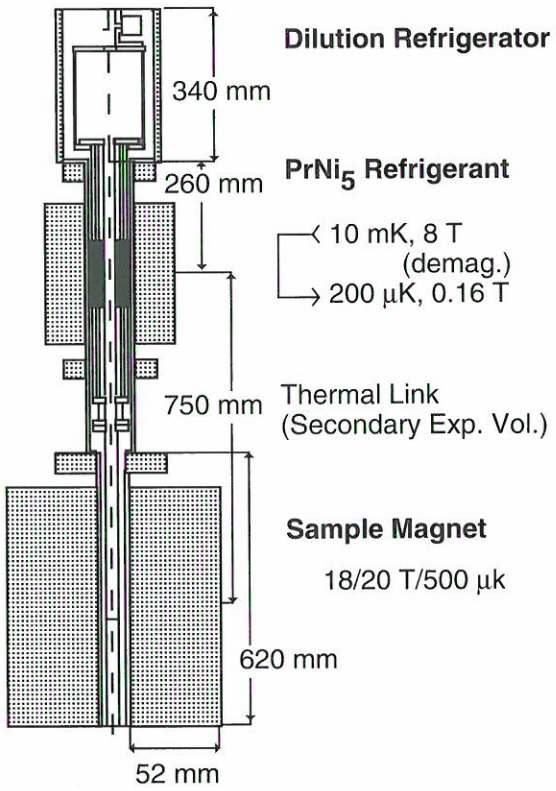

Ultra-High B/T Facility at UF (B≤20 T, T≥500 μK).

The dilution refrigerator and dewar have been installed and tested. With a minimum temperature of 4 mK, the high-cooling power dilution refrigerator reaches 10 mK in 10 hours. Infrequent transfers of helium will be required since the vapor shielded dewar has a hold-time of a week. Rapid bottom-loading of samples can be accomplished using a slide tube–and–bellows arrangement that allows the dilution refrigerator to be withdrawn from the dewar, then reinserted, without warming the dewar and magnets. The turn-around time from 10 mK is about 24 hours. Additionally, samples may be top loaded with some loss in the minimum temperature.

Assembling, installation, and testing of the PrNi5 demagnetization stage will be completed in January, 1996, with delivery of the high-field magnet expected about the same time. After commissioning of the magnet and testing on in-house experiments, the facility will be open to external users. A full-time research scientist, Jian-Sheng Xia, has been part of the design team and will be available to coordinate and assist with the assembly and design of the experiments.

Center for Interdisciplinary Magnetic Resonance (CIMAR)

Institutional Integration

The magnetic resonance program spans all three institutions of the NHMFL. The primary facilities for nuclear magnetic resonance (NMR), electron magnetic resonance (EMR, including electron paramagnetic, and cyclotron resonance), and ion cyclotron resonance (ICR) are housed in Tallahassee. The primary site for magnetic resonance imaging and *in vivo* spectroscopy (MRIS) is at the University of Florida (UF), which offers extensive animal care and surgical facilities. Furthermore, UF is developing a new Center for Structural Biology, and the NHMFL has contributed resources for equipping that Center. Strong ties have been established with the Structural Biology Program, the Center for Materials and Research Technology, and the Supercomputing Computational Research Institute at Florida State University (FSU); the Center for Structural Biology and the Department of Radiology of the College of Medicine at UF; the Chemical Science and Technology Division at Los Alamos National Laboratory; as well as with individual research groups in Biology, Biochemistry, Chemistry, Materials Science, and Physics at the three NHMFL institutions. Thus, the NHMFL magnetic resonance program is strengthened by taking advantage of the combined resources at its three host institutions.

Scientific Integration

A unique feature of CIMAR is its large-scale integration of NMR, MRIS, EMR, and ICR spectroscopies, which share many concepts and techniques. Continued cross-fertilization among these fields is facilitated at NHMFL in several ways through a broad external and internal user program.

In addition to "monodisciplinary" seminars, which tend to focus on special areas of NMR, EMR or ICR, frequent "multidisciplinary" seminars are targeted at the full range of magnetic resonance researchers. Visits by eminent speakers ensure regular injection of new ideas.

In December, 1995, NHMFL and CIMAR hosted the Southeastern Magnetic Resonance Conference (SEMRC). This high-level meeting provided an opportunity for many prominent scientists from the United States and abroad to visit the NHMFL and appreciate our achievements.

CIMAR faculty meetings have been held, approximately once every six weeks since June 1995, in Tallahassee, Gainesville, or Steinhatchee. These meetings provide a forum where investigators, research staff, postdoctoral associates, and graduate students with an interest in magnetic resonance can meet and exchange their views. The meetings feature scientific presentations by selected investigators who present work related to CIMAR, and provide an opportunity to discuss matters of scientific priorities, staffing, and

budget. Weekly meetings of the CIMAR committee (Bodenhausen, Brunel, Mareci, and Marshall) ensure a high level of coordination.

The magnetic resonance research groups in Tallahassee are housed in shared or contiguous laboratory and office space, including a shared reading room to encourage cross-talk and education across disciplinary lines. Close proximity of the research groups allows for efficient sharing of space and equipment: a common biochemical sample preparation laboratory, shared rf and microwave frequency synthesizers, counters, amplifiers, etc., and a computer network for interactive molecular graphics and other computations.

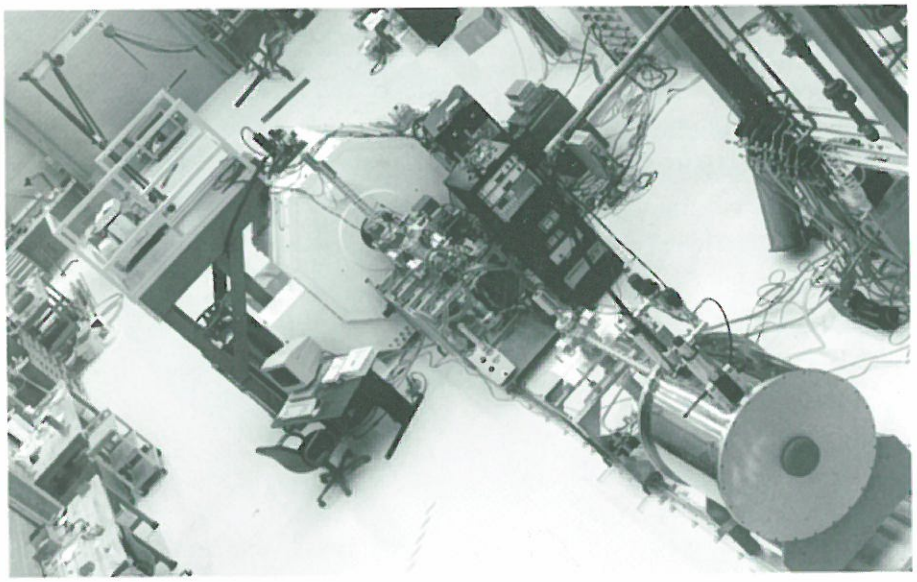

The 9.4 T FT-ICR mass spectrometer. The large white object just left of center is the shielded 9.4 T magnet. The darker objects in the center are the electrospray ion source and system controls. A 6 T, 150 mm bore magnet is shown lower right.

The NHMFL has hired and will continue to hire experts in the field of magnetic resonance to build strong in–house programs in NMR, MRIS, EMR, and ICR. External users are expected to be attracted to the NHMFL not only for its high–field spectrometers, but also because of new techniques, instruments, and applications developed by its in-house researchers.

A great deal of attention has been paid to the needs and interests of potential users, and a growing number of external users are beginning to make use of NHMFL's exceptional magnetic resonance facilities. Users are normally requested to give seminars about their work, so that the NHMFL staff can appreciate the scope of their research, thus providing improved opportunities for constructive collaboration.

Like all NHMFL facilities, CIMAR facilities are open to qualified users from anywhere in the world. For further information, contact

- Dr. Geoffrey Bodenhausen (NMR/MRIS), (904) 644-5044, boden@magnet.fsu.edu
- Dr. Louis-Claude Brunel (EMR), (904) 644-1647, brunel@magnet.fsu.edu
- Dr. Alan G Marshall (ICR), (904) 644-0529, marshall@magnet.fsu.edu.

All three individuals share the same fax (904)-644-1366.

NMR Program

Several NMR systems have been delivered and put into operation in the course of 1995. Continued efforts have been made to attract highly-qualified staff. Research and development has concentrated on a wide range of areas:

- Engineering of stable power supplies, flux stabilization, and field-frequency lock for magnetic resonance using resistive magnets (24.5 T).
- Development of probes and receiver systems for use at very high fields.
- Development of probes for double-rotation (DOR) of quadrupolar nuclei.
- ^{7}Li NMR and ^{139}La NQR in Lanthanum cuprates.
- High-field ^{17}O NMR of $YBa_2Cu_3O_7$.
- ^{77}Se NMR of spin density waves in $(TMTSF)_2PF_6$.
- Studies of ion-channel-forming peptides in biological membranes by solid-state NMR.
- NMR studies of the physiology of superfused muscle of marine organisms *in vivo*.
- Development of NMR methods for monitoring the metabolism of lactic acid *in vivo*.
- Microimaging of biological systems at high field (14 T).
- Measurements of diffusion of water and macromolecules in gels and gel-like media.
- Measurements of intracellular diffusion of phosphorous metabolites in skeletal muscle.
- Studies of protein folding dynamics.
- High resolution proton spectroscopy in partly deuterated solid materials, using novel methods for deuterium decoupling.
- Excitation of quadrupolar echoes in deuterated materials, using new rf modulation methods.
- Broadband decoupling in isotropic solution by frequency-modulated "chirp" pulses and other modulation schemes.
- Investigation of the field dependence of relaxation, particularly of cross-correlation of dipolar and chemical shift anisotropy (CSA) interactions in proton NMR.
- Selective measurement of nuclear Overhauser effects in various proteins and nucleic acids in isotropic solution, with inhibition of spin–diffusion, for accurate determination of internuclear distances.
- Measurement of nuclear Overhauser effects for accurate determination of the structure of cofactors bound to enzymes.
- Determination of the molecular structure of natural products by computer-supported analysis of multi-dimensional NMR spectra.
- Extraction of scalar coupling constants and chemical shifts by computer–supported analysis of multiplets in multi-dimensional NMR.
- Numerical simulations of the time-evolution of nuclear magnetization, including relaxation and chemical exchange. The NHMFL is developing into a world-wide "hub" for calculations of this type.

NMR Imaging and In Vivo Spectroscopy

NMR provides a unique, non–destructive method of imaging materials. By use of the resonance of abundant spins (mostly ^{1}H), magnetic field gradients can be used to map the distribution and physical environment of the material under study. In addition to important applications in materials research, NMR imaging has extensive applications in medicine. Currently, magnetic resonance imaging (MRI) is the premier tool of diagnostic radiology giving unsurpassed definition of soft tissue anatomy. However, the rich information content (relaxation, chemical shift, coupling constants, and diffusion) available with NMR can provide a detailed picture of the material under study that is not available with any other technology.

In addition to imaging, NMR can provide a direct measure of the biochemical processes in living tissue with *in vivo* spectroscopy. As examples, important compounds in the brain can be measured with ^{1}H spectroscopy and the metabolic status of various tissues determined using ^{31}P spectroscopy. At higher fields, other spins of great interest in biology (^{13}C, ^{15}N, ^{17}O) become accessible to direct measurement. There is no other technique that compares to *in vivo* NMR spectroscopy for the direct, non–invasive, dynamic study of biochemistry in living systems.

The NMR Program of the NHMFL is developing capabilities for imaging and *in vivo* spectroscopy at its sites in Tallahassee and Gainesville. At the Health Sciences Center of the University of Florida in Gainesville, two NMR instruments, which received partial support from NHMFL, have been developed for NMR microscopy. Both a 7 T, 50 mm bore and a 14 T, 50 mm bore spectrometer have been equipped with gradients and used to study excised human and animal (rat and cat) spinal cord samples. At the Tallahassee site of the NHMFL, a 14 T, 89 mm bore magnet was recently installed. The larger bore of this magnet system allows microscopy of larger samples.

This 4.7 T, 330 mm bore magnet system is part of a small animal imaging spectrometer at UF.

In addition to instruments directly supported by the NHMFL, the College of Medicine of the University of Florida houses other NMR imaging spectrometers used for research. Studies of whole animal systems are performed on a 4.7 T, 33 cm bore magnet system, and human studies are carried out on a 1.5 T, 1 m bore magnet system. Also a 3 T, 80 cm bore magnet system for human studies was installed in the Veterans Administration Medical Center during the fall of 1995. The magnet system was acquired though a collaborative effort of the Veterans Administration Medical Center, the Shands Hospital at the University of Florida, and the University of Florida Brain Institute (through the UF Office of Research, Technology, and Graduate Education). This system is used for imaging, angiography and *in vivo* spectroscopy. Of particular interest at this time is the development of functional brain and spinal cord imaging for the study of neuronal processing. Other important applications include localized *in vivo* spectroscopy in cancer studies.

In order to investigate the use of high-field NMR in biological systems, extensive studies have been undertaken to measure the field dependence of longitudinal and transverse relaxation of ^{31}P NMR in important phosphorus containing compounds (creatine phosphate, and adenosine triphosphate) and to evaluate gains in signal-to-noise ratio that can be expected at high fields.

The following are some specific projects on which substantial progress was made in 1995:

- Development of novel radiofrequency coils for large bore magnets for MRIS.
- Development of novel transverse field gradient assemblies for large bore magnets and for NMR microscopy.
- Development of novel contrast agents for MRI.
- Relaxation mechanisms of particulate suspension MRI contrast agents, especially related to water diffusion through local susceptibility gradients, and the field dependence of that relaxation.
- Structure and dynamics of peptide substrates and inhibitors of HIV proteinase (PR), and of inhibitor-HIV PR complexes.
- ^{31}P magnetic resonance spectroscopic imaging (MRSI) of *in vivo* intact human gastrocnemius (calf) muscle under physiologic stress (reduced blood flow) in low-intensity exercise trained and untrained individuals.
- ^{31}P MRSI of *in vivo* intact human gastrocnemius (calf) muscle under physiologic stress (cardiac insufficiency) in untrained and low-intensity exercise trained individuals with and without L-carnitine supplementation.
- ^{31}P MRSI of the *in vivo* intact human cardiac muscle in normal and cardiac heart failure individuals.
- ^{31}P MRSI of cell growth and cell death of a humanosteosarcoma cell line perfused in a bioreactor or implanted into nude mice.
- ^{31}P MRSI of cell growth and cell death of treated and untreated therapy sensitive and therapy resistant human osteosarcoma cell line perfused in a bioreactor and implanted into nude mice.
- ^{31}P MRSI therapy monitoring of patients with muscluloskeletal tumors of the leg.
- Measurements of diffusion anisotropy in excised spinal cord tissue.

Instrumentation for NMR and MRIS available in Tallahassee and Gainesville in December, 1995

FREQUENCY (MHz)	FIELD (T) BORE (mm)	HOMO-GENEITY	SUPPORTED RESEARCH
850*	18/20, 31	100 ppb	Solid–state NMR
720*	16.9, 50	1ppb	Solution–state NMR; Test bed for powered mode and 2.2 K operation aimed at ≥21 T system development
600*	14, 89	1 ppb	Solid-state NMR; Diffusion studies; *in-vivo* spectroscopy; and micro–imaging
600**	14, 50	1 ppb	Solution-state NMR; NMR microscopy
500*	11.75, 50	1 ppb	Solution-state NMR
500**	11.75, 50	1 ppb	Solution- and solid-state NMR
300*	7, 89	1 ppb	Developing new solid–state methods, including magic angle spinning techniques
300*	7, 50	1 ppb	Developing new solution–state methods
200**	4.7, 330	0.1 ppm	MRI and MRSI of animals
125**	3, 800	0.1 ppm	Whole body MRI and MRSI

* Tallahassee ** Gainesville

Electron Magnetic Resonance Spectroscopy

Electron Magnetic Resonance (EMR) includes electron cyclotron resonance and electron paramagnetic resonance (EPR). Electron cyclotron resonance has long been a major tool for physicists in high magnetic field laboratories. The cyclotron frequency of an electron in a magnetic field depends on the inverse of the "effective" electron mass; this is used to study the band structure of semiconductors. This technique has been used at the NHMFL with a Fourier Transform Infrared Spectrometer (Bruker 113uv) and with the newly acquired, optically pumped, Far Infrared Laser (Edinburgh FIRL 100).

In EPR, an unpaired electron is often used to probe the structure or the rigidity of its environment in materials ranging from metals to biomolecules. Because of the nature of the interaction between electromagnetic radiation and paramagnetic centers, it is far more difficult to observe EPR than to measure electron cyclotron resonance. The EMR program at the NHMFL has developed two spectrometers, a high field instrument based on the resistive magnets, and a high resolution instrument with a superconducting magnet. The scientific projects of the in-house scientists are drawn from physics (high T_c superconductors), chemistry (molecular magnetism), and biology (photosynthesis and proteins).

High Field EMR Spectrometer

On July 5, 1995, the EMR group obtained the first EPR spectrum with a resistive magnet at the NHMFL. The sample was BDPA, a molecule commonly used as a standard for EPR spectroscopy; the source was a

phase locked Gunn diode from ABmm (ESA 1-110); and the detector was an InSb fast electron bolometer from QMC Instruments. The experiments performed on July 5 allow us to evaluate precisely the possibilities of the NHMFL resistive magnet facilities:

- Maximum magnetic field: 30 T now, higher in the future.
- Maximum frequency: 3 THz with the FIR Laser (useful for systems with large zero field splittings like metalloproteins).
- Resolution: 1 mT for a cubic sample of 5x5x5 mm^3, at 10 T. This is limited by the inhomogeneity of the magnet and the ripple noise of the resistive magnet power supplies.
- Sensitivity: better than 10^{13} spins/gauss for a sample at 4.2 K.
- Temperature of the sample: 4.2 K - 300 K.

These specifications will be improved as soon as EPR calibrations are run in the 24.5 T resistive "enhanced homogeneity" magnet. NMR measurements have shown that the homogeneity and stability are at least ten times better than in standard magnets.

High Resolution EMR Spectrometer

In another major development that came to fruition late in 1995, high resolution EMR (0.01 mT) is now possible with a 15/17 T, 52 mm superconducting magnet specially designed for EMR experiments up to 450 GHz. Research by in-house and visiting users has already begun with this system. One user has been successful in observing spectra of iron-based proteins over an extremely broad frequency range: 44 to 330 GHz, and zero field splittings have been measured. Another user measured high field EPR at 330 GHz of linear-chain Heisenberg anti-ferromagnets.

An EPR X-band spectrometer (Bruker ECS 106)is available in the laboratory to check samples at 9 GHz .

ICR Program

Fourier transform ion cyclotron resonance (FT–ICR) provides the most versatile and highest–performance mass analysis: e.g., mass resolving power of 1,000,000 for protein ions up to 30,000 Da, and detection of a single (multiply–charged) ion up to 10^8 Da; determination of ion–molecule reaction pathways, kinetics, equilibria, energetics, and mechanism by manipulation of mass–selected trapped ions; mixture analysis; surface analysis; high sensitivity (e.g., attomole (10^{-18} moles) detection of peptides and phospholipids); speed (typically 1 second for a full mass spectrum); etc. During 1995, the number of FT-ICR systems worldwide increased by about 10% (to 185).

Although ion cyclotron resonance was not included in the original mission and funding of the NHMFL, an ICR program was initiated in 1993 from State of Florida funds, with the hiring of Alan G. Marshall (Director of the ICR Program) and Shenheng Guan (Associate Director). In 1994, these two investigators combined with UF's John R. Eyler for a $5 million five-year NSF High–Field Fourier Transform Ion Cyclotron Resonance Mass Spectrometry Facility designed to develop and provide state–of–the–art FT–ICR capabilities to external users (university, government, and industrial labs) nationwide. NHMFL's critical role lies in providing the infrastructure and high–field magnets that will make possible the highest–performance FT–ICR experiments in the world.

As in FT–NMR spectroscopy, resolving power in FT–ICR mass spectrometry scales linearly with magnetic field, B_0. Thus, the magnets available to NHMFL's ICR Facility [9.4 T (supercon), 20 T (resistive, available in early 1996), and 25 T (resistive, proposed for 1997)] project improvement in ICR mass resolving power by factors of 34% to 357% compared to the largest–field (7 T) ICR magnets anywhere else. Moreover, a higher magnetic field offers a host of additional advantages for FT–ICR, as outlined briefly in Table 1. Apart from obvious major improvements in mass resolving power and upper mass limit (which scale as B_0 and B_0^2), the higher magnetic field also greatly reduces the rate of ion loss by radial diffusion (which scales as B_0^{-2}), and thus improves all FT–ICR experiments because ions remain confined to the center of the ion trap. Finally, various non–linearities are greatly reduced at higher magnetic field: e.g., unwanted coalescence of closely–spaced peaks scales as B_0^{-2}.

Table 1. Improvement factors (relative to 7 tesla) for various FT–ICR performance parameters.

FT–ICR/MS performance parameter	9.4 T	20 T	25 T
Mass resolving power, $m/\Delta m \propto B_0$	1.3	2.9	3.6
Upper mass limit $\propto B_0^2$	1.8	8.2	12.8
Ion translational energy $\propto B_0^2$	1.8	8.2	12.8
Maximum number of trapped ions $\propto B_0^2$	1.8	8.2	12.8
Ion radial diffusion (loss) rate $\propto 1/B_0^2$	0.55	0.12	0.078
ICR orbital radius $\propto 1/B_0$	0.74	0.35	0.28
Maximum number of trapped ions $\propto B_0^2$	1.8	8.2	12.8
Coalescence of close–spaced resonances	0.55	0.12	0.078

During 1995, the FSU ICR group's main activity was the design, construction, and assembly of new instruments. As new techniques and experiments are developed on the NHMFL instruments, those methods will be implemented on external–user instruments in the NSF National High–Field FT–ICR Mass Spectrometry Facility. In addition to the construction program, the FSU ICR group produced 12 refereed publications and 52 invited and contributed talks at scientific meetings, universities, and government and industrial laboratories (see lists elsewhere in this Report) during the present reporting period. Specific highlights include:

- Design, construction, and testing of homebuilt high-performance data systems, with Pentium platform, LabWindows command structure, and VXI bus-mounted modules for control of r.f. and DC voltages, stored waveform excitation, up to 96-channel experimental event sequence pulse programmer, high-resolution (21-bit) 5 MHz analog-to-digital converter, broad-band receiver preamp, FFT data reduction, and menu-driven command structure with no more than three mouse clicks to reach any command. Five systems are under construction (two of which are hardware-complete), and several other research groups have expressed interest in helping to develop and use the system.
- Design and construction of 9.4 tesla FT-ICR mass spectrometer with homebuilt electrospray source and dual octupole ion guides. This instrument awaits only final delivery of a flange-mounted Penning trap, and should be completed early in 1996. Preliminary results are quite promising.

- Design and construction of 7.0 tesla FT-ICR mass spectrometer with homebuilt matrix-assisted laser desorption/ionization (MALDI) source and wire-in-cylinder ion guide. This instrument is currently under test and should be operational early in 1996.
- Design and construction of 3 tesla FT-ICR mass spectrometer for detection of fluorescence from mass-selected gas-phase trapped ions. This system is currently under test.
- Design of 20 tesla resistive-magnet FT-ICR mass spectrometer with homebuilt (MALDI) fiber-optic source. This small-bore system is currently under construction and should be ready for testing by the second quarter of 1996.
- New record for detection limit (9×10^{-18} moles) achieved for a peptide produced by matrix-assisted laser-desorption/ionization (MALDI).
- Record mass resolving power (1,500,000) achieved for MALDI of a peptide.
- Identification and structural analysis of phospholipids (polar head group, fatty acid side chains) from femtomole amounts of sample, including mixtures.
- Magnitude-mode multiple-derivative spectra for resolution enhancement without loss in signal-to-noise ratio (applies to all forms of FT spectroscopy).
- Simulation and construction of a wire-in-cylinder ion guide, for transfer of ions from an external ion source to the center of a solenoidal superconducting magnet. Based on our design, such an ion guide has been installed in an FT-ICR instrument at Oak Ridge National Laboratory.
- Simulation of a "matrix-shimmed" Penning trap that promises to provide near-perfect electric excitation, detection, and trapping potentials based on simple cubic geometry. Design and fabrication of such a trap are under way.
- The UF group developed a DC glow-discharge elemental ion source, coupled to an FT-ICR instrument. Their work on a separate inductively-coupled plasma elemental ion source is now under way.

Ion Cyclotron Resonance Spectrometers Available in December, 1995

The NHMFL Tallahassee site ICR capabilities derive from the magnets listed below. All have 10 ppm inhomogeneity. Additional superconducting magnet-based FT-ICR instruments at UF serve as development sites for other applications (e.g., DC glow-discharge ion source, inside-the-bore electrospray ion source).

FIELD (T) BORE(mm)	SUPPORTED RESEARCH
9.4, 210	Electrosprayed multiply-charged biomolecular ions of high molecular weight
7, 150	MALDI-generated singly-charged ions of peptides and polymers; and analysis and reaction chemistry of elemental ions generated by r.f. glow-discharge
6, 150	Test bed for an inside-the-bore electrospray ion source being developed and constructed by Prof. Laude's group at U. of Texas
3, 150	Excitation and detection of fluorescence from mass-selected trapped ions
3, 150	Routine ICR applications and tests to see whether higher-field performance is needed for a particular sample

Isotope Geochemistry Program

Program Description

The inclusion of isotope geochemistry and isotope ratio mass spectrometry (IRMS) in the in-house research program has broadened the research base of the facility. The program was initiated in 1994. 1995 was devoted mostly to construction of the laboratory facilities and the commissioning of the instrumentation. The construction of an 800 square foot Ultra-Clean Chemistry Laboratory was completed in 1995, and two isotope ratio mass spectrometers were put into operation. A new faculty member (Yang Wang) was hired jointly with the FSU Department of Geology. 1996 will be the first fully operational year of the Isotope Geochemistry/Mass Spectrometry Laboratory.

The isotope geochemistry facility specializes in the precise and accurate determination of trace metal concentrations at very low levels in both natural and synthetic materials as well as the measurement of the natural variation in isotopic composition of materials. In addition to dating processes that occur on the timescale of thousands to billions of years, the techniques are also used to investigate the chemical structure of the earth as well as to allow investigations into the sources, severity, and remediation of heavy metal pollution in the environment.

The addition of new faculty has broadened our expertise to include the "light" elements (hydrogen, carbon, oxygen and sulfur). The isotopic composition of these elements reveal information about the cycle of these elements in the environment and the anthropogenic influence on the hydrosphere.

Access to the facilities in Isotope Geochemistry are open to any user on a collaborative basis. Requests should be made by contacting one of the investigators. The operating cost of the facility is primarily borne by grants to the individual investigators.

Instrumentation

The Isolab 54 secondary ionization mass spectrometer represents the state of the art in secondary ion IRMS, and is used primarily for the determination of thorium and hafnium isotopes. Experiments involving the measurement of mercury isotopes have shown great promise and the technique for mercury isotopes will be further developed in 1996.

A Finnegan MAT 262 RPQ was purchased with an NSF grant and state matching funds and delivered in September 1995. The 262RPQ is a thermal ionization mass spectrometer outfitted with nine collectors, an ion counting system and a Retarding Potential Quadrupole (RPQ). The RPQ addition to the mass spectrometer allows filtering of ions that interacted with the residual gas on their path to the analyzer, thereby increasing the abundance sensitivity. The 262RPQ currently defines the cutting edge in moderate mass resolution, high abundance sensitivity thermal ionization mass spectrometry. It will be used for the determination of the isotopic compositions of Sr, Nd, Pb, U, Th, Hf, and Os as well as for measuring the concentration of a large variety of trace elements using isotope dilution techniques.

NHMFL - DC High Field Facility

USER	INSTITUTION	FUNDING	PROJECT
Agosta, C.C. Ivanov, S.A. Howe, D.A.* Immer, C.* Hannahs, S. T.	Clark Univ. Clark Univ. Clark Univ. FSU NHMFL	Air Force URI Program Grant F49620-92-J-0525	Superconductivity and Correlated Electron Properties of Molecular Conductors
Aronson, M. Tozer, S. Fisk, Z.	Univ. of Mich. NHMFL FSU	DOE	Angular Dependence of High Pressure Magneto-Resistance in Smb_6
Awschalom, D. Samarth, N. Crooker, S.* Flack, F.* Schmiedel, T.	UC, Santa Barbara Penn State Univ. UC, Santa Barbara UC, Santa Barbara NHMFL	AFOSR	Magneto-Optical Spectroscopy in Digital Magnetic Heterostructures
Awschalom, D. Mann, S. Gider, S.	UC, Santa Barbara Univ.Bath; UK UC, Santa Barbara	AFOSR	Torque Anisotropy of Ferritin
Bowers, C. R. Kuhns, P. L. Kleinhammes, A. Schmiedel, T. Sloan, S.* Chabrier, P. Moulton, W. G.	Univ. of Florida NHMFL NHMFL NHMFL Univ. of Florida FSU FSU & NHMFL	NSF	NMR Detected Optical Dynamic Nuclear Polarization Studies of ^{69}Ga in GaAs and ^{115}In in InP
Brandt, B. Liu, D.* Courts, S. S. Holmes, D. S.	NHMFL FSU Lake Shore Cryo., Inc Lake Shore Cryo., Inc	NSF	Magnetoresistance Measurement of Cernox Sensors
Brooks, J. S. Fisk, S. Z. Uji, S.* Terashima, T. Aoki, H. Valfells, S. Sandhu, P. Sarrao, J. Goettee, J.	FSU FSU FSU NRIM-Japan NRIM - Japan Boston Univ. Boston Univ. NHMFL LANL	NSF-DMR-95-10427	SdH Oscillations, Fermi Surface, and Phase Transitions in h-Mo_4O_{11}

USER	INSTITUTION	FUNDING	PROJECT
Brooks, J. S. Athas, G. J. Tanaka, Y. Kinoshita, T. Kinoshita, N. Tokumoto, M. Anzai, H.	FSU Boston Univ. Electro. Tech. Lab.., Japan Electro Tech. Lab.., Japan Electro Tech. Lab.., Japan Electro Tech. Lab.., Japan Himeji Institute of Technology, Japan	NSF-DMR-95-10427	Angular Dependence of Quantum Oscillations, Magnetoresistance, and Magnetic Field Induced Phase Transitions in Quasi-Two-Dimensional Organic Molecular Conductors
Brooks, J. S. Campos, C. E. van Bentum, P. J. M. Perenboom, A. A. J. Sandhu, P. Valfells, S. Tanaka, Y. Kinoshita, T. Kinoshita, N. Tokumoto, M. Anzai, H.	FSU Boston Univ. HMFL & RIM, Univ. of Nijmegen - Netherlands HMFL & RIM, Univ. of Nijmegen - Netherlands Boston Univ. Boston Univ. Electro Tech. Lab.., Japan Electro Tech. Lab.., Japan Electro Tech. Lab.., Japan Electro Tech. Lab.., Japan Himeji Institute of Technology, Japan	NSF-DMR-95-10427	Alteration of Density Wave and Superconducting Behavior in Quasi-Two Dimensional Organic Conductors under Uniaxial Stress
Brooks, J. S. Hill, S. O. Seeger, L.	FSU NHMFL NHMFL	NSF-DMR-95-10427	High Frequency Studies of the Complex Conductivity in an Organic Superconductor
Brooks, J. S. Sandhu, P. S. Campos, C. E. Ziman, T.	FSU Boston Univ. Boston Univ. Univ. Paul Sabatier - France	NSF-DMR-95-10427	Effects of Pressure and Uniaxial Stress on Organic Metals
Brooks, J. Valfells, S. Moulton, B. Kuhns, P. Kleinhammes, A. Anzai, H. Takasaki, S. Yamada, J.	FSU Boston Univ. FSU NHMFL NHMFL Hemeji Inst. of Tech. - Japan Hemeji Inst. of Tech. - Japan Hemeji Inst. of Tech. - Japan	NSF-DMR-95-10427	^{77}Se NMR Investigation of Spin Density Wave States of $(TMTSF)_2PF_6$

USER	INSTITUTION	FUNDING	PROJECT
Brooks, J. Valfells, S. Wang, Z. Anzai, H. Takasaki, S. Yamada, J. Tokumoto, M.	FSU Boston Univ. Boston Univ. Hemeji Inst. of Tech. - Japan Hemeji Inst. of Tech. - Japan Hemeji Inst. of Tech. - Japan Electro-Tech. Inst. - Japan	NSF-DMR-95-10427	Temperature Dependence of the Integer Quantum - Hall Effect in $(TMTSF)_2PF_6$
Brunel, L.-C. Crow, J. Hassan, A.* Hill, S. Sarrao, J. Moulton, W. Whitaker, H.* McCarthy, A.*	NHMFL NHMFL NHMFL NHMFL NHMFL NHMFL NHMFL NHMFL	NSF	EPR Measurements and Cyclotron Resonance in Mo_4O_{11}, $PrBa_2$, DBPA, Cu_3O_7, and $Y_{1-x}Tb_xBa_2Cu_3O_7$
Chaikin, P. M. Hannahs, S. Immer, C. * Danner, G. Scheven, U.	Princeton Univ. NHMFL NHMFL Princeton Univ. Princeton Univ.		Heat Capacity of $(TMTSF)_2ClO_4$
Chaparala, M.	NHMFL	NSF	Magnetization Measurement of $(ET)_2Cu(NCS)_2$
Chaparala, M. Immer, C. *	NHMFL NHMFL	NSF	Mercury Superconductivity at High Pressures
Chen, C. Pai, V.* Haik, Y. *	FAMU/FSU College of Eng. FSU FAMU/FSU College of Eng.	NSF	Effects of Magnetic Fields on Biological Fluids
Cheong, S. W. Hwang, H. Tozer, S. Batlogg, B.	AT&T Bell Labs AT&T Bell Labs NHMFL AT&T Bell Labs	AT&T	Field and Pressure Effects on the Interplay Among Charge, Spin, and Lattice in Doped $Lamno_3$
Cross, T. Soghomonian, V. Kuhns, P. Kleinhammes, A. Rosanski, R.	FSU NHMFL NHMFL NHMFL FSU	MCB 9317111	NMR Spectroscopy in High Homogeneity Resistive Magnets
Douglas, E. Smith, M.	LANL LANL	DOE	Processing of Polymers in Magnetic Fields
Du, R. Cunningham, J. Zudov, M.	Univ of Utah AT&T Bell Labs. Univ. of Utah	Univ. of Utah	Magneto Transport in 2D Electron System

USER	INSTITUTION	FUNDING	PROJECT
Furdyna, J. Schmiedel, T. Pareek, A.* Yin, A.* Dobrowolska, M.	Univ. of Notre Dame NHMFL Univ. of Notre Dame Univ. of Notre Dame Univ. of Notre Dame	NSF	Investigation of Spin Interactions in MnSe/ZnSe Superlattice at High Magnetic Fields
Goodrich, R. G. Lowndes, D. Hebard, A. Hall, D.* Godbole, M.	LSU Oak Ridge Nat'l. Lab. AT&T Bell Labs. LSU Oak Ridge Nat'l. Lab.	NSF & DOE	deHaas van Alphen Measurements on Superconductors
Goodrich, R. G. Lowndes, D. Hall, D.* Teklu, A.	LSU Oak Ridge Nat'l. Lab. LSU LSU	NSF & DOE	Hc_2 Measurement of BkBO
Graybeal, J. Schmiedel, T. Moore, S.*	Univ. of Florida NHMFL Univ. of Florida	NSF	Hall Magnetoresistance in Photodoped Copper Oxides
Gschneidner, K.A. Pecharsky, V. Chaparala, M.	Iowa State Univ. Iowa State Univ. NHMFL	DOE	Advanced Materials for Magnetic Refrigeration
Gubser, D. Soulen, B. Fuller-Mora, W. Datta, T.	Naval Research Lab. NRL NRL Univ. of S. Carolina	NRL	Critical Currents of Bismuth-Cuprate Superconductor Tapes
Hallock, R. Taylor, J. Joshi, R. J.	Univ. of Mass. Alfred Univ. Univ. of Mass., Amherst		Critical Exponents of the Superconducting Transition in High Fields in Granular YBCO from Non-Linear I-V Curve Measurements
Halperin, W. P. Reyes, A. P. Moulton, B. Kuhns, P. L. Kleinhammes, A. Hammel, P. C. Martindale, J. A.	Northwestern Univ. Northwestern Univ. FSU NHMFL NHMFL LANL LANL	NSF	High Field ^{17}O NMR Studies of $YBa_2Cu_3O_7$
Hannahs, S. Immer, C. * Tozer, S. Kang, W.	NHMFL NHMFL NHMFL Univ. of Chicago	NSF	Studies of the Bechgaard Salts at High Field and High Pressure
Hascicek, Y.	NHMFL	NHMFL	J_c Measurements Associated with *in situ* Lorentz Force Strain Induced in OST Bi - 2212/Ag PIT Tape by Field Jump

USER	INSTITUTION	FUNDING	PROJECT
Hettinger, J. Gray, K. E. Washburn, B.* Paulikas, P. Veal, B. Kostic, P.	Argonne Nat'l. Lab. and Rowan College of N. J. Argonne Nat'l. Lab. Argonne Nat'l. Lab. Argonne Nat'l. Lab. Argonne Nat'l. Lab. Argonne Nat'l. Lab.	DOE	Investigations of Intrinsic Josephson Coupling between Cu-O Bilayers in a High Temperature Superconductor
Jiang, H.-W. Wong, L.* Palm, E.	UCLA UCLA NHMFL	NSF	Breakdown Studies of the Integer Quantum Hall Effect
Jiang, H.-W. Wong, L.-R.* Palm, E.	UCLA UCLA NHMFL	NSF-DMR-93-13786	Collapse of Spin Splitting in the Quantum Hall Effect
Jones, E. D. Kurtz, S. R. Schmiedel, T. Houghton, D. C. Lee, K.-S. Lee, H.	Sandia Nat'l. Lab. Sandia Nat'l. Lab. NHMFL NRC - Canada Elec. & Telecomm. Res. Inst. - S. Korea Sandia Nat'l. Lab. & Kyunghee Univ. - Korea	DOE- DE-AC04-94AL85000	Optical Determination of Effective Mass and Binding Energy for a SiGe/Si Quantum Well
Kang, W. Young, J. B. Hannahs, S. T. Campman, K. Gossard, A.	Univ. of Chicago Univ. of Chicago NHMFL UC Santa Barbara UC Santa Barbara		Studies of 2-Dimensional Electron Systems Under Hydrostatic Pressure
Kleinhammes, A. Kuhns, P. L. Moulton, W.G. Sarrao, J. L. Fisk, Z. Sullivan, N. S.	NHMFL NHMFL FSU NHMFL FSU Univ. of Florida	NSF/NHMFL	^{7}Li NMR & ^{139}La NQR in $La_2Cu_{1-x}Li_xO_4$
Maley, M. Coulter, J.* Safar, H.* Cho, J. H. * Bulaevskii, L. N.	LANL LANL LANL LANL LANL	DOE	High Field C-Axis Transport in Anistropic Superconductors and Critical Current Behavior
Markiewicz, D. Bonney, L. Martinez, R. Pickard, K.	NHMFL NHMFL NHMFL NHMFL	NSF	High Current J_c Testing for Development of 900 MHz NMR Magnet
McCombe, B. D. Schmiedel, T. Fu, L. P.	SUNY at Buffalo NHMFL Emory University	NSF	Magnetophoto Luminescence Study of D Center in GaAs/AlGAAs Quantum Wells

USER	INSTITUTION	FUNDING	PROJECT
Meisel, M. Granroth, G. * Chou, L. Talham, D. R. Chaparala, M.	Univ. of Florida Univ. of Florida Univ. of Florida Univ. of Florida NHMFL		Critical Field of Oriented Single Crystals of TMNIN
Miller, J. Miller, G.	NHMFL NHMFL	NSF	Test of Hybrid Coil Insert
Musfeldt, J. L. Wang, Y.-J. Poirier, M. Jandl, S.	SUNY at Binghamton NHMFL Univ. de Sherbrooke Univ. de Sherbrooke	NSF	FIR/MIR Investigation of the Broken Symmetry Ground State in $GeCuO_3$
Naughton, M. Laukhin, V.N. Lee, I. Kutsch, N. Petrov, D. K. Chaparala, M.	SUNY at Buffalo SUNY, Buffalo and ICP–Chernogolvka SUNY at Buffalo ICP–Chernogolvka SUNY at Buffalo NHMFL	NSF	dHvA and SdH Study of (BEDT-$TTF)_2TlHg(SeCN)_4$
Pearton, S. Geerts, W. Schmiedel, T. Crooker, S.*	Univ. of Florida Univ. of Florida NHMFL UC, Santa Barbara	NSF	Magneto Transport Measurements on GaN and Highly Doped GaAs Structures
Petrou, A. Schmiedel, T. Yu, W.* Haetty, J.* Mountziaris, T. J. Jonker, B.	SUNY at Buffalo NHMFL SUNY at Buffalo SUNY at Buffalo SUNY at Buffalo Naval Res. Lab.	NSF	Magneto Excitons in ZnSe Strained and Unstrained Epilayers
Petrou, A. Schmiedel, T. Wang, Y. Salib, M.* Yu, Willy*	SUNY at Buffalo NHMFL NHMFL SUNY at Buffalo SUNY at Buffalo	NSF	Optically Detected Cyclotron Resonance in Semiconductor Heterostructures
Petrou, A. Schmiedel, T. Lee, S. T.* Dutta, M. Pamulapati, J. Salib, M.*	SUNY at Buffalo NHMFL SUNY at Buffalo SUNY at Buffalo SUNY at Buffalo SUNY at Buffalo	NSF	Magneto Optical and Transport Studies of Quantum Well Structures
Ranganathan, R. Schmiedel, T. Abernathy, C.	Cal State University Northridge NHMFL Univ. of Florida	NSF	Interband Magneto Optics in III-V Nitrides

USER	INSTITUTION	FUNDING	PROJECT
Schneider, D. Wang, Y.-J.	Tech. Univ. Braunschweig NHMFL	NSF	FIR Transmission
Schwartz, J. Nakamae, S.* Howton, J. Wei, W.* Hilton, D. Rigal, L. Miller, V. Kessler, G.	FAMU/FSU College of Engineering FSU NHMFL FSU NHMFL NHMFL NHMFL NHMFL	NSF	High T_c Superconducting Wire Development
Sessoli, R. Chaparala, M.	Univ. of Firenze NHMFL	NSF	Magnetization of Fe_8
Shayegan, M. Lay, T.-S.*	Princeton Univ. Princeton Univ.		Quantum Hall Effect in a Bilayer System in Tilted Magnetic Fields
Siddall, M. McKinnell, J.	Teledyne - Wah Chang Teledyne - Wah Chang	Teledyne/Wah Chang	Critical Current of Superconducting Wires
Stewart, G. H. Andraka, B. Thomas, S. Lumpe, H. Chaparala, M. Kim, J. S.	Univ. of Florida Univ. of Florida Univ. of Florida Univ. of Augsburg NHMFL Univ. of Florida	NSF	Magnetization of Spin Fluctuation Systems in High Fields
Sullivan, N. S. Moulton, B. Garcia, B.* Bodart, J.	Univ. of Florida FSU Univ. of Florida Univ. of Florida	NSF	Effects of Large Magnetic Fields on the Performance of an FET Marginal Oscillator Used for a CW-NMR Spectrometer
Summers, T. Gottstein, G. Herringhaus, F.* Leffers, R.*	FAMU/FSU College of Engineering RWTH Technical University NHMFL RWTH Tech.Univ	NSF	Wire Development for Pulsed Magnets (Magnetoresistivity of Cu-Ag Alloy Wires)
Tanner, D. Liu, H.-L.* Zibold, A.	Univ. of Florida Univ. of Florida Univ. of Florida	NSF	Flux-Flow Resistance of High -T_c Superconductors
Tanner, D. Wang, Y.-J. Zibold, A. Liu, H.-L.* Gruninger, M.*	Univ. of Florida NHMFL Univ. of Florida Univ. of Florida Univ. of Karlsruhe	NSF	Magnetic Interactions in the Insulating Phases of the Cuprates

USER	INSTITUTION	FUNDING	PROJECT
Tanner, D. Zibold, A.* Liu, H.-L.* Wang, Y.-Ji. Gruninger, M.* Geserich, H. P. Li, M. Y. Wu, M. K.	Univ. of Florida Univ. of Florida Univ. of Florida NHMFL Univ. of Karlsruhe - Germany Univ. of Karlsruhe - Germany Nat'l.'l. Tsing Hua Univ. - Taiwan Nat'l.'l. Tsing Hua Univ. - Taiwan	NSF	Magnetotransmittance Studies of Spin Wave Excitations in Insulating Phases of YBCO Thin Films
Tozer, S. Hannahs, S.	NHMFL NHMFL	NSF	High Pressure Electrical Transport Properties of Organic Conductors
Tsui, D. C. Störmer, H. L. Du, R.R.	Princeton Univ. AT&T Bell Lab. Univ. of Utah		Fractional Quantum Hall Measurements as a Function of Angle
Van Sciver, S. Bartholomew, K. Baudouy, B.* Cochran, V.	FAMU/FSU College of Engineering NHMFL NHMFL NHMFL	NSF	Test of AC Losses in Superconducting Cable
Van Winkle, D. Rill, R.	FSU FSU	NSF	Alignment of Xanthan Liquid Crystals in the Magnetic Field and Relaxation at Zero Field
Wang, Y.-J. Kaplan, R. Ng, H.-K. Doverspike, K. Gaskill, D. K. Ikedo, T. Amano, H. Akasaki, I.	NHMFL Naval Research Lab. FSU Naval Research Lab. Naval Research Lab. Meijo Univ. - Japan Meijo Univ. - Japan Meijo Univ. - Japan	NSF & NRL	Cyclotron Resonance Studies of GaN
Wang, Y. J. McCombe, B. D.	NHMFL SUNY at Buffalo		Electron Cyclotron Resonance Studies of Si Multiple Quantum Well Systems
Weinstein, R. Ren, Y. Foster, C. Liu, J. Obot, V. Parks, D.	Univ. of Houston Univ. of Houston Univ. of Indiana Univ. of Houston Texas S. Univ. Univ. of Houston	NSF	Temperature Dependance of Creep and Trapped Field for Trapped Field Magnets

* Graduate Student

NHMFL - Pulse Field Facility

USER	INSTITUTION	FUNDING	PROJECT
Lacerda, A.	Los Alamos	NHMFL	Kondo Insulators
Goettee, G. D.	Los Alamos	DoE	
Smith, J. L.	Los Alamos	DoE	
Kebede, A.	NC A&T	DoE	
Canfield, P.C.	Ames Labs.	DoE	
Buford, M.#	NC A&T	DoE	
Alexander, J.*	NM Tech.	DoE	
McLendon, T.#	NC A&T	DoE	
Lima, K.#	UFPE/Brazil		
Lacerda, A	Los Alamos	NHMFL	CeB_6
Torikachvili, M.S.	San Diego State Univ.	NHMFL	
Sarrao, J.L.	Tallahassee	NHMFL	
Fisk, Z.	Tallahassee	NHMFL	
Thompson, J.D.	Los Alamos	DoE	$YbInCu_4$
Lacerda, A.	Los Alamos	NHMFL	
Sarrao, J.L.	Tallahassee	NHMFL	
Fisk, Z.	Tallahassee	NHMFL	
Mielke, C.H.*	Clark Univ.	Air Force	Molecular Metals
Agosta, C.C.	Clark Univ.	Air Force	
Goettee, J.D.	Los Alamos	DoE	
Lacerda, A.	Los Alamos	NHMFL	
Smith, M.E.	Los Alamos	DoE	Polymers, Liquid Crystals
Armijo, E.V.	Los Alamos	DoE	
Benicewicz, B.C.	Los Alamos	DoE	
Douglas, E.P.	Los Alamos	DoE	
Lacerda, A.	Los Alamos	NHMFL	
Earls, J.D.	Dow Chemical		
Priester, R.D.	Dow Chemical		
Wei, X.	Los Alamos	DoE	Magneto-Raman-Spectroscopy
Donohoe, R.J.	Los Alamos	DoE	
Safar, H.	Los Alamos	DoE	YBaCuO
Coulter, Y.	Los Alamos	DoE	
Maley, M.	Los Alamos	DoE	
Wu, X.D.	Los Alamos	DoE	
Foltyn, S.	Los Alamos	DoE	
Arendt, P.	Los Alamos	DoE	
Willis, J.O.	Los Alamos	DoE	
Bruck, E.	Amsterdam Univ.	Netherlands	Magnetization of Intermetallics
Zhao, Z.G.	Amsterdam Univ.	Netherlands	
de Boer, F.R.	Amsterdam Univ.	Netherlands	
Haanappel, E.	Los Alamos	NHMFL	

USER	INSTITUTION	FUNDING	PROJECT
Havela, L.	Charles Univ.	Czech	UNiAl & UNiGe
Bruck, E.	Amsterdam Univ.	Netherlands	
Sechovsky, V.	Charles Univ.	Czech	
Nakotte, H.	Los Alamos	DoE	
Lacerda, A.	Los Alamos	NHMFL	
Canfield. P.C.	Ames Labs.	DoE	$HoNi_2B_2C$
Cho, B.K.*	Iowa State Univ.		
Lacerda, A.	Los Alamos	NHMFL	
Svoboda, P.	Charles Univ.	Czech	$NdCu_2$
Divis, M.	Charles Univ.	Czech	
Sechovsky, V.	Charles Univ.	Czech	
Nakotte, H.	Los Alamos	DoE	
Lacerda, A.	Los Alamos	NHMFL	
Onuki, Y.	Osaka Univ.		
Sugawara, H.	Tokyo Univ.		
Prokes, K.*	Amsterdam Univ.	Netherlands	U_2T_2X
de Boer, F.R.	Amsterdam Univ.	Netherlands	
Havela, L.	Charles Univ.	Czech	
Sechovsky, V.	Charles Univ.	Czech	
Pereira, L.C.*	European Commission		
Nakotte, H.	Los Alamos	DoE	
Haanappel, E.	Los Alamos	NHMFL	
Lacerda, A.	Los Alamos	NHMFL	
Nakotte, H.	Los Alamos	DoE	$UCu_{3.5}Al_{1.5}$
Lacerda, A.	Los Alamos	NHMFL	
Torikachvili, M.S.	San Diego State Univ.	NHMFL	
Bruck, E.	Amsterdam Univ.	Netherlands	
Prokes, K.*	Amsterdam Univ.	Netherlands	
de Boer, F.R.	Amsterdam Univ.	Netherlands	
Continentino, M.A.	UFF	Brazil	Warwickites
Fernandes, J.C.	UFF	Brazil	
Guimaraes, R.B.	UFF	Brazil	
Boechat, B.	UFF	Brazil	
Borges, H.	PUC	Brazil	
Valarelli, J.V.	USP	Brazil	
Silva, P.R.J.	CBPF	Brazil	
Haanappel, E.	Los Alamos	NHMFL	
Lacerda, A.	Los Alamos	NHMFL	
Torikachvili, M.S.	San Diego State Univ.	NHMFL	(La,Sr)CuO
Rodriguez, J.P.	LASU		
Lacerda, A.	Los Alamos	NHMFL	
Sarrao, J.L.	Tallahassee	NHMFL	
Fisk, Z.	Tallahassee	NHMFL	

USER	INSTITUTION	FUNDING	PROJECT
Montenegro, F.C. Lima, K.# Torikachvili, M.S. Lacerda, A.	UFPE UFPE San Diego State Univ. Los Alamos	Brazil Brazil NHMFL NHMFL	$Fe_xZn_{1-x}F_2$
Lawrence, J.M. Lacerda, A.	UC Irvine Los Alamos	NSF/DoE NHMFL	CePtPb
Mentink, S.A.M. Mason, T.E. Mydosh, J.A. Goettee, J.D.	Univ. Toronto Univ. Toronto Leiden Univ. Los Alamos	Univ. Univ. Univ. DoE	URu_2Si_2
Moehleck, S. Alexander, J.* Torikachvili, M.S. Lacerda, A.	UNICAMP NM Tech San Diego State Univ. Los Alamos	Brazil DoE NHMFL NHMFL	Bi2212+Zn
Meisel, M. Lee, Y.* Torikachvili, M.S. Lacerda, A.	Univ. of Florida Northeastern Univ. San Diego State Univ. Los Alamos	NSF Univ. NHMFL NHMFL	Gadolinium Sulfate Octh Ydrate
Haanappel, E. Alexander, J.* Lacerda, A.	Los Alamos NM Tech. Los Alamos	NHMFL DoE NHMFL	Transport Q- Crystals
Graf, T. Lacerda, A.	Autonoma Madrid Los Alamos	Spain NHMFL	Thin Films
Neumeier, J. Torikachvili, M.S. Lacerda, A.	Los Alamos San Diego State Univ. Los Alamos	DoE NHMFL NHMFL	GMR
Moshopoulou, E. Thompson, J.D. Smith, J.L. Lacerda, A.	Los Alamos Los Alamos Los Alamos Los Alamos	DoE DoE DoE NHMFL	$UBe_{1-x}B_x$
Jones. E. Kim, Y.* Perry, C.	Sandia Nat'l. Labs. Los Alamos Northeastern Univ.	DoE NHMFL NHMFL	InGaP alloy
Brooks, J. Kim, Y.* Perry, C.	FSU Los Alamos Northeastern Univ.	NSF NHMFL NHMFL	KHg - Polarization and Photoluminescence
Brooks, J. Valfells, S.* Lacerda, A.	FSU FSU Los Alamos	NSF NHMFL NHMFL	$(TMTSF)PF_6$

USER	INSTITUTION	FUNDING	PROJECT
Lacerda, A. Cho, J.-H.	Los Alamos Los Alamos	NHMFL DoE	(La, Sr)CuO
Agosta, C.C. Mielke, C.* Lacerda, A.	Clark Univ. Clark Univ. Los Alamos	Air Force Air Force NHMFL	$(BETS)_2GaCl_4$
Laukhin, V.N. Naughton, M. J. Haanappel, E.	Inst. Chem. Phys. SUNY at Buffalo Los Alamos	NSF NSF NHMFL	Magnetoresistance and Quantum Osc. in BEDT-TTF
Vuillemin, J. J. Haanappel, E. Mueller, F. M.	Univ. of Arizona Los Alamos Los Alamos	AWU NHMFL DoE	dH-vA in AuAg Alloys and Pd
Haanappel, E. Mueller, F. M. Canfield, P. Kycia, S. Goldman, A. Rabson, D. Harmon, B.	Los Alamos Los Alamos Ames Lab Cornell Univ. Ames Lab Los Alamos Ames Lab	NHMFL DoE DoE DoE DoE DoE	Quasicrystals
M. Torikachvili Haanappel, E.	San Diego State Univ. Los Alamos	Univ. NHMFL	Magnetization of $U Fe_4 P_{12}$, $Yb Fe_4 P_{12}$
Jones, E.D. Kim, Y. Perry, C. H. Tozer, S. W. Rickel, R. G.	Sandia Nat'l. Labs. Los Alamos Northeastern Univ. NHMFL-FSU Los Alamos	DoE NHMFL NHMFL NHMFL NHMFL	Pressure/Field Studies of Single Quantum Wells, (InGaAs-GaAs)
Perry, C.H. Kim, Y. Rickel, R. G.	Northeastern Univ. Los Alamos Los Alamos	NHMFL NHMFL NHMFL	Semiconductor Heterostructures
Perry, C.H. Kim, Y. Rickel, R. G. Lee, K.-S.	Northeastern Univ. Los Alamos Los Alamos ETRI, Korea	NHMFL NHMFL NHMFL MICK	PL of Mod-doped (Al-GaAs)/ GaAs SHJ
Perry, C.H. Kim, Y. Lee, K.-S. Rickel, R. G.	Northeastern Univ. Los Alamos ETRI, Korea Los Alamos	NHMFL NHMFL MICK NHMFL	PL of Si Delta-doped GaAS...
Lee, K.-S. Lee, C.D. Noh, S.K. Kim, Y. Perry, C.H. Rickel, R. G.	ETRI, Korea KRISS KRISS Los Alamos Northeastern Univ. Los Alamos	MICK MICK MICK NHMFL NHMFL NHMFL	Mag-opt. Determination of Carrier Effect Masses of InGaAs AlAs/ GaAs QWs

USER	INSTITUTION	FUNDING	PROJECT
Petrou, A.	SUNY at Buffalo	NSF/ONR	Indirect Transitions in AlAs-GaAs QWs
Dutta, M.	Army Res. Labs	ARO	
Perry, C.H.	Northeastern Univ.	NHMFL	
Kim, Y.	Los Alamos	NHMFL	
Rickel, R. G.	Los Alamos	NHMFL	
Namavar, F.	Spire Corp.	AFOSR	Magneto-PL of Porous Silicon
Perry, C.H.	Northeastern Univ.	NHMFL	
Kim, Y.	Los Alamos	NHMFL	
Rickel, R. G.	Los Alamos	NHMFL	
Simmons, J.A.	Sandia Nat'l. Labs.	DoE	EPL Studies of Mod-Doped Couple Double Quantum Wells
Jones, E.D.	Sandia Nat'l. Labs.	DoE	
Kim, Y.	Los Alamos	NHMFL	
Perry, C.H.	Northeastern Univ.	NHMFL	
Rickel, R. G.	Los Alamos	NHMFL	
Brooks, J.	FSU	NSF	PL & Polarization, KHg
Kim, Y.	Los Alamos	NHMFL	
Perry, C.H.	Northeastern Univ.	NHMFL	

KRISS is Korea Research Inst. of Standards and Science

MICK is Ministry of Information and Communication, Korea

* Graduate Student

\# Undergraduate Student

NHMFL - NMR Facility

USER	INSTITUTION	FUNDING	PROJECT
720 NMR #5 (Varian)			
Meersmann, T.	NHMFL	NHMFL	Transverse Relaxation in Coupled Spin Systems
Bodenhausen, G.			
Jeannerat, D.	NHMFL	NHMFL	Accurate Determination of Scalar Coupling Constants
Bodenhausen, G.			
Peng, C.	NHMFL	NHMFL	Automated Spectral Analysis
Bodenhausen, G.			
Vincent, S. J.F.	NHMFL	NHMFL	Suppression of Spin Diffusion in Nuclear Overhauser Spectroscopy
Zwahlen, C.			
Bodenhausen, G.			

USER	INSTITUTION	FUNDING	PROJECT
Murali, N. Bolton, P. H.	NHMFL Wesleyan Univ.	NHMFL NSF, NIH	Molecular Aignment in High Field
Logan, T.	FSU/NHMFL	FSU	Structure-Function Study of Proteins
Trewhella, J.	LANL	LANL	Study of Complexes Formed by Ca^{2+} Binding Proteins and Their Regulatory Targets

USER	INSTITUTION	FUNDING	PROJECT
500 NMR #3 (Varian)			
Robert, J.	Univ. So. Fla.		Study of Polypeptides and Proteins
Gochin, M.	Univ. Calif., San Francisico	NIH (GMS)	Use of Paramagnetic Shifts in NMR for Structure Determination
Bodenhausen, G. Gochin, M. Fu, R.	NHMFL/FSU Univ. of Calif, San Francisco NHMFL	NHMFL NHMFL	Broadband Decoupling of Paramagnetic Macromolecules

USER	INSTITUTION	FUNDING	PROJECT
600 WB NMR #4 (Bruker)			
Kinsey, S. Ellington, R.	FSU/NHMFL	NSF	NMR Studies of Lactate Permeation Mechanisms in Singlecells and Cell Bundles
Combs, C. Ellington, R.	FSU/NHMFL	NSF	NMR Studies of the Impact of Severe Acidosis on Cellular Energetics

USER	INSTITUTION	FUNDING	PROJECT
Combs, C. Kinsey, S. Ellington, R. Doeller, J. Kraus, D.	FSU/NHMFL Univ. of AL, at Birmingham	NSF	NMR Studies of Mitochondrial Sulfide Oxidation
Kinsey, S., Locke, B. Moerland, T.	FSU/NHMFL	NASA	Studies of Water and Diffusion in Gels

USER	INSTITUTION	FUNDING	PROJECT
300 - WB & NB NMR #1 & 2 (Bruker)			
Bodenhausen, G. Post, C.B. Burgner, J.W. Zwahlen, C. Vincent, S.J.F.	NHMFL/FSU Purdue Univ., at W. Lafayette Purdue Univ., at W. Lafayette NHMFL NHMFL	NHMFL NHMFL NHMFL	Study of Enzyme Co-Factor Complex
Bodenhausen, G. Roe, D.C. Fu, R. Zwahlen, C. Vincent, S.J.F.	NHMFL DuPont NHMFL NHMFL NHMFL	NHMFL DuPont NHMFL NHMFL NHMFL	Study of Chemical Exchange and Membranes Properties
Bodenhausen, G. Bolton, P.H. Zwahlen, C. Vincent, S.J.F.	NHMFL/FSU Wesleyan Univ., Middletown NHMFL NHMFL	NHMFL NHMFL NHMFL	Study of a New DNA Structure
Bodenhausen, G. Leroy, J.L. Guéron, M. Zwahlen, C. Vincent, S.J.F.	NHMFL/FSU Ecole Polytechnique, France Ecole Polytechnique, France NHMFL NHMFL	NHMFL NHMFL NHMFL	Study of a DNA Tetrad
Bodenhausen, G. Logan, T.M. Zwahlen, C. Vincent, S.J.F.	NHMFL/FSU FSU NHMFL NHMFL	NHMFL NHMFL NHMFL NHMFL	Study of Proteins Using Isotopically (^{13}C,^{15}N) Enriched Samples
Zwahlen, C. Vincent, S.J.F. Malliavin, T.	NHMFL NHMFL Univ. Montpellier I, France	NHMFL NHMFL CNRS	Study of a Calcium Binding Protein by NMR
Bodenhausen, G. Logan, T.M. Jeannerat, D. *	NHMFL/FSU FSU NHMFL	NHMFL NHMFL NHMFL	Study of Peptides

USER	INSTITUTION	FUNDING	PROJECT
Bodenhausen, G. Holton, R.A. Meersmann, T. * Jeannerat, D. * Peng, C.	NHMFL/FSU FSU NHMFL NHMFL NHMFL	NHMFL FSU NHMFL NHMFL NHMFL	Study of Taxol
Bodenhausen, G. Yuan, S. Zheng, C. Peng, C.	NHMFL/FSU Chinese Academy of Sciences Chinese Academy of Sciences NHMFL	NHMFL NHMFL	Computer Analysis of NMR Spectra
Berthault, P. Desvaux, H. Birlirakis, N. Rubinstenn, G. Sinaÿ, P.	CEA, France CEA/NHMFL CEA, France ENS, France ENS, France	CEA CEA/NHMFL CEA Univ. Paris VI Univ. Paris VI	Study of a Lewis^X Analog
Lippens, G. Desvaux, H.	Pasteur Institute, France CEA/NHMFL	CNRS CEA/NHMFL	Study of a Cyclic Glucan
Bodenhausen, G. Rosanske, D. Gullion, T. Schaefer, J. Fu, R.	NHMFL/FSU FSU FSU Washington Univ. NHMFL	NHMFL FSU FSU NHMFL	Transmission-Line Probe
Bodenhausen, G. Gullion, T. Samoson, A. Fu, R.	NHMFL/FSU FSU Estonian Academy of Science NHMFL	NHMFL NATO NHMFL	Instrumentation for Studying Quadrupolar Nuclei
Grant, D.M. Mayne, C. Chenon, M.T. Smith, S.	Univ. Utah Univ. Utah Univ. Utah NHMFL	Univ. Utah Univ. Utah Univ. Utah NHMFL	Investigation of Coupled Relaxation in Methyl Groups
Mayne, C. Smith, S.	Univ. Utah NHMFL	Univ. Utah NHMFL	Multi-mode Relaxation in Molecules Strong Scalar Coupling
Smith, S. Bodenhausen, G. Skrynnikov, N.	NHMFL NHMFL/FSU McGill Univ., Montreal	NHMFL NHMFL	Relaxation and Exchange Effects in NMR Experiments

* Graduate Students

NHMFL - EMR Facility

USER	INSTITUTION	FUNDING	PROJECT
Dalal, N.	Univ. of West Virginia	NSF	Linear Magnetism
Singh, K.	Univ. of West Virginia		
Hassan, A.	NHMFL		
Krzystek, J.	NHMFL		
Pardi, L.	NHMFL		
Brunel, L. C.	NHMFL		
Gaffney, B. J.	Johns Hopkins Univ.	NIH	Biochemistry
Maguire, B.C.	Johns Hopkins Univ.		
Doctor, K.S.	Johns Hopkins Univ.		
Tevelrakh, E.	Johns Hopkins Univ.		
Hassan, A.	NHMFL		
Krzystek, J.	NHMFL		
Pardi, L.	NHMFL		
Brunel, L. C.	NHMFL		
Janossy, A.	Univ. of Budapest		EPR of High T_c
Brunel, L. C.	NHMFL		
Cooper, J. R.	Cambridge Univ.		
Brunel, L. C.	NHMFL		EPR of Biradicals
Chachati, C.	C. E. N. Saclay, France		
Fabre, C.	Ecole Normale Superieure Paris		
Gambarelli, S.	Ecole Normale Superieure Paris		
Jaouen, D.	Ecole Normale Superieure Paris		
Rassat, A.	Ecole Normale Superieure Paris		
Pardi, L.	NHMFL		Magnetism
Gatteschi, D.	Univ. of Florence		
Sessoli, R.	Univ. of Florence		
Caneschi, A.	Univ. of Florence		
Gillon, B.	Univ. of Florence		
Hennion, M.	Univ. of Florence		
Mirabeau, I.	Univ. of Florence		
Kahn, O.	Univ. of Bordeaux		
Brunel, L-C.	NHMFL		
Rettori, C.	San Diego State Univ.		High T_c
Oseroff, S.	San Diego State Univ.		
Rao, D.	Univ. Estadual de Campinas		
Valdivia, J. A.	Univ. Estadual de Campinas		
Barberis, G. E.	Univ. Estadual de Campinas		
Martins, G.	NHMFL		
Sarrao, J.	NHMFL		
Fisk, Z.	NHMFL		
[illegible]	NHMFL		
[illegible]	Centro Atomico [illegible]iloche (Brazil)		

NHMFL - ICR Facility

USER	INSTITUTION	FUNDING	PROJECT
FTMS-2000 (3 tesla)			
Costello, C. Reinhold, B. B.#	Boston Univ.	NSF ICR Facility	Oligosaccharide Identific'n and Sequencing
Instrument and Technique Development			
Amster, I. J. Pitsenberger, C.*	Univ. Georgia	NSF ICR Facility	Electrospray Vacuum System AutoCad Design
Blair, L. Xin, T.*	Berea College	NSF ICR Facility	Ion Axialization in ICR Mass Spectrometry
Dunbar, R. C. Ho, Y.-P.* Lin, E.*	Case Western Reserve Univ.	NSF ICR Facility	Ion Heating During Quadrupolar Excitation; Optical Spectroscopy of Ions
Buchanan, M. Eyler, J. R. Lang, L.*	Oak Ridge Nat'l. Lab. Univ. of Florida	NSF ICR Facility NSF ICR Facility	Matrix-Assisted Laser Desorption/ Ionization of Nucleotides
Freiser, B. S. Auberry, K.* Jiao, C.*	Purdue Univ.	NSF ICR Facility	Platinum Cluster Ion Stoichiometry
Gross, F. Hodge, K.-N.†	Florida A&M Univ.	NSF ICR Facility	Quadrupolar Ion Guide Trajectory Simulations
Laude, D. A. Drader, J.*	Univ. of Texas	NSF ICR Facility	ICR Data System Development
Rice, J.A. Brown, T.*	South Dakota State Univ.	NSF ICR Facility	Humic Substances Analysis by MALDI FT-ICR MS
Yost, R. Degnore, J. P.*	Univ. of Florida	Marshall NSF Operating Grant	Ion Trajectory Simulations

† Undergraduate Researcher
* Graduate Student
# Postdoctoral Fellow

COMMITTEES 9

External Advisory Committee

Members of the External Advisory Committee are appointed by the Chancellor of the State University System of Florida. The committee reviews and evaluates overall performance and provides recommendations to the Chancellor. It meets once or twice a year.

Eric Jones, Chair
Sandia National Laboratories

Theoren Smith, Chair Elect
IBM Corporation

George Crabtree
Argonne National Laboratory

Donald Gubser
Naval Research Laboratory

Brian Maple
University of California at San Diego

Eric Oldfield
University of Illinois at Urbana-Champaign

Raymond Orbach
University of California at Riverside

Peter Roemer
Advanced Mammography Systems

Carl Rosner
Intermagnetics General Corporation

Ray Shaw
Varian Associates, Inc.

William Sibley
The University of Alabama at Birmingham

Peter Wyder
High Field Magnet Laboratory
Grenoble, France

Users' Committee

Members of the Users' Committee are appointed by the Director in consultation with the National Science Foundation and the NHMFL user community. The committee provides guidance on the needs and policies related to the development and utilization of the magnet laboratory's facilities and equipment in support of the users.

Horst Störmer, Chair
AT&T Bell Laboratories

David Awschalom
University of California at Santa Barbara

James Brooks
National High Magnetic Field Laboratory

Paul Chaikin
Princeton University

Naresh Dalal
Florida State University

Roy Goodrich
Louisiana State University

Eric Jones
Sandia National Laboratories

Martin Maley
Los Alamos National Laboratory

Mike Naughton
SUNY Buffalo

Stan Tozer
National High Magnetic Field Laboratory

Regitze Vold
University of California at San Diego

Erik Zuiderweg
University of Michigan

Science Program Committee

Members of the Science Program Committee are appointed by the Director from the three consortium institutions in consultation with the National Science Foundation. The committee recommends science programs and innovative research that advance the facilities. It also reviews requests for use of the facilities.

J. Robert Schrieffer, Chair

Lev Gor'kov, Associate Chair

Kevin Bedell

Geoffrey Bodenhausen

James Brooks

Zachary Fisk

John Graybeal

Chris Hammel

Kevin Ingersent

Tom Mareci

Alan Marshall

Stan Tozer

Stephan von Molnár

Ex Officio Members:

Jack Crow

Don Parkin

Neil Sullivan

Bruce Brandt

Larry Campbell

Hans Schneider-Muntau

Joe Thompson

RESEARCH REPORT APPENDIXES 10

Listing by Category

Biology

Chemistry

Superconductivity — Basic

Superconductivity — Applied

Kondo/Heavy Fermion Systems

Molecular Conductors

Semiconductors

Magnetism and Magnetic Materials

Other Condensed Matter

Magnetic Resonance Techniques

Authors Index